SOUTHERN AFRICAN DUST CHARACTERISTICS AND POTENTIAL IMPACTS ON THE SURROUNDING OCEANS

By:

KAUKURAUEE ISMAEL KANGUEEHI

Supervisor: Dr Susanne Fietz

Co-supervisor: Prof Frank Eckardt

Dissertation presented in fulfilment of the requirements for the degree of Doctorate of Earth Sciences in the Faculty of Science at Stellenbosch University

This page is intentionally left blank

DECLARATION

This is a declaration that this dissertation, in its entirety is my own original work and that I am the sole author thereof (save to the extent explicitly otherwise stated), that the reproduction and publication thereof by Stellenbosch University will not infringe any third party rights and that I have not previously in its entirety or in part submitted it for obtaining any qualification.

This dissertation includes three manuscripts, one that is under-review and two that are in the final stages in preparation for journal submission.

December 2021

This page is intentionally left blank

ACKNOWLEDGEMENTS

First of all, I would like to thank the Almighty God for carrying me and guiding through this long journey of my PhD dissertation. To my two supervisors Susanne and Frank, words cannot explain how grateful I am for your guidance and supervision during this journey.

Susanne, your open door policy meant I could pop in whenever I had a new idea or was struggling with a new concept, that became priceless through this PhD.. To Susanne I would like to acknowledge you for guiding me through all these years of my postgraduate career and allowing me to grow as a researcher. To Frank, your calmness and patience during this journey is admirable and will always be appreciated. I would also like to thank Proff Roy and Dr Jore for always being ready to help and being available to share your knowledge during this study.

In addition, I would also like to thank the TraceEx team (JL, Saumik, Andrea, Johan, Ryan, Jean, Margaret, Asmitta, Tara, Raya, Thato, Natasha, Houda, Jennifer), for all the coffee breaks, science discussions, meetings and outings discussing the science that we all love will always be highly valued and be missed as we finish this one chapter of our lives. Yet, we are excited at what the future holds and looking forward to working with you guys in the near future.

A special thank you goes to the captain and entire crew of the vessels RV Agulhas II and RV Welwitschia for helping me collect my dust samples during the Winter 2017, Winter 2019, Spring 2019 as well as sediment core during the May 2019.

Then last but least, I would like to thank my family (Tareere, Kuvee, Puvitanda, Utarera, Mekahako, Kahepako, Vetondouua, Veueza, Coco, Kasukona, Kangeri, Tjiuatu, Nandeesora, Ratandaije, Uakaeta, Ndiriraro, Kavii, Katukoo (lol) etc, I know I forgot a lot of names) for supporting during this journey. To my parents your believe and passion for education is incredible considering you guys never had the opportunity to go varsity. I will always cherish that about you guys and I am definitely blessed to call you guys my parents.

To my RUNNING TONIGHT sports club family, thank you for always encouraging us to try and do better. Surely nothing is impossible if you are willing to put in the work.

And to my brother Uaisapo Noks Kangueehi, I know you are smiling down on us from heaven and laughing at me with this words “Hapo utja morihongo ngatu rune?” which loosely translates as till when are going to study? This piece of work is dedicated you. I miss and love you. Continue resting in peace my brother.

To my great friend for as long as I can remember, Cynthia Kandorozu, words cannot explain your love, kindness, joy and support for me during this journey, I will forever be indebted to you, as you always say, this is our PhD.

A special word goes to my partner in everything Athina Kenned, you continue to amaze daily and thank you for all the support during this journey. I have surely found my person in you. Thank you for all the late nights of encouragement and support through all this years, will forever be indebted to you. I would also like to acknowledge your family for all their support during this journey as well.

This page is intentionally left blank

ABSTRACT

This study supports understanding the potential impact of dust aerosols from southern Africa have on the proximal ocean ecosystems. Dust can release essential nutrients and thus fertilize the ocean, which affects the food-web and the carbon dioxide concentrations in ocean waters, i.e. climate. Dust that fertilizes the phytoplankton communities in open oceans stimulates the drawdown of carbon dioxide from the atmosphere through the process of photosynthesis. Key here is that the nutrients must be released from the aerosol particles, as they can only be uptaken by biological organisms in soluble form. However, mineral dust emitted from arid environments differ from dust emitted through industrial activities; as a result the solubility and, by extent, potential impact on the ocean may also differ. In this study, I investigated mineral characteristics and solubility of dust from three distinct regions, one with a strong human footprint (Saldanha Bay), one with mostly natural mineral dust (Namib Desert) and one off shore over the Southern Ocean.

The first study targeted Saldanha Bay, a town that hosts the largest port in South Africa, with exports of up to 60 million tons of iron and manganese ore annually and is home of a steel plant and a smelter. Satellite images and photos from the area have shown extensive dispersion of dust from the area. Solubility leaching experiments revealed that dust collected in this town is highly soluble (bioaccessible) for trace metals such as Fe (up to 28%), Cu (up to 33%), Pb (up to 45%) and Zn (up to 38%). Phytoplankton communities in open oceans are sometimes depleted in these trace metals, and thus, such high solubility of dust from Saldanha Bay can prove to be an important nutrient supplier to surrounding oceans. In addition, air mass trajectories revealed that this readily available dust most likely affects the southeast Atlantic and Indian Ocean. The major implication was that harbour towns can be essential sources of trace metals to proximal oceans.

Secondly, I present results from the largest non-playa environment in the Namib Desert. Some of the prominent dust emitters located in the Namib Desert provide, feed and source of hundreds of tons of mineral dust to proximal surface ocean waters. The solubility of the mineral dust, in contrast to the mixed (anthropogenic and natural sourced) dust mentioned above, is much lower (e.g. up to 2 % for Fe, up to 7.8 % for Cu, up to 16% for Zn, up to 9% for Mn, 8% for Pb). These solubilities are in similar range to other semi-arid to arid major global dust sources such as the Sahara Desert in the Northern Hemisphere. Differences in mineralogy and particle size distribution at the sampling stations are the main drivers of the solubility. For example, the solubility of trace metals such as Fe, Zn and Pb is higher at the inland station than at the coastal station. The aggregated particles along the

coastal stations are less soluble probably because of persistent foggy conditions and less sunlight. The inland stations had less foggy conditions and more fine-grained particles which are rich in FeO oxides. Air mass trajectory modelling indicated that this mineral dust, with its low solubility, typically travels towards the southeast Atlantic Ocean, but can also reach the nutrient poor areas in the Southern Ocean in some cases. This study highlighted the role of non-playa environments as important dust sources and that mineralogy coupled with particle size are closely related to trace metal solubility.

In addition, to assessing the solubility and potential impact of dust with natural and anthropogenic imprint, we investigated the solubility of aerosols collected over the Southern Ocean south of South Africa on board on the research vessel SA Agulhas II. The solubility of the trace metals over the Southern Ocean ranges from 0.5 to 41% Fe, 9 to 48% Al, 0.1 to 88 % Mn, 25 to 72 % Zn and 3.3 to 39 % Co.

This study found large variability in trace metal composition and fractional solubility in dust aerosols collected from three distinct environments in southern Africa and south of southern Africa. Our study highlighted the importance of southern African dust of both anthropogenic and natural sources as a nutrient supplier to surrounding coastal and open oceans.

OPSOMMING

Hierdie studie ondersteun die begrip van die potensiële impak van stof-aërosole van Suider-Afrika op die proksimale oseaan-ekosisteme. Stof kan noodsaaklike voedingstowwe vrystel en sodoende die see bemes, wat die voedselweb en die kool stof dioksied konsentrasies in seewater, dit wil sê klimaat, beïnvloed. Stof wat die fitoplankton gemeenskappe in oop oseane bemes, stimuleer die onttrekking van koolstofdioksied uit die atmosfeer deur die proses van fotosintese. Sleutel hier is dat die voedingstowwe uit die aërosol deeltjies vrygestel moet word, aangesien dit slegs deur biologiese organismes in oplosbare vorm opgeneem kan word. Minerale stof wat uit droë omgewings vrygestel word verskil egter van stof wat deur industriële aktiwiteite vrygestel word; gevolglik kan die oplosbaarheid en, in mate, potensiële impak op die see ook verskil. In hierdie studie het ek mineraalkenmerke en oplosbaarheid van stof van drie afsonderlike streke ondersoek, een met 'n sterk menslike voetspoor (Saldanhabaai), een met meestal natuurlike minerale stof (Namib-woestyn) en een van die kus af oor die Suidelike Oseaan.

Die eerste studie was gerig op Saldanhabaai, 'n dorp wat die grootste hawe in Suid-Afrika huisves, met uitvoere van tot 60 miljoen ton yster- en mangaanerts jaarliks en is die tuiste van 'n staalaanleg en 'n smelter. Satellietbeelde en foto's van die gebied het uitgebreide verspreiding van stof uit die gebied getoon. Oplosbaarheidslogingseksperimente het aan die lig gebring dat stof wat in hierdie dorp versamel word hoogs oplosbaar (biotoeganklik) is vir spoormetale soos Fe (tot 28%), Cu (tot 33%), Pb (tot 45%) en Zn (tot 38%) %). Fitoplankton gemeenskappe in oop oseane is soms uitgeput in - bane aan die lig gebring dat hierdie geredelik beskikbare stof heel waarskynlik die suidoos-Atlanties hierdie spoormetale, en so 'n hoë oplosbaarheid van stof van Saldanhabaai kan dus 'n belangrike voedingstofverskaffer aan omliggende oseane blyk te wees. Daarbenewens het lugmassa e en Indiese Oseaan affekteer. Die belangrikste implikasie was dat hawedorpe noodsaaklike bronne van spoormetale tot proksimale oseane kan wees.

Tweedens bied ek resultate van die grootste nie playa-omgewing in die Namibwoestyn aan. Sommige van die prominente stofuitstralers wat in die Namib-woestyn geleë is, verskaf, voed en bron van honderde tonne minerale stof na die proksimale oppervlak-oseane water. Die oplosbaarheid van die mineraalstof, in teenstelling met die gemengde (antropogenese en natuurlike afkomstig) stof hierbo genoem, is baie laer (bv. tot 2 % vir Fe, tot 7.8 % vir Cu, tot 16 % vir Zn, tot en met 9% vir Mn, 8% vir Pb). Hierdie oplosbaarheid is in soortgelyke omvang as ander semi-droë tot dorre groot globale stofbronne soos die Sahara-woestyn in die Noordelike Halfrond. Verskille in mineralogie en deeltjiegrootteverspreiding by die monsternemingstasies is die hoofdrywers van die oplosbaarheid.

Byvoorbeeld, die oplosbaarheid van spoormetale soos Fe, Zn en Pb is hoër by die binnelandse stasie as by die kusstasie. Die saamgevoegde deeltjies langs die kusstasies is minder oplosbaar, waarskynlik as gevolg van aanhoudende mistige toestande en minder sonlig. Die binnelandse stasies het minder mistige toestande gehad en meer fynkorrelige deeltjies wat ryk is aan FeO oksiede. Lugmassa-trajekmodellering het aangedui dat hierdie mineraalstof, met sy lae oplosbaarheid, tipies na die suidoostelike Atlantiese Oseaan beweeg, maar in sommige gevalle ook die voedingsarm gebiede in die Suidelike Oseaan kan bereik. Hierdie studie het die rol van nie-playa omgewings as belangrike stofbronne uitgelig en dat mineralogie tesame met deeltjiegrootte nou verwant is aan spoormetaaloplosbaarheid.

Daarbenewens, om die oplosbaarheid en potensiële impak van stof met natuurlike en antropogenese afdruk te bepaal, het ons die oplosbaarheid van aërosols wat oor die Suidelike Oseaan suid van Suid-Afrika aan boord op die navorsings vaartuig SA Agulhas II versamel is, ondersoek. Die oplosbaarheid van die spoormetale oor die Suidelike Oseaan wissel van 0,5 tot 41 % Fe, 9 tot 48 % Al, 0,1 tot 88 % Mn, 25 tot 72 % Zn en 3,3 tot 39 % Co.

Hierdie studie het groot variasie in spoormetaalsamestelling en fraksionele oplosbaarheid in stof aërosols gevind wat van drie verskillende omgewings in Suider-Afrika en suid van Suider-Afrika versamel is. Ons studie het die belangrikheid van Suider-Afrikaanse stof van beide antropogenese en natuurlike bronne uitgelig as 'n voedingstofverskaffer aan omliggende kus- en oop oseane.

This page is intentionally left blank

TABLE OF CONTENTS

Declaration i

Acknowledgements iii

Abstract……..……iii

Opsomming…….iiix

Table of Contents xi

List of Figures xviii

List of Tables xxvi

CHAPTER 1: Overview 31

1.1. Introduction 31

1.1.1. The importance of dust in biogeochemical systems 31

1.1.2. Global dust sources and atmospheric dust transport 33

1.1.3. Major advances on dust research and its significance to understanding biogeochemical cycles 36

1.1.4. Recent advances recognizing the importance of solubility 37

1.1.5. Southern African dust sources and their relevance to surrounding open ocean regions.. 38

1.1.6. Knowledge Gap 41

1.2. Aim and objectives 41

1.2.1. Objective 1: Fertilizing potential and characteristics of dust that presumably has a strong anthropogenic imprint 42

1.2.2. Objective 2: Fertilizing potential and dust characteristics from predominantly natural source 42

1.2.3. Objective 3: Fertilizing potential and dust characteristics of aerosols collected over the Southern Ocean 42

1.3. Regional Setting 43

1.3.1. Saldanha Bay 43

1.3.2. Namib Desert 44
1.3.3. Proximal oceans 45
1.4. Thesis outline 47
1.5. Methods 49
1.5.1. Sample collection 49
1.6. Analysis 51
1.6.1. Trace elemental concentrations 51
1.6.2. Mineralogical characteristics 52
1.6.3. Leaching experiments 52
1.7. Hysplit Backward and Forward Trajectories 53
1.8. Chapter 1 References 54

CHAPTER 2: : Origin, solubility, and ocean impact of trace metal aerosols collected over a major iron port 70
2.1. Abstract 72
2.2. Introduction 73
2.2.1. Study Area 75
2.3. Methods 77
2.3.1. Five-year long record of bulk dust metal load 77
2.3.2. Target BSNEs sampling and bulk trace metal analysis 78
2.3.3. Aerosol trace metal leaching experiments 78
2.3.4. Milli-Q water leachate to determine the instantaneous water dissolvable fraction 79
2.3.5. Weak acid leachate to determine the labile trace metal fraction 79
2.3.6. Statistical analysis 80
2.3.7. Enrichment factor 80
2.3.8. Scanning Electron Microscope (SEM) analysis 80
2.3.9. Air Mass Pathways 81
2.3.10. Polar Plots 81

2.3.11. Data availability 82

2.4. Results 82
2.4.1. Synthesis of the five-year long dust monitoring 82
2.4.2. Total weight and total trace metal concentrations in the 2019 BSNE samples 83
2.4.3. Mineralogical characteristics 84
2.4.4. Trace metal solubility in the BSNE samples 88
2.4.5. Milli-Q leach 88
2.4.6. Hydroxylamine hydrochloride leach 90
2.4.7. Local and long-range dust transport 92
2.5. Discussion 95
2.5.1. Source attribution of dust in the Saldanha Bay area 95
2.5.2. Assessing the potential impact of the dust collected over Saldanha Bay 99
2.6. Conclusion 103
2.7. Author contributions 103
2.8. Funding 103
2.9. Acknowledgements 104
2.10. Conflict of Interest Statement 104
2.11. Chapter 2 References 104
2.12. S.1. Supplementary Material 116
S.1.1. Five year long monitoring of monthly metal load 117
S.1.1.1. Monitoring methods 117
S.1.1.2. Dust fall-out rates and trace metal composition, 2015-2019 118
S.1.1.2.1. Dust fall-out rates 118
S.1.1.2.2. Bulk trace metal concentrations, 2015-2019 119
S.2. Volumetric Flow Controlled (VFC) sample supporting bulk metal composition and mineralogical characteristics 126
S.2.1. VFC Methods 126
S.2.2. VFC mineralogical characteristics and bulk metal load 126
S.3. Supplementary References 130

CHAPTER 3: Solubility of trace metals in dust from one of the dustiest non-playa environments in the Namib Desert 131

3.1. Abstract 133

3.2. Introduction 134

3.3. Methods 135

3.3.1. Study Site 135

3.3.2. Sampling sites 139

3.3.3. Sample collection 139

3.3.4. Analytical techniques used for determination of dust load, mineralogical characteristics, bulk metal composition, and leaching experiments 140

3.4. Results 143

3.4.1. Dust loads 143

3.4.2. Dust particle characteristics (MWAC samples) 143

3.4.3. Total trace metal and leached concentrations (BSNE samples) 147

3.4.4. Air mass trajectories and wind directions 150

3.5. Discussion 152

3.5.1. Dust loads and potential contributions to open oceans 152

3.5.2. Particles shape and their role in transport 153

3.5.3. Particle sizes and their role in transport and potential impact on oceans 153

3.5.4. Mineralogical composition as an indicator of the dust sources and trace element content and solubility 154

3.5.4.1. Influence of meteorological conditions and anthropogenic impact on the trace metal solubility 155

3.6. Total and bioaccessible trace metals 155

3.6.1. Air mass pathways, directions and potential impact on the ocean 156

3.7. Conclusion 157

3.8. Author contributions 157

3.9. Funding 157

3.10. Acknowledgements 157

3.11. Conflict of Interest Statement 157
3.12. References 158
3.13. Supplementary Table 168
3.14. Supplementary Figures 169

CHAPTER 4: Atmospheric trace metal deposition in the oceans south of southern Africa 173
4.1. Abstract 175
4.2. Introduction 176
4.3. Methods 178
4.3.1. Cruise track and aerosol sampling 178
4.3.2. Bulk trace metal analysis 181
4.3.3. Leaching experiments 182
4.3.4. Milli-Q leachate to determine the instantaneous water dissolvable (soluble) fraction 182
4.3.5. Weak acid leachate to determine the labile trace metal fraction: “berger leach” 183
4.3.6. Air Mass Pathways 184
4.4. Results 184
4.4.1. Bulk aerosol trace metal concentration 184
4.4.2. Soluble and labile fraction 189
4.4.3. Enrichment factors 192
4.5. Backward trajectories and possible sources 193
4.6. Discussion 196
4.6.1. Bulk trace metals 196
4.6.2. Trace metal bioaccessibility 198
4.6.3. Potential Impact on Phytoplankton Communities 200
4.7. Conclusion 201
4.8. Author contributions 201
4.9. Funding 201

4.10. Acknowledgements 201

4.11. Conflict of Interest Statement 202

4.12. Chapter 4: References 203

4.13. Supplementary Figures 213

CHAPTER 5: Synopsis 218

5.1. Recommendations 221

5.2. Synopsis References 222

LIST OF FIGURES

CHAPTER 1: Overview

Figure 1.Earth as a complex system including the dust cycle (D-Cycle) and the Carbon cycle (C-cycle), along with their interactions with the Energy cycle (E-cycle (Shao et al., 2011). 32

Figure 2. Some of the major sources of micronutrients in the Southern Ocean, with prominent wind directions at the different regions. The proximal ocean regions around southern Africa are mainly supplied by dust, anthropogenic aerosols, wildfires, fluvial river inflows and upwelling as the main drivers of nutrient supply close to the continental masses. The supply from melting sea ice and biological internal cycling becomes an important source at the higher latitudes (Source: Henley et al., 2020) 34

Figure 3. Global distribution of major dust sources (based on initial work from Prospero et al., 2002). The shades of yellow represent the number of days when the aerosol index (AI) was high. The dominant seasonal wind directions are also highlighted for the major sources (Engelbrecht and Derbyshire, 2010)..... 35

Figure 4. The Southern African large scale atmospheric and ocean circulation patterns and features. Image from Hutchings et al., (2009). 39

Figure 5. The number of potential dust sources in (a) spring: September, October and November and (b) summer: December, January, and February, based on Moderate Resolution Imaging Spectroradiometer Deep Blue (MODIS DB) Level 2 aerosol products with dust optical depth (DOD)>2 over the continental southern African (Ginoux et al., 2012). The main focus of this study is on areas circled as 1, Namib Desert and 2, the west coast of South Africa. While the Namib is considered mainly as natural dust emitter, the west coast of South Africa is impacted by anthropogenic activity. 40

Figure 6. Saldanha Bay iron ore storage facilities showing the stockpiles of ore stored and handled prior to export (Source: Mr Van Rooyen). 44

Figure 7. The area close to the Namibian coastline showing dust emissions on the 9 June 2004, from the region transported and deposited on ocean surface (Source: NASA, 2008). 45

Figure 8 Schematic diagram showing all the research components conducted during this study. 48

Figure 9. An automated meteorological monitoring station and measuring types of equipment at Saldanha Bay.....49

Figure 10. BSNE sampling site in the Namib Desert. 50

Figure 11. The high volume dust sampler positioned on the monkey island on the SA Alguhas II during the winter cruise in 2019. 51

Figure 12. Schematic showing the different leaching stages (steps) to extract the soluble, labile and total trace metals. The leaching protocol begins with the dust loaded on the filter, then the dust loaded filters are leached with Milli-Q, followed by leaching with weak to determine the soluble and labile fractions in aerosols.....53

CHAPTER 2: Origin, solubility, and ocean impact of trace metal aerosols collected over a major iron port

Figure 1. (a, b, c). Red iron-ore rich stain that can often be observed around Saldanha Bay. (d) Open wagon trains that transport iron ore from the Northern Cape mines approximately 800 kilometres away from Saldanha Bay. 75

Figure 2. Sampling locations in Saldanha Bay and neighbouring Vredenburg. Vredenburg is in the northern part of the greater Saldanha Bay area (Stations NNA and NEA) and Saldanha Bay is located in the southern part (Stations SWA and CA), close to the harbour. Coordinates for all stations are given in Table 1. The railway line that services the Bay is located close to NEA. The insert shows the location of Saldanha Bay in a map of Southern Africa. 77

Figure 3. Particles, including iron microspherules also known as ferrospheres observed using SEM-EDS in a Saldanha Bay dust sample collected at Station NEA (close to the railway area; see Fig 2 for location). (a) agglomerates including spherular particles, (b) micrograph of a agllomerated particles spot indicated by the square box in panel (a), (c) micrograph of a spherule particle from an individual spherular particle showing high iron content, (d) magnified image of the spherular particles, showing much smaller particles within the larger agglomerate (e) micrographs that was obtained at position Spectrum 17 indicated in panel (a), (f) magnified image of the agglomerated particles, showing sub-angular particles. 85

Figure 4. SEM elemental maps showing the abundance of selected elements in particles collected at station NEA (see Figure 2 for location) using the BSNE sampler. Individual elemental maps for some of the trace metals of interest as well as Si and S which are abundant in the area. 87

Figure 5. Solubility as concentration in leachate per bulk concentration (%) of the different trace metals when leached with Milli-Q water and a weak acid. 89

Figure 6. Solubility (%) at the four sampling locations in the Milli-Q and the weak acid leachates combined. 91

Figure 7. Map of Saldanha Bay including polar plots showing the particle transport calculated for stations SWA and NNA. Both polar plots were calculated for the year 2019 (January to December) using wind speed and direction data along with the PM10 and PM2.5 concentrations. In addition, a wind rose shows the wind speed and direction at station SWA averaged for each month of the year from January 2015 to December 2019.Figure 7. Map of Saldanha Bay including polar plots

showing the particle transport calculated for stations SWA and NNA. Both polar plots were calculated for the year 2019 (January to December) using wind speed and direction data along with the PM_{10} and $PM_{2.5}$ concentrations. In addition, a wind rose shows the wind speed and direction at station SWA averaged for each month of the year from January 2015 to December 2019.....93

Figure 8. Hysplit 7-day forward dispersion models showing the possible monthly dust pathways from Saldanha Bay. The change in colour is an indication of change in time with distance. Brown and yellow indicate dispersion close to Saldanha Bay, and pink indicates the air masses furthest from Saldanha Bay. The dispersed particles are shown at different time intervals. 94

Figure S1. Annual mean net metal mass in ppm in bulk dust measured from 2015 to 2019, see Figure 1 and Table 1 for station locations. Mn was only analysed from 2016 to 2019. One Cu outlier value was removed for interpretation purposes. The error bars represent the standard deviation of the monthly data for each annual mean. 124

Figure S3. Dust fall-out rate vs concentration of trace metals Fe and Pb showing that stations that had high trace metal concentrations often had a low dust fall-out rate. The axes are plotted at log-scale to better visualise the relationship between the dust fall-out rate and trace metal concentration. 125

Figure S4. SEM images of from station SWA mineral dust particles collected on a Whatman 41 filter. Take note of the micrometer individual particles and agglomerated angular grains. There are also a few platey particles. The much finer particles will potentially be part of the filter matrix. ..128

Figure S5. SEM elemental mapping of a Saldanha Bay filter dust sample from station SWA, with micrographs showing individual dominant minerals in the area. 129

CHAPTER 3: Solubility of trace metals in dust from one of the dustiest non-playa environments in the Namib desert

Figure 1. Map of the sampling sites in the Namib Desert, Namibia. Station location coordinates are given in Table 2. Station names correspond to SASSCAL Monitoring Observation network (http://data.sasscal.org/metadata/view.php?view=station_meta&id=5699&ident=580240755916261319). 136

Figure 2. A monitoring station with various meteorological instruments including the (A) BSNE dust collector set at 2 m height from the central station shown for illustration of the BSNE sampling effort. (b) Persistent dust plumes being emitted from the Namib Desert towards the Atlantic Ocean (Credit: USGS/Landsat 8/OLI). 140

Figure 3. Size fractions of the dust particles collected from four sites in the Namib Desert. The x-axis represents the particle size classes. The y-axis represents the mass percentage of particles for the classified size as mass percentage of total sample. The black dots are the outliers. 144

Figure 4. Example of the roundness distribution of observed samples, at the Coastal station which was similar at the four stations. 145

Figure 5. Examples of mineral aggregates from the four stations in the Namib Desert, (a) Chlorite aggregated with aluminosilicates and Fe oxides at the Coastal station, (b) Iron-oxides intertwined with pyroxenes at Coastal station, (c) Chlorite intertwined with with micas and clays at inland station. The mineral particles shown in panels a, b, and c are not to scale. 146

Figure 6.The forward trajectories after 7 days from the Namib Desert at different seasons (a) Autumn, (b) Spring, (c) Summer and (d) Winter. Calculated and plotted using the R package: SplitR. 151

Figure S1. Map of the sampling sites in the Namib Desert, Namibia. Station location coordinates are given in Table 2. In addition, the ephemeral rivers and the Great Escarpment are also shown in this figure. 169

Figure S2. Wind roses for Garnet Koppie for data ranging from 2016 to 2017. 170

Figure S3. Wind roses for Aussinanis for data ranging from 2016 to 2017. 170

Figure S4. Monthly wind roses of Vogelfederberg for wind data from 2016 to 2017. 170

Figure S5. Wind roses for Coastal Met for data ranging from 2016 to 2017. 171

Figure S6. The grid displaying the roundness of particles from angular to round. Sample from Coastal station used as an example. 172

CHAPTER 4: Atmospheric trace metal deposition in the oceans south of southern Africa

Figure 1. Sample locations for the Southern oCean seAsonal Experiment 2019 (SCALE 2019) Winter Cruise (WAer) 2019 and Spring Cruise (SAer) 2019. In this study we use three operationally defined categories for the samples: samples collected in the coastal area, samples collected in the mid-ocean zone and samples collected furthest away from the continent. 179

Figure 2. The high-volume air sampler (Tisch Environmental) positioned on the monkey island on the SA Agulhas II during the winter cruise in 2019. In the background are pan cake ice sheets from approximately 58°S in the Atlantic sector of the Southern Ocean. 181

Figure 3. Bulk total trace metal concentration of the different zones combining data gathered from winter and spring cruises 2019..... 187

Figure 4. Soluble fraction in (%) using Milli-Q water as a leachate (Milli-Q (%)) in aerosols collected in winter and spring 2019 over the Southern Ocean. The black dots represent the outliers. The reader is referred to figure 1 and Table 1 for zonal grouping of the samples..... 190

Figure 5. Solubility (%) of labile fraction using a weak acid as a leachate in aerosols collected in winter and spring 2019 over the Southern Ocean. The black dots represent the outliers. The reader is referred to Figure 1 and Table 1 for zonal grouping of the samples..... 191

Figure 6. Representative backward trajectories for the coastal stations. 193

Figure 7. Representative backward trajectories for the 40s South station. 194

Figure 8. Representative backward trajectories for the 50s South stations 195

Figure S1. Box and whisker plots showing the percentage of labile fraction of trace metal collected in winter and spring 2019 over the Southern Ocean. The black dots represent the outliers. 213

Figure S2. Box and whisker plots showing the percentage of soluble fraction trace metal from spring 2019 collected over the Southern Ocean. The black dots represent the outliers. 214

Figure S3 Backward air masses trajectories showing the direction of air masses from two selected stations. 216

Figure S4. Some of the dust plumes from the agricultural fields in the Free State on the 23 September 2008 that can be seen exported through the Eastern Cape (EC) can be exported through this area. Image NASA MODIS satellite image. 217

LIST OF TABLES

CHAPTER 2: Origin, solubility, and ocean impact of trace metal aerosols collected over a major iron port

Table 1. Station coordinates for BSNE (2019) samplers. All locations are shown in Figure 2.....76

Table 2. Total trace metal concentrations of aerosols from Saldanha Bay collected using the BSNE traps from January 2019 to January 2020. All trace metal concentrations are reported in ppm.....83

Table 3. Enrichment factors in dust aerosols from Saldanha Bay collected using the BSNE samples from January 2019 to January 2020.....84

Table 4. Solubility of example trace metals expressed as concentration in leachate per bulk concentration (%) when leached with Milli-Q water and a weak acid. The sum of the two fractional solubilities (not shown) is considered the labile or bioaccessible fraction.....90

Table 5. Approximate contribution to dominant air mass pathways for the forward and backward trajectories averaged over the years 2015 to 2019. N – north, NW – northwest, NE – northeast, E – east, SE – southeast, W – west, SW – southwest, S – south, T – terrestrial origin, M- marine origin. 95

Table 6. Examples of locations reported with high trace metal concentrations in aerosols. The locations selected here either have steel factory, mining activities or a smelter to facilitate a comparison with the Saldanha Bay area. 97

Table 7. Classification of the different stations based on the observations from pollution roses, enrichment factors and mineralogical particles and background trace metal chemistry. The classification scheme includes three categories, (1) “oceanic”, which refers to likely sea spray origin, (2) “terrestrial”, which refers to sources from natural lithogenic inputs, and (3) “anthropogenic” which refers to influence by mineral ore. All seven stations were assessed based on the five year-long monitoring. In addition, stations CA, NEA, NNA and SWA were classified based on the BNSE bulk metal compositions and mineralogical characteristics.....99

Table 8. Examples of concentrations of soluble fractions (%) of iron in major iron ore emitting regions.....101

Table S1. Station coordinates for the dust buckets used for the five-year long (2015 to 2019) monitoring and VFC (two weeks in 2019) samplers. 118

Table S2. Summary of dust fall-out rates and annual trace metal concentrations from the seven municipal monitoring stations between 2015 to 2019. bdl refers to samples below detection limit. Dust fall-out rates were determined by dividing the weight of the insoluble material collected by the cross-sectional area of the funnel and the number of days over which the sample was taken. Net masses of metals obtained within the five year-year long monitoring are reffered here in ppm. 120

Table S3. Summary of all dust fall-out rates (mg/m2/day) at the seven municipal monitoring stations 2015 to 2019..... 122

Table S4. Summary of the trace metal concentrations in dust samples collected using buckets between 2015 and 2019. In addition, the table shows a summary of statistically significant differences in annual mean trace metal concentrations between years..... 123

Table S5. Trace metal concentrations of aerosols from Saldanha Bay collected using the VFC sampler collected from 03 May 2018 to 20 May 2018. All trace metal concentrations are reported in ppm. 127

Table S6. Enrichment factors in dust aerosols from Saldanha Bay collected using the VFC samples. 127

CHAPTER 3: Solubility of trace metals in dust from one of the dustiest non-playa environments in the Namib desert

Table 1. Coordinates and basic meteorological conditions defining the three main dust sampling sites. The sites are classified in three different locations based on the various climatic conditions. 138

Table 2. Sample weights (g) from the four collection sites. Values represent averages and standard deviations from duplicates samples except for station GK due to the low sample yield. Source areas are added based on the prevalent wind pattern at 2 and 3 m heights (Table 1) 143

Table 3. Minerals composition observed in the dust collected at the four stations in the Namib Desert. 147

Table 4. Total trace metal concentrations for the four stations in the Namib Desert. Concentrations are presented in ppm as average of two and standard deviation were duplicates could be analysed. 148

Table 5. Soluble trace metal concentrations for the four stations in the Namib Desert when leached with Milli-Q water. Concentrations are presented in ppm as average of duplicates and standard deviation. 149

Table 6. Labile trace metal concentrations for the four stations in the Namib Desert when leached with weak acid leach. Concentrations are presented in ppm as an average duplicates and standard deviation where available 149

Table 7. Range of trace metal concentrations and fractional solubilities of the Namib dust when leached with Milli-Q water and a weak acid solution (“Berger leach”). 150

Table S1. MWAC samples from the two year period. These samples were used for Qemscan analysis. 168

CHAPTER 4: Atmospheric trace metal deposition in the oceans south of southern Africa

Table 1. Aerosol sampling dates and number of samples collected during the South African led Southern oCean seAsonal Experiment 2019 (SCALE 2019) cruises into the Southern Ocean. Sampling duration was 48 hours for all samples. 180

Table 2. Mean and standard error (duplicates samples) of elemental composition (concentration in ppm) of Arizona Test Dust determined in this study and Baker et al. (2020). 181

Table 3. Bulk trace metal concentrations (ng m^{-3}) at the different dust sampling locations grouped according to the distance from the South African coast (cf. Figure 1). Bdl refers to below detection limit. 185

Table 4. Total and fractional aerosol trace metal concentrations range in the proximal and distant open ocean water regions around Southern Africa for the Winter Cruise 2019. See Figure 1, Table 1 for sample locations. Bdl refers to below detection limit 185

Table 5. Total and fractional aerosol trace metal concentrations ranges in the proximal and distant open ocean water regions around Southern Africa for the Spring Cruise 2019. See Figure 1, Table 1 for sample locations. Bdl refers to below detection limit. 186

Table 6. Enrichment factors at the different dust sampling locations grouped according to the distance from the South African coast. 192

CHAPTER 4: Synopsis

Table 1 Comparison of trace metal concentrations and solubility in aerosol particles from different dust sources that were investigated in this dissertation. The data shown here represent a synthesis from (i) Paper 1 (Chapter 2 of Section 2.4.4.) for the anthropogenic and mixed sources, (ii) Paper 2 (Chapter 3 of Section 3.3.3.) for the natural dust sources, and (iii) Paper 3 (Chapter 3 of Section 4.3.1.) for the samples collected over the ocean. 220

CHAPTER 1: OVERVIEW

1.1. INTRODUCTION

1.1.1. The importance of dust in biogeochemical systems

Dust events and plumes are regarded as a nuisances, disturbing everyday life, reducing visibility, and causing ear, eyes and nose irritations (Amato, 2000). However, the input of dust is also key to the functioning of the biogeochemical cycles in many open ocean systems (Baker et al., 2006; Martin et al., 1990; Perron et al., 2020), as dust is a major supplier of micronutrients. More than half of all primary productivity in the world occurs in oceans (Behrenfeld et al., 2001), and phytoplankton communities can absorb up to 25% of anthropogenically emitted CO_2 in oceans annually (Falkowski, 2012), hence acting as an important sink of CO_2 from the atmosphere. However, the phytoplankton as the primary producers rely on the trace metals for essential processes such as photosynthesis (Jickells and Moore, 2015; Moore et al., 2013). For example, trace metals are utilized in enzymes that are required for photosynthesis, or in the process of respiration or nitrogen fixation (Moore et al., 2013). Dust however might also have detrimental effects on living organisms if the dust contains trace metals in toxic concentrations (Paytan et al., 2009). Despite this biogeochemical importance (Figure 1), the long-term transport and deposition of dust on surface oceans in some regions are yet not well understood. Knowledge gaps remain between dusts geochemical composition and physical characteristics from emission sources to depositional sites in open oceans.

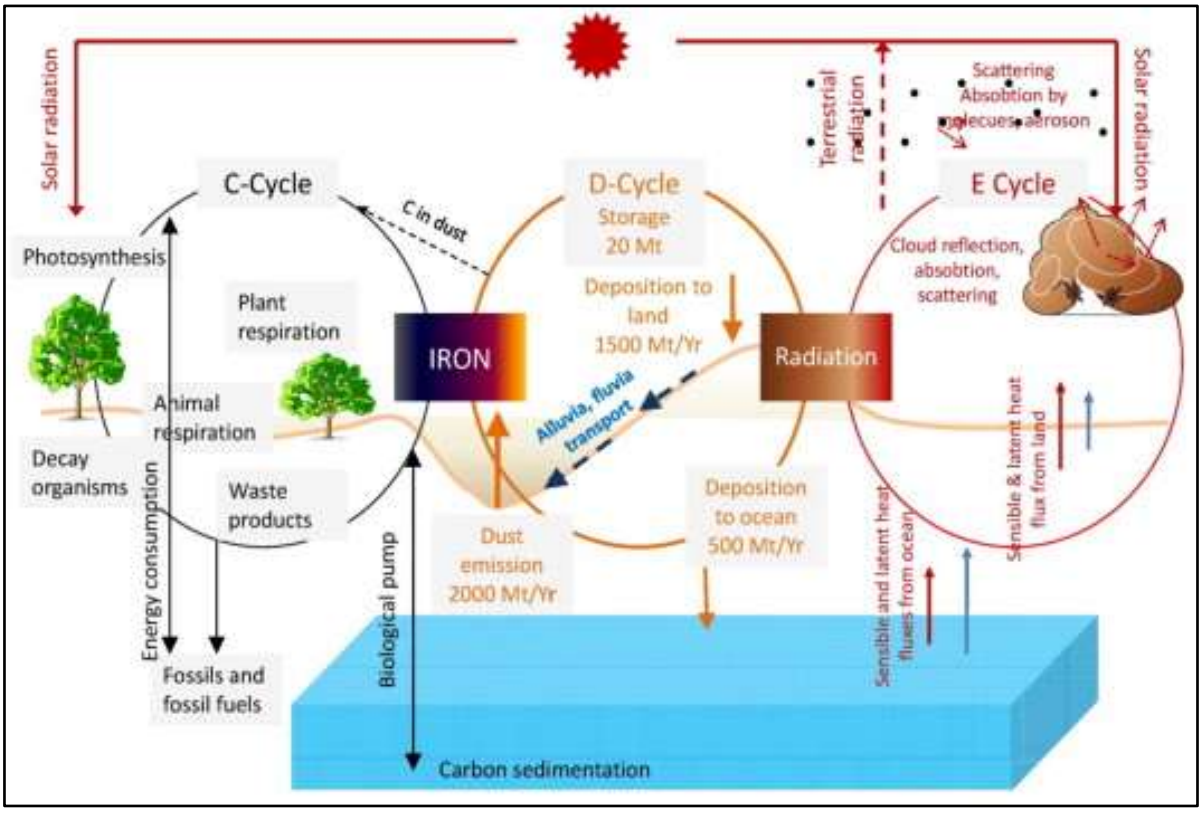

Figure 1*.Earth as a complex system including the dust cycle (D-Cycle) and the Carbon cycle (C-cycle), along with their interactions with the Energy cycle (E-cycle (Shao et al., 2011).*

The particle size distribution and mineralogical composition of the dust aerosols influence the fertilization potential of the aerosols to the open oceans (Jickells et al., 2005; Journet et al., 2008; Mahowald et al., 2008). For example, clay minerals have a higher solubility than iron hydroxides (Journet et al., 2008) and smaller grained particles also usually have a higher solubility (Buck et al., 2010). In addition, various atmospheric processes also tend to influence the fertilization potential of aerosols from sources to deposition and most studies hypothesized that the potential fertilization increases during atmospheric transport to depositional sites (Mahowald et al., 2005; Rodríguez et al., 2021). This means that trace metals solubility at depositional sites should be higher compared to sources because of atmospheric processing (e.g. photochemical reduction) which can increase the bioavailability of dust (Scanza et al., 2018). Studies investigating solubility at sources and depositional sites are limited in southern Africa and our study aims to contribute to these questions.

Phytoplankton communities are responsible for approximately half of net global primary productivity (Field et al., 1998). The phytoplankton communities at the deposition sites and their nutrient requirements also influence whether fertilization occurs (Moore et al. 2013). If phytoplankton is not limited spatially, fertilization potential from dust addition might be lower than in areas depleted in

essential nutrients. Different trace metals such as Zn, Cu, Ni and Mn might be required at different doses by the phytoplankton communities. For example, iron is required in enzymes to catalyze carbon and nitrogen fixation processes, while Mn plays an important role as an enzyme in photosynthesis in oxidation of water; but the cellular requirements are typically species-specific (Twining and Baines, 2013). In addition, environmental conditions at deposition site such as light availability, also change the trace metal requirements in the surface oceans (Viljoen et al., 2018). This illustrates that the dust fertilization potential depends on the initial composition, and processes during transport, as well as on the community and conditions in seawater upon deposition. For example, dust emissions correlate with phytoplankton growth in High Nutrient Low Chlorophyll (HNLC) regions (Moore et al., 2013) and were also predicted to play a role in open oceans around southern Africa (Dansie et al., 2018).

1.1.2. Global dust sources and atmospheric dust transport

The major sources of nutrients to open oceans range from mineral dust (Jickells, 2005), via hydrothermal vents (Ardyna et al., 2019; Tagliabue et al., 2010), rivers (Poulton and Raiswell, 2002), volcanoes (Duggen et al., 2007) and melting of sea ice in the Polar regions (Pereira et al., 2018) (Figure 2). Fluvial deposits are the largest suppliers of sediments and nutrient-rich trace metals, especially to marginal oceans (Syvitski, 2003), while aerosol deposits are the second largest suppliers, especially to open oceans (Mahowald et al., 2005). Some of these sources tend to be either of short temporal duration or provide a supply to small areas, whereas dust is more frequent and can travel long distances.

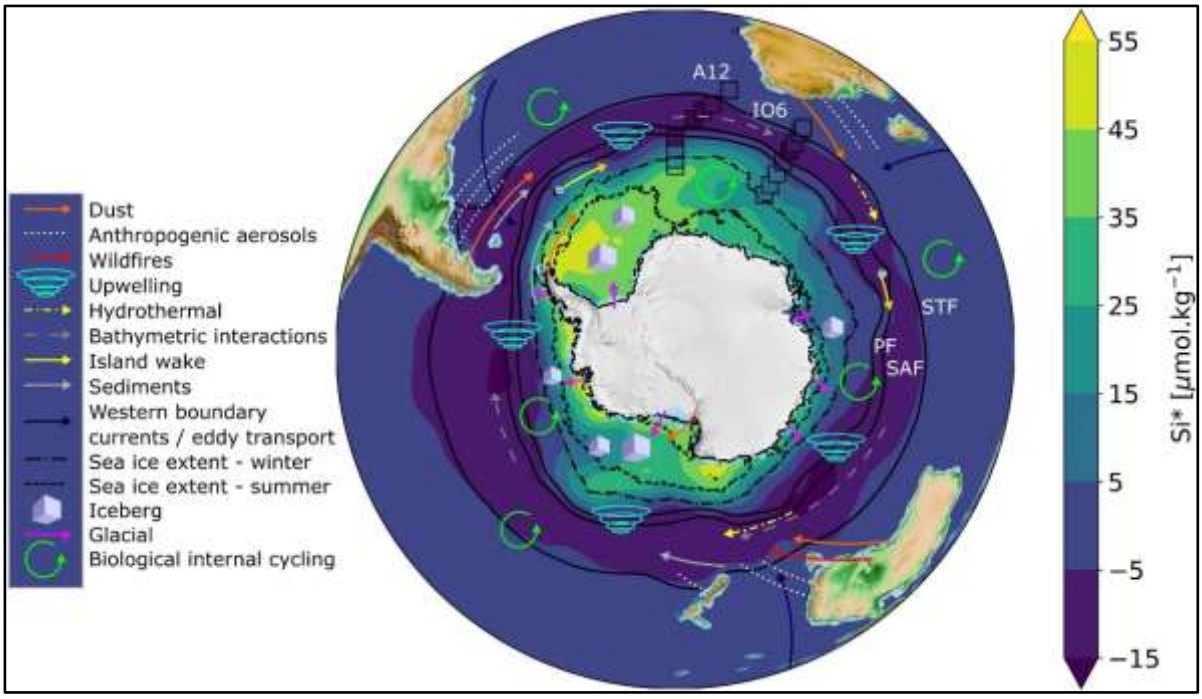

Figure 2. *Some of the major sources of micronutrients in the Southern Ocean, with prominent wind directions at the different regions. The proximal ocean regions around southern Africa are mainly supplied by dust, anthropogenic aerosols, wildfires, fluvial river inflows and upwelling as the main drivers of nutrient supply close to the continental masses. The supply from melting sea ice and biological internal cycling becomes an important source at the higher latitudes* (Source: Henley et al., 2020)

Major sources of mineral dust are mostly semi-arid to arid dryland environments such as deserts, ephemeral lakes and rivers (Mahowald et al., 2005; Prospero et al., 2002a), but a considerable portion of dust is also derived from combustion, biomass burning and other anthropogenic sources (Guieu et al., 2005; Jickells, 2005). Globally, 1536 $Tg.yr^{-1}$ is the estimated emission of dust annually (Ginoux et al., 2012). Majority of tons of sediments are eroded from Saharan Desert soils (51-69% of the global dust emissions), transported across the Atlantic Ocean westward, and deposited as far as the Amazon Basin and the Barbados and Caribbean Islands (Goudie and Middleton, 2001; Prospero, 1996; Prospero et al., 2020; Swap et al., 2002; Yu et al., 2015). In the Southern Hemisphere, southern Africa (i.e. Etosha and Makgadikgadi Pans and the ephemeral rivers along the Namibian coastline), Australia (i.e. Lake Eyre), and South America (i.e. Patagonian Desert) are the three dominant dust sources (Piketh et al., 1999). These Southern Hemisphere sources are much smaller compared in size (contribute ~10% (1.8-3.2 Tg)), and emit less dust than the Northern Hemisphere counterparts (Gao et al., 2001; Prospero et al., 2002) (Figure 3).

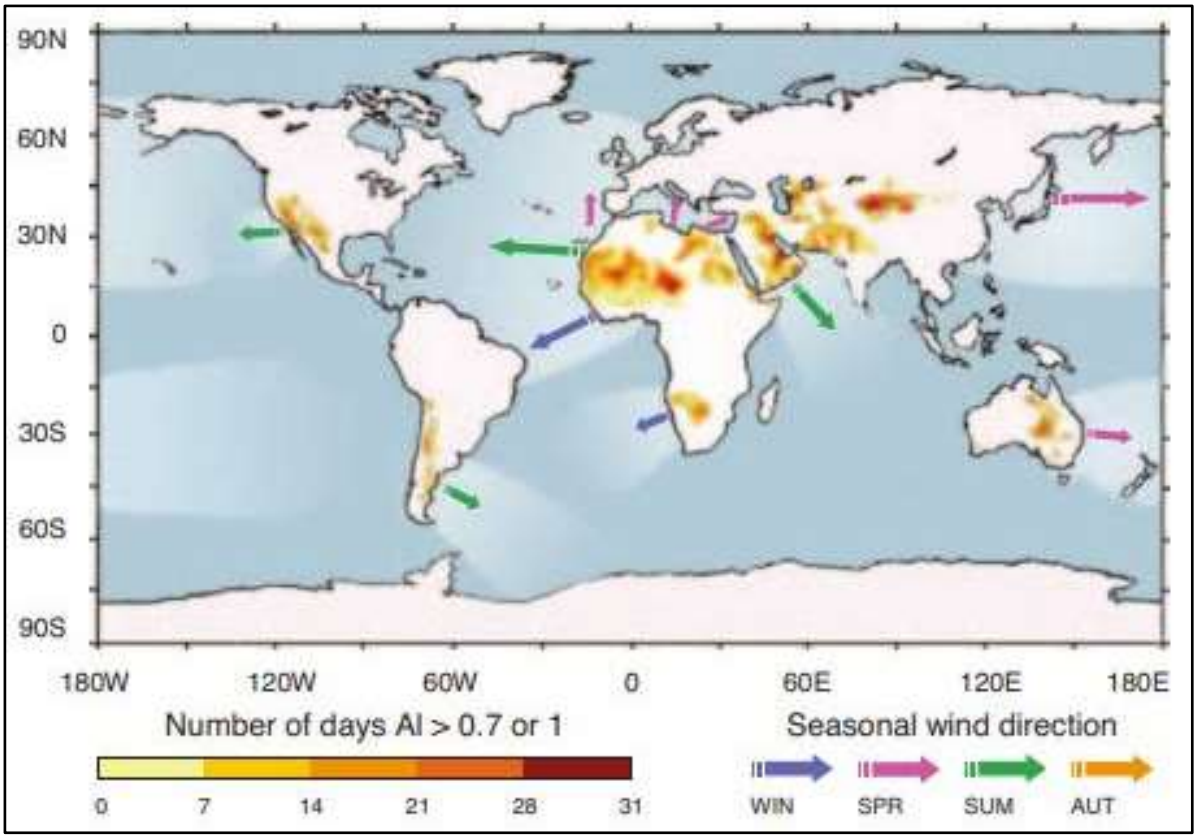

Figure 3*. Global distribution of major dust sources (based on initial work from Prospero et al., 2002). The shades of yellow represent the number of days when the aerosol index (AI) was high. The dominant seasonal wind directions are also highlighted for the major sources* (Engelbrecht and Derbyshire, 2010).

Dust can travel long distances and affect local areas as particles drop out during transport (Uno et al., 2009). Dust plumes are especially capable of carrying large quantities of soil material hundreds of kilometers from sources (Neff and Bertler, 2015). For example, Saharan dust can be transported for about 4 to 11 days over a distance of over 5000 km to the Amazon in South America (Prospero and Carlson, 1972; Swap et al., 2003). Dust fluxes from southern Africa average 30 million tons annually moving towards the western Atlantic Ocean, while almost 50 million tons is blown towards the Indian Ocean in an easterly direction (Tyson et al., 1996). Southern African dust can travel for over 4000 km to the tropical Atlantic Ocean (Swap et al., 1996). In the process, a substantial amount of dust is deposited in the ocean, providing vital nutrients for phytoplankton communities. Most of the dust emissions in southern Africa, occur during winter, peaking around late winter (August and September) (Vickery et al., 2013). Southern African dust sources have so far been proposed as having a localized rather than global impact due to smaller sources and weaker wind systems, compared to Patagonia and Australia, for example (Li et al., 2008). As such the impact to high latitudes may be

limited, while more localized, mid-latitude impact prevails because of the location of these sources and the long distance towards the high latitudes and the Polar regions.

1.1.3. Major advances on dust research and its significance to understanding biogeochemical cycles

Recent advancements in modern technology has made it easier to identify dust sources (Bryant, 2003; Eckardt and Kuring, 2005; Ginoux et al., 2001; Vickery et al., 2013; von Holdt et al., 2019; Washington et al., 2003). Remote sensing techniques such as Landsat, MODIS and Google Earth can help identify dust hotspots and classify them based on their frequency, time periods and magnitude (Vickery, 2010; Vickery et al., 2013; von Holdt et al., 2019; Washington et al., 1995; Wiggs et al., 2018). Similarly, there have been advances on modelling techniques to simulate and better predict the long-distance transport pathway directions towards the depositional sites (Bhattachan et al., 2015; Mcgowan and Clark, 2008; Prospero, 1999; Rodríguez et al., 2021; Tatlhego et al., 2020). Other satellite imagery techniques such as the Total Ozone Mapping Spectrometer (TOMS) Aerosol Index was also used extensively to identify ancient low-lying ephemeral pans such as the Etosha and Makgadikgadi pans in southern Africa as the most prominent dust sources (Prospero et al., 2002; Washington et al., 2003). These advances have provided important platforms to better study the processes that are involved in the transport from the source areas to the depositional regions. Field based passive sampling methods such as meteorological stations, Big Spring Number Eight sampler (BSNE) and the modified Wilson and Cooke sampler (MWAC), or collection of surface samples have been set-up based on information from these remote sensing techniques (e.g. Bhattachan et al., 2015; Dansie et al., 2017a; Goossens and Offer, 2000; Jeanneau et al., 2019).

Currently, most studies in this region focused on the mineral dust properties at southern African sources (Dansie et al., 2018, 2017b, 2017a; Eltayeb et al., 1993, 1992; Formenti et al., 2011; Klopper et al., 2020). However, dust composition at source can differ from dust composition at depositional site, for example dust being transported and collected across the Northeast Atlantic Ocean has a different composition compared to their initial sources (Perrone et al., 2021). The properties of dust particles change with transport, and dependent on dry and windy weather conditions. In addition, dust particles sources are usually rich in trace metals such as Al, Fe, Mn, Zn, Cu, Cd and Mo (Moore et al., 2013), but trace metal contents tend to diminish with traveling distance due to gravitational settling (Wagener et al., 2008). This could be explained, for example, by gravitational settling (Friese et al., 2016; Schepanski, 2018; Shi et al., 2012), with some of the coarser particles being dropped from suspension faster compared to the fine particles (van der Does et al., 2018; Van Der Does et al.,

2016). On-board, sampling allows for a better understanding of the aerosol content that is eventually deposited on surface oceans, but aerosols in the open oceans are challenging to measure and predict (Remenyi, 2013). Sampling in remote open oceans is expensive and cruises occur over limited time periods, which might be different to when emissions occur (Anderson et al., 2016). Sampling dust at depositional sites over the ocean proximal to the southern African continent is rare with few exceptions (Baker et al., 2006; Chance et al., 2015; Witt et al., 2006, 2010). These studies observed that not all trace metals behave similarly, and the solubility increased with distance from sources, especially for Fe and Mn. There were large ranges in fractional solubility with median range from below 20% to 70% (Chance et al., 2015).

1.1.4. Recent advances recognizing the importance of solubility

The total trace metal concentration in the dust in the source region or at the depositional site is not necessarily the most important factor that determines the fertilization of dust. Most research focus on the bioaccessible fraction (Barbeau, 2006; Shi et al., 2009), which is the phase in which trace metals can be taken up and utilized by phytoplankton (Boyd et al., 2010; Guieu and Thomas, 1996). Often, solubility is used as measurable proxy for bioaccessibility and as such the bioaccessible fraction is calculated by determining the soluble fraction of the total concentration (Duce and Tindale, 1991; Fung et al., 2000). A common way of determining the solubility of dust is through leaching experiments (Mahowald et al., 2018). Two common leaching methods are the batch and a continuous flow through method (Aguilar-Islas et al., 2010; Simonella et al., 2014; Wu et al., 2007). Batch method involves calculating the soluble fraction from the total composition when the dust is left in a specific reagent (Wu et al., 2007). However, with this method, Fe tends to precipitate on the bottle walls (Aguilar-Islas et al., 2010). Continuous flow through involves the instantaneous leaching of trace metals, were the aerosol samples have very short leaching time to prevent trace metals from precipitating. One of the recent most widely used approach is the so-called “Berger leach” consisting of 25% acetic acid and 0.02 M hydroxylamine hydrochloride (Na_2OH HCl) (Berger et al., 2008; Perron et al., 2019; Shelley et al., 2018; Winton et al., 2015). There are many other methods of determining the bioavailability, but there is no universal standard method (Perron et al., 2020). The use of different leaching methods has made it challenging to compare results from different studies. For example, as a result of using different approaches, solubility estimates range from 0.01 to 90% for iron due to difference in experimental methods and compositional variation at source areas (Mahowald et al., 2009). Further studies using dust from different sources and testing different leaching approaches are still required.

1.1.5. Southern African dust sources and their relevance to surrounding open ocean regions

1.1.5.1. Natural sources

The southern African continent along the Namibian coastline and the Namib Desert has numerous dust sources emitting thousands of tonnes of sediments to surface oceans (Vickery et al., 2013). This dust can be transported towards southwest Africa (e.g., Western Cape) (Molepo et al., 2019), as well as towards the Southern Ocean (Li et al., 2008). Recent isotopes work has revealed that dust from southern Africa was even a significant contributor to remote areas, such as the eastern Antarctica continent (Gili et al., 2021) and the Amazon basin (Nogueira et al., 2021). This further highlights the importance of understanding the fertilizing capacity of dust from southern Africa. One of the important regions receiving natural dust from southern Africa is the Southern Ocean (including several HNLC regions), that is located in close proximity. The HNLC open water areas are often depleted in trace metals such as Fe, which results in low primary productivity (Martin and Fitzwater, 1988), and an addition of Fe on these surface oceans may result into phytoplankton growth (Aumont and Bopp, 2006; Boyd et al., 2000; Cassar et al., 2007; Quéguiner, 2013).

Another important oceanic region likely to be impacted by natural southern African dust is the Benguela Upwelling System (BUS) (Figure 4). The BUS forms part of the highly productive Eastern Boundary Upwelling Systems (EBUS), located along the western coastal waters of northern and southern Africa. Although, EBUS may only account for 1% of all oceanic surface regions, it accounts for the highest of global productivity rates (up to 20% of the global fish catch) (Lachkar and Gruber, 2012). During upwelling, nutrient-rich waters at the surface can be Fe-limited (Capone and Hutchins, 2013; Messié and Chavez, 2015). Dansie et al. (2017, 2018) highlighted the impact of natural aerosols phytoplankton communities in the region, while most studies focus on the impact from upwelling. In this study, we aim to emphasize the importance of dust to surface ocean waters in this region. There is still a lack of studies in Southern Africa that has used dust to understand its potential impact of local ocean regions.

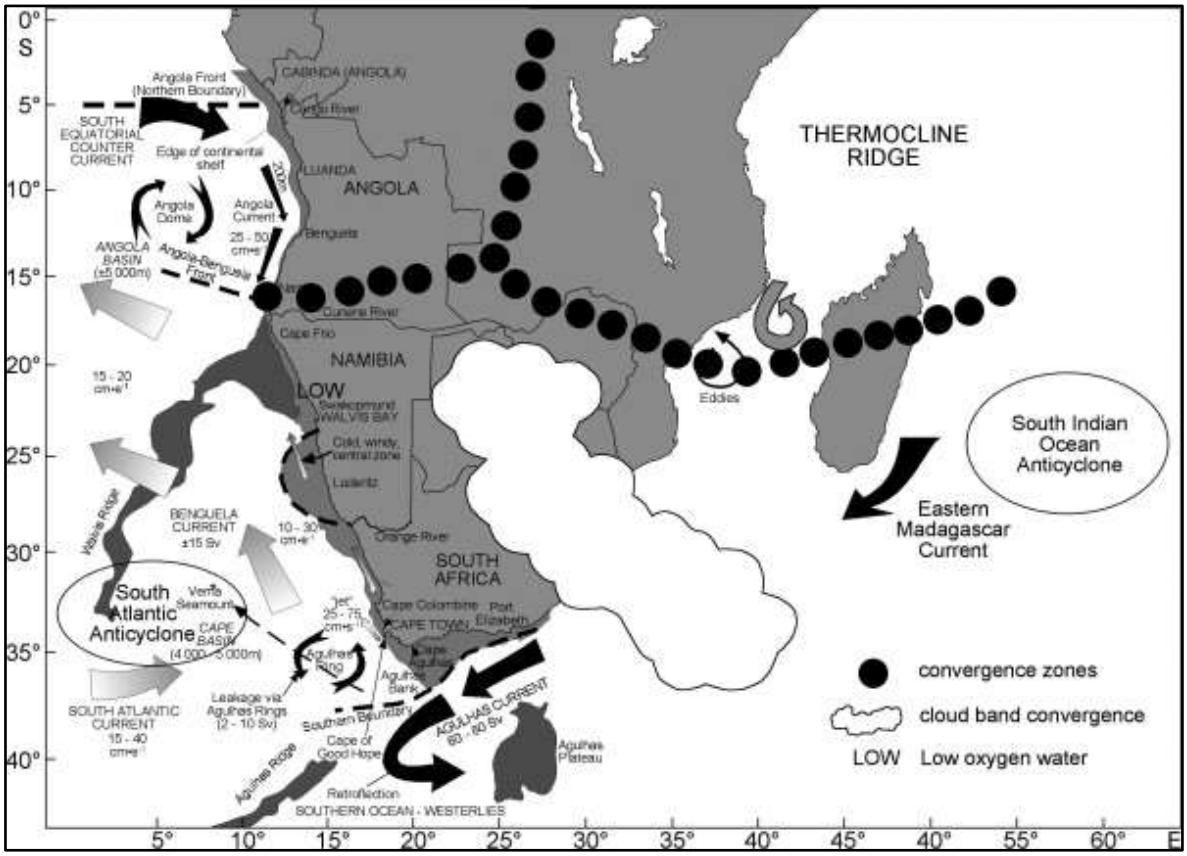

Figure 4. *The Southern African large scale atmospheric and ocean circulation patterns and features. Image from Hutchings et al., (2009).*

1.1.5.2. Anthropogenic sources

At global level, industrial activities have increased emissions from combustions, biomass burning, fossil fuels and agricultural land use (Engelbrecht and Derbyshire, 2010; Mahowald et al., 2010; Prospero et al., 2002). Nowadays, anthropogenic dust can contribute up to 25% of all global dust emissions (Ginoux et al., 2012). For example,in the East China Sea,, anthropogenic dust is already considered the primary source of trace metals to open oceans rather than mineral dust (Ho et al., 2010). The worldwide stronger industrial dust emissions, releasing nutrients into the ocean, leads to large-scale fertilization (Chen et al., 2012; Sedwick et al., 2007; Sholkovitz et al., 2012, 2009), and as a result, it is estimated that industrialization has contributed up to 6% of primary productivity in open oceans (Mahowald et al., 2010).

As an example, the Fe deposit flux in the Southern Ocean has increased by up to 73% in the current industrial era compared to pre-industrial conditions (Matsui et al., 2018), hence possibly providing more Fe that can be used by phytoplankton (Ito and Shi, 2016). The solubility of the anthropogenic dust also differs from natural dust, because anthropogenic dust is a major source of acidic and organic

compounds in the atmosphere that can increase the solubility of trace metals (Ito and Shi, 2016; Meskhidze et al., 2017). Anthropogenic dust from oil combustion products for instance has up to 80% soluble Fe compared to approximately 1% soluble Fe in dry soil environments (Schroth et al., 2009). Studies investigating the impact of anthropogenic dust to oceans in southern Africa are still missing. Anthropogenic dust from coal emissions, the smelting operations in some of southern Africa industrial towns, combustions from burning of fossil fuels and the burning biomass could all contribute to the anthropogenic dust from the region that can impact oceans.

1.1.5.3. Mixed Sources

Mineral and anthropogenic dust are not fully decoupled in the atmosphere. Typically, anthropogenic emissions occur in the pathway of natural dust transport and vice versa. The mixing of mineral dust with anthropogenic dust can increase the solubility of dust during long distance transport (Fan et al., 2006). Southern Africa has experienced an increase in industrial activities over the Anthropocene (Bauer et al., 2019) and hence Southern African dust will increasingly be expected to be of mixed origin in future (Figure 5). Biomass burning and wildfires have become more frequent in southern Africa, and these emissions will be an essential contributor to soluble Fe fluxes between the atmosphere and open oceans (Barkley et al., 2019; Hamilton et al., 2020b, 2020a).

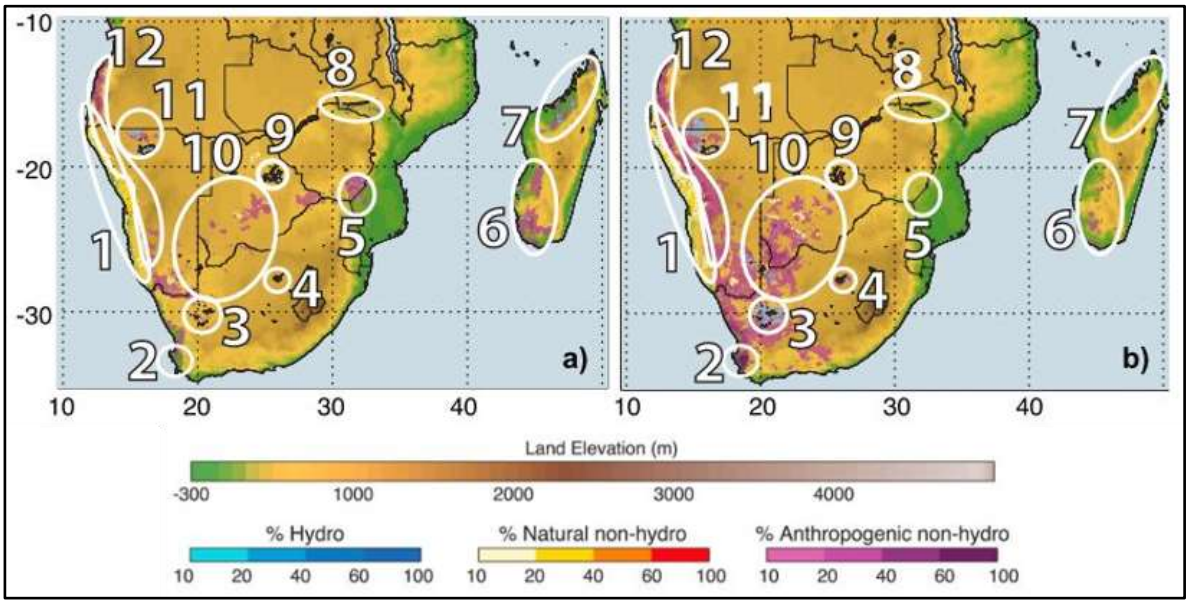

Figure 5*. The number of potential dust sources in (a) spring: September, October and November and (b) summer: December, January, and February, based on Moderate Resolution Imaging Spectroradiometer Deep Blue (MODIS DB) Level 2 aerosol products with dust optical depth (DOD)>2 over the continental southern African (Ginoux et al., 2012). The main focus of this study is on areas circled as 1, Namib Desert and 2, the west coast of South Africa. While the Namib is*

considered mainly as natural dust emitter, the west coast of South Africa is impacted by anthropogenic activity.

1.1.6. Knowledge Gap

To date, in southern Africa, most studies have focused on the major known dryland dust sources and playa environments, such as ephemeral rivers and pans (Annegarn et al., 1983; Dansie et al., 2017b, 2017a, 2018; Eckardt and Kuring, 2005; Eltayeb et al., 1992, 1993; Klopper et al., 2020; Vickery et al., 2013a). Non-playa environments have so far been overlooked despite remote sensing techniques showing that they can be essential sources of dust (Vickery et al., 2013a; von Holdt et al., 2019). This study aims to close this gap by investigating the geochemical composition and bioaccessibility of dust from these non-playa natural dust sources. Secondly, anthropogenic dust has been shown to be one of the major sources of soluble iron to open oceans (Ito et al., 2019; Jenner and Abiodun, 2013; Li et al., 2017; Perron et al., 2019; Strzelec et al., 2020). To the best knowledge of this study, no studies have investigated the solubility of dust from Southern African anthropogenic sources as potential supplier of micronutrients to open oceans. The proximity of anthropogenic dust sources to essential coastal regions prompted this study to improve the understanding of the potential impact of aerosols on surface oceans.

In addition, most studies have investigated the dust at or close to the sources on land, while studies over the ocean are limited. Most of the on shipboard sampling for aerosols in the Southern Ocean is conducted during summer (Chance et al., 2015; Witt et al., 2006, 2010), despite the fact that most of emissions in southern Africa occur during the winter and spring (Vickery et al., 2013). Hence, our understanding of the dust composition and trace metal solubility over the coastal and remote oceans in summer and winter is limited. This study aims to cover these knowledge gaps.

1.2. AIM AND OBJECTIVES

Considering these knowledge gaps, this thesis will provide insights into dust composition and solubility at sources and depositional sites, to conclude on the potential impact on the ocean ecosystem. The major research question driving this work is how important southern African dust is for the global atmospheric and ocean biogeochemistry. The thesis focusses on southern Africa and the Southern Hemisphere, as both are still under-represented in the global aeolian trace metal research.

The main tasks included to determine the mineralogical characteristics, trace metal composition, fractional solubility (bioaccessibility) and air masses pathways of dust from prominent sources in southern Africa. In addition, aerosols were collected on ship-based sampling in order to estimate fractional solubility at the depositional sites. To achieve this, several objectives were established:

1.2.1. Objective 1: Fertilizing potential and characteristics of dust that presumably has a strong anthropogenic imprint

Dust was sampled from Saldanha Bay, a port town where more than 60 million tons of ore annually are processed. Dust aerosols were used to understand if and how dust that includes an anthropogenic source, can impact proximal oceans. This was achieved by (i) determining the bulk trace metal composition, (ii) characterizing the mineralogical composition (iii) attempting a source assessment (iv) determining the trace metal fractional solubility and (v) project how the dust may impact proximal oceans.

1.2.2. Objective 2: Fertilizing potential and dust characteristics from predominantly natural source

Dust samples were collected from four different stations to provide information on the importance of non-playa environments as potential fertilisers to proximal open oceans. In addition, this study linked fractional solubility of dust from these four investigated sites with the mineralogical characteristics. This was achieved by (i) determining the bulk trace metal composition (ii) characterizing the mineralogical composition (iii) attempting a source assessment (iv) determining the trace metal fractional solubility and (v) predict the air masses pathways and how they may impact the ocean.

1.2.3. Objective 3: Fertilizing potential and dust characteristics of aerosols collected over the Southern Ocean

Ship-based aerosols sampling was conducted in winter and spring 2019 over the Southern Ocean. The trace composition and fractional solubility in the dust aerosols collected from coastal to open ocean areas was determined. In addition, this study provides an understanding of prevalent air mass pathway at all sampling sites to link the trace metal content with potential source regions. Hence, this study (i) determined the bulk trace metal composition and the trace metal fractional solubility, (iii) attempted a source assessment, and (iv) projected the potential impact on the ocean.

1.3. REGIONAL SETTING

This section introduces the major areas that this thesis focusses on. Detailed information on the respective areas relevant to each of the above mentioned objectives are given in the respective chapters (manuscripts).

1.3.1. Saldanha Bay

Saldanha Bay is a small industrial town located on the southernmost portion of the Western Cape`s, known for its large port. The area experiences intense industries such as steel manufacturing, shipping, ballast water discharges, mining activities, importing and storage of crude oil, which leads to the area becoming a high-risk anthropogenic area (Clark et al., 2020). Most of the Northern Cape iron ore mines export their ore through this town. More than 60 million tons of iron ore and coal are exported through this town annually by rail wagons onto ships using the iron ore terminal. There are plans to increase the handling and storage of up to 80 million tons (Clark et al., 2020). These can potentially increase dust emissions in the area during the process of storage and handling. Manganese, phosphate, lead and zinc are some of the other ores also exported through this town (Clark et al., 2020). Red iron stains and colorations on properties and road signs are common in the area (Figure 6). Saldanha Bay is a semi-enclosed embayment area that receives winter rain and is located on the southern limb of the BUS (Joyce et al., 2005). The most prevalent winds are from the southeast to southwest blowing strongly from September and May (Heinecken et al., 2017). The upwelling system is an important region for the fisheries industry with a highly productive marine environment (Hutchings et al., 2009).

Figure 6. *Saldanha Bay iron ore storage facilities showing the stockpiles of ore stored and handled prior to export (Source: Mr Van Rooyen).*

1.3.2. Namib Desert

The Namibian coastline extends for more than 2000 km from South Africa to Angola northwards (Heine and Heine, 2002), with the highly productive Atlantic Ocean, the BUS, towards the west. Towards the east, the Namib Desert extends approximately 100-150 km inland, the Namib Sand Sea lies between two coastal towns, Walvis Bay and Luderitz. The Great Escarpment serves as an eastern boundary of the Namib Desert and also extends parallel to the Namibian coastline, with an elevation of ~ 1000m (Goudie and Eckardt, 1999). Most of the dust emissions in this region are associated with dry river beds and pans (Eckardt and Kuring, 2005; Ginoux et al., 2012; Vickery et al., 2013). There are approximately 12 east to west aligned rivers, with lengths ranging from 80 km (for the short rivers e.g. Khumib River) to 460 km (for the long rivers e.g. Ugab River) (Dansie et al., 2018). In addition, the Namib Desert valleys, deltas and the Great Escarpment are prime areas for ephemeral dust emission (Vickery, 2010; Vickery et al., 2013), that extend for more than 5 000 km^2 and have meagre annual precipitation. The annual precipitation gradually increases from west to east, ranging from 0 to 25 mm in the Namib Desert and steadily increasing to more than 500 mm annually east of the Great Escarpment (Jacobson et al., 1995). Satellite images have shown that dust from the ephemeral (Figure 7) along the Namibian coastline is transported offshore during the dry seasons (available at https://worldview. earthdata.nasa.gov). The coastal region where most of the terrestrial samples were collected for this study is mostly covered by gravel plains and silt sized sediments, with only a few outcrops being exposed (Figure 7).

Figure 7*. The area close to the Namibian coastline showing dust emissions on the 9 June 2004, from the region transported and deposited on ocean surface (Source: NASA, 2008). The coastal region where most of the dust sources are located are covered by gravel plains and silt-sized sediments.*

1.3.3. Proximal oceans

The oceans surrounding southern Africa are the most under-sampled (Schlitzer et al., 2018), especially for aerosols, with ~ 10 studies investigating trace metals in aerosols from this region. Most of the aerosol sampling efforts in the Southern Hemisphere have focussed on sampling at continental stations rather than ship sampling. Despite the underrepresentation in large sampling efforts, the proximal

oceanic regions around Southern Africa are important to global biogeochemical cycles. For example, the Southern Ocean includes the largest HNLC area in the high latitude regions and the limitation of micronutrients lowers the efficiency of the biological pump in sequestering CO_2 from the atmosphere (Boyd et al., 2000; Martin et al., 1990). Another example, is illustrated by the Benguela system, as a unique, highly productive area with rich marine organisms and contributing economically to the fishing industry in the region (Rossi et al., 2009). East of southern Africa, the Indian Ocean is known as region, which contributes to the net CO_2 drawdown.

1.4. THESIS OUTLINE

This thesis comprises three sections; the first section is chapter 1 that was outlined above and introduced the topic and provided the theoretical background for this study. Chapter 1 also did set out the aims and objectives of this study. The second section that follows hereafter comprises chapters 2, 3 and 4 and presents the research findings two periods. The third section (chapter 5) is outlined further below after this second section structure.

Section two is structured as follows:

Chapter 2 presents the distribution of bioactive trace metals in dust collected at the town of Saldanha Bay. The fractional solubility of dust from this industrial area was monitored as a potential source of micronutrients to phytoplankton in open oceans. The industrial activities in the town could be contributing to anthropogenic dust. Chapter 2 is under review in Atmospheric Environment: X (https://www.journals.elsevier.com/atmospheric-environment-x; manuscript reference number AEAOA-D-21-00065).

Chapter 3 looks at the dustiest non-playa environment in the Namib Desert. The mineralogy and the fractional solubility of dust from this region has been investigated as a potential source of micronutrient to the open oceans. This work will contribute to the understanding of the bioaccessibility of trace metals at source and potential impact on open oceans. This work is being prepared for submission to a peer-reviewed journal.

Chapter 4 presents the characteristics and fractional solubility of aerosols collected over the Southern Ocean during the austral winter and spring. This study helps to understand the bioaccessibility of dust at the depositional sites, from coast to open oceans. This work is being prepared for submission to a peer-reviewed journal.

The third section refers to Chapter 5, which is the concluding chapter that presents a short summary of the major findings in the study and links the different chapters. This chapter also provides recommendations on possible future research and knowledge gaps that should be included in future dust research.

The overall workflow of this dissertation it displayed in below.

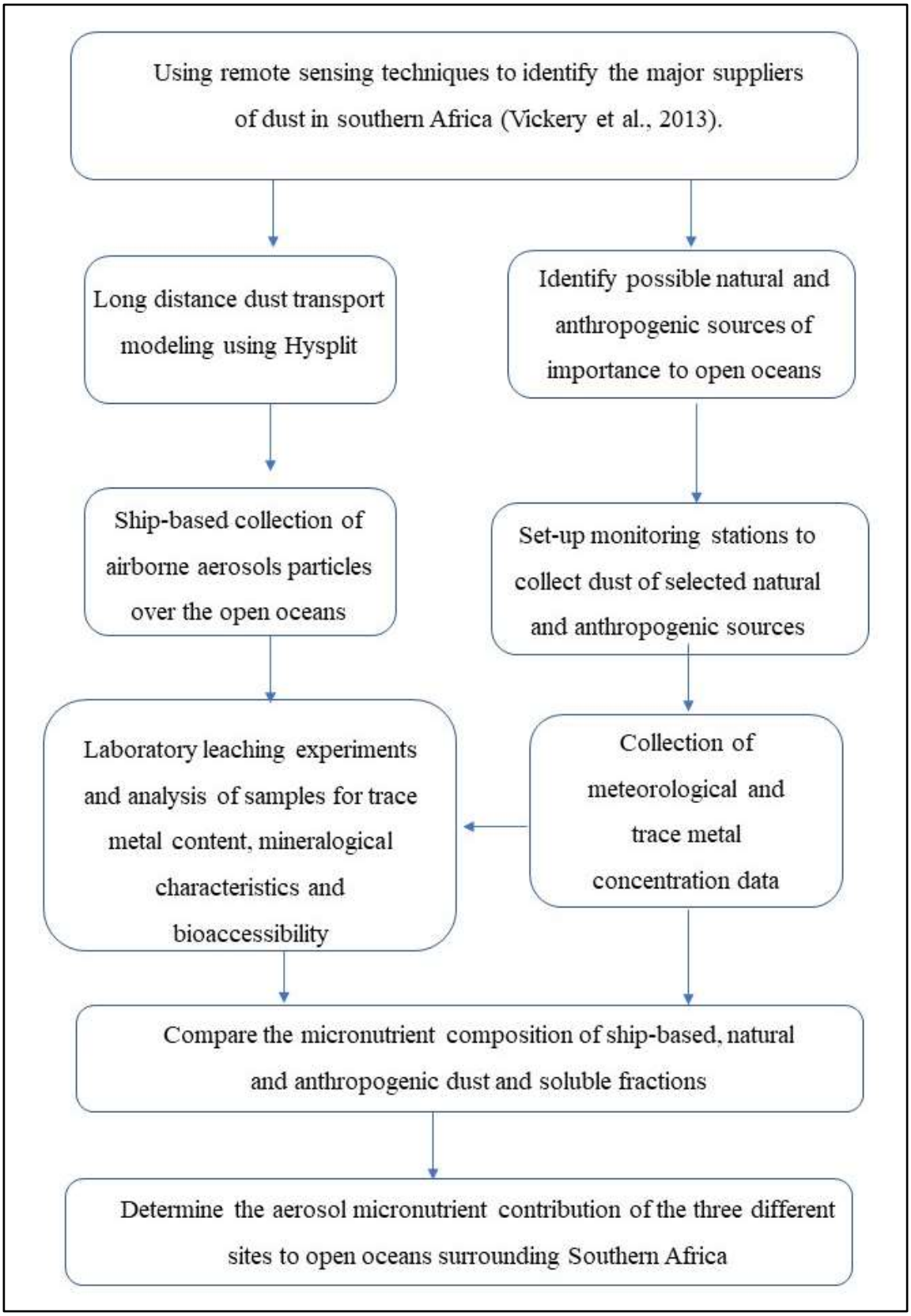

Figure 8. *Schematic diagram showing all the research components conducted during this study.*

1.5. METHODS

The following provides a very broad overview of approaches adopted in the projecton the three chapters (manuscripts) that address the three Objectives outlined above (cf. 3. Aims). Details for each sampling campaign, sample processing and analyses are given in each respective chapter (manuscript) of the second section of this thesis.

1.5.1. Sample collection

1.5.1.1. Saldanha Bay

To achieve the research objective 1 of this study, fieldwork (dust samplers) coupled with analytical work in the laboratory was conducted. Saldanha Bay Municipality has an existing dust bucket sampling program at seven stations (Figure 9), where samples are collected monthly and analysed for trace metals (https://sbm.gov.za/environmental/). Monthly dust bucket sampling data from January 2015 to December 2019 was used in this study. In addition, BSNEs samplers were set-up from February 2019 to February 2020 in Saldanha Bay at four stations. These samples were used to to characterize the mineralogical composition (iii) attempting a source assessment (iv) and to determine the trace metal fractional solubility.

Figure 9*. An automated meteorological monitoring station and measuring types of equipment at Saldanha Bay.*

1.5.1.2. Namib Desert

Setting up of the MWAC dust samplers started from April 2016 and lasted until October 2017, at four non-playa environments stations in the Namib Desert. The samples were used to partially achieve objective two of this study which was to characterize the mineralogical composition and attempting a source assessment. In addition, samples were collected using Big spring Number Eight (BSNE) aeolian dust samplers at 3-meter vertical height for two sites from March 2019 to January 2020 (Figure 10). The BNSE samples were used to achieve the remaining part of objective two of this study, which was to provide information on the importance of non-playa environments as potential fertilisers to proximal open oceans.

***Figure 10**. BSNE sampling site in the Namib Desert.*

1.5.1.3. Southern Ocean

Aerosols samples were collected from Cape Town towards the Southern Ocean on the research vessel SA Agulhas II on two cruises from July to August 2019 and October to December 2019. Bulk aerosol samples were collected on filters. Air was pumped through the filters using the total suspended particulate volumetric flow controlled high volume air sampler. The high-volume dust sampler was

deployed on the 11th deck approximately 30 m above the sea surface (Figure 11). The samples were not immediately subsampled for analyses but stored frozen at -20 ºC.

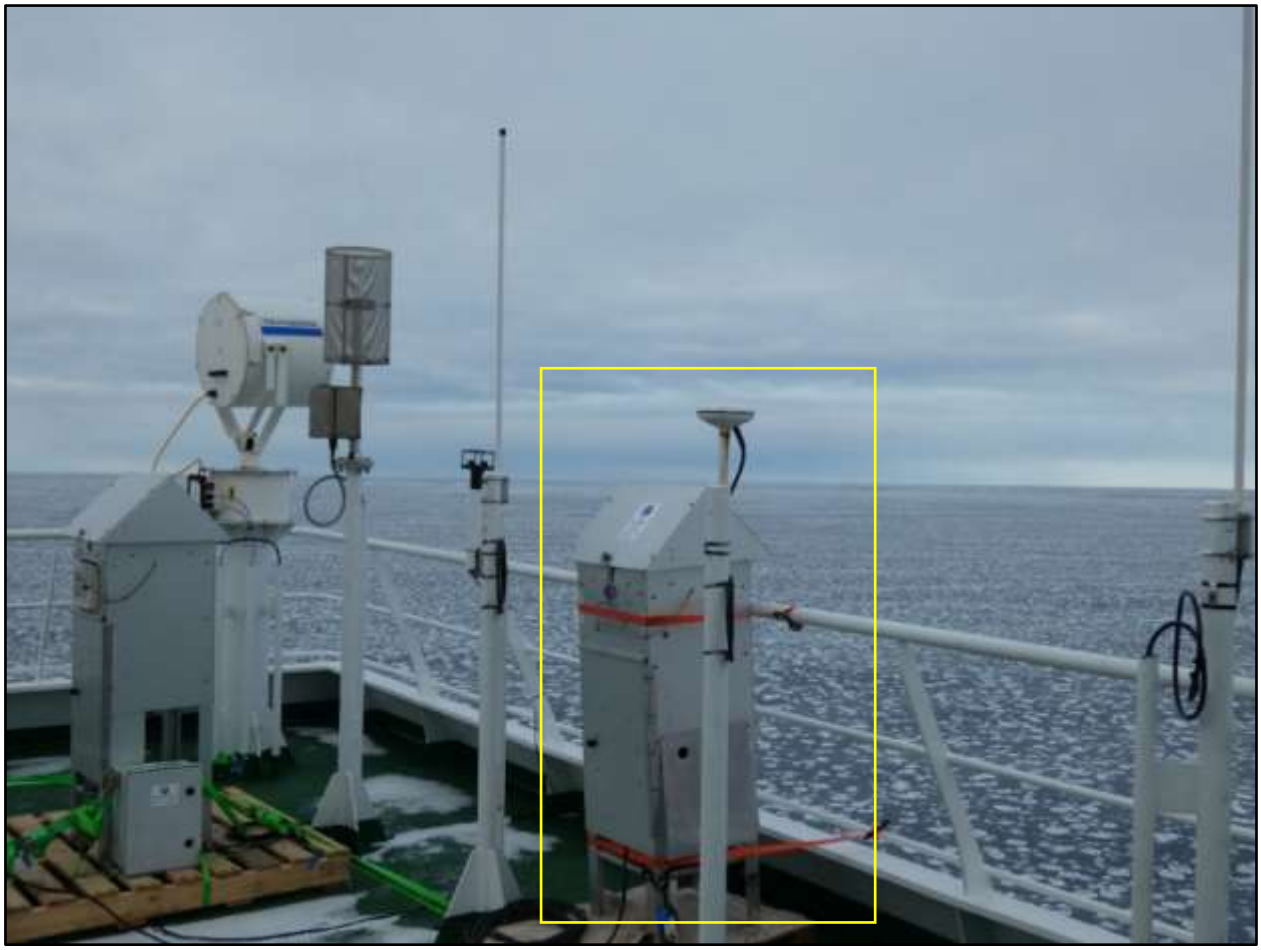

***Figure 11**. The high-volume dust sampler positioned on the monkey island on the SA Alguhas II during the winter cruise in 2019. The dust sampler is highlighted in the yellow rectangle.*

1.6. ANALYSIS

1.6.1. Trace elemental concentrations

In the laboratory, the processing and handling of the filters were conducted under a laminar flow to avoid external contaminations. The aerosol samples were digested in order to determine the trace elemental concentration using an Agilent 7900 inductively coupled plasma mass spectrometry (ICP-MS). The full digestion was conducted with HNO_3, with full details explained in the three manuscripts. Different trace elements are used as lithogenic tracers (Al), indicators for pollution (Pb, V) and or considered bioactive (Fe, Mn, Cu, Zn, Cd, Co).

1.6.2. Mineralogical characteristics

Mineralogical characteristics were assessed differently for the samples from Saldanha Bay and Namib Desert in this thesis (further described in Chapter 2 and 3). The Southern Ocean samples could not be seen under SEM due to the low aerosols load. For Saldanha Bay (chapter 1) samples was selected for mineralogical investigation due to logistical constraints, with sampling only allowed in specific areas. This selected samples was lightly coated with either carbon or gold before being examined using a Zeiss MERLIN FE-SEM at the Stellenbosch University Central Analytical Facilities. For mineral identification and characterization, Cryo-energy-dispersive X-ray spectrometry (cryo-EDS) was used. The EDS spectra particles were observed at an accelerating voltage of 15kV.

For the Namib Desert samples (chapter 2), mineralogical characteristics analysis was conducted for all samples using a Quantitative Evaluation of Minerals by Scanning Electron Microscopy (QEMSCAN) at the Centre for Minerals Research, University of Cape Town. QEMSCAN provides rapid mineralogical and morphological characteristically analysis of particles from a relatively small sample size.

1.6.3. Leaching experiments

Dissolution experiments were carried out in order to understand the solubility of the dust. Solubility is used as a proxy for dust bioaccessibility. Analytical leaching experiments were conducted in the laboratory at University of Stellenbosch.

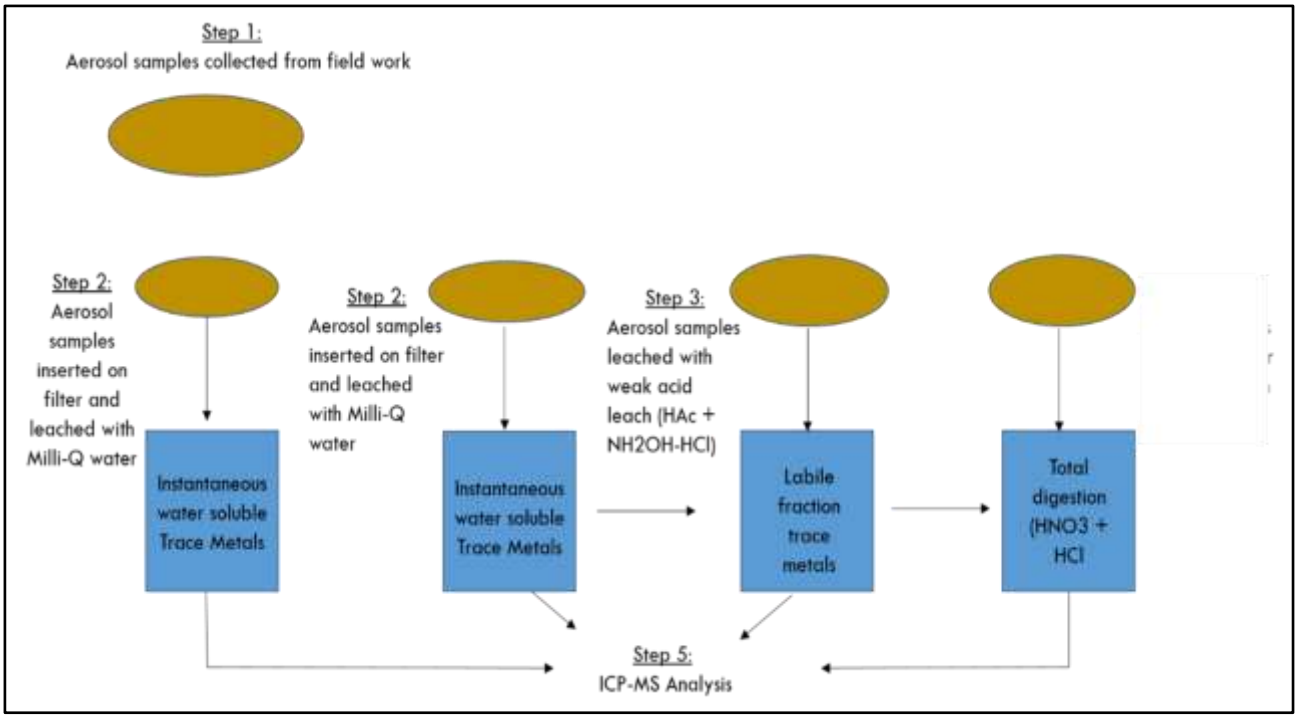

***Figure 12**. Flowchart showing the different leaching stages (steps) to extract the soluble, labile and total trace metals. The leaching protocol begins with the dust loaded on the filter, then the dust loaded filters are leached with Milli-Q, followed by leaching with weak acid to determine the soluble and labile fractions in aerosols.*

1.7. HYSPLIT BACKWARD AND FORWARD TRAJECTORIES

Hysplit determines the source of air masses possibly entraining the analyzed aerosol particles. For this purpose, 7-day (168 hours) air mass backward and forward trajectories were modelled for each aerosol dust sample to determine the source of the air masses. The GDAS meteorology on the online free available NOAA Air Resources Laboratory Hybrid Single-Particle Lagrangian Integrated Trajectory (HYSPLIT) model (Stein et al. 2015; Rolph 2016). The starting heights from the models were 100, 500, 1500 m.

1.8. CHAPTER 1 REFERENCES

Aguilar-Islas, A.M., Wu, J., Rember, R., Johansen, A.M., Shank, L.M., 2010. Dissolution of aerosol-derived iron in seawater: Leach solution chemistry, aerosol type, and colloidal iron fraction. Mar. Chem. 120, 25–33. https://doi.org/10.1016/j.marchem.2009.01.011

Amato, J.A., 2000. Dust: A History of the Small and the Invisible. University of Califonia Publishing, Califonia.

Anderson, R.F., Cheng, H., Edwards, R.L., Fleisher, M.Q., Hayes, C.T., Huang, K.F., Kadko, D., Lam, P.J., Landing, W.M., Lao, Y., Lu, Y., Measures, C.I., Moran, S.B., Morton, P.L., Ohnemus, D.C., Robinson, L.F., Shelley, R.U., 2016. How well can we quantify dust deposition to the ocean? Philos. Trans. R. Soc. A Math. Phys. Eng. Sci. 374. https://doi.org/10.1098/rsta.2015.0285

Annegarn, H.A.J., Van Grieken, R., Bibby, D.M., Von Blottnitz, F., 1983. Background Aerosol Composition in the Namib Desert, South West Africa (Namibia). Atmos. Environ. 17, 2045–2053.

Ardyna, M., Lacour, L., Sergi, S., d'Ovidio, F., Sallée, J.B., Rembauville, M., Blain, S., Tagliabue, A., Schlitzer, R., Jeandel, C., Arrigo, K.R., Claustre, H., 2019. Hydrothermal vents trigger massive phytoplankton blooms in the Southern Ocean. Nat. Commun. 10, 1–8. https://doi.org/10.1038/s41467-019-09973-6

Aumont, O., Bopp, L., 2006. Globalizing results from ocean in situ iron fertilization studies. Global Biogeochem. Cycles 20, n/a-n/a. https://doi.org/10.1029/2005GB002591

Baker, A. R., Jickells, T.D., Witt, M., Linge, K.L., 2006. Trends in the solubility of iron, aluminium, manganese and phosphorus in aerosol collected over the Atlantic Ocean. Mar. Chem. 98, 43–58. https://doi.org/10.1016/j.marchem.2005.06.004

Barbeau, K., 2006. Photochemistry of Organic Iron(III) Complexing Ligands in Oceanic Systems. Photochem. Photobiol. 82, 1505–1516. https://doi.org/10.1111/j.1751-1097.2006.tb09806.x

Barkley, A.E., Prospero, J.M., Mahowald, N., Hamilton, D.S., Popendorf, K.J., Oehlert, A.M., Pourmand, A., Gatineau, A., Panechou-Pulcherie, K., Blackwelder, P., Gaston, C.J., 2019. African biomass burning is a substantial source of phosphorus deposition to the Amazon, Tropical Atlantic Ocean, and Southern Ocean. Proc. Natl. Acad. Sci. U. S. A. 116, 16216–

16221. https://doi.org/10.1073/pnas.1906091116

Bauer, S.E., Im, U., Mezuman, K., Gao, C.Y., 2019. Desert Dust, Industrialization, and Agricultural Fires: Health Impacts of Outdoor Air Pollution in Africa. J. Geophys. Res. Atmos. 124, 4104–4120. https://doi.org/10.1029/2018JD029336

Behrenfeld, M.J., Randerson, J.T., McClain, C.R., Feldman, G.C., Los, S.O., Tucker, C.J., Falkowski, P.G., Field, C.B., Frouin, R., Esaias, W.E., Kolber, D.D., Pollack, N.H., 2001. Biospheric primary production during an ENSO transition. Science (80-.). 291, 2594–2597. https://doi.org/10.1126/science.1055071

Berger, C.J.M., Lippiatt, S.M., Lawrence, M.G., Bruland, K.W., 2008. Application of a chemical leach technique for estimating labile particulate aluminum, iron, and manganese in the Columbia River plume and coastal waters off Oregon and Washington. J. Geophys. Res. 113, 1–16. https://doi.org/10.1029/2007jc004703

Bhattachan, A, D'Odorico, P., Okin, G.S., 2015. Biogeochemistry of dust sources in Southern Africa. J. Arid Environ. 117, 18–27. https://doi.org/10.1016/j.jaridenv.2015.02.013

Bhattachan, Abinash, Wang, L., Miller, M.F., Licht, K.J., D'Odorico, P., 2015. Antarctica's Dry Valleys: A potential source of soluble iron to the Southern Ocean? Geophys. Res. Lett. 42, 1912–1918. https://doi.org/10.1002/2015GL063419

Boyd, P.W., Mackie, D.S., Hunter, K.A., 2010. Aerosol iron deposition to the surface ocean - Modes of iron supply and biological responses. Mar. Chem. 120, 128–143. https://doi.org/10.1016/j.marchem.2009.01.008

Boyd, P.W., Watson, A.J., Law, C.S., Abraham, E.R., Trull, T., Murdoch, R., Bakker, D.C.E., Bowie, A.R., Buesseler, K.O., Chang, H., Charette, M., Croot, P.L., Downing, K., Frew, R., Gall, M., Hadfield, M., Hall, J., Harvey, M., Jameson, G., LaRoche, J., Liddicoat, M., Ling, R., Maldonado, M.T., McKay, M.R., Nodder, S., Pickmere, S., Pridmore, R., Rintoul, S., Safi, K., Sutton, P., Strzepek, R., Tanneberger, K., Turner, S., Waite, A., Zeldis, J., 2000. A mesoscale phytoplankton bloom in the polar Southern Ocean stimulated by iron fertilization. Nature 407, 695–702.

Bryant, R.G., 2003. Monitoring hydrological controls on dust emissions: preliminary observations from Etosha Pan, Namibia. Geogr. J. 169, 131–141. https://doi.org/10.1111/1475-4959.04977

Buck, C.S., Landing, W.M., Resing, J.A., 2010. Particle size and aerosol iron solubility: A high-

resolution analysis of Atlantic aerosols. Mar. Chem. 120, 14–24. https://doi.org/10.1016/j.marchem.2008.11.002

Capone, D.G., Hutchins, D.A., 2013. Microbial biogeochemistry of coastal upwelling regimes in a changing ocean. Nat. Geosci. 6, 711–717. https://doi.org/10.1038/ngeo1916

Cassar, N., Bender, M.L., Barnett, B.A., Fan, S., Moxim, W.J., Levy, H., Tilbrook, B., 2007. The southern ocean biological response to aeolian iron deposition. Science (80-.). 317, 1067–1070. https://doi.org/10.1126/science.1144602

Chance, R., Jickells, T.D., Baker, A.R., 2015. Atmospheric trace metal concentrations, solubility and deposition fluxes in remote marine air over the south-east Atlantic. Mar. Chem. 177, 45–56. https://doi.org/10.1016/j.marchem.2015.06.028

Chen, H., Laskin, A., Baltrusaitis, J., Gorski, C.A., Scherer, M.M., Grassian, V.H., 2012. Coal fly ash as a source of iron in atmospheric dust. Environ. Sci. Technol. 46, 2112–2120. https://doi.org/10.1021/es204102f

Clark, B., Laird, M., Hutchings, K., Liebau, V., Biccard, A., Turpie, J., Parker-Mallick, N., 2020. The State of Saldanha Bay and Langebaan Lagoon 2020. Report 1581, 1–381.

Dansie, A.P., Thomas, D.S.G., Wiggs, G.F.S., Munkittrick, K.R., 2018. Spatial variability of ocean fertilizing nutrients in the dust-emitting ephemeral river catchments of Namibia. Earth Surf. Process. Landforms 43, 563–578. https://doi.org/10.1002/esp.4207

Dansie, A.P., Wiggs, G.F.S., Thomas, D.S.G., 2017a. Iron and nutrient content of wind-erodible sediment in the ephemeral river valleys of Namibia. Geomorphology 290, 335–346. https://doi.org/10.1016/j.geomorph.2017.03.016

Dansie, A.P., Wiggs, G.F.S., Thomas, D.S.G., Washington, R., 2017b. Measurements of windblown dust characteristics and ocean fertilization potential: The ephemeral river valleys of Namibia. Aeolian Res. 29, 30–41. https://doi.org/10.1016/j.aeolia.2017.08.002

Duce, R.A., Tindale, N.W., 1991. Chemistry and biology of iron and other trace metals in the ocean. Limnol. Oceanogr. 8, 1715–1726.

Duggen, S., Croot, P., Schacht, U., Hoffmann, L., 2007. Subduction zone volcanic ash can fertilize the surface ocean and stimulate phytoplankton growth: Evidence from biogeochemical experiments and satellite data. Geophys. Res. Lett. 34, 1–5.

https://doi.org/10.1029/2006GL027522

Eckardt, F.D., Kuring, N., 2005. SeaWiFS identifies dust sources in the Namib Desert. Int. J. Remote Sens. 26, 4159–4167. https://doi.org/10.1080/01431160500113112

Eltayeb, M.A.H., van Grieken, R.E., Maenhaut, W., Annegarn, H., 1993. Aerosol-soil fractionate for Namib Desert samples. Atmos. Environ. 27A, 669–678.

Eltayeb, M.A.H., Van Grieken, R.E., Maenhaut, W., Annegarn, H.A.J., 1992. Aerosol-soil fractionationation for Namib desert samples. Aerosol Sci. 23, 983–986.

Engelbrecht, J.P., Derbyshire, E., 2010. Airborne mineral dust. Elements 6, 241–246. https://doi.org/10.2113/gselements.6.4.241

Falkowski, P., 2012. Ocean science: The power of plankton. Nature 483, S17–S20. https://doi.org/10.1038/483S17a

Fan, S.M., Moxim, W.J., Levy, H., 2006. Aeolian input of bioavailable iron to the ocean. Geophys. Res. Lett. https://doi.org/10.1029/2005GL024852

Field, C.B., Behrenfeld, M.J., Randerson, J.T., Falkowski, P., 1998. Primary production of the biosphere: Integrating terrestrial and oceanic components. Science (80-.). 281, 237–240. https://doi.org/10.1126/science.281.5374.237

Formenti, P., Schütz, L., Balkanski, Y., Desboeufs, K., Ebert, M., Kandler, K., Petzold, A., Scheuvens, D., Weinbruch, S., Zhang, D., 2011. Recent progress in understanding physical and chemical properties of African and Asian mineral dust. Atmos. Chem. Phys. 11, 8231–8256. https://doi.org/10.5194/acp-11-8231-2011

Friese, C.A., van der Does, M., Merkel, U., Iversen, M.H., Fischer, G., Stuut, J.B.W., 2016. Environmental factors controlling the seasonal variability in particle size distribution of modern Saharan dust deposited off Cape Blanc. Aeolian Res. 22, 165–179. https://doi.org/10.1016/j.aeolia.2016.04.005

Fung, I.Y., Meyn, S.K., Tegen, I., Doney, S.C., John, J.G., Bishop, J.K.B., 2000. Iron supply and demand in the upper ocean. Global Biogeochem. Cycles 14, 281–295. https://doi.org/10.1029/1999gb900059

Gao, Y., Kaufman, Y.J., Tanré, D., Kolber, D., Falkowski, P.G., 2001. Seasonal distributions of

Aeolian iron fluxes to the global ocean. Geophys. Res. Lett. 28, 29–32. https://doi.org/10.1029/2000GL011926

Gili, S., Vanderstraeten, A., Cazaunau, M., Chaput, A., Doussin, J.-F., Di Biagio, C., Formenti, P., King, J.S., Magnold, A., Mattielli, N., Pangui, E., Van Overmeiren, P., Walgraeve, Christop, C., 2021. The role of Southern Africa as a dust precursor to East Antarctica (No. id. 18441). Online.

Ginoux, P., Chin, M., Tegen, I., Goddard, T., Ina, G., Prospero, J.M., Holben, B., Dubovik, O., Lin, S.-J., 2001. Sources and distributions of dust aerosols simulated with the GOCART model. J. Geophys. Res. 106, 20,255-20,273.

Ginoux, P., Prospero, J.M., Gill, T.E., Hsu, N.C., Zhao, M., 2012. Global-scale attribution of anthropogenic and natural dust sources and their emission rates based on MODIS Deep Blue aerosol products. Rev. Geophys. 50, 1–36. https://doi.org/10.1029/2012RG000388

Goossens, D., Offer, Z.Y., 2000. Wind tunnel and field calibration of six aeolian dust samplers. Atmos. Environ. 34, 1043–1057. https://doi.org/10.1016/S1352-2310(99)00376-3

Goudie, A.S., Eckardt, F., 1999. The evolution of the morphological framework of the Central Namib Desert, Namibia, since the Early Cretaceous. Geogr. Ann. Ser. A Phys. Geogr. 81, 443–458. https://doi.org/10.1111/j.0435-3676.1999.00073.x

Goudie, A.S., Middleton, N.J., 2001. Saharan dust storms: Nature and consequences. Earth-Science Rev. 56, 179–204. https://doi.org/10.1016/S0012-8252(01)00067-8

Guieu, C., Bonnet, S., Wagener, T., Loÿe-Pilot, M.D., 2005. Biomass burning as a source of dissolved iron to the open ocean? Geophys. Res. Lett. 32, 1–5. https://doi.org/10.1029/2005GL022962

Guieu, C., Thomas, A.J., 1996. Saharan Aerosols: From the Soil to the Ocean. Springer, Dordrecht, pp. 207–216. https://doi.org/10.1007/978-94-017-3354-0_20

Hamilton, D.S., Moore, J.K., Arneth, A., Bond, T.C., Carslaw, K.S., Hantson, S., Ito, A., Kaplan, J.O., Lindsay, K., Nieradzik, L., Rathod, S.D., Scanza, R.A., Mahowald, N.M., 2020a. Impact of Changes to the Atmospheric Soluble Iron Deposition Flux on Ocean Biogeochemical Cycles in the Anthropocene. Global Biogeochem. Cycles 34, e2019GB006448. https://doi.org/10.1029/2019GB006448

Hamilton, D.S., Scanza, R.A., Rathod, S.D., Bond, T.C., Kok, J.F., Li, L., Matsui, H., Mahowald, N.M., 2020b. Recent (1980 to 2015) Trends and Variability in Daily-to-Interannual Soluble Iron Deposition from Dust, Fire, and Anthropogenic Sources. Geophys. Res. Lett. 47. https://doi.org/10.1029/2020GL089688

Heine, K., Heine, J.T., 2002. A paleohydrologic reinterpretation of the Homeb Silts, Kuiseb River, central Namib Desert (Namibia) and paleoclimatic implications. Catena 48, 107–130. https://doi.org/10.1016/S0341-8162(02)00012-7

Heinecken, C., Japp, D., Olivier, D., 2017. Concept for a Proposed Sea-Based Aquaculture Development Zone in Saldanha Bay, South Africa. Capricorn Mar. Environ. 1–56.

Henley, S.F., Cavan, E.L., Fawcett, S.E., Kerr, R., Monteiro, T., Sherrell, R.M., Bowie, A.R., Boyd, P.W., Barnes, D.K.A., Schloss, I.R., Marshall, T., Flynn, R., Smith, S., 2020. Changing Biogeochemistry of the Southern Ocean and Its Ecosystem Implications, Frontiers in Marine Science. https://doi.org/10.3389/fmars.2020.00581

Ho, T.-Y., Chou, W.-C., Wei, C.-L., Lin, F.-J., Wong, G.T.F., Line, H.-L., 2010. Trace metal cycling in the surface water of the South China Sea: Vertical fluxes, composition, and sources. Limnol. Oceanogr. 55, 1807–1820. https://doi.org/10.4319/lo.2010.55.5.1807

Hutchings, L., van der Lingen, C.D., Shannon, L.J., Crawford, R.J.M., Verheye, H.M.S., Bartholomae, C.H., van der Plas, A.K., Louw, D., Kreiner, A., Ostrowski, M., Fidel, Q., Barlow, R.G., Lamont, T., Coetzee, J., Shillington, F., Veitch, J., Currie, J.C., Monteiro, P.M.S., 2009. The Benguela Current: An ecosystem of four components. Prog. Oceanogr. 83, 15–32. https://doi.org/10.1016/j.pocean.2009.07.046

Ito, A., Myriokefalitakis, S., Kanakidou, M., Mahowald, N.M., Scanza, R.A., Hamilton, D.S., Baker, A.R., Jickells, T., Sarin, M., Bikkina, S., Gao, Y., Shelley, R.U., Buck, C.S., Landing, W.M., Bowie, A.R., Perron, M.M.G., Guieu, C., Meskhidze, N., Johnson, M.S., Feng, Y., Kok, J.F., Nenes, A., Duce, R.A., 2019. Pyrogenic iron: The missing link to high iron solubility in aerosols. Sci. Adv. 5, eaau7671. https://doi.org/10.1126/sciadv.aau7671

Ito, A., Shi, Z., 2016. Delivery of anthropogenic bioavailable iron from mineral dust and combustion aerosols to the ocean. Atmos. Chem. Phys. 16, 85–99. https://doi.org/10.5194/acp-16-85-2016

Jacobson, P.J., Jacobson, K.M., Seely, M.K., 1995. Ephemeral Rivers and their Catchments:

Sustaining People and Development in Western Namibia., Eds. ed. Desert Research Foundation of Namibia, Windhoek.

Jeanneau, A.C., Ostendorf, B., Herrmann, T., 2019. Relative spatial differences in sediment transport in fire-affected agricultural landscapes: A field study. Aeolian Res. 39, 13–22. https://doi.org/10.1016/j.aeolia.2019.04.002

Jenner, S.L., Abiodun, B.J., 2013. The transport of atmospheric sulfur over Cape Town. Atmos. Environ. 79, 248–260. https://doi.org/10.1016/j.atmosenv.2013.06.010

Jickells, T., Moore, C.M., 2015. The Importance of Atmospheric Deposition for Ocean Productivity. Annu. Rev. Ecol. Evol. Syst. 46, 481–501. https://doi.org/10.1146/annurev-ecolsys-112414-054118

Jickells, T.D., 2005. Global Iron Connections Between Desert Dust, Ocean Biogeochemistry, and Climate. Science (80-.). 308, 67–71. https://doi.org/10.1126/science.1105959

Jickells, T.D., An, Z.S., Andersen, K.K., Baker, A.R., Bergametti, C., Brooks, N., Cao, J.J., Boyd, P.W., Duce, R.A., Hunter, K.A., Kawahata, H., Kubilay, N., LaRoche, J., Liss, P.S., Mahowald, N., Prospero, J.M., Ridgwell, A.J., Tegen, I., Torres, R., 2005. Global iron connections between desert dust, ocean biogeochemistry, and climate. Science (80-.). https://doi.org/10.1126/science.1105959

Journet, E., Desboeufs, K. V., Caquineau, S., Colin, J.L., 2008. Mineralogy as a critical factor of dust iron solubility. Geophys. Res. Lett. 35, 1–5. https://doi.org/10.1029/2007GL031589

Joyce, L.B., Pitcher, G.C., Randt, A. Du, Monteiro, P.M.S., 2005. Dinoflagellate cysts from surface sediments of Saldanha Bay, South Africa: An indication of the potential risk of harmful algal blooms. Harmful Algae 4, 309–318. https://doi.org/10.1016/j.hal.2004.08.001

Klopper, D., Formenti, P., Namwoonde, A., Cazaunau, M., Chevaillier, S., Feron, A., Gaimoz, C., Hease, P., Lahmidi, F., Mirande-Bret, C., Triquet, S., Zeng, Z., Piketh, S., 2020. Chemical composition and source apportionment of atmospheric aerosols on the Namibian coast. Atmos. Chem. Phys. Discuss. 1–43. https://doi.org/10.5194/acp-2020-388

Lachkar, Z., Gruber, N., 2012. A comparative study of biological production in eastern boundary upwelling systems using an artificial neural network. Biogeosciences 9, 293–308. https://doi.org/10.5194/bg-9-293-2012

Li, F., Ginoux, P., Ramaswamy, V., 2008. Distribution, transport, and deposition of mineral dust in the Southern Ocean and Antarctica: Contribution of major sources. J. Geophys. Res. Atmos. 113, 1–15. https://doi.org/10.1029/2007JD009190

Li, W., Xu, L., Liu, X., Zhang, J., Lin, Y., Yao, X., Gao, H., Zhang, D., Chen, J., Wang, W., Harrison, R.M., Zhang, X., Shao, L., Fu, P., Nenes, A., Shi, Z., 2017. Air pollution–aerosol interactions produce more bioavailable iron for ocean ecosystems. Sci. Adv. 3, 1–7. https://doi.org/10.1126/sciadv.1601749

Mahowald, N., Jickells, T.D., Baker, A.R., Artaxo, P., Benitez-Nelson, C.R., Bergametti, G., Bond, T.C., Chen, Y., Cohen, D.D., Herut, B., Kubilay, N., Losno, R., Luo, C., Maenhaut, W., McGee, K.A., Okin, G.S., Siefert, R.L., Tsukuda, S., 2008. Global distribution of atmospheric phosphorus sources, concentrations and deposition rates, and anthropogenic impacts. Global Biogeochem. Cycles 22, 1–19. https://doi.org/10.1029/2008GB003240

Mahowald, N.M., Baker, A.R., Bergametti, G., Brooks, N., Duce, R.A., Jickells, T.D., Prospero, J.M., Tegen, I., 2005. Atmospheric global dust cycle and iron inputs to the ocean. Global Biogeochem. Cycles 19, 1–15. https://doi.org/10.1029/2004GB002402

Mahowald, N.M., Engelstaeder, S., Luo, C., Sealy, A., Artaxo, P., Benitez-Nelson, C.R., Bonnet, S., Chen, Y., Chuang, P.Y., Cohen, D.D., Dulac, F., Herut, B., Johansen, A.M., Kubilay, N., Losno, R., Maenhaut, W., Paytan, A., Prospero, J.M., Shank, L.M., Siefert, R.L., 2009. Atmospheric Iron Deposition : Global Distribution , Variability , and Human Perturbations. Ann. Rev. Mar. Sci. 245–278. https://doi.org/10.1146/annurev.marine.010908.163727

Mahowald, N.M., Hamilton, D.S., Mackey, K.R.M., Moore, J.K., Baker, A.R., Scanza, R.A., Zhang, Y., 2018. Aerosol trace metal leaching and impacts on marine microorganisms. Nat. Commun. 9. https://doi.org/10.1038/s41467-018-04970-7

Mahowald, N.M., Kloster, S., Engelstaedter, S., Moore, J.K., Mukhopadhyay, S., McConnell, J.R., Albani, S., Doney, S.C., Bhattacharya, A., Curran, M.A.J., Flanner, M.G., Hoffman, F.M., Lawrence, D.M., Lindsay, K., Mayewski, P.A., Neff, J., Rothenberg, D., Thomas, E., Thornton, P.E., Zender, C.S., 2010. Observed 20th century desert dust variability: Impact on climate and biogeochemistry. Atmos. Chem. Phys. 10, 10875–10893. https://doi.org/10.5194/acp-10-10875-2010

Martin, J.H., Fitzwater, S.E., 1988. Iron deficiency limits phytoplankton growth in the north-east Pacific subarctic. Nature. https://doi.org/10.1038/331341a0

Martin, J.H., Fitzwater, S.E., Gordon, R.M., 1990. Iron deficiency limits phytoplankton growth in Antarctic waters. Global Biogeochem. Cycles 4, 5–12. https://doi.org/10.1029/GB004i001p00005

Matsui, H., Mahowald, N.M., Moteki, N., Hamilton, D.S., Ohata, S., Yoshida, A., Koike, M., Scanza, R.A., Flanner, M.G., 2018. Anthropogenic combustion iron as a complex climate forcer. Nat. Commun. 9. https://doi.org/10.1038/s41467-018-03997-0

Mcgowan, H., Clark, A., 2008. Identification of dust transport pathways from Lake Eyre , Australia using Hysplit. Atmos. Environ. 42, 6915–6925. https://doi.org/10.1016/j.atmosenv.2008.05.053

Meskhidze, N., Hurley, D., Royalty, T.M., Johnson, M.S., 2017. Potential effect of atmospheric dissolved organic carbon on the iron solubility in seawater. Mar. Chem. 194, 124–132. https://doi.org/10.1016/j.marchem.2017.05.011

Messié, M., Chavez, F.P., 2015. Seasonal regulation of primary production in eastern boundary upwelling systems. Prog. Oceanogr. 134, 1–18. https://doi.org/10.1016/j.pocean.2014.10.011

Molepo, K.M., Abiodun, B.J., Magoba, R.N., 2019. The transport of PM10 over Cape Town during high pollution episodes. Atmos. Environ. 213, 116–132. https://doi.org/10.1016/j.atmosenv.2019.05.041

Moore, C.M., Mills, M.M., Arrigo, K.R., Berman-Frank, I., Bopp, L., Boyd, P.W., Galbraith, E.D., Geider, R.J., Guieu, C., Jaccard, S.L., Jickells, T.D., La Roche, J., Lenton, T.M., Mahowald, N.M., Marañón, E., Marinov, I., Moore, J.K., Nakatsuka, T., Oschlies, A., Saito, M.A., Thingstad, T.F., Tsuda, A., Ulloa, O., 2013a. Processes and patterns of oceanic nutrient limitation. Nat. Geosci. 6, 701–710. https://doi.org/10.1038/ngeo1765

Neff, P.D., Bertler, N.A.N., 2015. Trajectory modeling of modern dust transport to the Southern Ocean and Antarctica. J. Geophys. Res. 120, 9303–9322. https://doi.org/10.1002/2015JD023304

Nogueira, J., Evangelista, H., Valeriano, C. de M., Sifeddine, A., Neto, C., Vaz, G., Moreira, L.S., Cordeiro, R.C., Turcq, B., Aniceto, K.C., Neto, A.B., Martins, G., Barbosa, C.G.G., Godoi, R.H.M., Shimizu, M.H., 2021. Dust arriving in the Amazon basin over the past 7,500 years came from diverse sources. Commun. Earth Environ. 2, 1–11. https://doi.org/10.1038/s43247-020-00071-w

Paytan, A., Mackey, K.R.M., Chen, Y., Lima, I.D., Doney, S.C., Mahowald, N., Labiosa, R., Post, A.F., 2009. Toxicity of atmospheric aerosols on marine phytoplankton. PNAS 106, 4601–4605.

Perron, M.M.G., Proemse, B.C., Strzelec, M., Gault-Ringold, M., Boyd, P.W., Sanz Rodriguez, E., Paull, B., Bowie, A.R., 2019. Origin, transport and deposition of aerosol iron to Australian coastal waters. Submitted 228, 117432. https://doi.org/10.1016/j.atmosenv.2020.117432

Perron, M.M.G., Strzelec, M., Gault-Ringold, M., Proemse, B.C., Boyd, P.W., Bowie, A.R., 2020. Assessment of leaching protocols to determine the solubility of trace metals in aerosols. Talanta 208, 120377. https://doi.org/10.1016/j.talanta.2019.120377

Piketh, S.J., Annegarn, H.J., Tyson, P.D., 1999. Lower tropospheric aerosol loadings over South Africa: The relative contribution of aeolian dust, industrial emissions, and biomass burning. J. Geophys. Res. Atmos. 104, 1597–1607. https://doi.org/10.1029/1998JD100014

Poulton, S.W., Raiswell, R., 2002. The low-temperature geochemical cycle of iron: From continental fluxes to marine sediment deposition. Am. J. Sci. 302, 774–805. https://doi.org/10.2475/ajs.302.9.774

Prospero, J.M., 1999. Long-range transport of mineral dust in the global atmosphere: Impact of African dust on the environment of the southeastern United States. Proc. Natl. Acad. Sci. U. S. A. 96, 3396–3403. https://doi.org/10.1073/pnas.96.7.3396

Prospero, J.M., 1996. The Atmospheric Transport of Particles to the Ocean, in: Ittekkot, V., Schafer, P., Honjo, S., Depetris, P.J. (Eds.), Particle Flux in the Ocean. John Wiley & Sons Ltd, pp. 19–52.

Prospero, J.M., Barkley, A.E., Gaston, C.J., Gatineau, A., Sansano, A.C. y, Panechou, K., 2020. Characterizing and Quantifying African Dust Transport and Deposition to South America: Implications for the Phosphorus Budget in the Amazon Basin. Global Biogeochem. Cycles 34, e2020GB006536. https://doi.org/10.1029/2020GB006536

Prospero, J.M., Carlson, T.N., 1972. Vertical and areal distribution of Saharan dust over the western equatorial north Atlantic Ocean. J. Geophys. Res. 77, 5255–5265. https://doi.org/10.1029/JC077i027p05255

Prospero, J.M., Ginoux, P., Torres, O., Nicholson, S.E., Gill, T.E., 2002a. Environmental characterization of global sources of atmospheric soil dust identified with the Nimbus 7 Total

Ozone Mapping Spectrometer (TOMS) absorbing aerosol product. Rev. Geophys. 40, 2-1-2–31. https://doi.org/10.1029/2000RG000095

Prospero, J.M., Ginoux, P., Torres, O., Nicholson, S.E., Gill, T.E., 2002c. Environmental characterization of global sources of atmospheric soil dust identified with the Nimbus 7 Total Ozone Mapping Spectrometer (TOMS) absorbing aerosol product. Rev. Geophys. 40, 2-1-2–31. https://doi.org/10.1029/2000RG000095

Quéguiner, B., 2013. Iron fertilization and the structure of planktonic communities in high nutrient regions of the Southern Ocean. Deep. Res. Part II Top. Stud. Oceanogr. 90, 43–54. https://doi.org/10.1016/j.dsr2.2012.07.024

Remenyi, T.A., 2013. Investigating the impact of aeolian deposition to the Southern Ocean using dissolved aluminium concentrations. University of Tasmania.

Rodríguez, S., Prospero, J.M., López-Darias, J., García-Alvarez, M.I., Zuidema, P., Nava, S., Lucarelli, F., Gaston, C.J., Galindo, L., Sosa, E., 2021a. Tracking the changes of iron solubility and air pollutants traces as African dust transits the Atlantic in the Saharan dust outbreaks. Atmos. Environ. 246, 118092. https://doi.org/10.1016/j.atmosenv.2020.118092

Rossi, V., López, C., Hernández-García, E., Sudre, J., Garçon, V., Morel, Y., 2009. Surface mixing and biological activity in the four Eastern Boundary Upwelling Systems, Nonlin. Processes Geophys.

Schepanski, K., 2018. Transport of mineral dust and its impact on climate. Geosci. 8. https://doi.org/10.3390/geosciences8050151

Schlitzer, R., Anderson, R.F., Dodas, E.M., Lohan, M., Geibert, W., Tagliabue, A., Bowie, A., Jeandel, C., Maldonado, M.T., Landing, W.M., Cockwell, D., Abadie, C., Abouchami, W., Achterberg, E.P., Agather, A., Aguliar-Islas, A., van Aken, H.M., Andersen, M., Archer, C., Auro, M., de Baar, H.J., Baars, O., Baker, A.R., Bakker, K., Basak, C., Baskaran, M., Bates, N.R., Bauch, D., van Beek, P., Behrens, M.K., Black, E., Bluhm, K., Bopp, L., Bouman, H., Bowman, K., Bown, J., Boyd, P., Boye, M., Boyle, E.A., Branellec, P., Bridgestock, L., Brissebrat, G., Browning, T., Bruland, K.W., Brumsack, H.J., Brzezinski, M., Buck, C.S., Buck, K.N., Buesseler, K., Bull, A., Butler, E., Cai, P., Mor, P.C., Cardinal, D., Carlson, C., Carrasco, G., Casacuberta, N., Casciotti, K.L., Castrillejo, M., Chamizo, E., Chance, R., Charette, M.A., Chaves, J.E., Cheng, H., Chever, F., Christl, M., Church, T.M., Closset, I., Colman, A., Conway, T.M., Cossa, D., Croot, P., Cullen, J.T., Cutter, G.A., Daniels, C.,

Dehairs, F., Deng, F., Dieu, H.T., Duggan, B., Dulaquais, G., Dumousseaud, C., Echegoyen-Sanz, Y., Edwards, R.L., Ellwood, M., Fahrbach, E., Fitzsimmons, J.N., Russell Flegal, A., Fleisher, M.Q., van de Flierdt, T., Frank, M., Friedrich, J., Fripiat, F., Fröllje, H., Galer, S.J.G., Gamo, T., Ganeshram, R.S., Garcia-Orellana, J., Garcia-Solsona, E., Gault-Ringold, M., George, E., Gerringa, L.J.A., Gilbert, M., Godoy, J.M., Goldstein, S.L., Gonzalez, S.R., Grissom, K., Hammerschmidt, C., Hartman, A., Hassler, C.S., Hathorne, E.C., Hatta, M., Hawco, N., Hayes, C.T., Heimbürger, L.E., Helgoe, J., Heller, M., Henderson, G.M., Henderson, P.B., van Heuven, S., Ho, P., Horner, T.J., Hsieh, Y. Te, Huang, K.F., Humphreys, M.P., Isshiki, K., Jacquot, J.E., Janssen, D.J., Jenkins, W.J., John, S., Jones, E.M., Jones, J.L., Kadko, D.C., Kayser, R., Kenna, T.C., Khondoker, R., Kim, T., Kipp, L., Klar, J.K., Klunder, M., Kretschmer, S., Kumamoto, Y., Laan, P., Labatut, M., Lacan, F., Lam, P.J., Lambelet, M., Lamborg, C.H., Le Moigne, F.A.C., Le Roy, E., Lechtenfeld, O.J., Lee, J.M., Lherminier, P., Little, S., López-Lora, M., Lu, Y., Masque, P., Mawji, E., Mcclain, C.R., Measures, C., Mehic, S., Barraqueta, J.L.M., van der Merwe, P., Middag, R., Mieruch, S., Milne, A., Minami, T., Moffett, J.W., Moncoiffe, G., Moore, W.S., Morris, P.J., Morton, P.L., Nakaguchi, Y., Nakayama, N., Niedermiller, J., Nishioka, J., Nishiuchi, A., Noble, A., Obata, H., Ober, S., Ohnemus, D.C., van Ooijen, J., O'Sullivan, J., Owens, S., Pahnke, K., Paul, M., Pavia, F., Pena, L.D., Peters, B., Planchon, F., Planquette, H., Pradoux, C., Puigcorbé, V., Quay, P., Queroue, F., Radic, A., Rauschenberg, S., Rehkämper, M., Rember, R., Remenyi, T., Resing, J.A., Rickli, J., Rigaud, S., Rijkenberg, M.J.A., Rintoul, S., Robinson, L.F., Roca-Martí, M., Rodellas, V., Roeske, T., Rolison, J.M., Rosenberg, M., Roshan, S., Rutgers van der Loeff, M.M., Ryabenko, E., Saito, M.A., Salt, L.A., Sanial, V., Sarthou, G., Schallenberg, C., Schauer, U., Scher, H., Schlosser, C., Schnetger, B., Scott, P., Sedwick, P.N., Semiletov, I., Shelley, R., Sherrell, R.M., Shiller, A.M., Sigman, D.M., Singh, S.K., Slagter, H.A., Slater, E., Smethie, W.M., Snaith, H., Sohrin, Y., Sohst, B., Sonke, J.E., Speich, S., Steinfeldt, R., Stewart, G., Stichel, T., Stirling, C.H., Stutsman, J., Swarr, G.J., Swift, J.H., Thomas, A., Thorne, K., Till, C.P., Till, R., Townsend, A.T., Townsend, E., Tuerena, R., Twining, B.S., Vance, D., Velazquez, S., Venchiarutti, C., Villa-Alfageme, M., Vivancos, S.M., Voelker, A.H.L., Wake, B., Warner, M.J., Watson, R., van Weerlee, E., Alexandra Weigand, M., Weinstein, Y., Weiss, D., Wisotzki, A., Woodward, E.M.S., Wu, J., Wu, Y., Wuttig, K., Wyatt, N., Xiang, Y., Xie, R.C., Xue, Z., Yoshikawa, H., Zhang, J., Zhang, P., Zhao, Y., Zheng, L., Zheng, X.Y., Zieringer, M., Zimmer, L.A., Ziveri, P., Zunino, P., Zurbrick, C., 2018. The GEOTRACES Intermediate Data Product 2017. Chem. Geol. 493, 210–223. https://doi.org/10.1016/j.chemgeo.2018.05.040

Schroth, A.W., Crusius, J., Sholkovitz, E.R., Bostick, B.C., 2009. Iron solubility driven by speciation in dust sources to the ocean. Nat. Geosci. 2, 337–340. https://doi.org/10.1038/ngeo501

Sedwick, P.N., Sholkovitz, E.R., Church, T.M., 2007. Impact of anthropogenic combustion emissions on the fractional solubility of aerosol iron: Evidence from the Sargasso Sea. J. Earth Sci. 8, 1–21. https://doi.org/10.1029/2007GC001586

Shao, Y., Wyrwoll, K.H., Chappell, A., Huang, J., Lin, Z., McTainsh, G.H., Mikami, M., Tanaka, T.Y., Wang, X., Yoon, S., 2011. Dust cycle: An emerging core theme in Earth system science. Aeolian Res. 2, 181–204. https://doi.org/10.1016/j.aeolia.2011.02.001

Shelley, R.U., Landing, W.M., Ussher, S.J., Planquette, H., Sarthou, G., 2018. Regional trends in the fractional solubility of Fe and other metals from North Atlantic aerosols (GEOTRACES cruises GA01 and GA03) following a two-stage leach. Biogeosciences 15, 2271–2288. https://doi.org/10.5194/bg-15-2271-2018

Shi, Z., Krom, M.D., Bonneville, S., Baker, A.R., Jickells, T.D., Benning, L.G., 2009. Formation of iron nanoparticles and increase in iron reactivity in mineral dust during simulated cloud processing. Environ. Sci. Technol. 43, 6592–6596. https://doi.org/10.1021/es901294g

Shi, Z., Krom, M.D., Jickells, T.D., Bonneville, S., Carslaw, K.S., Mihalopoulos, N., Baker, A.R., Benning, L.G., 2012. Impacts on iron solubility in the mineral dust by processes in the source region and the atmosphere: A review. Aeolian Res. https://doi.org/10.1016/j.aeolia.2012.03.001

Sholkovitz, E.R., Sedwick, P.N., Church, T.M., 2009. Influence of anthropogenic combustion emissions on the deposition of soluble aerosol iron to the ocean: Empirical estimates for island sites in the North Atlantic. Geochim. Cosmochim. Acta 73, 3981–4003. https://doi.org/10.1016/j.gca.2009.04.029

Sholkovitz, E.R., Sedwick, P.N., Church, T.M., Baker, A.R., Powell, C.F., 2012. Fractional solubility of aerosol iron: Synthesis of a global-scale data set. Geochim. Cosmochim. Acta 89, 173–189. https://doi.org/10.1016/j.gca.2012.04.022

Simões Pereira, P., van de Flierdt, T., Hemming, S.R., Hammond, S.J., Kuhn, G., Brachfeld, S., Doherty, C., Hillenbrand, C.D., 2018. Geochemical fingerprints of glacially eroded bedrock from West Antarctica: Detrital thermochronology, radiogenic isotope systematics and trace

element geochemistry in Late Holocene glacial-marine sediments. Earth-Science Rev. https://doi.org/10.1016/j.earscirev.2018.04.011

Simonella, L.E., Gaiero, D.M., Palomeque, M.E., 2014. Validation of a continuous flow method for the determination of soluble iron in atmospheric dust and volcanic ash. Talanta 128, 248–253. https://doi.org/10.1016/j.talanta.2014.04.076

Strzelec, M., Proemse, B.C., Gault-Ringold, M., Boyd, P.W., Perron, M.M.G., Schofield, R., Ryan, R.G., Ristovski, Z.D., Alroe, J., Humphries, R.S., Keywood, M.D., Ward, J., Bowie, A.R., 2020. Atmospheric trace metal deposition near the Great Barrier Reef, Australia. Atmosphere (Basel). 11. https://doi.org/10.3390/ATMOS11040390

Swap, R., Ulanski, S., Cobbett, M., Garstang, M., 1996. Temporal and spatial characteristics of Saharan dust outbreaks. J. Geophys. Res. Atmos. 101, 4205–4220. https://doi.org/10.1029/95JD03236

Swap, R.J., Annegarn, H.J., Suttles, J.T., Haywood, J., Helmlinger, M.C., Hely, C., Hobbs, P. V., Holben, B.N., Ji, J., King, M.D., Landmann, T., Maenhaut, W., Otter, L., Pak, B., Piketh, S.J., Platnick, S., Privette, J., Roy, D., Thompson, A.M., Ward, D., Yokelson, R., 2002. The Southern African Regional Science Initiative (SAFARI 2000): Overview of the dry season field campaign. S. Afr. J. Sci. 98, 125–130.

Swap, R.J., Annegarn, H.J., Suttles, J.T., King, M.D., Platnick, S., Privette, J.L., Scholes, R.J., 2003. Africa burning : A thematic analysis of the Southern African Regional Science Initiative (SAFARI 2000). J. Geophys. Res. 108, 1–15. https://doi.org/10.1029/2003JD003747

Syvitski, J.P.M., 2003. Supply and flux of sediment along hydrological pathways: Research for the 21st century. Glob. Planet. Change 39, 1–11. https://doi.org/10.1016/S0921-8181(03)00008-0

Tagliabue, A., Bopp, L., Dutay, J.-C., Bowie, A.R., Chever, F., Jean-Baptiste, P., Bucciarelli, E., Lannuzel, D., Remenyi, T., Sarthou, G., Aumont, O., Gehlen, M., Jeandel, C., 2010. Hydrothermal contribution to the oceanic dissolved iron inventory. Nat. Geosci. 3, 252–256. https://doi.org/10.1038/ngeo818

Tatlhego, M., Bhattachan, A., Okin, G.S., D'Odorico, P., 2020. Mapping Areas of the Southern Ocean Where Productivity Likely Depends on Dust-Delivered Iron. J. Geophys. Res. Atmos. 125, 1–10. https://doi.org/10.1029/2019JD030926

Twining, B.S., Baines, S.B., 2013. The trace metal composition of marine phytoplankton. Ann.

Rev. Mar. Sci. 5, 191–215. https://doi.org/10.1146/annurev-marine-121211-172322

Tyson, P.D., Garstang, M., Swap, R., Kallberg, P., Edwards, M., 1996. an Air Transport Climatology for Subtropical Southern Africa. Int. J. Climatol. 16, 265–291.

Uno, I., Eguchi, K., Yumimoto, K., Takemura, T., Shimizu, A., Uematsu, M., Liu, Z., Wang, Z., Hara, Y., Sugimoto, N., 2009. Asian dust transported one full circuit around theglobe. Nat. Geosci. 2, 557–560. https://doi.org/10.1038/ngeo583

van der Does, M., Knippertz, P., Zschenderlein, P., Giles Harrison, R., Stuut, J.B.W., 2018. The mysterious long-range transport of giant mineral dust particles. Sci. Adv. 4, 1–9. https://doi.org/10.1126/sciadv.aau2768

Van Der Does, M., Korte, L.F., Munday, C.I., Brummer, G.J.A., Stuut, J.B.W., 2016. Particle size traces modern Saharan dust transport and deposition across the equatorial North Atlantic. Atmos. Chem. Phys. 16, 13697–13710. https://doi.org/10.5194/acp-16-13697-2016

Vickery, K.J., 2010. Southern African dust sources as identified by multiple space borne sensors. University of Cape Town.

Vickery, K.J., Eckardt, F.D., Bryant, R.G., 2013a. A sub-basin scale dust plume source frequency inventory for southern Africa, 2005-2008. Geophys. Res. Lett. 40, 5274–5279. https://doi.org/10.1002/grl.50968

Viljoen, J.J., Philibert, R., Van Horsten, N., Mtshali, T., Roychoudhury, A.N., Thomalla, S., Fietz, S., 2018. Phytoplankton response in growth, photophysiology and community structure to iron and light in the Polar Frontal Zone and Antarctic waters. Deep. Res. Part I Oceanogr. Res. Pap. 141, 118–129. https://doi.org/10.1016/j.dsr.2018.09.006

von Holdt, J.R.C., Eckardt, F.D., Baddock, M.C., Wiggs, G.F.S., 2019. Assessing Landscape Dust Emission Potential Using Combined Ground-Based Measurements and Remote Sensing Data, Journal of Geophysical Research: Earth Surface. https://doi.org/10.1029/2018JF004713

Wagener, T., Guieu, C., Losno, R., Bonnet, S., Mahowald, N., 2008. Revisiting atmospheric dust export to the Southern Hemisphere ocean: Biogeochemical implications. Global Biogeochem. Cycles 22. https://doi.org/10.1029/2007GB002984

Washington, R., Todd, M., Middleton, N.J., Goudie, A.S., 2003. Dust-storm source areas determined by the total ozone monitoring spectrometer and surface observations. Ann. Assoc.

Am. Geogr. 93, 297–313. https://doi.org/10.1111/1467-8306.9302003

Washington, R., Wiggs, G., King, J., Haustein, K., Thomas, D., Brindley, H., Murray, J., Bryant, R., Eckardt, F., Hewitson, B., Vickery, K., Nield, J., Woodwood, S., Jones, R., 1995. Dust Observations for Models – DO4Models 6.

Wiggs, G.F.S., Baddock, M.C., Bryant, R.G., Thomas, D.S.G., Eckardt, F., Washington, R., Engelstaedter, S., Nield, J., 2018. Combining field-based observations and remote sensing data to resolve aeolian dust dynamics at a globally significant source : Etosha Pan , Namibia 2018.

Winton, V., Bowie, A., Edwards, R., Keywood, M., Townsend, A., van der Merwe, P., Bollhfer, A., 2015. Fractional iron solubility of atmospheric iron inputs to the Southern Ocean. Mar. Chem. 177, 20–32. https://doi.org/10.1016/j.marchem.2015.06.006

Witt, M., Baker, A.R., Jickells, T.D., 2006. Atmospheric trace metals over the Atlantic and South Indian Oceans: Investigation of metal concentrations and lead isotope ratios in coastal and remote marine aerosols. Atmos. Environ. 40, 5435–5451. https://doi.org/10.1016/j.atmosenv.2006.04.041

Witt, M.L.I., Mather, T.A., Baker, A.R., De Hoog, J.C.M., Pyle, D.M., 2010. Atmospheric trace metals over the south-west Indian Ocean: Total gaseous mercury, aerosol trace metal concentrations and lead isotope ratios. Mar. Chem. 121, 2–16. https://doi.org/10.1016/j.marchem.2010.02.005

Wu, J., Rember, R., Cahill, C., 2007. Dissolution of aerosol iron in the surface waters of the North Pacific and North Atlantic oceans as determined by a semicontinuous flow-through reactor method. Global Biogeochem. Cycles 21, 1–10. https://doi.org/10.1029/2006GB002851

Yu, H., Chin, M., Yuan, T., Bian, H., Remer, L.A., Prospero, J.M., Omar, A., Winker, D., Yang, Y., Zhang, Y., Zhang, Z., Zhao, C., 2015. The fertilizing role of African dust in the Amazon rainforest: A first multiyear assessment based on data from Cloud-Aerosol Lidar and Infrared Pathfinder Satellite Observations. Geophys. Res. Lett. 42, 1984–1991. https://doi.org/10.1002/2015GL063040

CHAPTER 2: ORIGIN, SOLUBILITY, AND OCEAN IMPACT OF TRACE METAL AEROSOLS COLLECTED OVER A MAJOR IRON PORT

A presentation of the submitted research paper

This research manuscript has been submitted to the open access journal Atmospheric Environment: X. The submission is entitled “Origin, solubility and ocean impact of trace metal aerosols collected over a major iron port. I am the lead author of the manuscript. S. Fietz, F. D. Eckardt, R. Toesie and G. Ravenscroft are co-authors. I was responsible for the collection of field samples, all analyses, data processing and writing of the manuscript

This manuscript contributes the first information on trace metals and their solubility dust from a mixed (anthropogenic and natural) source. The data was compared to other similar sources, either natural or anthropogenic. This provided information on the fertilizing potential of this iron port as a source of micronutrients to the surrounding oceans. The aim is to better understand the impact that anthropogenic and mixed sources have on oceans as suppliers of micronutrients.

ORIGIN, SOLUBILITY, AND OCEAN IMPACT OF TRACE METAL AEROSOLS COLLECTED OVER A MAJOR IRON ORE PORT

K. Kangueehi [a], F. D. Eckardt [b], R. Toesie [c], G. Ravenscroft [d], S. Fietz [a*]

[a] Centre for Trace Metal and Experimental Biogeochemistry, Department of Earth Sciences, University of Stellenbosch, Stellenbosch, 7600, South Africa

[b] Department of Environmental and Geographical Sciences, University of Cape Town, Cape Town, 7701, South Africa

[c] Municipality of Saldanha Bay, Private bag x12, Vredenburg, 7380, South Africa

[d] Argos Scientific (Africa) Pty Ltd., INOSPACE (Metalheads) Business Park, Paarden Eiland, 7405, South Africa

*corresponding author: Department of Earth Sciences, Stellenbosch University, 7600 Stellenbosch, South Africa, sfietz@sun.ac.za, +27218083117

Keywords: Anthropogenic origin; GEOTRACES; Hysplit; Fractional solubility; Bioaccessilbility

2.1. ABSTRACT

Persistent red coloured dust experienced in town for most of the year prompted an investigation of the dust properties in the greater Saldanha Bay area, West Coast, South Africa. The town hosts the largest and deepest harbour as well as the largest ore terminal in South Africa. A large part of the dust in this area has presumably anthropogenic origins such as local industry combustion and mining ore exported through the port. Such dust can have local as well as far-reaching impact, for example, as a source of micronutrients to the open ocean, potentially fertilizing phytoplankton communities, and ultimately sequestering carbon dioxide from the atmosphere. Here, we are interested in the sources, pathways, and impact of dust from such an important economic hub in southern Africa. To achieve this, dust dispersion, mineralogy, trace metal composition and fractional solubility were investigated. Samples were collected with a Big Spring Number Eight (BSNE) in 2019 and used for mineralogical characteristics analysis and laboratory leaching experiments complementing five-year long dust bucket monitoring data. Scanning Electron Microscopy coupled with Energy Dispersive X-Ray (SEM-EDX) analysis revealed an abundance of quartz, magnetite, hematite, garnet, rutile, feldspars, galena and organic matter. Highest bulk trace metal concentrations were observed for Fe, Al, Zn, and Mn. Potentially toxic metals such as V, Pb, Cu occurred in bulk concentrations several orders of magnitude lower than Fe, Al, Mn and Zn. The trace metal soluble fractions in leaching experiments ranged from c. 0.1 to c. 5% of the bulk concentrations in pure water and c. 1 to c. 100% in weak acid. Sources and potential sites of deposition of the dust were further investigated for the period of the dust sampling. Polar plots showed that most particles originated inland (from northeast) although the dominant wind direction is from southwest. Forward trajectories indicated that most of the air masses, likely carrying the dust, travel either northwest along the west coast of southern Africa or southeast towards the southern Indian Ocean. In summary, our study suggests that a mixture of both natural and anthropogenic emissions through this important economic hub can supply highly soluble bioactive trace metals to surrounding oceans.

2.2. INTRODUCTION

The solubility of aerosols deposited into the ocean affects the nutrient, including trace metal, availability in the surface oceans. As a result, not only the total dust load, but also the aerosol solubility can stimulate or limit primary productivity, especially in the remote open ocean (Baker et al., 2006, 2016; Jickells, 2006; Schulz et al., 2012). The trace metal solubility and thus fertilising potential varies with the emission sources (Mahowald et al., 2018). The sources can either be natural, such as mineral dust (Schulz et al., 2012) and volcanic emissions (Olgun et al., 2011), or anthropogenic, such as industrial emissions and burning of biomass (Ginoux et al., 2012; Guieu et al., 2005; Hamilton et al., 2019; Piketh et al., 1999). In Africa most studies have focussed on the impact of natural dust on biogeochemical cycles due to the large number of sub-Saharan mineral dust emitters (Bhattachan et al., 2015; Dansie et al., 2017a,b, 2018). Nonetheless, globally, anthropogenic dust deposition on surface oceans also has an important impact on marine biogeochemical cycles (Ginoux et al., 2012; Mahowald et al., 2005) enhancing or potentially inhibiting primary productivity (Jordi et al., 2012; Paytan et al., 2009). This is especially important for southern Africa, because of its proximity to three different major oceanic regions, and strong reliance on the Blue Economy.

Aerosols sourced from industrial activities can provide essential trace metals to oceanic regions as they can contain concentrations of trace metals two orders of magnitude higher compared to natural sources (Sedwick et al., 2007; Sholkovitz et al., 2009). For example, aerosol particles that are produced from steel and iron ore industries are enriched in Fe, Mn, Zn, Cd and Cr (Dai et al., 2015; Hsu et al., 2021; Sylvestre et al., 2017). Primary productivity in oceans has increased by up to 6% in the 20th century due to industrialization (Mahowald et al., 2010), and it can reasonably be assumed that this is partially a consequence of elevated deposition of fertilising dust. The iron depositional flux in the Southern Ocean, for example, has increased by up to 73% in the current industrial era, compared to pre-industrial conditions (Matsui et al., 2018).

Several recent studies investigated the chemical composition and trace metal bioavailability in dust from natural southern African sources (Bhattachan et al., 2015; Dansie et al., 2017a,b). However, anthropogenic dust may be more soluble than natural mineral dust (Hamilton et al., 2019; Srinivas et al., 2012) and can contribute up to 80% of all soluble iron deposited in open oceans (Guieu et al., 2005; Luo et al., 2008; Sholkovitz et al., 2012). Investigations on the fractional solubility of anthropogenic dust from southern Africa are missing. Here, we will therefore contribute to the understanding of the potential impact of natural dust sources and anthropogenic activities on the marine environment, focussing on an important southern African economic hub, the harbour town of Saldanha Bay.

Port towns, such as Saldanha Bay (South Africa), can be hotspots of anthropogenic emissions due to the industrial activities related to the export and import of goods (Omidvarborna et al., 2021). Indeed, Saldanha Bay experiences persistent red coloured dust for most of the year (Figure 1), which prompted a five-year record (2015-2019) of bulk trace metal loads in dust aerosols that provides important context for this study. Complementing this long-term record of bulk metal loads, the first objective of this study is to determine the dust aerosol particle sizes and mineralogy that are influenced by the source geology and industrial chemical processing (e.g., mining and smelting of the ore) and in turn impact the suspension time and solubility (Desboeufs et al., 2005; Journet et al., 2008; Paris et al., 2011). The second objective of this study is to determine the bulk trace metal concentrations and actual solubility, because the impact on the marine environments such as on the primary productivity and biogeochemical cycles is particularly influenced by the bioavailable fraction in the dust (Chen et al., 2012; Spokes and Jickells, 1995).

In summary, the main aim of this study is to understand how the southern African dust of mixed, anthropogenic and natural origin can impact proximal oceans. For this purpose, we (i) characterize the mineralogical composition (ii) attempt a source assessment (iii) determine the trace metal bulk load and fractional solubility and (iv) project how the dust may impact proximal oceans.

***Figure 1**. (a, b, c). Red iron-ore rich stain that can often be observed around Saldanha Bay. (d) Open wagon trains that transport iron ore from the Northern Cape mines approximately 800 kilometres away from Saldanha Bay.*

2.2.1. Study Area

Saldanha Bay is located on the west coast of South Africa (33°02′05″S 18°00′35″E), approximately 100 km north of Cape Town and is directly adjacent to a shallow, tidal lagoon (Figure 2). Saldanha Bay covers an area of approximately 25 km by 10 km and in 2011 hosted a population of ca. 115 200 (Western Cape Government, 2019). The area experiences dry, hot summer months and cool winters with an annual average rainfall of 280 mm between April and September.

Dust emissions due to local industrial activities: Saldanha Bay and neighbouring Vredenburg are two of the fastest growing towns in the Western Cape, South Africa, with considerable industrial development occurring in the area. Base metals such as Mn, Zn and Pb are transported through the port, while a heavy mineral smelter and a crude oil storage near the port (Figure 2) might contribute to local anthropogenic emissions (Clark et al., 2020).

Emissions that result from ore transport and storage: Saldanha Bay is home to the deepest and largest natural port in southern Africa, exporting over 60 million tons of manganese and iron ore from the Northern Cape and North West Provinces of South Africa to the Middle East annually (Atkinson et al., 2006; Naidoo and Reddy, 2009). Approximately 2 million tons of iron ore is annually processed in the Saldanha Steel plant (Naidoo and Reddy, 2009). A relatively small fraction is exported directly from the mines through the port. The large remainder of the iron ore is stored before being exported. Dust emissions usually occur during this storage phase. Other pollutants may be a result of mining-related transport activities such as combustion. The metal ore is transported by train from these mining towns and then transferred to open conveyor belts before being loaded onto cargo ships. The export of iron ore from the port has been increasing since 2011 from less than 500 000 tons to more than 2 million tons in 2018 (Clark et al., 2009). Manganese export from the town started in 2013/2014 with approximately less than 100 000 tons of ore to more than 4.5 million tons of ore in 2017/2018.

Table 1. *Station coordinates for BSNE (2019) samplers. All locations are shown in Figure 2.*

Sampling Stations	**Latitude [°N]**	**Longitude [°E]**
CA	-32.95	17.97
SWA	-32.99	17.97
NNA	-32.92	17.98
NEA	-32.93	18.07

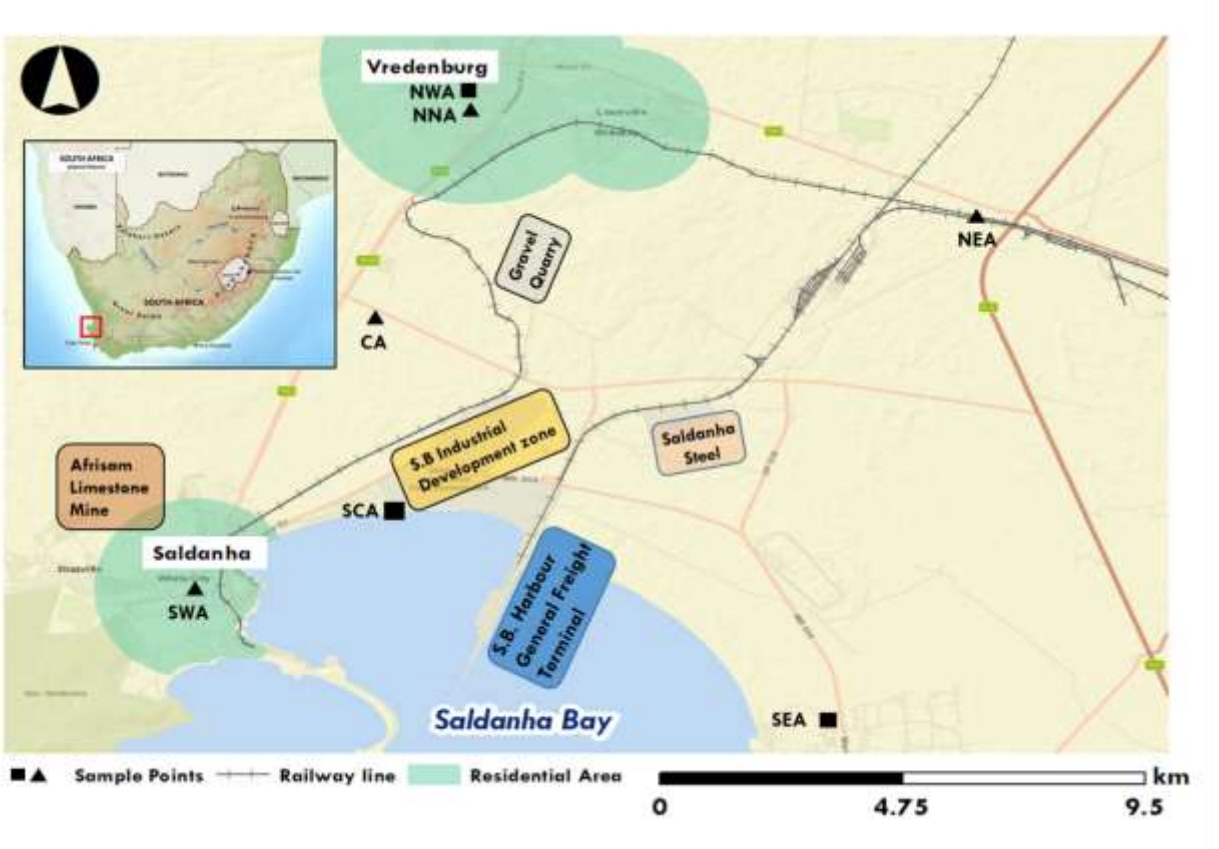

Figure 2. *Sampling locations in Saldanha Bay and neighbouring Vredenburg. Vredenburg is in the northern part of the greater Saldanha Bay area (Stations NNA and NEA) and Saldanha Bay is located in the southern part (Stations SWA and CA), close to the harbour. Coordinates for all stations are given Table 1. The railway line that services the Bay is located close to NEA. The insert shows the location of Saldanha Bay in a map of Southern Africa. The triangles show the BSNE samples, while the squares and triangles combined show the location of the dust bucket samples.*

2.3. METHODS

2.3.1. Five-year long record of bulk dust metal load

Monthly dust samples for metal load and composition were collected in seven dust buckets strategically situated in the greater Saldanha Bay area (i.e., close to potential sources of aerosol emissions in the area; (Figure 2) from 2015 and 2019. Fall-out rates per year were determined by dividing the samples total weight by sampled period. The data from the dust buckets were used to examine the spatial distribution of total dust fall-out rates and net metal masses (e.g., Pb, Mn, Fe, Cu and Zn). The analysis was conducted in the SGS Environmental Laboratory in Randburg, South Africa, a South African National Standards (SANS) 17025 accredited facility. An overview summary of the ranges will be provided in the main section of this paper to provide context to our target 2019

BNSE sampling. For details on the methodology and monitoring data, the reader is referred to the Section S.1.1. Five year long monitoring of monthly metal load.

2.3.2. Target BSNEs sampling and bulk trace metal analysis

The BSNE dust samplers were set-up at four stations (Figure 2, Table 1) for 12 months from January 2019 to January 2020. The BSNE-samples were split into two sub-samples and used for i) determination of trace metal composition of the bulk dust (~0.1 g), and ii) fractional solubility leaching experiments (~0.15 g). The bulk dust was analysed with an Agilent 7900 Inductively Coupled Plasma Mass Spectrometry (ICP-MS) at Stellenbosch University following digestion with HNO_3**.** The trace metals had an internal standard accuracy range from 96 to 108% by repeat analysis (n=10).

2.3.3. Aerosol trace metal leaching experiments

The bioavailability refers to the fraction of trace nutrients that can be utilised by microorganisms, and solubility serves as a suitable surrogate for bioavailability (Jickells et al., 2016; Moskowitz et al., 2016). Leaching experiments are widely used in the GEOTRACES community to determine the fractional solubility (Aguilar-Islas et al., 2010; Berger et al., 2008; Schlitzer et al., 2018; Winton et al., 2015) and have shown that trace metal solubility in dust aerosols can greatly vary. For example, a wide range of fractional solubility for iron ranging from 0.01% to c. 80% was observed. This variability was partially attributed to different mineralogical characteristics in dust derived from various sources and to differences in experimental methods (e.g., (Aguilar-Islas et al., 2010; Schroth et al., 2009; Baker et al., 2006; Shelley et al., 2018; Sholkovitz et al., 2012). Hence here we use two leaching experiments using a pure water and a weak acid approach.

The BSNEs sub-samples were used for these leaching experiments that were conducted in a sequential manner with a trace metal clean flow through method following Aguilar-Islas et al. (2010) and Winton et al. (2015). All bottles and filters used in the leaching experiments were acid cleaned according to GEOTRACES protocols (Cutter et al., 2017). The system consisted of acid-washed 47 mm diameter Whatman 41 cellulose filters with 20 µm nominal pore size, which were mounted to a single-staged PFA funnel stage connected to a front face. A peristaltic pump was used to pump the leachate at 24 rpm to push through 50 ml of solvent over approximately 10 min. The same set-up was used for a duplicate dust loaded filter and a blank.

2.3.4. Milli-Q water leachate to determine the instantaneous water dissolvable fraction

The Milli-Q water was used for the first leachate using the flow-through system described above (50 mL, 10 min). The leachates were analysed using the same Agilent 7900 ICP-MS at Stellenbosch University as used for bulk metal analysis (cf. 3.2). The leachates were acidified to 2% final acid concentration using ultra-pure HNO_3 and particulates were left to settle out prior to analysis. Previously published, similar continuous flow-through experiments indicated that the bioavailable and easily available iron and other trace metal fractions could be extracted with Milli-Q water within the first 10 minutes (Wu et al., 2007). This instantaneous water dissolvable trace metal fraction is calculated following Winton et al. (2015), Eq. 1:

$$TM_{MilliQ}(\%) = \frac{TM_{MilliQ-leach}}{TM_{bulk}} x100 \qquad \text{(Eq. 1).}$$

In Eq. 1, TM_{MilliQ} refers to the fractional solubility of the respective trace metal, TM_{bulk} refers to the trace metal's concentration in the bulk sample, and $TM_{MilliQ\text{-}leach}$ refers to the respective trace metal concentration in the Milli-Q leachate. After the leaching with Milli-Q water, the filters were used for further weak acid leaching experiments (cf. 3.3.2).

2.3.5. Weak acid leachate to determine the labile trace metal fraction

The reactive, labile fraction was determined following Berger et al. (2008) and Winton et al. (2015) using 25% glacial acetic acid (HAc) and hydroxylamine hydrochloride ($Na_2OH{\cdot}HCl$). After the Milli-Q water leaching (section 3.3.1), the same filters were transferred into acid-washed vials, dried in the laminar flow hood, and leached with 25% ultra-high purity HAc and 0.02 M ($NH_2OH{\cdot}HCl$) at 90 °C for 10-15 min. The heating process enables dissolution of an additional labile fraction and acid-soluble fraction (Winton et al., 2015), as the traditional 25% HAc room temperature leach tends to underestimate the labile metal fraction (Berger et al., 2008; Chester and Hughes, 1967). Such underestimation of the labile metal fraction is of particular concern in coastal areas such as Saldanha Bay with high abundance of terrestrial iron coated particles. In addition, the heating step also serves to liberate the trace metals found in intracellular proteins in phytoplankton (Berger et al., 2008) and assists to release trace materials such as iron and manganese oxyhydroxides from biogenic materials (Bayon et al., 2004). The leachates were acidified with 2% HNO_3 solution and analysed with an ICP-MS as described for bulk metal analysis above (cf. 3.2). The fractional solubility in the weak acid was calculated according to Eq. 2 following Winton et al. (2015) similarly as shown in Eq. 1 for Milli-Q leachates:

$$TM_{acid}(\%) = \frac{TM_{acid-leach}}{TM_{bulk}} x100 \quad \text{(Eq. 2).}$$

In Eq. 2, TM_{acid} refers to the fractional solubility of the respective trace metal, TM_{bulk} refers to the trace metal's concentration in the bulk sample, and $TM_{acid\text{-}leach}$ refers to the respective trace metal concentration in the weak acid leachate. The bioaccessible fraction is considered as sum of the fractional solubility in Milli-Q (cf. 3.3.1) and weak acid.

2.3.6. Statistical analysis

All solubility experiments were conducted as duplicates due to the limited amount of collected dust and average measurements were reported. The reported errors represent one standard deviation.

2.3.7. Enrichment factor

Enrichment factors are determined by calculating elemental ratios of trace metals relative to the crustal composition (Eq. 3).

$$EF = [\frac{X}{Al}]_{aerosol} / [\frac{X}{Al}]_{UCC} \quad \text{(Eq. 3).}$$

In Eq. 3, EF is the enrichment factor, $[X/Al]_{aerosol}$ is the molar ratio of element X to Al in the sample aerosol, while $[X/Al]_{UCC}$ is the reference ratio of element X to Al in the upper continental crustal (UCC) (Yaroshevsky, 2006). Such enrichment factors provides important information on the primary source of aerosols, i.e., whether they are natural or anthropogenic. For example, high EF ratios for elements such Pb and V are an indication of air pollution from fuel combustion emissions (Shelley et al., 2017).

2.3.8. Scanning Electron Microscope (SEM) analysis

One dust sample was used for petrographic characterization as well as to visualize particle types and to illustrate where specific trace metals are located within the different mineral particles. This sample was collected with a BSNE trap at station NEA (Figure 2). The dust sample was spread evenly on a thin section for preparation and then lightly coated with either carbon or gold before being examined using a Zeiss MERLIN FE-SEM at the Stellenbosch University Central Analytical Facilities. This instrument was operated at secondary electron with an accelerating voltage of 5 kV, sample current at 250 pA and the stage was set at 3mm working distance. For the backscattered electrons, the working

distance was set at 9.5 mm with a sample current of 11 nA. For mineral identification and characterization, Cryo-energy-dispersive X-ray spectrometry (cryo-EDS) was used. The EDS spectra particles were observed at an accelerating voltage of 15kV.

2.3.9. Air Mass Pathways

The Hybrid Single Particle Lagrangian Integrated Trajectory Model (Hysplit; Stein et al., 2015; Rolph et al., 2017) is widely utilized to study atmospheric dispersion and suspended aerosols transport for example in dust events and volcanic emission (Ashrafi et al., 2014; Bhattachan et al., 2012; Mcgowan and Clark, 2008; Stein et al., 2015; Tatlhego et al., 2020). The Hysplit modelling software was used in this study to generate backward and forward trajectories to determine the source and pathways of aerosols emissions into and from Saldanha Bay (-32.95 ◦S, 17.97 ◦E). The trajectories were calculated with one at each elevation of 50m, 500m and 1000 m above ground level. The simulations were calculated for seven days (168 hours) for both forward and backward trajectories. The first week of each month was used as dates for the models. The total simulated trajectories were classified based on different wind directions and percentages were calculated to determine the dominant air mass pathway direction.

In addition, dispersion models were run for the first five days of each month in 2019 using the splitR package in R (available from https://github.com/rich-iannone/SplitR) and Openair (Carslaw and Ropkins, 2012) packages from the open-source libraries. The parameters used were as follows: emission rate was set at 5 mass units per hour, starting height of 50 m above ground level, with the global NCEP Reanalysis data used for the synoptic state. The single particles were emitted for 2 hours at an emission rate of 5 mass units per hour. The particle diameter was set to 15 µm, density to 1.5 g/cm^3 and a shape factor to 0.8.

2.3.10. Polar Plots

Ambient concentrations of particulates of less than 10 and 2.5 µm in diameter were measured at the Saldanha Bay and Vredenburg monitoring site according to the latest South African Ambient Air Quality Standards methods (https://saaqis.environment.gov.za/). Polar plots were created using the 2019 data for wind speed and direction coupled with particulate matter (smaller than 10 µm (PM_{10}) and smaller than 2.5 µm ($PM_{2.5}$ in diameter). The wind speed and direction were measured using anemometers located on top monitoring containers in both Saldanha Bay (SWA) and Vredenburg (NNA). The wind data and PM_{10} and $PM_{2.5}$ data were recorded on 5 minute averages between January

and December 2019. The polar plots were plotted using the Openair package (Carslaw and Ropkins, 2012) using the Rstudio interface.

2.3.11. Data availability

Data for the five-year long monitoring study are publicly available through the Municipality of Saldanha Bay (https://sbm.gov.za/environmental/). Data for bulk metal concentrations and soluble fractions is noted in Section 2.12 (.cvs).

2.4. RESULTS

2.4.1. Synthesis of the five-year long dust monitoring

The monthly dust samples for metal load and composition were collected in seven dust buckets strategically situated (close to potential sources of aerosol emissions in the area) from 2015 and 2019. Details are provided in Supplemental Material Section S1. The total suspended dust particles fall-out annual average rates between 2015 and 2019 ranged from 63 to 135 mg m^{-2} d^{-1} (Table S2). 92% of all samples collected at all seven stations (i.e., 315 out of 342 samples) had annual average dust fall-out rates lower than 250 mg m^{-2} d^{-1}. As such all mean dust fall-out rates can be categorised as "low" following South Africa governmental air quality guidelines (https://saaqis.environment.gov.za/). A high spatial variability was observed among the seven different stations (Supplemental Material S.1.3.a). Among the four stations used for the BSNE sampling, the central station (CA; Table 2) had the highest (254 ± 161, Table S3) and the southwest (SWA) station had the lowest (40 ± 23; Table S3) mean dust fall-out rate over the five-year period. The bulk dust collected from 2015 to 2019 contained elevated annual mean net metal masses, such as Fe (110092 ± 40900 ppm, five-year average ± SD), Pb (2051 ± 1284 ppm), Cu (38 919 ± 1089 ppm), Zn (3578 ± 1620 ppm) and Mn (13 636 ± 9310 ppm) (Table S2).

Trace metal spatial distribution was not homogenous, likely reflecting the industrial activity in the area. Importantly, stations with the highest dust collected by weight mass did not have the highest net metal masses as illustrated in Figure S1. For example, southwestern and northern stations (SWA, NNA) with lowest dust load had relatively high net metal masses, whereas the central station (CA) had a high average dust load but relatively low net metal masses (Figure S1). Occasionally, monthly data revealed extremely high net metal masses. The greatest monthly spikes in trace metals were found at north-eastern station (NEA) for example for Pb (7563 ppm) in 2017 and Fe (110 092 ppm) in 2015 (Figure S1).

Bulk dust load and metal composition also differed between years, and even some significant interannual differences were observed (for details, the reader is referred to S.1.1). Here, we are particularly interested to provide context for our 2019 BSNE sampling. Annual average dust fall-out rate in 2019 was 112 ± 144 mg m^{-2} d^{-1} (Table S1), and it was not significantly different from previous years. We thus consider our sampling year 2019 and our selected stations CA, SWA, NEA and NNA as reasonable representatives of the area and years. This selected stations were strategically positioned in all the parts of the town were high dust yield was observed from the five-year dust bucket data.

Table 2*. Total trace metal concentrations of aerosols from Saldanha Bay collected using the BSNE traps from January 2019 to January 2020. All trace metal concentrations are reported in ppm.*

Stations	Dry weight (mg/y)	V	Cu	Pb	Al	Mn	Fe	Zn
CA	127	15.5	20.5	28.0	14 121	437	13 669	4 366
NEA	163	15.9	30.1	14.0	12 402	1141	19 115	15 983
NNA	87	17.8	66.8	1175	17 620	1830	33 380	24 778
SWA	99	14.7	35.2	30.5	26 029	200	11 440	24 63

2.4.2. Total weight and total trace metal concentrations in the 2019 BSNE samples

The 2019 BSNE bulk dust collection is largely in agreement with the five-year long monitoring. For example, stations CA and NEA had some of the highest dust loads throughout the 2015-2019 municipal monitoring (20 – 741 and 6 - 2021 mg/m^2/day, respectively; Table S3), as well as when collected using the BSNE traps in 2019 (127 and 163 mg/y, respectively; Table 2). Furthermore, the dust load collected using the BSNE traps in 2019 was lowest at NNA and SWA (87 and 99, respectively; Table 2) similar to the 2015-2019 municipal monitoring (4 - 122 and 8 – 105 mg/m^2/day, respectively; Table S3).

As had been mentioned for the five-year long monitoring (Figure S3), dust loads were not necessarily reflected in trace metal concentrations (Table 2). For example, the northern station NNA had lowest dust load of all stations, but particularly high concentrations for most trace metals, such as Pb (~1175 ppm), Cu (~67 pppm), Mn (~ 1830) and Fe (~33 380 ppm) (Table 2). In comparison, Pb only ranged between ~14 and ~31 ppm and Cu only between ~20 and ~35 ppm at stations CA, NEA and SWA

(Table 2). Southwestern station SWA, in contrast, had highest concentrations of Al (26 029 ppm). The V concentrations ranged from ~15 to 18 ppm at all stations. Vanadium was not analysed in the 2015-2019 monthly long-term monitoring (cf. 4.1), but is documented here for the 2019 BSNE samples because it can be used as a proxy for combustion and anthropogenic emissions (Shelley et al., 2017).

Enrichment factors for V, Pb, Fe, Mn, Zn and Cu were calculated to support distinguishing natural from anthropogenic dust sources. Most stations displayed enrichment factors below 10 (Table 3) for trace metals V, Mn, Cu and Fe which is an indication that these stations receive mainly lithogenic dust. However, Zn displayed a strong enrichment at all stations (Table 3).

Table 3*. Enrichment factors in dust aerosols from Saldanha Bay collected using the BSNE samples from January 2019 to January 2020.*

Stations	**V**	**Cu**	**Pb**	**Mn**	**Fe**	**Zn**
CA	1.0	2.5	9.7	2.5	1.7	327
NEA	1.1	4.1	5.6	7.3	2.7	1255
NNA	0.9	6.5	334	8.3	3.2	1239
SWA	0.5	2.3	5.9	0.6	0.8	849

2.4.3. Mineralogical characteristics

SEM imagery and chemical mapping using false coloration were used to identify dominant minerals for samples collected at the northeastern station NEA. Station NEA was chosen amongst the BSNE samples because of its proximity to the railway line that imports iron ore from the Northern Cape mines. SEM allows assessing the dust grain sizes, shapes and aggregate assemblages. The grain shapes in Saldanha Bay can be grouped into two different types, (i) spherical type and (ii) angular/clustered and agglomarated grains. An additional sample collected using VFC from the south-western station SWA illustrating especially the angular/clustered and agglomarated grains grain types is outlined in Section S.2. Volumetric Flow Controlled (VFC) sample supporting bulk metal composition and mineralogical characteristics

The spherular shaped particles were dark red or black in color and fine grained while the angular clustered grains were coarser than spherical grains. Most of the grains ranged from single to clustered sharp edged with sizes ranging from 20 to 5000 nm. Some of the larger (~10 µm) spherical particles had rough surfaces, while medium to fine grained particles were smooth and with soft edges,

especially the very fine grained particles (~5 µm) (` 3). Some spherical particles showed porous texture, which could be an indication that the particles are soluble.

In addition to the shape characteristics, SEM-EDS microanalysis was conducted to study mineralogical composition with emphasis on the trace metals of interest identified above (section 4.1 and 4.2). Most of the spherular particles were ferromagnetic particles (Figure 4). Such iron micro-spherules characteristically have a perfect spherical shape with a very complicated texture (Zhang et al., 2014). This may cause the red dust colouration that is prominent especially during the winter months (Clark et al., 2020) and can be observed everywhere in Saldanha Bay, ranging from building roofs, stains on house walls, on roads and along the railway line (Figure 2) (Naidoo and Reddy, 2009). The spherular particles were collected in the central to eastern part of Saldanha Bay at station NEA located close to a smelter and railway line where ore is transported through the town (Figure 2) and the dust collected at this station also had high Fe, Mn and Pb concentrations (Table 2). The elemental maps of samples from NEA showed that metals such Fe, Pb, S and Al prevailed in the particles (Figure 4). In addition, the elemental mapping showed an overlapping of Pb, Fe and S. Approximately 50% of the coarse particles (>5 µm) were coated with S, which is an indication that sulfate precipitated from gas to particle interactions in the atmosphere (Li et al., 2017).

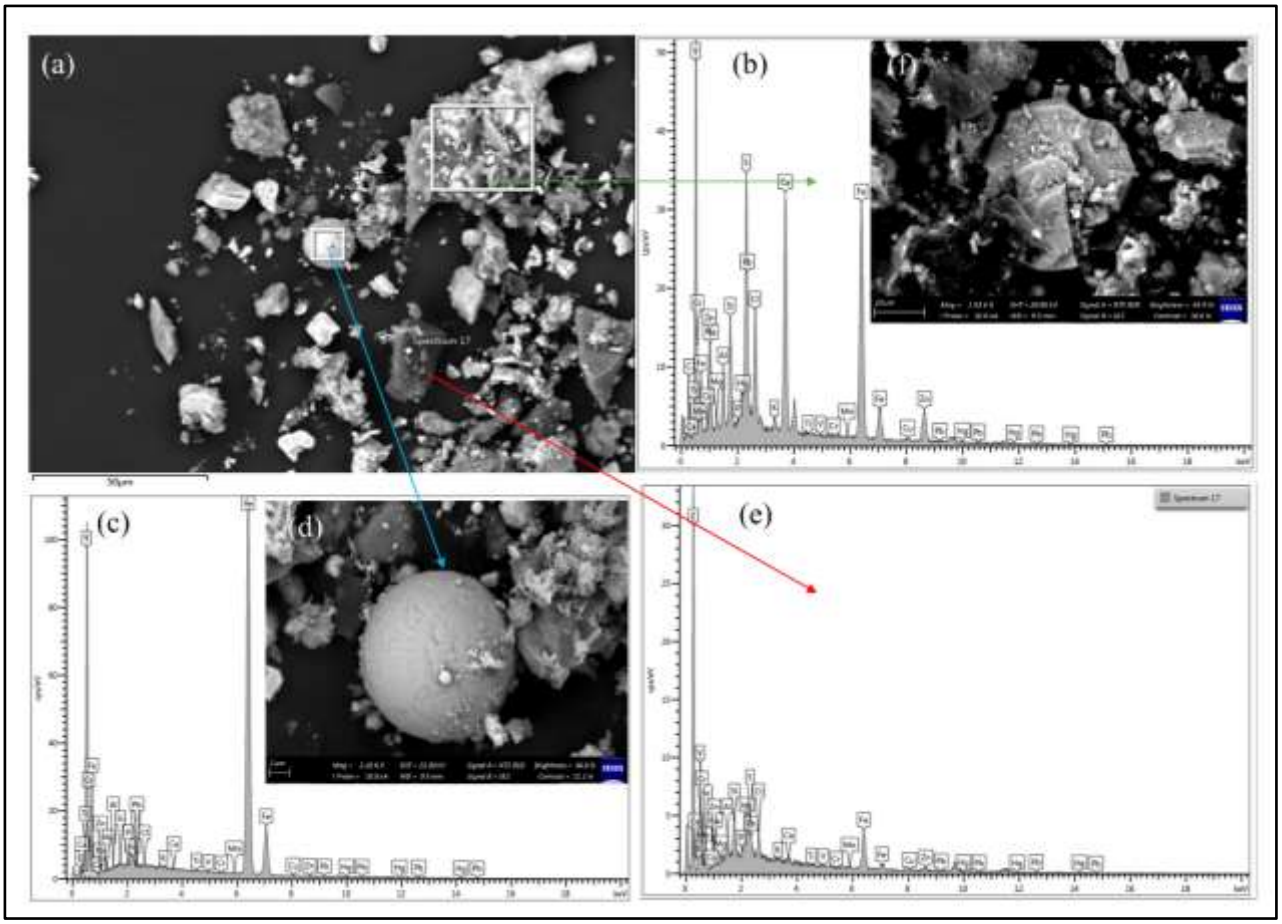

***Figure 3**. Particles, including iron microspherules also known as ferrospheres observed using SEM-EDS in a Saldanha Bay dust sample collected at Station NEA (close to the railway area; see Fig 2 for location). (a) agglomerates including spherular particles, (b) micrograph of a agllomerated particles spot indicated by the square box in panel (a), (c) micrograph of a spherule particle from an individual spherular particle showing high iron content, (d) magnified image of the spherular particles, showing much smaller particles within the larger agglomerate (e) micrographs that was obtained at position Spectrum 17 indicated in panel (a), (f) magnified image of the agglomerated particles, showing sub-angular particles.*

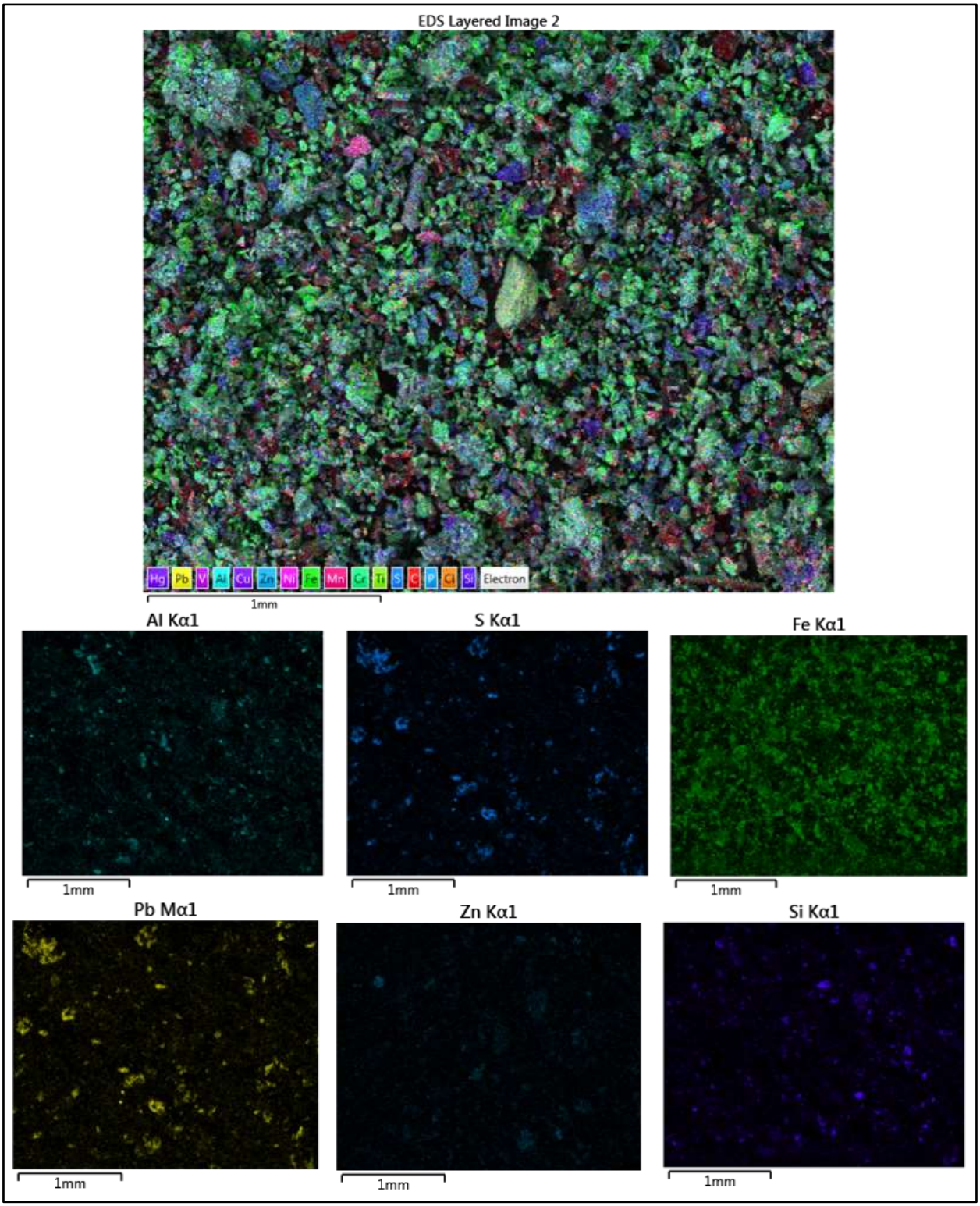

Figure 4*. SEM elemental maps showing the abundance of selected elements in particles collected at station NEA (see Figure 2 for location) using the BSNE sampler. Individual elemental maps for some of the trace metals of interest as well as Si and S which are abundant in the area.*

2.4.4. Trace metal solubility in the BSNE samples

The results presented in this section are from leaching experiments using the dust from Saldanha Bay collected using the BSNE samplers at stations NEA, NNA, CA, and SWA. Milli-Q® as well as hydroxylamine hydrochloride were used as leachates.

2.4.5. Milli-Q leach

The highest concentrations of some trace metals in the Milli-Q leachates were found at station NNA, especially for Fe (c. 140 ppm) and Pb (c. 8 ppm) (cf. Figure 5). Highest concentrations of Al and Mn in the Milli-Q leachates were found at station CA (c. 210 and c. 20 ppm, respectively). Other trace metals such as V (<0.15 ppm) and Cu (<1.7 ppm) were observed in low concentrations in the Milli-Q leachates at all stations (see Section 2.12).

The fractional solubility in Mill-Q (i.e., the portion of trace metals leached with Mill-Q water as a percentage fraction of the bulk trace metals presented in section 4.2) ranged from 0.06 to 0.9 % for Pb, 0.08 to 0.5 % for Fe, 0.1 to 1.5 % for Al, 0.07 to 1.9 % for Zn, 0.6 to 4.2 % for Cu and 0.25 to 0.75 % for V (Table 4, Figure 5). The spatial distribution of highest and lowest solubilities is similar to the aforementioned distribution in concentrations, i.e., highest fractional solubility was observed at NNA for Fe and Pb, while highest fractional solubility for Al and Mn was found at CA (Figure 5).

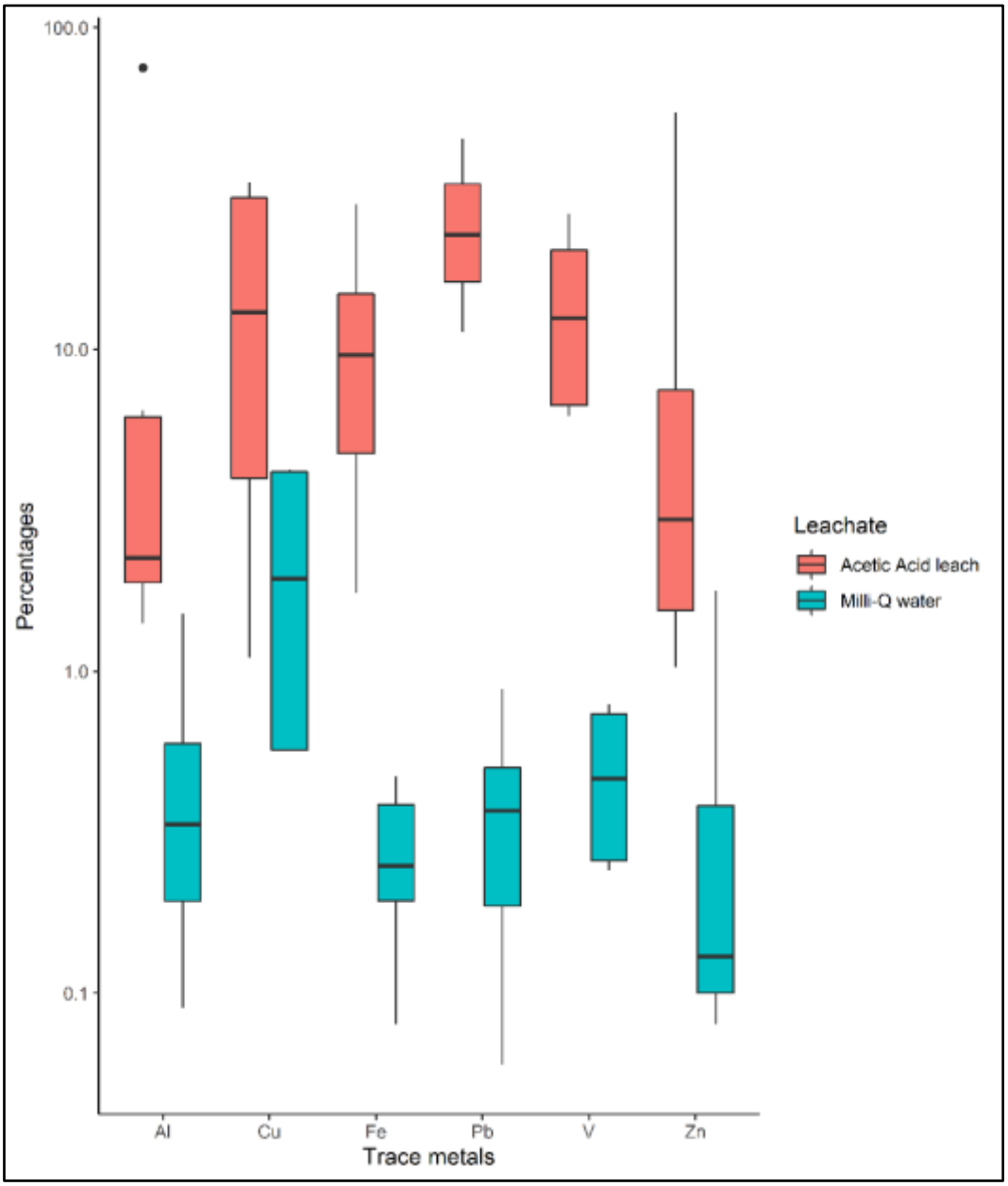

Figure 5*. Solubility as concentration in leachate per bulk concentration (%) of the different trace metals when leached with Milli-Q water and a weak acid. The line shows the upper and lower limit while the single dots represents the outliers.*

***Table 4**. Solubility of example trace metals expressed as concentration in leachate per bulk concentration (%) when leached with Milli-Q water and a weak acid. The sum of the two fractional solubilities (not shown) is considered the labile or bioaccessible fraction.*

Trace metals	Solubility (%) in Milli-Q water	Solubility (%) in weak acid leach
Fe	0.2 to 0.5	1.8 to 28
Al	0.1 to 1.5	1.4 to ~100
Zn	0.07 to 1.9	1.0 to 54
Pb	0.07 to 0.9	11 to 45
Cu	0.6 to 4.2	1.1 to 33

2.4.6. Hydroxylamine hydrochloride leach

In the weak acid leachate, the solubility pattern differed from the solubility in the Mill-Q leachate. Highest concentrations of Al in the weak acid leachates were found at station CA (c. 13300 ppm), while highest concentrations of Fe, Mn and Cu were all observed at station CA and NEA (Table S2). In contrast, weak acid leached Pb was highest at NNA (c. 440 ppm) (Figure 6). These labile soluble fractions (i.e., the portion soluble with the hydroxylamine hydrochloride acid) ranged from c. 2 to c. 28% for Fe, c. 4 to c. 100 % for Al, c. 11 to 45 % for Pb, c. 1 to 33% for Cu, and c. 3 to 30% for V (Figure 5)

The leaching by hydroxylamine hydrochloride acid is significantly stronger compared to the Milli-Q leaching for V and Pb ($p < 0.05$), as well as Al, Mn, Fe and Zn ($p < 0.01$). For example, Pb concentrations leached with hydroxylamine hydrochloride at some stations, such as NEA and CA were more than 100 times higher than when leached with Milli-Q water. However, there was no significant difference for Cu ($p = 0.3$) between the Milli-Q and hydroxylamine hydrochloride leachate. This indicates that the often-assumed stronger leaching with hydroxylamine hydrochloride acid compared to Milli-Q leaching is selective, i.e., some metals are released much stronger, while leaching for others does not differ significantly.

As mentioned above (Section 4.1; Figure S1), the dust load did not necessarily reflect the highest bulk trace metal concentrations. In addition, the leaching experiments show that dust load with low trace metal concentrations, can carry very soluble particles. For example, station CA was characterised by relatively high dust load and relatively low bulk metal concentrations (Table 2), but the sum of the soluble fractions at this station was highest for most trace metals (Figure 6). In contrast,

station NNA that experienced lowest dust loads, but relatively high bulk metal concentrations (Table 2), was characterised by mostly low (except for Pb) solubility (Figure 6).

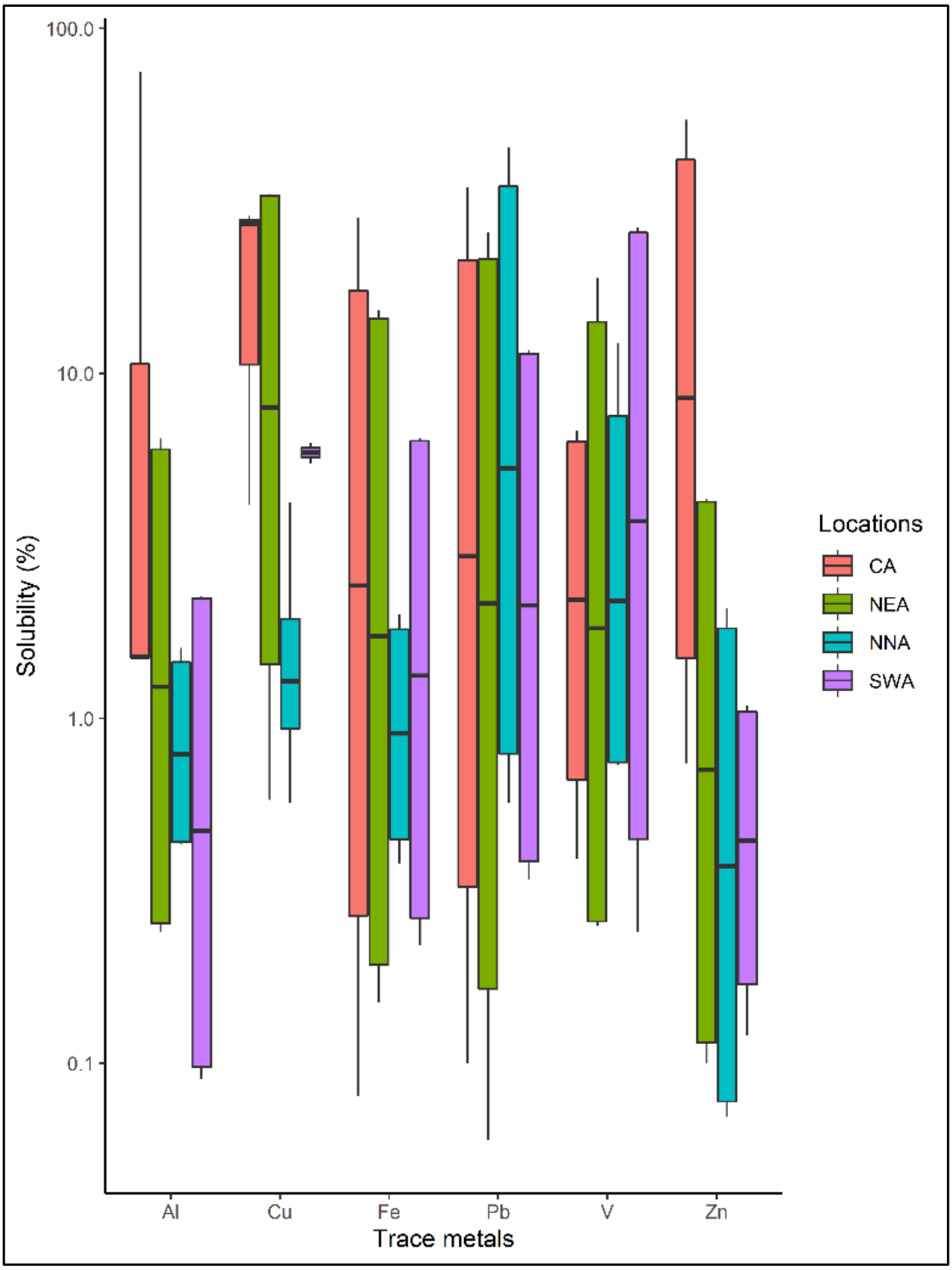

Figure 6. *Solubility (%) at the four sampling locations in the Milli-Q and the weak acid leachates combined. The line shows the upper and lower limit while the single dots represents the outliers.*

2.4.7. Local and long-range dust transport

2.4.7.1. Dust sources

Strong winds from the southwest dominate close to Saldanha Bay. Hysplit backward modelling indeed indicated that long-range air masses over Saldanha Bay are influenced predominantly by southwesterly and to a lesser extent by westerly winds. The Hysplit models indicated that ~63% of the air masses originate from the Atlantic Ocean. The second dominant wind direction is from the south and southeast, while few air masses are from inland (from northeast), either over the Kalahari Desert or along the Namib Desert (not shown). These occasional strong winds from the northeast, however, are prone to transport most of the particles. To support our understanding of the local transport and distribution of aerosol particles, wind roses in combination with PM_{10} and $PM_{2.5}$ data were used to construct polar plots (Figure 7). The polar plots indicate that particles at station SWA were sourced mostly from east and northeast probably affected by the Saldanha Bay freight terminal and industrial area located in this pathway (Figure 7). The distribution of PM_{10} and $PM_{2.5}$ appeared to be not influenced by wind directions. At station NNA, PM_{10} particles are mainly originate from south-to-southwest, likely influenced by the Saldanha Bay industrial area and potentially by the gravel quarry. The polar plots further indicated that at this station (NNA), most of the fine particles were sourced from the northeast potentially from the sand mines located northeast of Vredenburg (Figure 7). Most particles are being transported from the dominant southwestern wind direction, most likely due to lack of strong emitters.

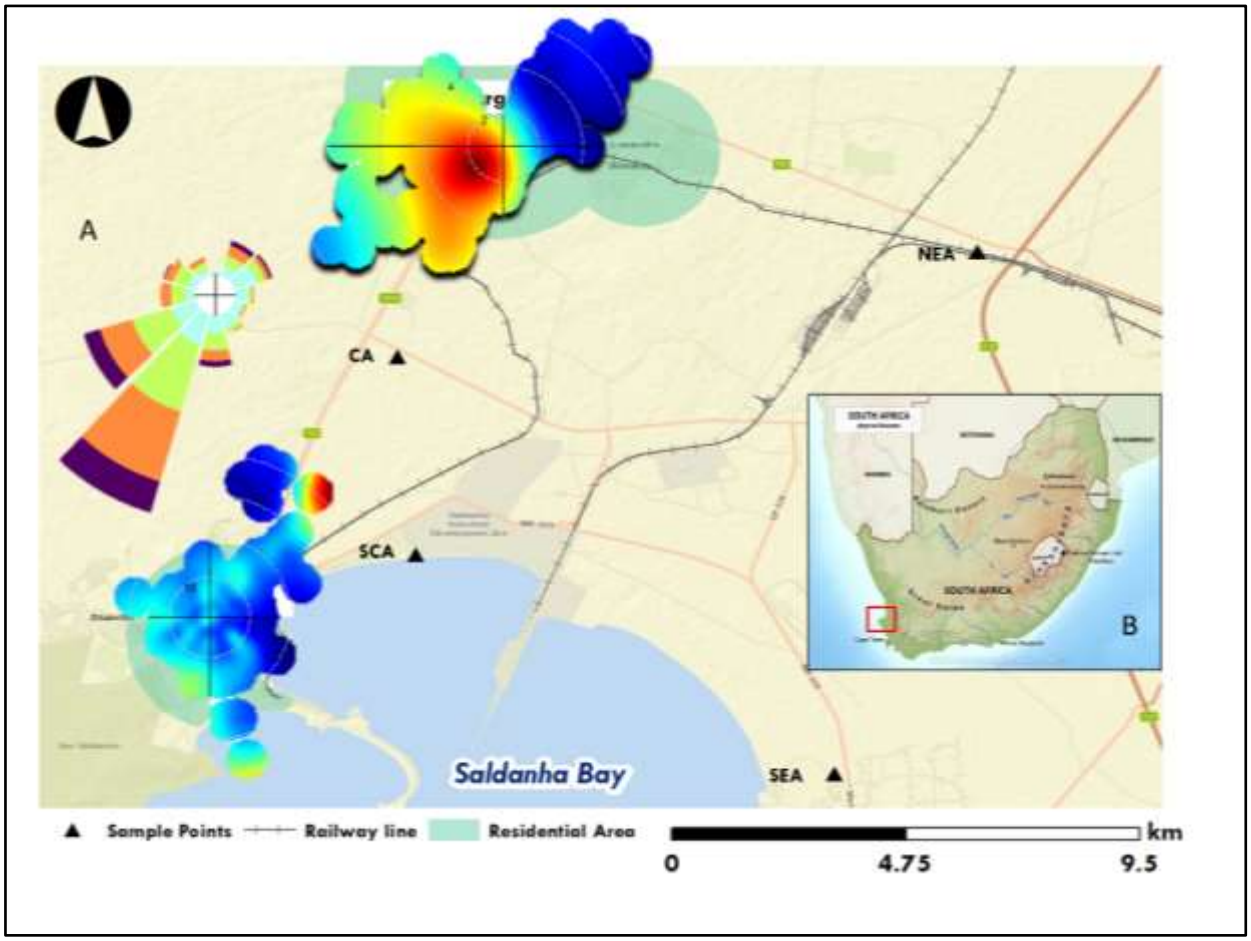

Figure 7*. Map of Saldanha Bay including polar plots showing the particle transport calculated for stations SWA and NNA. Both polar plots were calculated for the year 2019 (January to December) using wind speed and direction data along with the PM_{10} and $PM_{2.5}$ concentrations. In addition, a wind rose shows the wind speed and direction at station SWA averaged for each month of the year from January 2015 to December 2019.*

2.4.7.2. Long-range dust transport

Hysplit modelling can support the projection of the long-range transport of the dust, that is providing key information on i) where the dust collected in Saldanha Bay may originate from and ii) where this dust may travel before deposition. Forward trajectories indicate potential pathways for far-reaching open oceans deposition, especially along the South African coastline (Figure 8). In the forward trajectories, approximately 40% of the air masses over Saldanha Bay (and thus potentially the suspended dust aerosols) travel north and northwest (Table 5). The northwest directed air masses travel along the east coast of the Atlantic Ocean. Secondly, ~ 45% of the air masses travel east and northeast towards South Africa`s interior. Roughly 11% of the air masses from Saldanha Bay travel

southeast, towards the Indian Ocean. Hence, in terms of ocean impact, the dust collected at Saldanha Bay can potentially be deposited into the southeast Atlantic and the southwest Indian Ocean.

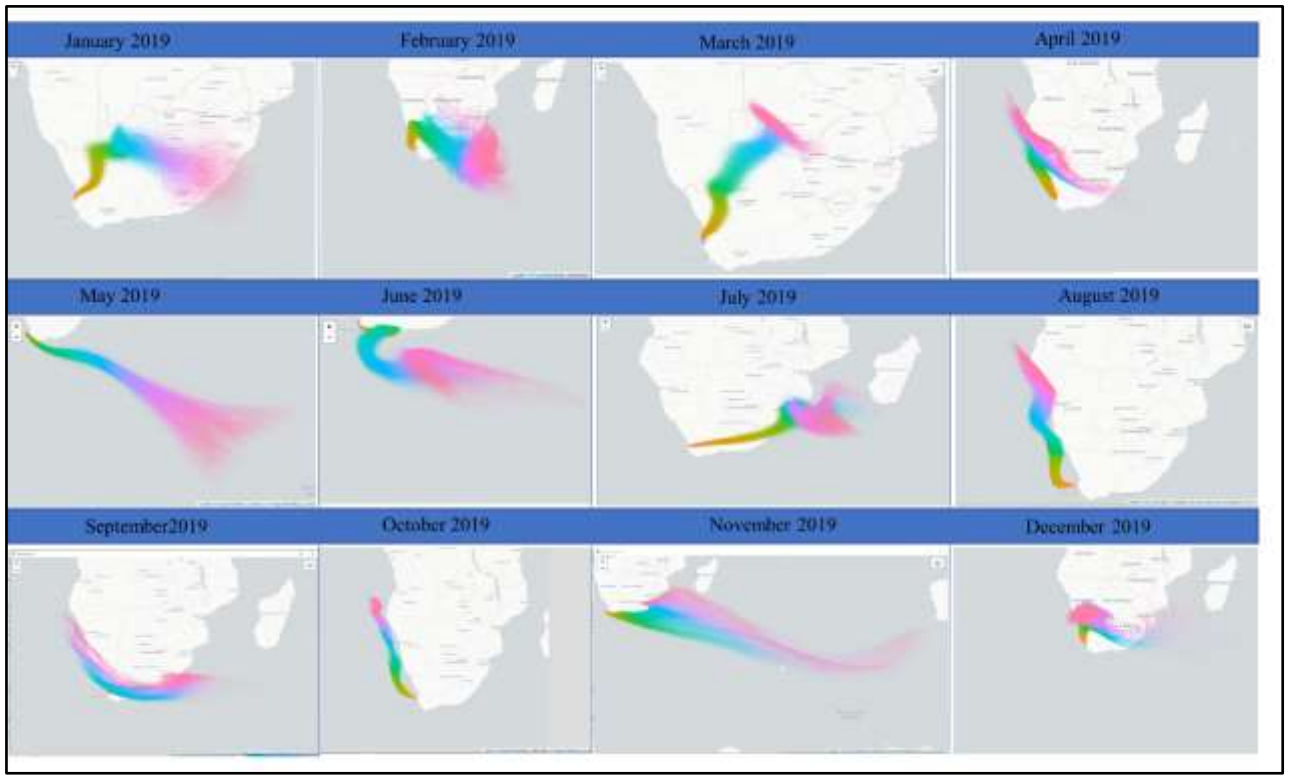

Figure 8. *Hysplit 7-day forward dispersion models at a height of 500m showing the possible monthly dust pathways from Saldanha Bay. The change in colour is an indication of change in time with distance. Brown and yellow indicate dispersion close to Saldanha Bay, and pink indicates the air masses furthest from Saldanha Bay. The dispersed particles are shown at different time intervals.*

Table 5. *Approximate contribution to dominant air mass pathways for the forward and backward trajectories averaged over the years 2015 to 2019. N – north, NW – northwest, NE – northeast, E – east, SE – southeast, W – west, SW – southwest, S – south, T – terrestrial origin, M- marine origin.*

Dominant wind directions	North (T)	NW (M)	NE (T)	E (T)	SE (T)	W (M)	SW (T)	S (M)
Backward trajectories (%)	0	6	10	0	17	0	63	4
Forward trajectories (%)	16	24	25	20	12	0.7	0.7	3

2.5. DISCUSSION

2.5.1. Source attribution of dust in the Saldanha Bay area

Saldanha Bay is popularly known as a dusty town, and here, we first assess potential sources to improve our understanding of the controlling factors of the dust characteristics.

2.5.1.1. Oceanic source

The Hysplit trajectories and polar plots revealed that local air masses are likely strongly influenced by sea spray. The extent of the marine influence may vary between the sampled stations as some stations seem to have a stronger marine imprint than others. For example, mineralogical analysis revealed that most of the particles collected at station SWA have an oceanic origin (cf. S.2). As such, medium grained Na particles were observed in SEM elemental maps for station SWA (Figure S4). Sea salt particles can be concentrated in coastal cities (Li et al., 2011) and the occurrence of such particles can be explained by the proximity of the samples to the ocean and favourable wind direction. The sea salt in our Saldanha Bay samples was mostly found in the coarse-grained fraction (>3 µm) conforms to findings by Shelley et al., (2015), who observed medium grained sea salt particles aboard during the US-GEOTRACES North Atlantic Zonal transect. The ocean contribution to particle composition may explain that station SWA had lower annual mean concentrations of Fe, Mn and Pb compared to the northern stations NNA and NEA. The high trace metal concentrations measured in most of our samples however, is an indication that despite some air masses originating from the southwest, demonstrating oceanic impact, the local natural terrestrial and anthropogenic sources may have a stronger impact.

2.5.1.2. Terrestrial (natural and anthropogenic) sources

Most of the terrestrial sources are from the Namibian coastline or the interior of southern Africa. Backward trajectories and polar plots showed that there is input from the northeastern interior such as the Kalahari and Namib Deserts. Our results are in agreement with Molepo et al. (2019), showing similar trajectories from the Kalahari and Namib Deserts. However, in addition to these natural dust sources, the terrestrial influence includes an anthropogenic component. For example, at station SWA, the polar plots indicated that PM_{10} is partially sourced from the northeast and southeast, an indication that the PM_{10} can originate from the export terminal and the industrial area, including Saldanha steel smelter. At station NNA, the polar plots showed high PM_{10} contribution from the northeast and northwest, which includes industrial areas. For example, northeast of Vredenburg is a sand mine that could potentially contribute to the PM_{10} emission and c. four kilometres south of NNA is a gravel quarry that also potentially emits dust. The area close to the quarry is proposed for a new phosphate mine which could increase the dust emissions in future.

2.5.1.3. Enrichment factors

The calculated enrichment factors enabled us to further constrain the sources and distinguish between natural and anthropogenic impact. Saldanha Bay dust aerosols revealed low enrichment factors for most of the trace metals except for Zn (for all stations). Stations NNA showed generally highest enrichment factors, especially noteworthy for Pb, indicating anthropogenic input. This could be contributed by the steel plant and industrial zones, which are located less than 20 kilometres from NNA. The enrichment in Pb could be associated with metal smelting and combustion of fossil fuels (Bridgestock et al., 2017; Buck et al., 2019; Wozniak et al., 2015). The dominant wind could transport fine particles from the industrial zone and steel plant towards the northern stations. In contrast, dust of lithogenic origin seem to prevail in central Saldanha Bay, which may, however, be affected by local dust emissions from the quartz quarry. Station NNA also shows relatively high V concentrations. In this area, V could be sourced from high temperature combustions sources such as shipments and vehicles in the town (Shelley et al., 2015).

2.5.1.4. Dust load and bulk element content

Some stations such as NEA and NNA have relatively low dust fall-out rates but high bulk trace metal concentrations (Figure S1). Trapp et al. (2010) previously documented areas in the equatorial Atlantic with low dust load and high trace elemental concentrations. These stations, potentially influenced by emissions from the smelter or industrial activities, are characterised by particles from anthropogenic

activities that are usually fine grained and enriched in trace metals (cf. 4.4) (López-García et al., 2017; Meskhidze, 2005). We argue that the area is influenced by both natural and anthropogenic sources, including lithogenic and combustion emissions. These factors can lead to high trace metal concentrations in areas characterised by low dust fall-out rates, especially evident in the northern stations.

Several bulk trace metal concentrations were found to be similar or higher compared to known contaminated areas in the world. For example, in the Hebei Province in China, close to an iron ore steel plant, Mn and Fe concentrations occurred in ranges (Lin et al., 2020) comparable to concentrations in Saldanha Bay (Table 6). Iron dust collected close to a steel plant in Oman also had Fe concentrations ranges comparable to those observed in Saldanha Bay (Table 6). In southern Africa, Kříbek et al., (2014) found Pb and Zn enrichment in windblown material collected at the Rosh Pinah mine tailings dam, Namibia, where trace metal concentrations were higher than in our Saldanha Bay samples (Table 6). Only the annual mean concentration of bulk Mn at Saldanha Bay is surprisingly almost ten times higher compared to a town (Tielong, China) located in a region where a Zn-Cu poly-metallic deposit was mined (Xie et al., 2017) (Table 6).

Table 6. *Examples of locations reported with high trace metal concentrations in aerosols. The locations selected here either have steel factory, mining activities or a smelter to facilitate a comparison with the Saldanha Bay area.*

Location	**Trace metal concentrations**	**References**
Tielong, China	173 ppm Mn	Xie et al., (2017)
Hebei Province, China	1500 to 8500 ppm Mn 28 600 to 41 900 ppm Fe	Lin et al., (2020)
Rosh Pinah Mine, Namibia	11 000 ppm Mn 1210 ppm Cu 38 240 ppm Pb	Kříbek et al. (2014)
Liwa, Sohar, Sea of Oman	4780 to 17180 ppm Fe	Omidvarborna et al. (2018); Omidvarborna et al. (2021)
Saldanha Bay, 2019	**200 to 1830 ppm Mn** **11 440 to 33 380 ppm Fe** **20.5 to 66.8 ppm Cu** **14 to 1175 ppm Pb**	**This study** (cf. Table 2 for other metals in 2019; cf. Table S1 for range of net metal mass during the five-year long monitoring, 2015-2019)

2.5.1.5. Mineralogical characteristics

Most of the particles collected at the northeastern station NEA showed angular, agglomerated and spherule, shaped particles. The magnetic spherules can originate from diagenetic, volcanic, or anthropogenic sources (Itambi et al., 2010). Since there have been no recent reported volcanic eruption, or deposition, in the area, Saldanha Bay dust contains material that is either anthropogenically or diagenetically sourced. The NEA single or agglomerated soft particles or sharp and angular or spherical particles, are similar to particles studied in the Sohar Industrial Port in Oman (Omidvarborna et al., 2018). The particles found in Oman are also iron-rich with coatings of sulfate (known to enhance acidity and solubility), similar to the particles collected at Saldanha Bay. This coating is observed as overlapping of Fe, Pb, Mn and S in the SEM elemental mapping images (Figure 3). The Fe- and Mn- bearing minerals could thus be from the mining ore transported by trucks and trains since the NEA station is close to the railway line, or from industrial and smelter activities to the south. Iron-spherules usually form due to condensation of iron being emitted into the atmosphere due to cooling from high-temperature industrial activities such as metal smelting (e.g., Riffault et al., 2015). The spherical morphology of the particles from Saldanha Bay is an indication that particles were formed at high-temperature processes with rapid cooling effects or volcanic rocks (Itambi et al., 2010; Li et al., 2017). Such particles are produced from anthropogenic industrial processes and steel processing plant. In summary, a mixed origin of natural and anthropogenic origin is most likely in the collected aerosols, while only two monitoring stations (SWA and SEA) likely had a predominant marine imprint (Table 7).

Table 7. *Classification of the different stations based on the observations from pollution roses, enrichment factors and mineralogical particles and background trace metal chemistry. The classification scheme includes three categories, (1) "oceanic", which refers to likely sea spray origin, (2) "terrestrial", which refers to sources from natural lithogenic inputs, and (3) "anthropogenic" which refers to influence by mineral ore. All seven stations were assessed based on the five year-long monitoring. In addition, stations CA, NEA, NNA and SWA were classified based on the BNSE bulk metal compositions and mineralogical characteristics.*

Sample Sites	Oceanic	Terrestrial natural	Anthropogenic
CA		x	
NEA			x
NNA			x
NWA			x
SCA	x	x	
SEA		x	
SWA	x		x

2.5.2. Assessing the potential impact of the dust collected over Saldanha Bay

2.5.2.1. Role of mineralogical composition for trace metal dissolution

Particle size and mineralogy are both critical factors in the solubility of the dust (Journet et al., 2008), constraining or facilitating solubility. Our SEM analyses showed there is an abundance of very fine particles (mostly less than 100 µm in size). There is a general agreement that finer grained particles are more soluble than coarse grain counterparts (Baker et al., 2006; Baker and Jickells, 2006; Buck et al., 2006). Hence, we expect a relatively high solubility in our samples as further supported in the experimental analysis discussed below.

The mineralogy also corresponded with major pattern in observed solubility in our samples. For example, the SEM results of the Saldanha Bay particles showed iron oxide phases containing goethite and hematite, which can reduce the solubility (Scanza et al., 2018) and increase leaching time (Shi et al., 2011a). This may explain the observed low solubility of Fe in some of the Milli-Q leachates. Elemental mapping also revealed fine-grained (~500 nm) Mn-bearing particles, although they did not coincide with S, which could indicate occurrence of oxides. Mn oxydroxides have high adsorption capacities and can hence constrain the solubility and subsequent release of trace metals that can be either toxic or enhance bioavailability in marine settings (Tebo et al., 2004).

On the other hand, higher contents of aluminosilicate minerals were observed at some stations, such as SWA, in which the trace metals also had a higher solubility. The aluminosilicates at SWA might be attributed by natural dust emissions in the area; hence, the origin and its influence on the mineralogy matters for the ocean impact. The elemental mapping in the SEM also indicated a strong overlapping of sulfate and iron which can enhance the solubility of iron. Sulfate can cause acidity when in contact with water and potentially increase solubility (Zhu et al., 2020). The coating of iron might have been secondary due to industrial activities, and hence resulted in a more soluble iron form such as iron sulfate (Li et al., 2017). Furthermore, some of the coarse-grained particles showed an overlapping of Pb and S in the elemental mapping images which could be due to occurrence of galena (PbS) particles. The leaching of Pb was one of the most efficient and this may be explained by sulfate and the presence of galena. Hence, these results show that at least some of the particles collected over Saldanha Bay can easily dissolve when deposited into surface oceans. This has been further tested with flow-through leaching experiments discussed in the following section.

2.5.2.2. Simulating potential dissolution during transport and upon deposition in surface ocean

Different methodological procedures and leaching solutions have resulted in a variety of aerosol dissolution estimates (Baker et al., 2014; Mahowald et al., 2018; Morton et al., 2013; Sholkovitz et al., 2012) and hence it is important here to distinguish the leaching solution. Most studies use Milli-Q and acetic acid as reagents, partially because they are readily available and used to investigate metal dissolution in atmospheric dust (Duggen et al., 2010; Shi et al., 2011b). Milli-Q as a leaching solution is representative of seawater because the difference between leaching with Milli-Q and seawater is not significant (Aguilar-Islas et al., 2010; Buck et al., 2006; Shelley et al., 2018). However, leaching with Milli-Q causes more acidity and reaches lower pH values faster compared to seawater because Milli-Q is not a buffered solution (Aguilar-Islas et al., 2010). This reflects processes that occur during atmospheric transport, resulting in more acidic conditions and trace metals becoming more soluble before being deposited in the seawater. These patterns are strengthened using a weak acid leachate. Therefore, here, we used the Milli-Q and weak acid leachates as representatives of dissolution during transport and in open ocean seawater.

As observed on aerosols from Australia and South American top soils (Perron et al., 2020; Simonella et al., 2014; Winton et al., 2015), the solubility of trace metals in the Saldanha Bay dust in Milli-Q was low, while the solubility in the weak acid was higher confirming that low pH condition is an important contributing factor to solubility. The higher extraction efficiency found in the weak acid is also an indication of the influence of atmospheric processing.

2.5.2.3. Comparison of Saldanha Bay aerosol dissolution in a global context

Fractional solubilities in the weak acid in our aerosols of mixed origin are higher in comparison to dust aerosols from natural sources that had solubility ranging from 0.003 to 5.3 % in minerals such as iron oxides, magnetites, clays, feldspars, orthoclase and hematite with particle sizes of less than 100 µm when using HNO_3 with a low pH of 2 as a leachate (Journet et al., 2008). This confirms that the solubility of mineral dust at source is lower than after atmospheric transport when collected as aerosols. Generally, the solubility of dust sources is lower compared to what is reported over the open oceans. In addition, solubilities determined for our aerosols of mixed origin were generally higher than those observed in mineral dust, even when collected as aerosols. We argue that the higher fractional solubilities at Saldanha Bay might be attributed to influence of particles resulting from industrial activities (Ito and Kok, 2017). Spokes and Jickells (1995) for example, recorded very low solubility (~0.1 to 0.3%) in Saharan aerosols when the leachate solution had a pH of 5.5 and 8, similar to observations by Sedwick et al. (2007)(0.44%). Sedwick et al. (2007) recorded much higher fractional solubility of 19% in dust close to North America, and attributed the increase to anthropogenic combustion products. Biomass burning has also been shown to lead to very high solubilities, e.g. in recent studies (Perron et al., 2019, 2020) from Australia from sources influenced by biomass burning. However, Perron et al. (2020) used leaching with the very strong hydrofluoric acid, which might bias some of the observed solubility differences and challenges a direct comparison with our data. Thuróczy et al. (2010) in contrast, testing coal ash collected in Cape Verde Islands reported a solubility range of only <0.1 to 0.2% of anthropogenically sourced Zn when dissolved in seawater. These solubility ranges are much lower than what we observed over Saldanha Bay (Table 8). In summary, we argue that dust aerosols at an industrial site such as Saldanha Bay have relatively large fractional solubility ranges and often include peak solubilities due the influence of both natural mineral dust and anthropogenic aerosols from industrial activities. We also argue that the pH plays an important role in the solubility of dust, with low pH conditions enhancing the solubility.

Table 8. *Examples of concentrations of soluble fractions (%) of iron in major iron ore emitting regions.*

Sample type	Reference	Experimental leaching time	leachate used, pH of leachate	Concentration of soluble fraction of iron (%)
feldspar/oligoclase, orthoclase, < 100 µm	Journet et al. (2008)	1 hour	HNO_3, pH2	5.25, 4.26

Clay/illite, <100 µm				0.95 to 1.39
Iron oxide/goethite, magnetite, hematite, 100 µm				0.003 to 0.01
				2.6
Clay/montmorillonite, <100 µm				
Dust from Arizona	Cwiertny et al. (2008)	1-day	HCl_1, pH1	13.6 ± 0.6
			pH1 HNO_3, pH1	11.9 ± 0.5
			HSO_4, pH1	15.7 ± 0.8
Saharan aerosol collected at the North African coast	Spokes and Jickells (1995)	1 day	pH2	4.7 ± 0.2
			pH5.5	0.3
			pH8	0.1
Tibetsi and Beijing dust samples sieved to three size fractions (PM_{20}; PM_{10}; $PM_{2.5}$)	Shi et al. (2011)	Up to 1000 hours	0.1, 0.01N H_2SO_4	0.5 – 2
			0.001N H_2SO_4	1 – 3
			pH1, 2, 3	15 – 40
Saldanha Bay dust (cf. section 4.4 for mineralogy)	**This study**	**10 min**	**UHPW** **25% acetic acid**	**0.08 - 0.47** **1.8-28**

2.5.2.4. Potential impact of Saldanha Bay to surrounding marine systems

Anthropogenic dust is known to supply trace nutrients to oceans (Ito et al., 2019; Sedwick et al., 2007). Agglomerates of aerosols and atmospheric gases have previously been reported as being transported from southern Africa towards the Indian Ocean and some towards the Atlantic (Ginoux et al., 2004; Piketh et al., 1999, 2002; Swap et al., 1996). Our air mass trajectories also show that most pathways are directed towards the Indian and Atlantic Ocean, but about 5% travel towards the Southern Ocean and Antarctica. Most of the trajectories showed that air masses travel towards the continental regions such as towards the N, NE, E and SE. The latter confirms previous models that have shown air mass pathways directed towards the Southern Ocean and Antarctica (Albani et al., 2012; Li et al., 2008; Neff and Bertler, 2015; Tatlhego et al., 2020). Some of these marine systems are key regions for CO_2 capturing, but also known for conditions of excess macro- but limited micronutrients (e.g., Henley et al. 2020). Hence, such southern African, highly soluble dust of mixed

(mineral and anthropogenic) origin can be important to external micronutrient fluxes. In addition, the forward air mass trajectories have shown that dust captured in Saldanha Bay can travel northwest towards the Benguela Upwelling System. The Benguela Upwelling System is one of the most productive systems (Hutchings et al., 2009). Since soluble (bioactive) trace metals such as Fe, Mn and Zn are important for maintaining these high levels of productivity (Capone and Hutchins, 2013), we argue that the mixture of anthropogenic and natural dust as observed at the port town Saldanha Bay can be a major contributor to the Benguela Upwelling System.

2.6. CONCLUSION

This study investigated the aerosol particle composition at a major iron ore export town, incorporating trace metals and mineralogical characteristics and assessing the potential bioaccessility to open oceans. The aerosols collected at Saldanha Bay have different sources, such as oceanic, terrestrial, and industrial. Despite some stations indicating relatively low dust loads, the corresponding high trace metal concentration and the high solubility means that these aerosols could provide essential and highly soluble trace metals to the surrounding oceans, especially the Indian Ocean and the South Atlantic, including the Benguela Upwelling System. Emissions from anthropogenic sources in the port town samples might be relatively small compared to natural ones but are more soluble and thus could play key roles in primary producer fertilisation and ultimately carbon dioxide sequestration.

2.7. AUTHOR CONTRIBUTIONS

S.F., K. K., and F. E., conceived and designed the study and acquired funding; K.K., R.T., and G.R. contributed data and interpretation. K.K., F.D. and S.F. wrote the manuscript. All co-authors reviewed and edited this or previous versions of the manuscript and gave final approval for publication.

2.8. FUNDING

The work leading to these results received funding from the National Research Foundation (NRF) under the SANAP (110715, 110731), Bilateral (114677) and CPRR (105826) programmes. K. Kangueehi acknowledges funding from NRF through a Masters Innovation Scholarship.

2.9. ACKNOWLEDGEMENTS

The authors thank the Saldanha Bay municipality for providing the long-term monitoring data included in this study.

2.10. CONFLICT OF INTEREST STATEMENT

All authors declare no competing interests.

2.11. CHAPTER 2 REFERENCES

Aguilar-Islas, Ana M., Wu, J., Rember, R., Johansen, A.M., Shank, L.M., 2010. Dissolution of aerosol-derived iron in seawater: Leach solution chemistry, aerosol type, and colloidal iron fraction. Mar. Chem. 120, 25–33. https://doi.org/10.1016/j.marchem.2009.01.011

Albani, S., Mahowald, N.M., Winckler, G., Delmonte, B., Maggi, V., 2012. Comparing modeled and observed changes in mineral dust transport and deposition to Antarctica between the Last Glacial Maximum and current climates. Clim. Dyn. 38, 38.

Ashrafi, K., Shafiepour-Motlagh, M., Aslemand, A., Ghader, S., 2014. Dust storm simulation over Iran using HYSPLIT. J. Environ. Heal. Sci. Eng. 12, 9. https://doi.org/10.1186/2052-336X-12-9

Atkinson, L., Hutchings, K., Clark, B., Turpie, J., Steffani, N., Robinson, T., Duffell-Canham, A., 2006. State of the Bay 2006 : Saldanha Bay and Langebaan Lagoon, Technical report 127.

Baker, A.R., Jickells, T.D., 2006. Mineral particle size as a control on aerosol iron solubility. Geophys. Res. Lett. 33, 1–4. https://doi.org/10.1029/2006GL026557

Baker, A.R., Jickells, T.D., Witt, M., Linge, K.L., 2006. Trends in the solubility of iron, aluminium, manganese and phosphorus in aerosol collected over the Atlantic Ocean. Mar. Chem. 98, 43–58. https://doi.org/10.1016/j.marchem.2005.06.004

Baker, A.R., Laskina, O., Grassian, V.H., 2014. Processing and ageing in the atmosphere, in: Mineral Dust: A Key Player in the Earth System. https://doi.org/10.1007/978-94-017-8978-3_4

Baker A.R., Landing W.M. , Bucciarelli E., Cheize M., Fietz S., Hayes C.T., Kadko D., Morton P.L., Rogan N., Sarthou G., Shelley R.U. , Shi Z., Shiller A., van Hulten M.M.P., 2016. Trace

Element and Isotope Deposition across the Air – Sea Interface: Progress and Research Needs. Philosophical Transactions of the Royal Society A.374, 20160190. http://rsta.royalsocietypublishing.org/content/374/2081/20160190

Bayon, G., German, C.R., Burton, K.W., Nesbitt, R.W., Rogers, N., 2004. Sedimentary Fe-Mn oxyhydroxides as paleoceanographic archives and the role of aeolian flux in regulating oceanic dissolved REE. Earth Planet. Sci. Lett. 224, 477–492. https://doi.org/10.1016/j.epsl.2004.05.033

Berger, C.J.M., Lippiatt, S.M., Lawrence, M.G., Bruland, K.W., 2008. Application of a chemical leach technique for estimating labile particulate aluminum, iron, and manganese in the Columbia River plume and coastal waters off Oregon and Washington. J. Geophys. Res. 113, 1–16. https://doi.org/10.1029/2007jc004703

Bhattachan, A., D'Odorico, P., Baddock, M.C., Zobeck, T.M., Okin, G.S., Cassar, N., 2012. The Southern Kalahari: a potential new dust source in the Southern Hemisphere? Environ. Res. Lett. 7, 024001. https://doi.org/10.1088/1748-9326/7/2/024001

Bhattachan, A., D'Odorico, P., Okin, G.S., 2015. Biogeochemistry of dust sources in Southern Africa. J. Arid Environ. 117, 18–27. https://doi.org/10.1016/j.jaridenv.2015.02.013

Bridgestock, L., Rehkämper, M., van de Flierdt, T., Murphy, K., Khondoker, R., Baker, A.R., Chance, R., Strekopytov, S., Humphreys-Williams, E., Achterberg, E.P., 2017. The Cd isotope composition of atmospheric aerosols from the Tropical Atlantic Ocean. Geophys. Res. Lett. 44, 2932–2940. https://doi.org/10.1002/2017GL072748

Buck, C.S., Aguilar-Islas, A., Marsay, C., Kadko, D., Landing, W.M., 2019. Trace element concentrations, elemental ratios, and enrichment factors observed in aerosol samples collected during the US GEOTRACES eastern Pacific Ocean transect (GP16). Chem. Geol. 511, 212–224. https://doi.org/10.1016/j.chemgeo.2019.01.002

Buck, C.S., Resing, W.M., Resing, J.A., Lebon, G.T., 2006. Aerosol iron and aluminum solubility in the northwest Pacific Ocean: Results from the 2002 IOC cruise. J. Earth Sci. 7, 1–21. https://doi.org/10.1029/2005GC000977

Capone, D.G., Hutchins, D.A., 2013. Microbial biogeochemistry of coastal upwelling regimes in a changing ocean. Nat. Geosci. 6, 711–717. https://doi.org/10.1038/ngeo1916

Carslaw, D.C., Ropkins, K., 2012. Openair - An r package for air quality data analysis. Environ.

Model. Softw. 27–28, 52–61. https://doi.org/10.1016/j.envsoft.2011.09.008

Chen, H., Laskin, A., Baltrusaitis, J., Gorski, C.A., Scherer, M.M., Grassian, V.H., 2012. Coal fly ash as a source of iron in atmospheric dust. Environ. Sci. Technol. 46, 2112–2120. https://doi.org/10.1021/es204102f

Chester, R., Hughes, M.J., 1967. A chemical technique for the separation of ferro-manganese minerals, carbonate minerals and adsorbed trace elements from pelagic sediments. Chem. Geol. 2, 249–262. https://doi.org/10.1016/0009-2541(67)90025-3

Clark, B., Laird, M., Hutchings, K., Liebau, V., Biccard, A., Turpie, J., Parker-Mallick, N., 2020. The State of Saldanha Bay and Langebaan Lagoon 2020. Report 1581, 1–381.

Clark, B., Orr, K., Hutchings, K., Steffani, N., Angel, A., Turpie, J., 2009. State of Saldanha Bay 2018 : Saldanha Bay and Langebaan Lagoon. Saldanha Bay Water Qual. Trust 1581, 1–351.

Cutter, G., Casciotti, K., Croot, P., Geibert, W., Geochemistry, M., Heimbürger, L.-E., Lohan, M., 2017. Sampling and Sample-handling Protocols for GEOTRACES Cruises.

Cwiertny, D.M., Baltrusaitis, J., Hunter, G.J., Laskin, A., Scherer, M.M., Grassian, V.H., 2008. Characterization and acid-mobilization study of iron-containing mineral dust source materials. J. Geophys. Res. Atmos. 113, 1–18. https://doi.org/10.1029/2007JD009332

Dai, Q.L., Bi, X.H., Wu, J.H., Zhang, Y.F., Wang, J., Xu, H., Yao, L., Jiao, L., Feng, Y.C., 2015. Characterization and source identification of heavy metals in ambient PM10 and PM2.5 in an integrated Iron and Steel industry zone compared with a background site. Aerosol Air Qual. Res. 15, 875–887. https://doi.org/10.4209/aaqr.2014.09.0226

Dansie, A.P., Thomas, D.S.G., Wiggs, G.F.S., Munkittrick, K.R., 2018. Spatial variability of ocean fertilizing nutrients in the dust-emitting ephemeral river catchments of Namibia. Earth Surf. Process. Landforms 43, 563–578. https://doi.org/10.1002/esp.4207

Dansie, A P, Wiggs, G.F.S., Thomas, D.S.G., 2017. Iron and nutrient content of wind-erodible sediment in the ephemeral river valleys of Namibia. Geomorphology 1–42. https://doi.org/10.1016/j.geomorph.2017.03.016

Dansie, A. P., Wiggs, G.F.S., Thomas, D.S.G., Washington, R., 2017. Measurements of windblown dust characteristics and ocean fertilization potential: The ephemeral river valleys of Namibia. Aeolian Res. 29, 30–41. https://doi.org/10.1016/j.aeolia.2017.08.002

Desboeufs, K. V., Sofikitis, A., Losno, R., Colin, J.L., Ausset, P., 2005a. Dissolution and solubility of trace metals from natural and anthropogenic aerosol particulate matter. Chemosphere 58, 195–203. https://doi.org/10.1016/j.chemosphere.2004.02.025

Duggen, S., Olgun, N., Croot, P., Hoffmann, L., Dietze, H., Delmelle, P., Teschner, C., 2010. The role of airborne volcanic ash for the surface ocean biogeochemical iron-cycle: A review. Biogeosciences 7, 827–844. https://doi.org/10.5194/bg-7-827-2010

Ginoux, P., Prospero, J.M., Gill, T.E., Hsu, N.C., Zhao, M., 2012. Global-scale attribution of anthropogenic and natural dust sources and their emission rates based on MODIS Deep Blue aerosol products. Rev. Geophys. https://doi.org/10.1029/2012RG000388

Ginoux, P., Prospero, J.M., Torres, O., Chin, M., 2004. Long-term simulation of global dust distribution with the GOCART model : correlation with North Atlantic Oscillation. Environ. Model. Softw. 19, 113–128. https://doi.org/10.1016/S1364-8152(03)00114-2

Guieu, C., Bonnet, S., Wagener, T., Loÿe-Pilot, M.D., 2005. Biomass burning as a source of dissolved iron to the open ocean? Geophys. Res. Lett. 32, 1–5. https://doi.org/10.1029/2005GL022962

Hamilton, D.S., Scanza, R.A., Feng, Y., Guinness, J., Kok, J.F., Li, L., Liu, X., Rathod, S.D., Wan, J.S., Wu, M., Mahowald, N.M., 2019. Improved methodologies for Earth system modelling of atmospheric soluble iron and observation comparisons using the Mechanism of Intermediate complexity for Modelling Iron (MIMI v1.0). Geosci. Model Dev 12, 3835–3862. https://doi.org/10.5194/gmd-12-3835-2019

Hsu, C.Y., Chi, K.H., Wu, C. Da, Lin, S.L., Hsu, W.C., Tseng, C.C., Chen, M.J., Chen, Y.C., 2021. Integrated analysis of source-specific risks for PM2.5-bound metals in urban, suburban, rural, and industrial areas. Environ. Pollut. 275, 116652. https://doi.org/10.1016/j.envpol.2021.116652

Hutchings, L., van der Lingen, C.D., Shannon, L.J., Crawford, R.J.M., Verheye, H.M.S., Bartholomae, C.H., van der Plas, A.K., Louw, D., Kreiner, A., Ostrowski, M., Fidel, Q., Barlow, R.G., Lamont, T., Coetzee, J., Shillington, F., Veitch, J., Currie, J.C., Monteiro, P.M.S., 2009. The Benguela Current: An ecosystem of four components. Prog. Oceanogr. 83, 15–32. https://doi.org/10.1016/j.pocean.2009.07.046

Itambi, A.C., Von Dobeneck, T., Dekkers, M.J., Frederichs, T., 2010. Magnetic mineral inventory

of equatorial Atlantic Ocean marine sediments off Senegal-glacial and interglacial contrast. Geophys. J. Int. 183, 163–177. https://doi.org/10.1111/j.1365-246X.2010.04736.x

Ito, A., Kok, J.F., 2017. Do dust emissions from sparsely vegetated regions dominate atmospheric iron supply to the Southern Ocean? J. Geophys. Res. 122, 3987–4002. https://doi.org/10.1002/2016JD025939

Ito, A., Myriokefalitakis, S., Kanakidou, M., Mahowald, N.M., Scanza, R.A., Hamilton, D.S., Baker, A.R., Jickells, T., Sarin, M., Bikkina, S., Gao, Y., Shelley, R.U., Buck, C.S., Landing, W.M., Bowie, A.R., Perron, M.M.G., Guieu, C., Meskhidze, N., Johnson, M.S., Feng, Y., Kok, J.F., Nenes, A., Duce, R.A., 2019. Pyrogenic iron: The missing link to high iron solubility in aerosols. Sci. Adv. 5. https://doi.org/10.1126/sciadv.aau7671

Jickells, T., 2006. The role of air-sea exchange in the marine nitrogen cycle, Biogeosciences.

Jickells, T.D., Baker, A.R., Chance, R., 2016. Atmospheric transport of trace elements and nutrients to the oceans. Philos. Trans. R. Soc. A Math. Phys. Eng. Sci. 374. https://doi.org/10.1098/rsta.2015.0286

Jordi, A., Basterretxea, G., Tovar-Sánchez, A., Alastuey, A., Querol, X., 2012. Copper aerosols inhibit phytoplankton growth in the Mediterranean Sea. Proc. Natl. Acad. Sci. U. S. A. 109, 21246–21249. https://doi.org/10.1073/pnas.1207567110

Journet, E., Desboeufs, K. V., Caquineau, S., Colin, J.L., 2008. Mineralogy as a critical factor of dust iron solubility. Geophys. Res. Lett. 35, 3–7. https://doi.org/10.1029/2007GL031589

Kříbek, B., Majer, V., Pašava, J., Kamona, F., Mapani, B., Keder, J., Ettler, V., 2014. Contamination of soils with dust fallout from the tailings dam at the Rosh Pinah area, Namibia: Regional assessment, dust dispersion modeling and environmental consequences. J. Geochemical Explor. 144, 391–408. https://doi.org/10.1016/j.gexplo.2014.01.010

Li, F., Ginoux, P., Ramaswamy, V., 2008. Distribution, transport, and deposition of mineral dust in the Southern Ocean and Antarctica: Contribution of major sources. J. Geophys. Res. Atmos. 113, 1–15. https://doi.org/10.1029/2007JD009190

Li, W., Shao, L., Li, R., Yang, S., Wang, Z., Tang, U., 2011. Internally Mixed Sea Salt, Soot, and Sulfates at Macao, a Coastal City in South China. J. Air Waste Manag. Assoc. 61, 1166–1173. https://doi.org/10.1080/10473289.2011.603996

Li, W., Xu, L., Liu, X., Zhang, J., Lin, Y., Yao, X., Gao, H., Zhang, D., Chen, J., Wang, W., Harrison, R.M., Zhang, X., Shao, L., Fu, P., Nenes, A., Shi, Z., 2017. Air pollution–aerosol interactions produce more bioavailable iron for ocean ecosystems. Sci. Adv. 3, 1–7. https://doi.org/10.1126/sciadv.1601749

López-García, P., Gelado-Caballero, M.D., Collado-Sánchez, C., Hernández-Brito, J.J., 2017. Solubility of aerosol trace elements: Sources and deposition fluxes in the Canary Region. Atmos. Environ. 148, 167–174. https://doi.org/10.1016/j.atmosenv.2016.10.035

Luo, C., Mahowald, N., Bond, T., Chuang, P.Y., Artaxo, P., Siefert, R., Chen, Y., Schauer, J., 2008. Combustion iron distribution and deposition. Global Biogeochem. Cycles 22. https://doi.org/10.1029/2007GB002964

Mahowald, N.M., Baker, A.R., Bergametti, G., Brooks, N., Duce, R.A., Jickells, T.D., Kubilay, N., Prospero, J.M., Tegen, I., 2005. Atmospheric global dust cycle and iron inputs to the ocean. Global Biogeochem. Cycles 19. https://doi.org/10.1029/2004GB002402

Mahowald, N.M., Hamilton, D.S., Mackey, K.R.M., Moore, J.K., Baker, A.R., Scanza, R.A., Zhang, Y., 2018. Aerosol trace metal leaching and impacts on marine microorganisms. Nat. Commun. 9. https://doi.org/10.1038/s41467-018-04970-7

Mahowald, N.M., Kloster, S., Engelstaedter, S., Moore, J.K., Mukhopadhyay, S., McConnell, J.R., Albani, S., Doney, S.C., Bhattacharya, A., Curran, M.A.J., Flanner, M.G., Hoffman, F.M., Lawrence, D.M., Lindsay, K., Mayewski, P.A., Neff, J., Rothenberg, D., Thomas, E., Thornton, P.E., Zender, C.S., 2010. Observed 20th century desert dust variability: Impact on climate and biogeochemistry. Atmos. Chem. Phys. 10, 10875–10893. https://doi.org/10.5194/acp-10-10875-2010

Mahowald, N.M., Luo, C., 2003. A less dusty future? Geophys. Res. Lett. 30, 1903. https://doi.org/10.1029/2003gl017880

Matsui, H., Mahowald, N.M., Moteki, N., Hamilton, D.S., Ohata, S., Yoshida, A., Koike, M., Scanza, R.A., Flanner, M.G., 2018. Anthropogenic combustion iron as a complex climate forcer. Nat. Commun. 9. https://doi.org/10.1038/s41467-018-03997-0

Mcgowan, H., Clark, A., 2008. Identification of dust transport pathways from Lake Eyre, Australia using Hysplit. Atmos. Environ. 42, 6915–6925. https://doi.org/10.1016/j.atmosenv.2008.05.053

Meskhidze, N., 2005. Dust and pollution: A recipe for enhanced ocean fertilization? J. Geophys. Res. 110, D03301. https://doi.org/10.1029/2004JD005082

Meskhidze, N., Nenes, A., Chameides, W.L., Luo, C., Mahowald, N., 2007. Atlantic Southern Ocean productivity: Fertilization from above or below? Global Biogeochem. Cycles 21. https://doi.org/10.1029/2006GB002711

Molepo, K.M., Abiodun, B.J., Magoba, R.N., 2019. The transport of PM10 over Cape Town during high pollution episodes. Atmos. Environ. 213, 116–132. https://doi.org/10.1016/j.atmosenv.2019.05.041

Morton, P.L., Landing, W., Hsu, S., Milne, A., Aguilar-Islas, A., Baker, A., Bowie, A., Buck, C., Gao, Y., Gichuki, S., 2013. Methods for the sampling and analysis of marine aerosols: results from the 2008 GEOTRACES aerosol intercalibration experiment. Limnol. Oceanogr. 11, 62–78. https://doi.org/10.4319/lom.2013.11.62

Moskowitz, B.M., Reynolds, R.L., Goldstein, H.L., Berquó, T.S., Kokaly, R.F., Bristow, C.S., 2016. Iron oxide minerals in dust-source sediments from the Bodélé Depression, Chad: Implications for radiative properties and Fe bioavailability of dust plumes from the Sahara. Aeolian Res. 22, 93–106. https://doi.org/10.1016/j.aeolia.2016.07.001

Naidoo, D., Reddy, V.., 2009. Saldanha Air Quality Permit Amendment Basic Assessment : Air Quality Specialist Baseline Study and Impact Assessment. http://www.transnet.net/BUSINESSWITHUS/EnvPubDoc/saldanhaironore/SpecialistStudies/AirQualitySpecialistReport/1.%20Air%20Quality%20Specialist%20Report.pdf

Neff, P.D., Bertler, N.A.N., 2015. Trajectory modeling of modern dust transport to the Southern Ocean and Antarctica. J. Geophys. Res. 120, 9303–9322. https://doi.org/10.1002/2015JD023304

Olgun, N., Duggen, S., Croot, P.L., Delmelle, P., Dietze, H., Schacht, U., Óskarsson, N., Siebe, C., Auer, A., Garbe-Schönberg, D., 2011. Surface ocean iron fertilization: The role of airborne volcanic ash from subduction zone and hot spot volcanoes and related iron fluxes into the Pacific Ocean. Global Biogeochem. Cycles 25, 1–15. https://doi.org/10.1029/2009GB003761

Omidvarborna, H., Baawain, M., Al-Mamun, A., Al-Muhtaseb, A.H., 2018. Dispersion and deposition estimation of fugitive iron particles from an iron industry on nearby communities via AERMOD. Environ. Monit. Assess. 190. https://doi.org/10.1007/s10661-018-7009-4

Omidvarborna, H., Baawain, M., Al-Mamun, A., Siddiqi, S., 2021. Characterizing the unknown contribution of iron industries in atmospheric iron emissions using sensitivity analysis. J. Aerosol Sci. 151. https://doi.org/10.1016/j.jaerosci.2020.105630

Paris, R., Desboeufs, K. V., Journet, E., 2011. Variability of dust iron solubility in atmospheric waters: Investigation of the role of oxalate organic complexation. Atmos. Environ. 45, 6510–6517. https://doi.org/10.1016/j.atmosenv.2011.08.068

Paytan, A., Mackey, K.R.M., Chen, Y., Lima, I.D., Doney, S.C., Mahowald, N., Labiosa, R., Post, A.F., 2009. Toxicity of atmospheric aerosols on marine phytoplankton. Proc. Natl. Acad. Sci. 106, 4601–4605. https://doi.org/10.1073/pnas.0811486106

Perron, M.M.G., Proemse, B.C., Strzelec, M., Gault-Ringold, M., Boyd, P.W., Sanz Rodriguez, E., Paull, B., Bowie, A.R., 2019. Origin, transport and deposition of aerosol iron to Australian coastal waters. Atmospheric Environment 228,117432. https://doi.org/10.1016/j.atmosenv.2020.117432

Perron, M.M.G., Strzelec, M., Gault-Ringold, M., Proemse, B.C., Boyd, P.W., Bowie, A.R., 2020. Assessment of leaching protocols to determine the solubility of trace metals in aerosols. Talanta 208, 120377. https://doi.org/10.1016/j.talanta.2019.120377

Piketh, S.J., Annegarn, H.J., Tyson, P.D., 1999. Lower tropospheric aerosol loadings over South Africa: The relative contribution of aeolian dust, industrial emissions, and biomass burning. J. Geophys. Res. Atmos. 104, 1597–1607. https://doi.org/10.1029/1998JD100014

Piketh, S.J., Swap, R.J., Maenhaut, W., Annegarn, H.J., Formenti, P., 2002. Chemical evidence of long-range atmospheric transport over southern Africa. J. Geophys. Res. Atmos. 107, 1–13. https://doi.org/10.1029/2002JD002056

Riffault, V., Arndt, J., Marris, H., Mbengue, S., Setyan, A., Alleman, L.Y., Deboudt, K., Flament, P., Augustin, P., Delbarre, H., Wenger, J., 2015. Fine and Ultrafine Particles in the Vicinity of Industrial Activities: A Review. Crit. Rev. Environ. Sci. Technol. 45, 2305–2356. https://doi.org/10.1080/10643389.2015.1025636

Rolph, G., Stein, A., and Stunder, B., (2017). Real-time Environmental Applications and Display sYstem: READY. Environmental Modelling & Software, 95, 210-228, https://doi.org/10.1016/j.envsoft.2017.06.025

Scanza, R.A., Hamilton, D.S., Perez Garcia-Pando, C., Buck, C., Baker, A., Mahowald, N.M.,

2018. Atmospheric processing of iron in mineral and combustion aerosols: Development of an intermediate-complexity mechanism suitable for Earth system models. Atmos. Chem. Phys. 18, 14175–14196. https://doi.org/10.5194/acp-18-14175-2018

Schlitzer, R., Anderson, R.F., Dodas, E.M., et al., 2018. The GEOTRACES Intermediate Data Product 2017. Chem. Geol. 493, 210–223. https://doi.org/10.1016/j.chemgeo.2018.05.040

Schroth, A.W., Crusius, J., Sholkovitz, E.R., Bostick, B.C., 2009. Iron solubility driven by speciation in dust sources to the ocean. Nat. Geosci. 2, 337–340. https://doi.org/10.1038/ngeo501

Schulz, M., Prospero, J.M., Baker, A.R., Dentener, F., Ickes, L., Liss, P.S., Mahowald, N.M., Nickovic, S., García-Pando, C.P., Rodríguez, S., Sarin, M., Tegen, I., Duce, R. a, 2012. Atmospheric transport and deposition of mineral dust to the ocean: implications for research needs. Environ. Sci. Technol. 46, 10390–404. https://doi.org/10.1021/es300073u

Sedwick, P.N., Sholkovitz, E.R., Church, T.M., 2007. Impact of anthropogenic combustion emissions on the fractional solubility of aerosol iron: Evidence from the Sargasso Sea. Geochemistry, Geophys. Geosystems 8. https://doi.org/10.1029/2007GC001586

Shelley, R.U., Landing, W.M., Ussher, S.J., Planquette, H., Sarthou, G., 2018. Regional trends in the fractional solubility of Fe and other metals from North Atlantic aerosols (GEOTRACES cruises GA01 and GA03) following a two-stage leach. Biogeosciences 15, 2271–2288. https://doi.org/10.5194/bg-15-2271-2018

Shelley, R.U., Morton, P.L., Landing, W.M., 2015. Elemental ratios and enrichment factors in aerosols from the US-GEOTRACES North Atlantic transects. Deep. Res. Part II Top. Stud. Oceanogr. 116, 262–272. https://doi.org/10.1016/j.dsr2.2014.12.005

Shelley, R.U., Roca-Martí, M., Castrillejo, M., Sanial, V., Masqué, P., Landing, W.M., Planquette, H., Sarthou, G., 2017. Quantification of trace element atmospheric deposition fluxes to the Atlantic Ocean (>40°N; GEOVIDE, GEOTRACES GA01) during spring 2014. Deep. Res. Part I Oceanogr. Res. Pap. 119, 34–49. https://doi.org/10.1016/j.dsr.2016.11.010

Shi, Z., Bonneville, S., Krom, M.D., Carslaw, K.S., Jickells, T.D., Baker, A.R., Benning, L.G., 2011. Iron dissolution kinetics of mineral dust at low pH during simulated atmospheric processing. Atmos. Chem. Phys. 11, 995–1007. https://doi.org/10.5194/acp-11-995-2011

Shi, Zongbo, Krom, M.D., Bonneville, S., Baker, A.R., Bristow, C., Drake, N., Mann, G., Carslaw,

K., McQuaid, J.B., Jickells, T., Benning, L.G., 2011. Influence of chemical weathering and aging of iron oxides on the potential iron solubility of Saharan dust during simulated atmospheric processing. Global Biogeochem. Cycles 25. https://doi.org/10.1029/2010GB003837

Sholkovitz, E.R., Sedwick, P.N., Church, T.M., 2009. Influence of anthropogenic combustion emissions on the deposition of soluble aerosol iron to the ocean: Empirical estimates for island sites in the North Atlantic. Geochim. Cosmochim. Acta 73, 3981–4003. https://doi.org/10.1016/j.gca.2009.04.029

Sholkovitz, E.R., Sedwick, P.N., Church, T.M., Baker, A.R., Powell, C.F., 2012. Fractional solubility of aerosol iron: Synthesis of a global-scale data set. Geochim. Cosmochim. Acta 89, 173–189. https://doi.org/10.1016/j.gca.2012.04.022

Simonella, L.E., Gaiero, D.M., Palomeque, M.E., 2014. Validation of a continuous flow method for the determination of soluble iron in atmospheric dust and volcanic ash. Talanta 128, 248–253. https://doi.org/10.1016/j.talanta.2014.04.076

Spokes, L.J., Jickells, T.D., 1995. Factors controlling the solubility of aerosol trace metals in the atmosphere and on mixing into seawater. Aquat. Geochemistry 1, 355–374. https://doi.org/10.1007/BF00702739

Srinivas, B., Sarin, M.M., Kumar, A., 2012. Impact of anthropogenic sources on aerosol iron solubility over the Bay of Bengal and the Arabian Sea. Biogeochemistry 110, 257–268. https://doi.org/10.1007/s10533-011-9680-1

Stein, A.F., Draxler, R.R., Rolph, G.D., Stunder, B.J.B., Cohen, M.D., Ngan, F., 2015. NOAA's HYSPLIT atmospheric transport and dispersion modeling system. Bull. Am. Meteorol. Soc. 96, 2059–2077. https://doi.org/10.1175/BAMS-D-14-00110.1

Swap, R., Garstang, M., Macko, S, A., Tyson, P, D., Maenhaut, W., Artaxo, P., Kalberg, P., Talbot, R., 1996. The long-range transport of southern African aerosols to the tropical South Atlantic. Geophysical 101, 777–791.

Sylvestre, A., Mizzi, A., Mathiot, S., Masson, F., Jaffrezo, J.L., Dron, J., Mesbah, B., Wortham, H., Marchand, N., 2017. Comprehensive chemical characterization of industrial PM2.5 from steel industry activities. Atmos. Environ. 152, 180–190. https://doi.org/10.1016/j.atmosenv.2016.12.032

Tatlhego, M., Bhattachan, A., Okin, G.S., D'Odorico, P., 2020. Mapping Areas of the Southern Ocean Where Productivity Likely Depends on Dust-Delivered Iron. J. Geophys. Res. Atmos. 125, e2019JD030926. https://doi.org/10.1029/2019JD030926

Tebo, B.M., Bargar, J.R., Clement, B.G., Dick, G.J., Murray, K.J., Parker, D., Verity, R., Webb, S.M., 2004. BIOGENIC MANGANESE OXIDES: Properties and Mechanisms of Formation. Annu. Rev. Earth Planet. Sci. 32, 287–328. https://doi.org/10.1146/annurev.earth.32.101802.120213

Thuróczy, C.E., Boye, M., Losno, R., 2010. Dissolution of cobalt and zinc from natural and anthropogenic dusts in seawater. Biogeosciences 7, 1927-1936. https://doi.org/10.5194/bg-7-1927-2010

Trapp, J.M., Millero, F.J., Prospero, J.M., 2010. Trends in the solubility of iron in dust-dominated aerosols in the equatorial Atlantic trade winds: Importance of iron speciation and sources. Geochemistry, Geophys. Geosystems 11, 1–22. https://doi.org/10.1029/2009GC002651

Western Cape Government, 2019. 2018 Socio-economic Profile: Saldanha Bay Municipality 30.

Winton, V.H.L., Bowie, A.R., Edwards, R., Keywood, M., Townsend, A.T., van der Merwe, P., Bollhofer, A., 2015. Fractional iron solubility of atmospheric iron inputs to the Southern Ocean. Mar. Chem. 177, 20–32. https://doi.org/10.1016/j.marchem.2015.06.006

Wozniak, A.S., Shelley, R.U., McElhenie, S.D., Landing, W.M., Hatcher, P.G., 2015. Aerosol water soluble organic matter characteristics over the North Atlantic Ocean: Implications for iron-binding ligands and iron solubility. Mar. Chem. 173, 162–172. https://doi.org/10.1016/j.marchem.2014.11.002

Wu, J., Rember, R., Cahill, C., 2007. Dissolution of aerosol iron in the surface waters of the North Pacific and North Atlantic oceans as determined by a semicontinuous flow-through reactor method. Global Biogeochem. Cycles 21, GB4010. https://doi.org/10.1029/2006GB002851

Xie, W., Peng, C., Wang, H., Chen, W., 2017. Health risk assessment of trace metals in various environmental media, crops and human hair from a mining affected area. Int. J. Environ. Res. Public Health 14, 1595. https://doi.org/10.3390/ijerph14121595

Yaroshevsky, A.A., 2006. Abundances of chemical elements in the Earth's crust. Geochemistry Int. 44, 48–55. https://doi.org/10.1134/S001670290601006X

Zhang, Y., Mahowald, N., Scanza, R., Journet, E., Desboeufs, K., Albani, S., Kok, J., Zhuang, G., Chen, Y., Cohen, D.D., Paytan, A., Patey, M.D., Achterberg, E.P., Engelbrecht, J.P., Fomba, K.W., 2014. Modeling the global emission, transport and deposition of trace elements associated with mineral dust. Biogeosciences 12, 5771 - 5792. https://doi.org/10.5194/bgd-11-17491-2014

Zhu, Y., Li, W., Lin, Q., Yuan, Q., Liu, L., Zhang, J., Zhang, Y., Shao, L., Niu, H., Yang, S., Shi, Z., 2020. Iron solubility in fine particles associated with secondary acidic aerosols in east China. Environ. Pollut. 264, 114769. https://doi.org/10.1016/j.envpol.2020.114769

2.12. S.1. SUPPLEMENTARY MATERIAL

Origin, solubility and ocean impact of trace metal aerosols collected over a major iron ore port

K. Kangueehi [a], F. D. Eckardt [b], R. Toesie [c], G. Ravenscroft[d] , S. Fietz [a*]

[a] Centre for Trace Metal and Experimental Biogeochemistry, Department of Earth Sciences, University of Stellenbosch, Stellenbosch, 7600, South Africa

[b] Department of Environmental and Geographical Sciences, University of Cape Town, Cape Town, 7701, South Africa

[c] Municipality of Saldanha Bay, Private bag x12, Vredenburg, 7380, South Africa

[d] Argos Scientific (Africa) Pty Ltd., INOSPACE (Metalheads) Business Park, Paarden Eiland, 7405, South Africa

In this broader study, three different dust sampling methods were used for determination of bulk dust load, mineralogical characterisation, metal composition and leaching experiments: (i) Dust buckets were used from 2015-2019 to collect samples that provided a long-term overview of dust loads and trace metal distribution in the greater Saldanha Bay area (including neighbouring town Vredenburg). The data from the dust buckets were used to examine the spatial distribution of total dust fall out rates and trace metals composition (e.g., Pb, Mn, Fe, Cu and Zn) in the greater Saldanha Bay area. A comprehensive overview of the results of this five year-long monitoring effort are presented here in the Supplemental Material Section 1. A synthesis of the monitoring is presented in the main text. (ii) Big Spring Number Eight (BSNE) trap dust samples were used in 2019; these 2019 BSNE bulk composition data were compared to the 2015-2019 bulk composition data and furthermore the 2019 BSNE samples were used for leaching experiments. These BSNE data are all presented in the main text of this study. (iii) Volumetric Flow Controlled (VFC) samples were collected for two weeks in 2019 and used to compare with the bulk composition data. These additional data are presented here in the Supplemental Material Section S.2.

S.1.1. FIVE YEAR LONG MONITORING OF MONTHLY METAL LOAD

S.1.1.1. MONITORING METHODS

Samples were collected monthly from seven different stations (Table S1) over a five-year period from January 2015 to December 2019. Sampling locations were chosen according to proximity to industrial activities, residential areas, high traffic areas and other anthropogenic sources (Figure 2). The dust collection buckets (~300 cm^2 diameter) were placed on poles at 3m height above the ground. The dust fall-out rates were determined by dividing the weight of the collected insoluble material by the cross-sectional area of the funnel and the number of days over which the sample was taken. Dust fall-out rates are reported in $mg/m^2/day$. After weighing, these bulk dust samples were digested in an *aqua regia* solution and analysed at the SGS Environmental Laboratory in Randburg, South Africa, a South African National Standards (SANS) 17025 accredited facility. Annual averages for the bulk dust fall-out and trace metal concentrations were obtained. Reported errors represent one standard deviation. T-test statistical analysis was used to analyse significant differences between the years 2015-2019. All trace metal concentrations obtained from the five-year long monitoring effort are referred here as net mass of metal expressed in ppm.

Table S1. Station coordinates for the dust buckets used for the five-year long (2015 to 2019) monitoring and VFC (two weeks in 2019) samplers.

Sampling Stations	Dust buckets	VFCs	Latitude [°N]	Longitude [°E]
CA	x		-32.95	17.97
SCA	x		-33.01	17.93
SEA	x		-33.03	18.05
SWA	x	x	-32.99	17.97
NNA	x		-32.92	17.98
NWA	x		-32.91	17.98
NEA	x		-32.93	18.07

S.1.1.2. DUST FALL-OUT RATES AND TRACE METAL COMPOSITION, 2015-2019

S.1.1.2.1. Dust fall-out rates

The average annual dust fall-out rates for the sampled years 2015 to 2019 are summarised in Table S2. Here, the dust bucket fall-out rates are classified following the South African Government`s Air Quality Guidelines (Regulation 6 of the National Dust Control Regulations, South Africa Government Gazette (36974) dated November 2013) (NEMA: AQA, 2013): 92% of the samples (i.e. 315 out of 342 samples) at all seven stations had dust fall out rates of 0- 250 mg/m^2/d; Table S2). Twenty-three samples out of the total 342 samples collected (6.7%) could be categorised as "moderate" (i.e. ranging between 250 and 500 mg/m^2/d), while only four samples (1.2%) could be categorised as "heavy" (500 to 1200 mg/m^2/d) (Table S2). On two occasions, the dust fall out rate was categorised as "very heavy" (> 1200 mg/m^2/d) (Table S2).

Inter-annual comparison of dust fall out rates: The annual dust fall-out rates ranged from below detection limit to 2021 mg/m^2/day (Table S2). Annual dust fall-out rates between 2015, 2016 and 2017 significantly increased ($p < 0.005$) from year to year. As such, the highest dust fall-out rates occurred in 2017. However, there was no significant difference between the annual dust fall-out rates in 2017 and 2018 and between 2018 and 2019 ($p > 0.1$).

Spatial comparison: The comparison of fall-out rates among the seven stations (Table S3) located in the greater Saldanha Bay area revealed a heterogeneous distribution, but few significant differences between the stations across the five year monitoring. Here we highlight a few examples to provide an

indication of the spatial variability. This understanding, along with the above mentioned inter-annual variability, is used to place the target BSNE sampling at selected four stations in 2019 in context. At station CA located in the central part of the greater Saldanha Bay area (Table S4). The dust fall-out rates 2015-2019 ranged from 20 to 741 mg/m^2/day and averaged 254 ± 161 mg/m^2/day. At station NEA, in the north eastern part of the area, the dust fall-out rates ranged from 6 to 2021 mg/m^2/day and averaged 171 ± 318 mg/m^2/day, with the highest rate found in 2016. At station NNA, in the north western part of the area the dust fall rates ranged from 4 to 122 mg/m^2/day and averaged 53±31 mg/m^2/day, with highest dust fall out rate occurring in 2017. At station NWA the dust fall-out rate ranged from 4-122 mg/m^2/day and averaged 56 ± 54 mg/m^2/day, with highest dust fall-out rate occurring in 2017.

S.1.1.2.2. BULK TRACE METAL CONCENTRATIONS, 2015-2019

Inter-annual comparison: Mean annual concentrations of trace metals Pb, Cu, Zn, Fe and Mn from the seven stations (Table S1) are presented in Table S2 and Table S4. The bulk Pb and Mn annual average concentrations generally increased over the five-year period from 2015 to 2019, although peak annual average concentrations are recorded in 2016 for Pb (2051 ± 1284 ppm) and 2017 for Mn (13 636 ± 9310 ppm). The annual average concentrations of Fe, Cu and Zn, in contrast, generally decreased over the four-year period with highest concentrations recorded in 2015 for Fe (110092 ± 40900 ppm), Cu (38 919 ± 1089 ppm), and Zn (3578 ± 1620 ppm).

Some significant inter-annual differences ($p < 0.05$) were observed (Table S4) indicating major variability in bulk trace metal concentration between the years. For example, annual average Pb concentrations were lower in 2015 compared to 2016, and between 2017 and 2018. Annual average Cu concentrations were lower in 2016 compared to 2017 and between 2018 and 2019. However, for Zn, Fe and Mn only few years showed significant differences in annual concentrations (Table S4).

Spatial comparison: The trace metal concentration at specific sites was highly variable, likely reflecting the main dust aerosol sources. During the study period between 2015 and 2019, concentrations of all investigated trace metals were relatively low at central station CA and south-eastern station SEA (e.g. annual means for station CA ranging from 30 to 175 ppm for Pb, 45 to 983 ppm for Cu, 210 to 994 ppm for Zn, 1590 to 20640 ppm for Fe and 202 to 2335 ppm for Mn) (Figure S1). In contrast, the rest of the stations (SWA, NNA, NWA and SEA) generally had high trace metal concentrations (e.g., annual means ranging from 87 to 610 ppm for Pb, 175 to 4824 ppm for Cu, 213 to 1143 ppm for Zn, 11 300 to 29 700 ppm for Fe and 784 to 4128 ppm for Mn) (Figure S1). Occasionally, monthly data revealed extremely high concentrations. The greatest spikes in trace metals were found at NEA for Pb (7563 ppm) in 2017, Fe (110 092 ppm) in 2015, Mn (15 484 ppm)

in 2019, Zn (9664 ppm) in 2017 and at NWA for Cu (38 919 ppm) in 2015. Cu concentrations were low (e.g., 4064 ppm ± 975) at south-eastern stations SEA for the years 2015 and 2019. This illustrates that the trace metal spatial distribution was not homogenous.

The stations with the highest dust collected by weight mass do not necessarily have the highest trace metal concentrations (Figure S3). For example, stations such as NNA and NWA recorded very low dust fall-out rates but contained high trace metal concentrations for Mn, Fe and Pb. In contrast, the highest bulk trace metal compositions were found at stations with low dust fall rates. Low Mn and Pb concentrations despite high dust fall-rate were observed at station CA close to the airport possibly because of the distance away from the railway.

Table S2*. Summary of dust fall-out rates and annual trace metal concentrations from the seven municipal monitoring stations between 2015 to 2019. bdl refers to samples below detection limit. Dust fall-out rates were determined by dividing the weight of the insoluble material collected by the cross-sectional area of the funnel and the number of days over which the sample was taken. Net masses of metals obtained within the five year-year long monitoring are reffered here in ppm.*

	n	Annual Minimum	Annual Maximum	Annual Mean	Standard Deviation (SD)
2015	63				
Net mass (mg/y)		0	43	50	80
No. of days		27	37	32	4
Dust fall-out rate (mg/m^2/day)		2	517	63	99
Pb (ppm)		bdl	1284	140	191
Cu (ppm)		14	38919	1714	4989
Zn (ppm)		83	3578	892	764
Fe (ppm)		253	110092	17970	20155
2016	58				
Net mass (mg/y)		0	133	70	17
No. of days		0	35	28	7.17
Dust fall-out rate (mg/m^2/day)		0	2021	107	267
Pb (ppm)		bdl	2051	316	368
Cu (ppm)		bdl	7171	865	1489
Zn (ppm)		bdl	1754	491	376
Fe (ppm)		bdl	63749	16429	13000
Mn (ppm)		bdl	11201	1092	1629
2017	44				
Net mass (mg/y)		20	56	10	10
No. of days		30	66	34	5.63

Dust fall-out rate (mg/m^2/day)		25	741	124	126
Pb (ppm)		9	1620	241	269
Cu (ppm)		13	1089	256	239
Zn (ppm)		29	1620	463	326
Fe (ppm)		1388	40090	17699	10333
Mn (ppm)		52	13636	1836	2804

Cont'd on page 6

2018	64				
Net mass (mg/y)		2	110	100	17
No. of days		12	41	30	4.05
Dust fall-out rate (mg/m^2/day)		0.00	1305	135	207
Pb (ppm)		bdl	1406	252	327
Cu (ppm)		17	9105	668	1411
Zn (ppm)		28	2281	442	377
Fe (ppm)		664	76868	17449	13174
Mn (ppm)		17	9310	1348	1685
2019	56				
Net mass (mg/y)		11	1000	77	100
No. of Days		24	33	29	2.47
Dust fall-out rate (mg/m^2/day)		14	866	112	144
Pb (ppm)		6	2748	226	452
Cu (ppm)		23	10394	1903	2986
Zn (ppm)		76	3068	615	523
Fe (ppm)		2685	80000	25217	18015
Mn (ppm)		102	15484	2620	1946

Table S3. Summary of all dust fall-out rates (mg/m2/day) at the seven municipal monitoring stations 2015 to 2019.

Sampling locations	**Range of average dust fall-out rates (mg/m^2/day)**	**Average (± SD) of all dust fall-out rates over the five year period**	**Year of peak dust load**
CA	20 - 741	254 ± 161	2017
NEA	6 - 2021	107 ± 192	2016
NNA	4 - 122	53 ± 31	2017
NWA	4 -124	56 ± 54	2017
SCA	9 - 297	77 ± 64	2017
SEA	9 - 1305	113 ± 183	2018
SWA	8 - 105	40 ± 23	2019

***Table S4**. Summary of the trace metal concentrations in dust samples collected using buckets between 2015 and 2019. In addition, the table shows a summary of statistically significant differences in annual mean trace metal concentrations between years.*

Trace element	**2015-2019 average (±SD) concentration in ppm**	**Year of peak concentration**	**Statistically significant differences in annual mean trace metal concentration between sampled years**
Mn	13 636 ± 9310	2017	(p = 0.02) between 2016 and 2017
Pb	2051 ± 1284	2016	(p = <0.001) between 2015 and 2016 (p = 0.045) between 2017 and 2018
Fe	110092 ± 40900	2015	(p = 0.02) between 2018 and 2019
Zn	3578 ± 1620	2015	(p = 0.004) between 2015 and 2016
Cu	38 919 ± 1089	2015	(p = 0.001) between 2016 and 2017 (p = 0.037) between 2018 and 2019

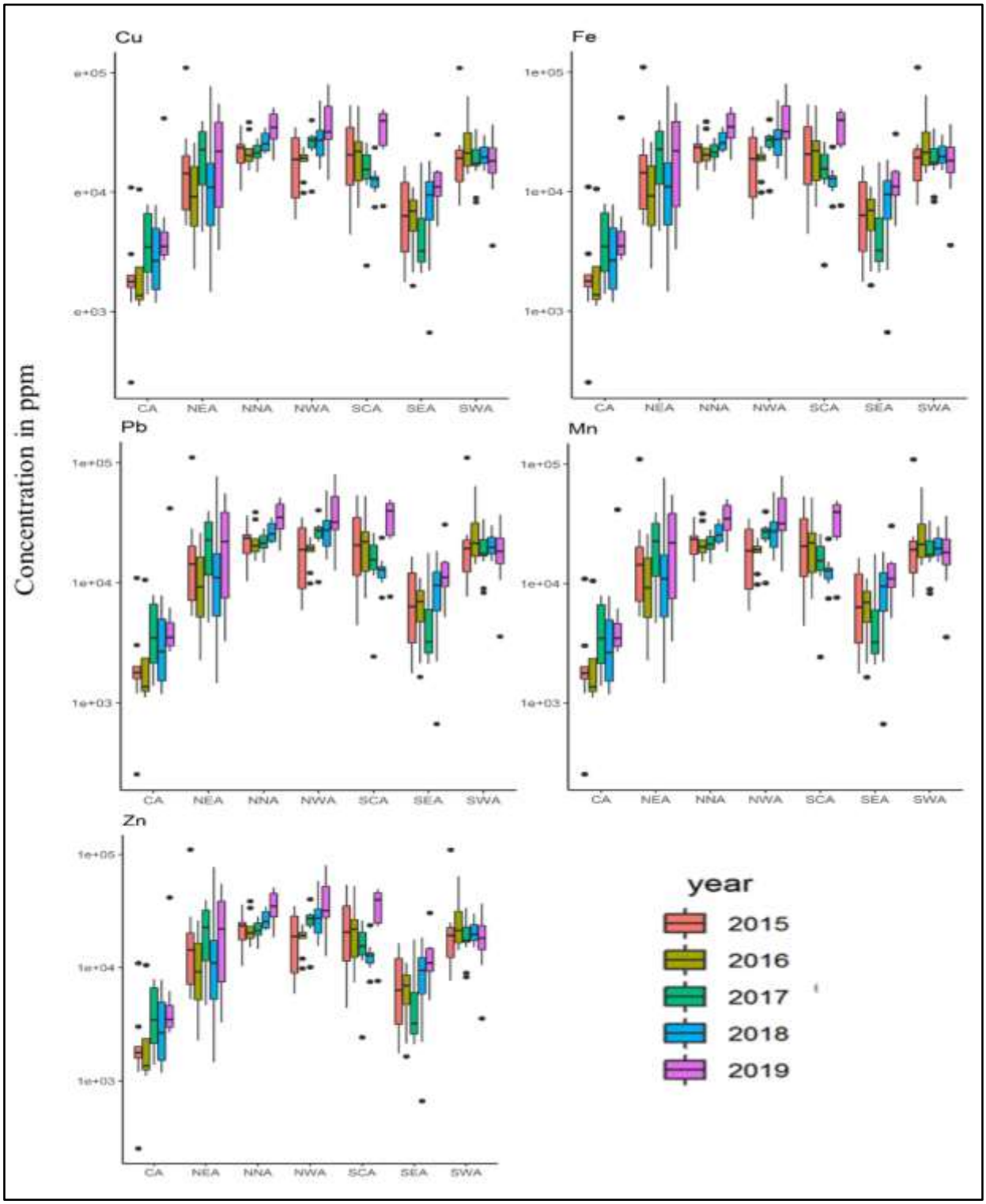

Figure S1. *Annual mean net metal mass in ppm in bulk dust measured from 2015 to 2019, see Figure 1 and Table 1 for station locations. Mn was only analysed from 2016 to 2019. One Cu outlier value was removed for interpretation purposes. The error bars represent the standard deviation of the monthly data for each annual mean.*

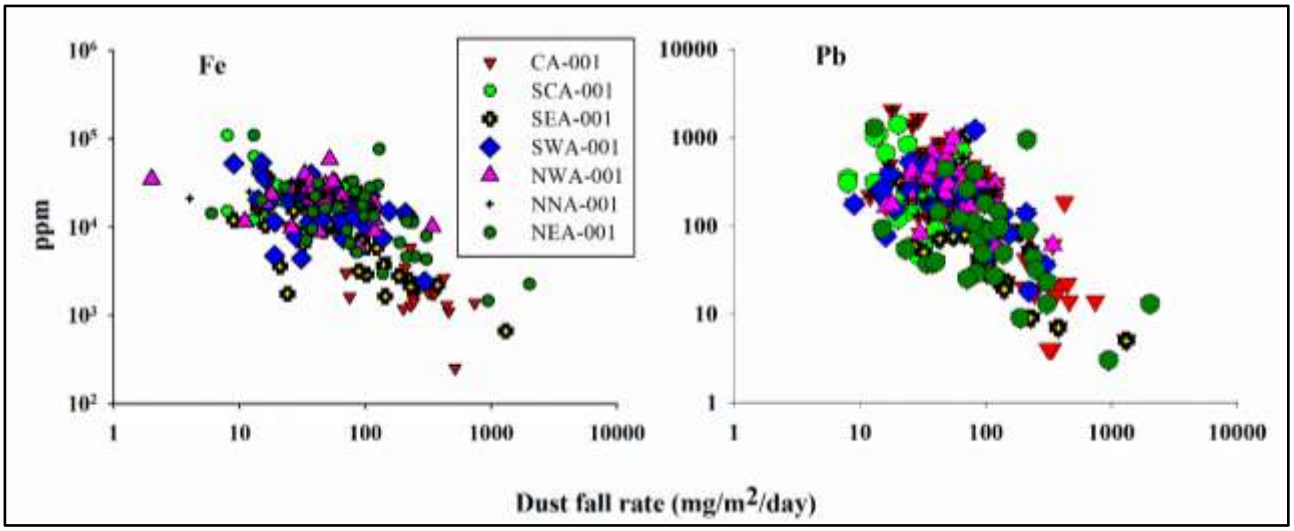

***Figure S3**. Dust fall-out rate vs concentration of trace metals Fe and Pb showing that stations that had high trace metal concentrations often had a low dust fall-out rate. The axes are plotted at log-scale to better visualise the relationship between the dust fall-out rate and trace metal concentration.*

S.2. VOLUMETRIC FLOW CONTROLLED (VFC) SAMPLE SUPPORTING BULK METAL COMPOSITION AND MINERALOGICAL CHARACTERISTICS

S.2.1. VFC METHODS

A dust sample for i) mineralogical characterization ii) further determination of trace metal composition of the bulk dust, as well as iii) further fractional solubility leaching experiments, was collected using a Volumetric Flow Controlled (VFC) high volume air sampler (Tisch Environmental, TE-5170V-BL), continuously for two weeks in March 2019 at one station (SWA, Figure 2; Table 1). Sampling followed trace metal clean sampling protocols (Morton et al., 2013) and particles were collected on a 12 x 47 mm Whatman 41 cellulose filter pre-cleaned in a 1 M HCl bath (Cutter et al., 2017). Prior to deployment, the filter was rinsed five times with Milli-Q (18 μΩ-Milli-Q Advance 10) before being dried under laminar flow. The filter was stored in a cleaned plastic zip-lock bag until deployment (Morton et al., 2013). After sampling, the filter was folded in half and stored in the freezer until analysis.

The 12 x 47 mm filter sheet was sub-sampled into 47 mm diameter discs with a ceramic knife and retained for analysis. The dust on the filter collected with the VFC sampler was analysed with the same ICP-MS system as described in the main text for BSNE bulk sample analysis. The filters were digested using 2% HNO_3 in a microwave prior to ICP-MS analysis.

S.2.2. VFC mineralogical characteristics and bulk metal load

Trace metal concentrations in the VFC sample (Table S5) followed a similar order as in most of the BSNE sample, i.e. Fe, Al, Zn > Mn > Pb > Cu > V. Some trace metals, such as Pb, Zn and Cu were strongly enriched in the particles collected using the VFC at station SWA (EF>>10; Table S6). Iron and V showed some enrichment (EF 4 and 10, respectively; Table S6). The angular and clustered grains dominated the dust collected at station SWA, close to the ocean (Figure S4). At this station, the angular, clustered grains were larger (mainly between 2- 200 μm) relative to the spherical particles and may have been derived from sea spray and natural dust. The larger fraction (> 5 μm) are enriched in silica minerals (Figure S5). The particles in the samples were dominated by hematite (Fe_2O_3), quartz (SiO_2), clay minerals, halite and zinc oxides possibly due to the oceanic influence, while the sample from NEA was richer in iron-oxide (Figure 4). The micrograph SEM analyses further indicate that station SWA has elevated concentrations of Na, Mg, Al, Si, and Cl, possibly a result of sea spray from oceanic sources and clay minerals from terrestrial sources.

***Table S5**. Trace metal concentrations of aerosols from Saldanha Bay collected using the VFC sampler collected from 03 May 2018 to 20 May 2018. All trace metal concentrations are reported in ppm.*

VFC Sample ID	**V**	**Cu**	**Pb**	**Al**	**Mn**	**Fe**	**Zn**
SWA	35.8	34.3	44.8	70 044	290	20 424	50.5

***Table S6**. Enrichment factors in dust aerosols from Saldanha Bay collected using the VFC samples.*

VFC Sample ID	**V**	**Mn**	**Cu**	**Zn**	**Pb**	**Fe**
SWA	9.7	0.2	22	57	70	4.2

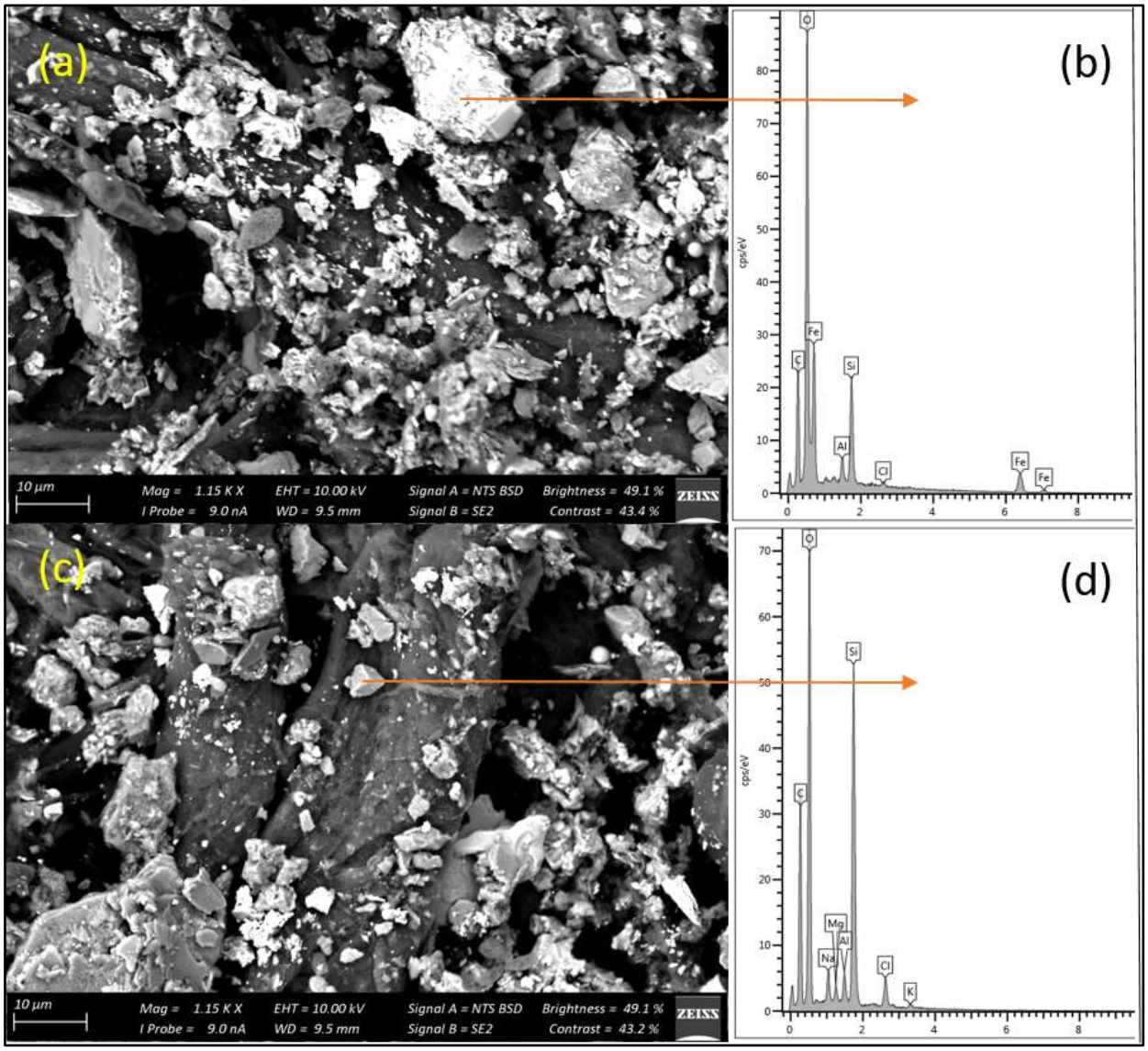

***Figure S4**. SEM images of from station SWA mineral dust particles collected on a Whatman 41 filter. Take note of the micrometer individual particles and agglomerated angular grains. There are also a few platey particles. The much finer particles will potentially be part of the filter matrix.*

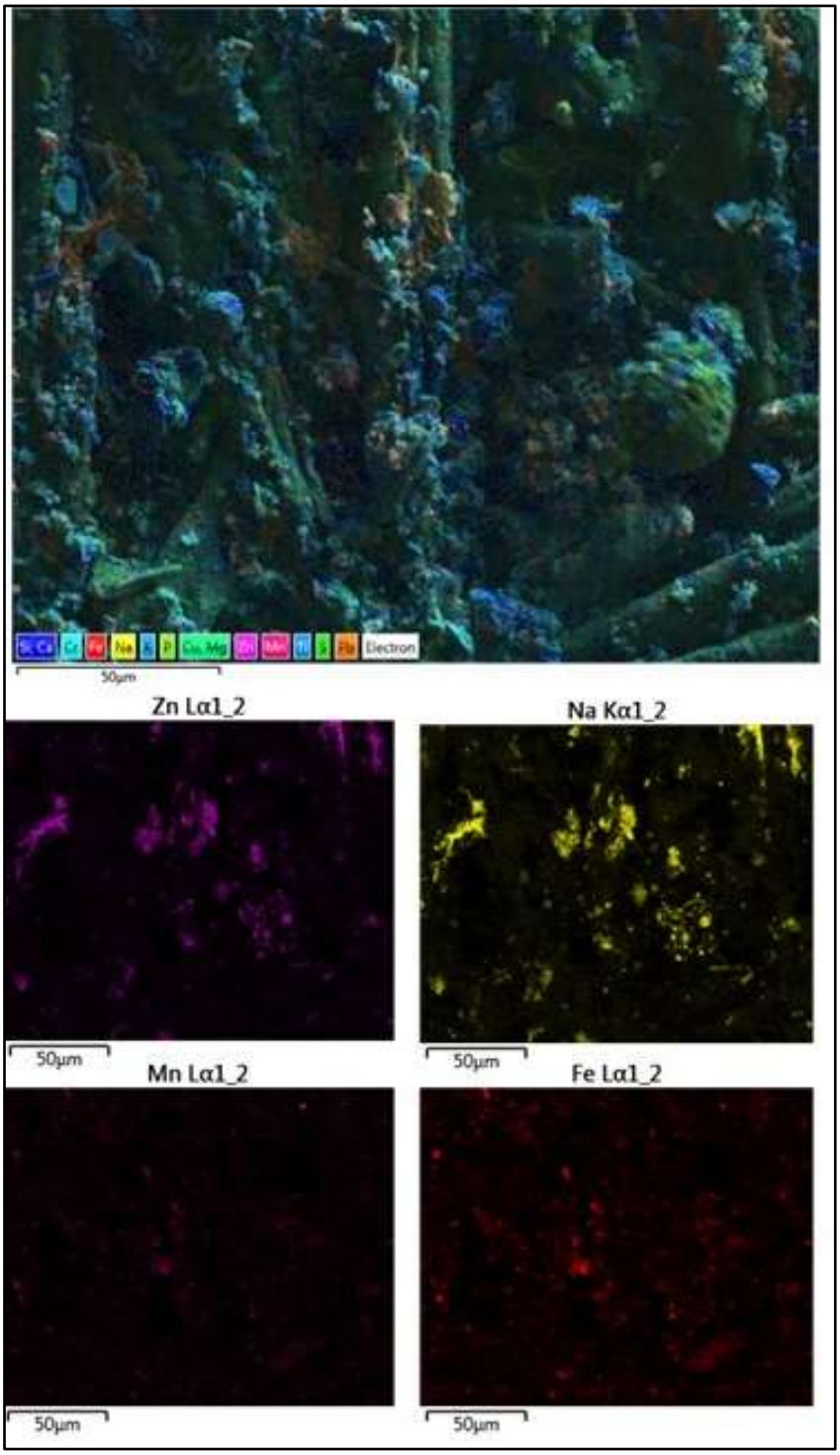

***Figure S5**. SEM elemental mapping of a Saldanha Bay filter dust sample from station SWA, with micrographs showing individual dominant minerals in the area.*

S.3. SUPPLEMENTARY REFERENCES

Cutter, Gregory, Casciotti, Karen, Croot, Peter, Geibert, Walter, Heimbürger, Lars-Eric, Lohan, Maeve, Planquette, Hélène, van de Flierdt, Tina (2017) Sampling and Sample-handling Protocols for GEOTRACES Cruises. Version 3, August 2017. Toulouse, France, GEOTRACES International Project Office, 139pp. & Appendices. DOI: http://dx.doi.org/10.25607/OBP-2.

Morton, P.L., Landing, W., Hsu, S., Milne, A., Aguilar-Islas, A., Baker, A., Bowie, A., Buck, C., Gao, Y., Gichuki, S., 2013. Methods for the sampling and analysis of marine aerosols: results from the 2008 GEOTRACES aerosol intercalibration experiment. Limnol. Oceanogr. 11, 62–78. https://doi.org/10.4319/lom.2013.11.62.

CHAPTER 3: SOLUBILITY OF TRACE METALS IN DUST FROM ONE OF THE DUSTIEST NON-PLAYA ENVIRONMENTS IN THE NAMIB DESERT

A presentation of the prepared research paper

This research manuscript has been prepared for submission to Aeolian Research. I am the lead author of the manuscript. S. Fietz, F. D. Eckardt, and J. Von Holdt were co-authors. I was responsible for the collection of field data, data processing and writing of the manuscript.

This manuscript contributes to understanding of the trace metal content and solubility of dust from a non-playa environment in the Namib Desert. The data was compared to other global natural dust sources. In addition, this provides information on the link between solubility and other mineralogical characteristics. The aim is to achieve a better understanding of the impact of these southern African non-playa environments to surrounding oceans.

SOLUBILITY OF TRACE METALS IN DUST FROM ONE OF THE DUSTIEST NON-PLAYA ENVIRONMENT IN THE NAMIB DESERT

Kaukurauee Ismael Kangueehi[1], Frank D. Eckardt[2], Johanna Von Holdt[3], Alakendra N. Roychoudhury[1], Susanne Fietz[1]*

[1]Centre for Trace Metal and Experimental Biogeochemistry, Department of Earth Sciences, University of Stellenbosch, 7600 Stellenbosch, South Africa

[2] Environmental and Geographical Science Department, University of Cape Town, South Africa

[3] Chemical Engineering Department, University of Cape Town

*corresponding author: Department of Earth Sciences, Stellenbosch University, 7600 Stellenbosch, South Africa, sfietz@sun.ac.za, +27218083117

Keywords: Hysplit, Fractional solubility, Bioaccessibility, Qemscan, GEOTRACES

3.1. ABSTRACT

Dust plays an essential role in the drawdown of atmospheric CO_2, as it can alter the biogeochemistry of marine environments supplying important trace metals such as iron, zinc, manganese and aluminum to open surface oceans. In this study, we investigate the total and soluble trace metal concentrations as well as mineralogical composition, particle size distribution and particle shape of dust from the dustiest non-playa sources in the Namib Desert. Big Spring Number Eight (BSNE) samplers and Modified Wilson and Coock (MWAC) dust sampling traps were used to collect mineral dust. We distinguished samples from coastal and inland settings since these represent contrasting environments. The dust samples were used for determination of mineralogical characteristics with Quantitative Evaluation of Minerals by Scanning Electron Microscopy (QEMSCAN). Most prominent mineralogical distinctions were observed in the fine particles (< 5 µm) while the mineralogy of the coarse-grained fraction was similar between stations. Total trace metal contents varied largely, ranging for example from 15 500 to 35 000 ppm for Fe, from 19 000 to 29 200 ppm for Al, and from 16 to 30 ppm for Cu. Milli-Q water and a weak acid were used in leaching experiments to mimic atmospheric conditions and to determine the soluble fractions. The fractional solubility of the trace metals in pure water was low especially for Fe and Al, ranging from 0.1 to 2% and 0.3 to 0.6% respectively. The solubility was higher for other trace metals such as Cu (1.5 to 7.8%), Zn (2 to 16%), Mn (2 to 9%) and Pb (0.2 to 8%). The mineralogy indicated that FeO and sulphides in the fine particles partially controlled the solubility, especially for Fe, Zn and Pb. Particle sizes distribution and shapes coupled with occasional occurrence of strong winds suggest that dust from these sources can travel long distances. Hysplit forward trajectories furthermore showed that air masses are transported towards ocean areas of high chlorophyll-concentrations and can potentially impact these regions. This study highlights the potential importance of the southern African natural dust emitters to proximal oceans.

3.2. INTRODUCTION

Desert dust is an important pathway of micronutrient re-supply in the surface ocean. Upon deposition in micronutrient depleted areas, such dust can temporarily increase primary productivity (Baker and Croot, 2010; Mahowald et al., 2009; Spokes et al., 2001), and alter the biogeochemical systems (Jickells et al., 2005; Mahowald et al., 2009; Tatlhego et al., 2020). For example, in modern times, dust from the Sahara drastically alters the biogeochemistry of the North Atlantic (e.g. Conway and John, 2014; Shelley et al., 2018). In addition, the role of mineral dust in primary production and biogeochemical cycling is an essential component in CO_2 and global climate fluctuations (Muhs, 2013). Paleo-reconstructions for example, showed that high dust supply is linked to high primary productivity in the Southern Ocean coupled with reduced global atmospheric CO_2 during the glacial maxima (Kohfeld and Harrison, 2001; Lambert et al., 2008; Lüthi et al., 2008).

Dust sources from the Southern Hemisphere only contribute ~5% of all global dust sources, hence most dust studies focused on the Northern Hemisphere that contributes >90% (Goudie and Middleton, 2001; Ginoux et al., 2012). However, in recent years, there has been a gradual rise in research investigating dust activities and sources in the Southern Hemisphere and more specifically in southern Africa (Bhattachan et al., 2015, 2012; Klopper et al., 2020; Vickery et al., 2013; von Holdt, 2013; 2021). Most of the studies in southern Africa focused on ephemeral dry river valleys and ephemeral inland pans (Bhattachan et al., 2015; Dansie et al., 2018; Vickery et al., 2013), which are visible on satellite images. Other non-playa environments such as gravel plains, sand seas and other inland sources, which are difficult to identify with remote sensing techniques, are potentially overlooked. In this study, we aim to investigate these non-playa sources in the Namib Desert.

Previous studies have revealed that Namibian dust has some of the highest Fe contents globally (Eltayeb et al. 1993). High contents of bulk trace metals and in some studies bioavailable Fe were reported along dry river valleys along the Namibian coastline (Dansie et al., 2018, 2017b; Formenti et al., 2019; Klopper et al., 2020). This dust can potentially travel long distances (Bhattachan et al., 2015, 2012; Tatlhego et al., 2020; Thomas and Leason, 2005) and fertilize surrounding surface oceans (Dansie et al., 2017, 2017b), such as the Southern Ocean and the Benguela Upwelling System (Capone and Hutchins, 2013; Jickells et al., 2005). In some regions the primary productivity is low despite high macronutrient availability because of limited micronutrient supply such as Fe, Zn, Mn, Co, Cu, and Cd and aeolian supply may therefore be important. In this study, we consider the suite of these essential trace elements in the Namibian dust.

To assess the potential impact of aeolian micronutrient supply, it is however, important not to only consider the total amount of trace metals, but to focus on the soluble fraction, which indicates bioaccessibility (Baker et al., 2006; Sholkovitz et al., 2012). The fractional solubility of trace metals in mineral dust from a variety of global sources, range from 0.01% to 90% (Aguilar-Islas et al., 2010; Baker et al., 2006; Mahowald et al., 2018; Sedwick et al., 2007; Wu et al., 2007). Among other factors, the solubility is controlled by morphological characteristics and geochemical and mineralogical composition (Baker et al., 2006; Desboeufs et al., 2005, 2001; Hettiarachchi et al., 2018; Mahowald et al., 2018). An example of the importance of mineralogical characteristics and composition is that iron oxides and hydroxides in mineral dust are often the principle contributors of Fe (Hettiarachchi et al., 2018; Meskhidze et al., 2005), while Fe solubility is higher in the alumino-silicates such as feldspars and clays (Desboeufs et al., 2005; Journet et al., 2008). Hence, trace metal content and solubility do not always match. In addition, different minerals have different surface properties and particle sizes, attributing a considerable variation in the solubility of clays and oxides (Journet et al., 2008a). The mineralogical composition, particle sizes and geomorphology of some prominent dust sources in southern Africa have been recently studied (von Holdt et al., 2021). Here, we assess the mineral characteristics and composition along with the fractional solubility in the Namibian dust (Journet et al., 2008; Koffman et al., 2021; Paris et al., 2011).

This study investigates mineral dust emitted from one of the dustiest non-playa environments in Namibia. We analyzed the mineralogy, chemistry, and particle morphology and size distribution from four sites situated in close proximity to the gravel plains, sand seas and sand dunes. In addition, this study links fractional solubility of dust from these four sites to their mineralogical characteristics and assesses the potential impact this dust can have on the proximal and remote oceans.

3.3. METHODS

3.3.1. Study Site

The Namib Desert stretches from the coast, approximately 150 kilometers eastwards (Figure 1) (Jacobson et al., 2000). Even though the Namib Desert is a coastal environment, it is hyper-arid, with a gradual decline in rainfall and temperature from the east to the west. At the eastern edge, the rainfall gradually rises to over 500 mm annually in the Khomas Highlands. The Namib Desert central area experiences very low rainfall with an annual average of 27 mm at Gobabeb (Lancaster et al., 1984), and an annual evaporation of approximately 3000 mm (Eckardt et al., 2013; Lancaster et al., 1984). The Namib Desert weather system is mainly influenced by the

subtropical anticyclonic zone located southwest and the cold Benguela current to the west (Armstrong et al., 2014). The coastal dryness is due to the widespread strong subsidence from the high-pressure belt and is increased and sustained by the temperature advection caused by east-northeasterly onshore winds from the South Atlantic anticyclone (Formenti et al., 2019; Heine, 2005). The cold Benguela Current System maintains coastal fog which can extend up to 60 km inland (Abrams et al., 1997; Eckardt et al., 2013; Eckardt and Schemenauer, 1998; Gottlieb et al., 2019) and results in relatively low temperatures, less radiation, stronger winds and higher humidity on land (Heine, 2005; Vogel, 1989).

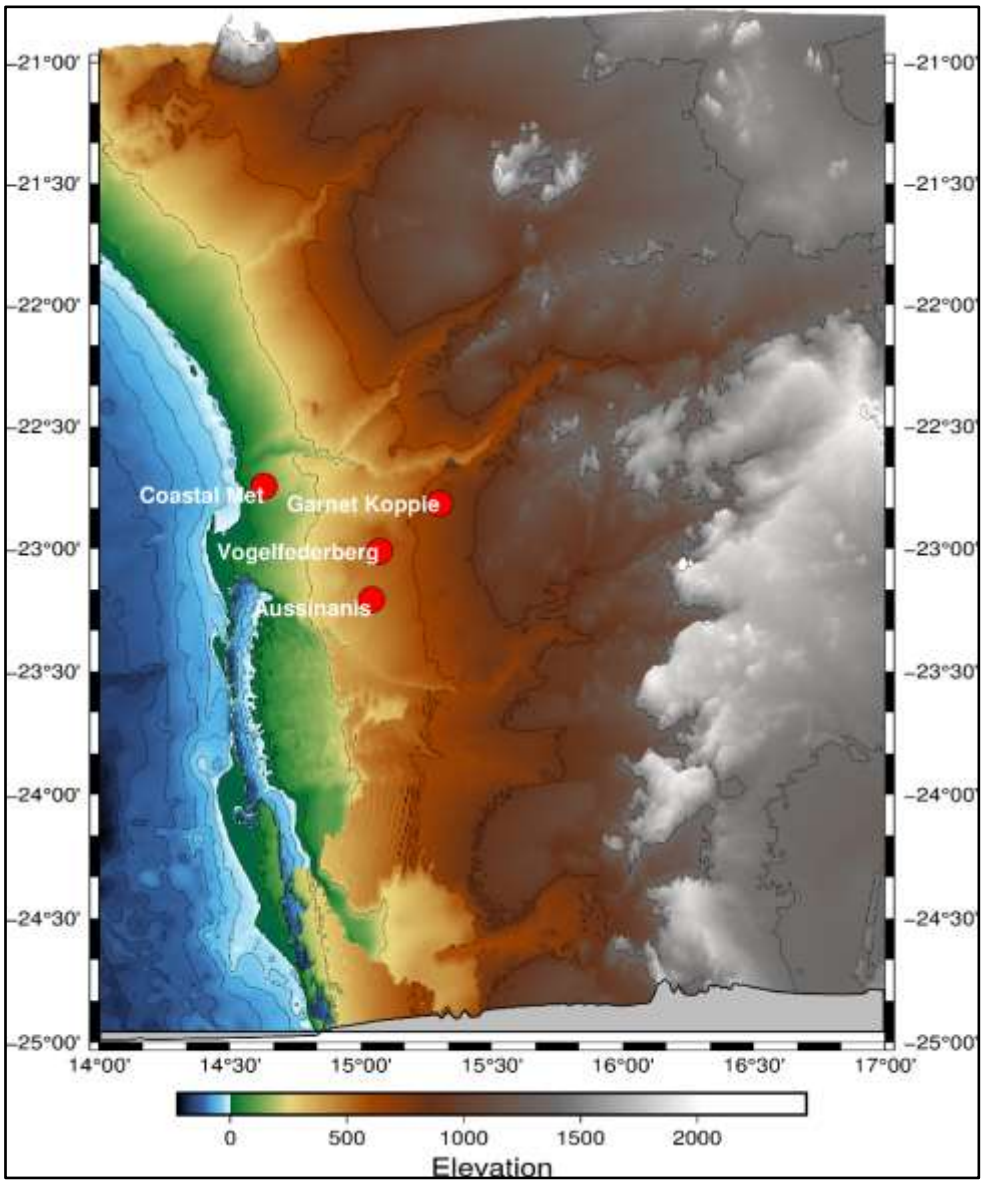

***Figure 1**. Map of the sampling sites in the Namib Desert, Namibia. Station location coordinates are given in Table 2. Station names correspond to SASSCAL Monitoring Observation network (http://data.sasscal.org/metadata/view.php?view=station_meta&id=5699&ident=580240755916261319).*

***Table 1**. Coordinates and basic meteorological conditions defining the three main dust sampling sites. The sites are classified in three different locations based on the various climatic conditions.*

	Coastal (**Coastal Met**) (CM)	Central (**Aussinanis)** (AS)	Central **(Vogelfederberg)** (VF)	Inland (**Garnet Koppie**) (GK)
Coordinates	(-23.05 S, 14.63 E)	(-23.45 S, 15.04 E)	(-23.28 S, 15.07 E)	(-23.11 S, 15.30 E)
Fog and Stratus	Frequent	Occasionally	Occasionally	None
Rainfall	Rarely (< 20 mm)	Infrequent (< 50 mm)	Infrequent (<50 mm)	High (50 – 100 mm)
Temperature	Low temperature	Higher temperature	Higher temperature	Highest temperature
Maximum Wind speed	Strong winds from E and SW (maximum wind speed (Max wind speed 23.4 m/s on 15 November 2017)	Strong winds from NE and NW (maximum wind speed 21.1 m/s on 19 April 2017)	Strong winds from NE and NW (maximum wind speed 21 m/s on 6 July 2016)	Moderate winds from NE and SW (Maximum wind speed of 30.7 m/s on 22 March 2017)
Average wind speeds and dominant direction	3.9 m/s (E/SW)	4.3 m/s (NW/NE)	5.4 m/s (NW/NE)	4.5 m/s (NE/SW)
Radiation	Least sunlight	Moderate sunlight	Moderate	Most sunlight
Elevation (meters above sea level)	92 m	431 m	496m	746m
MWAC orientations	60˚, 220˚	60˚, 200˚	35˚, 200˚	50˚, 220˚

3.3.2. Sampling sites

Dust monitoring and sample collection took place over a two-year period (2016-2017 (for MWAC) and 2019-2020 (for BSNE)). Four sites were investigated and classified as follows: the site located most inland (station "Garnet Koppie (GK) hereafter labelled "inland"), two sites in the central part considered intermediate (stations "Aussinanis (AS)" and "Vogelfederberg (VF)" hereafter labelled "central") and the site closest to the coast coastal site (station "Coastal Met (CM)" hereafter labelled "coastal") (Figure 1, Table 1). These four sites are distiguished based on background geology and meteorological conditions (Table 1). The two central stations are situated in a flat gravel plain where, most dust emitted from drainage channels and occasionally by sediment disturbances by off-vehicles touring the area (von Holdt et al., 2019). The coastal station is susceptible to strong winds and likely receives dust emissions from surrounding dunes and the Kuiseb River (Figure 1). The coastal station is located in close proximity to the Kuiseb Delta which has previously been identified as an important dust emitter in the area (Dansie et al., 2018; Eckardt and Kuring, 2005; Vickery et al., 2013; von Holdt et al., 2017). Satellite images show persistent dust emissions from the ephemeral rivers including the Kuiseb River being transported towards the Atlantic Ocean (Dansie et al., 2017b). The inland station is comprised of Precambrian Damara Orogen rocks, with commonly found intrusive granite outcrops (Eckardt et al., 2013). In addition, the Kuiseb Formation with abundant outcrops of schist outcrops and the Matchless Amphibolite Belt also passes through the Central Namib Desert (Miller et al., 2008).

3.3.3. Sample collection

Two sampling methods were used to trap dust at the four stations (Figure 2). The dust yield from the two sampling methods were expected to be different and were compared. The first sampling effort used a Modified Wilson and Cook (MWAC) samplers mounted and fixed towards the major southwest and east wind directions for a period of two years from January 2016 to December 2017 (Table 1). The MWAC samplers were set up at heights of 3 meters for all four stations to capture dust particles suspended in the air. In addition, the coastal station had a 6-meter sampling bottle. The fixed bearing angle directions for the samples were 60°, 220° for Coastal Met, 35°, 200° for Vogelfederberg, 60°, 200° for Aussinanis and 50°, 220° for Garnet Koppie. Samples were retrieved once a year except for the Coastal Met samples that were collected after the two-year period (January 2016 to October 2017). The second sampling effort used rotating Big Spring Number Eight (BSNE) samplers that were erected at 2m height (Figure 2). The BSNE samplers were able to rotate for a full 360°. The BSNE traps were deployed for a 10 month period between March 2019 and January 2020, to sample for the dry "dust season" between April and September. The samples were used for different analyses

as the low amount of dust collected did not allow to analyse all parameters on the same dust samples. This is further detailed below in section "2.4 Analytical techniques".

***Figure 2**. A monitoring station with various meteorological instruments including the (A) BSNE dust collector set at 2 m height from the central station shown for illustration of the BSNE sampling effort. (b) Persistent dust plumes being emitted from the Namib Desert towards the Atlantic Ocean (Credit: USGS/Landsat 8/OLI).*

3.3.4. Analytical techniques used for determination of dust load, mineralogical characteristics, bulk metal composition, and leaching experiments

3.3.4.1. Dust load

Samples were collected from the four stations for two consecutive years (from January- December 2016 and January-December 2017 for the MWAC samples. At some stations, more than one sample collected depending on the sampling orientation (see Table 3 below). The BSNE samples were collected after sampling from March 2019 to January 2020.

3.3.4.2. Mineralogical characteristics

All dust samples collected from the four sites using MWAC samplers were tested for physical (size and shape), mineralogical (mineral identification), and geochemical compositions using QEMSCAN, at the Centre of Mineral Research at the University of Cape Town. QEMSCAN combines scanning electron microscopy with energy dispersive spectroscopy, which allows automated, quantitative morphological and mineralogical analysis (Knappett et al., 2011; Nie and Peng, 2014). This can produce high-quality images and quantitative chemical analysis used to interpret the mineralogical characteristic of the dust. All MWAC samples were oven dried at 35°C for 24 hours, and split with a rotating microriffler to subsample roughly 0.1 g for each sample. The MWAC subsamples were then dry screened onto a resin mount, coated with graphite and stored at 35°C before analysis to minimize

the moisture on the hydrophilic salts. Approximately 10000 particles were scanned for each disc, generating data for mineralogy characteristics, particle sizes and shapes.

3.3.4.3. Bulk trace metal composition

All dust samples collected from the four sites using BNSE samplers were split into two and used for i) determination of trace metal composition of the bulk dust as well as ii) leaching experiments (see section 2.4.3). Approximately 0.1 g sample was used for bulk trace metal analysis and approximately 0.15 g sample was used for leaching experiment analysis. The bulk trace metals composition in the BSNE samples was analysed with an Agilent 7900 Inductively Coupled Plasma Mass Spectrometry (ICP-MS) at Stellenbosch University following digestion with HNO_3**.** The trace metals had an internal standard accuracy range from 96 to 108% by repeat analysis (n=10).

3.3.4.4. Dust trace metal leaching experiments

All bottles and filters used in the leaching experiments were acid cleaned following GEOTRACES protocols (Cutter et al., 2017; Jenkins et al., 2015). Sequential continuous experiments were conducted with a trace metal clean flow through method following Buck et al., (2006) and Aguilar-Islas et al., (2010). The system consisted of acid washed 0.45 µm quartz filters mounted to a single-staged PFA funnel stage connected to a front face. The reagent streams through the filter for up to 10-15 min. Duplicates were analysed for each BNSE sample. In addition, blanks were prepared as acid washed 0.45 µm quartz filters without dust. Two leaching experiments were conducted, one using Milli-Q water and one using a weak acid solution further described below.

3.3.4.5. Leaching using Milli-Q water

First, the instantaneous flow-through experiments using 50 ml of Milli-Q water were conducted for 10-15 min. Similar, previous experiments indicated that the instantaneous water dissolvable trace metal fraction can be extracted with de-ionized water for the first 10 minutes, and that there is an exponential decrease in Fe solubility with Milli-Q water leaching after the first 10 min (Aguilar-Islas et al., 2010; Perron et al., 2020). The instantaneous is used to show instant solubility of dust on surface oceans (Buck et al., 2006). The term solubility in this paper is loosely defined and the instantaneous leach can include fractions of particulate, colloidal and dissolved phases of trace metals such as Fe.

3.3.4.6. Leaching using weak acid reagent

To further identify the labile fraction, an acetic acid (HAc) and hydroxylamine hydrochloride ($Na_2OH{\cdot}HCl$) leachate was used (Berger et al., 2008; Winton et al., 2015). The Milli-Q water leached filters were transferred into new acid-washed vials, dried under laminar flow and further leached with 25% ultra-high purity HAc and 0.02 M $NH_2OH{\cdot}HCl$ at 90 °C for ~10 min. The heating process enables an additional labile fraction to be dissolved because the traditional 25% HAc room temperature leach underestimates the labile metal fraction (Chester and Hughes, 1967). This may be particularly important in areas with high abundance of terrestrial input. The heating step may also help to liberate the trace metals found in intracellular proteins in phytoplankton (Berger et al., 2008) and can assist in Fe and Mn oxyhydroxides to be released from biogenic materials (Winton et al., 2016).

3.3.4.7. Local winds and long range air mass pathways

Local wind speed and direction were measured using Young Model 05103 Wind Monitors. Measurements were recorded for each minute. Data is available on the SASSCAL WeatherNet website (http://www.sasscalweathernet.org/).

The Hybrid Single Particle Lagrangian Integrated Trajectory Model (Hysplit) dispersion model is widely utilized to study atmospheric dispersion and suspended aerosols transport for example in dust events and volcanic emission (Ashrafi et al., 2014; Goudie et al., 2015; Mcgowan and Clark, 2008; Stein et al., 2015). In this study, Hysplit was used to generate forward trajectories of air masses potentially carrying aerosols particles from the Namib Desert (-23,111ºS 15.304ºE). The trajectories were calculated from all four sampling stations (Figure 1), with one trajectory at each elevation of 50m, 500m and 1000 m above the ground level (Marx et al., 2014). The simulations were calculated for seven days (168 hours). The total simulated trajectories were classified based on different wind directions to determine the dominant air mass pathways. The trajectories were calculated using the R studio interface through the rich_iannone/splitR (available from https://github.com/rich-iannone/SplitR) and Openair (Carslaw and Ropkins, 2017) packages from the open-source libraries.

3.4. RESULTS

3.4.1. Dust loads

The highest dust yield was collected at the coastal station (CM) with a mass of 1.12 ± 0.54 g in the MWAC sampler annually, and 3.4 g in the BSNE sampler for 10 months. The inland station AS yields second highest dust loads ranging from 0.43 g (BSNE, over 10 months) and 0.24 g (MWAC for a year), while the VB and GK stations had lower yields with a range from 0.06 g (MWAC for a year) to 0.73 g (BSNE for 10 months) (Table 3).

***Table 2**. Sample weights (g) from the four collection sites. Values represent averages and standard deviations from duplicates samples except for station GK due to the low sample yield. Source areas are added based on the prevalent wind pattern at 2 and 3 m heights (Table 1)*

Sample ID	MWAC (Jan-Dec 2016 and – Jan-Dec 2017)	BSNE (April 2019 to Jan 2020)	Source Area
Garnet Koppie	0.5	0.73	Eastern Escarpment Foot
Aussinanis	0.24 ± 0.2	0.43	Central
Vogelfederberg	0.06 ± 0.01	0.17	Central
Coastal Met	1.12 ± 0.54	3.4	Coastal northern and western coast

3.4.2. Dust particle characteristics (MWAC samples)

3.4.2.1. Grain size distribution

A total of 180, 229 particles were scanned from the 15 samples collected from the four sites, with information on particle size, mineralogical composition and morphology for each particle at 2.5 µm per pixel resolution. The particle size distribution appeared in a narrow range. More than 50% of all collected particles from the four sites are less than 100 µm.

At the station collecting dust from inland (GK), all particles are smaller than 63 µm were most of the particles was in the range between 20 to 63 µm (Figure 3). The dust particles from all stations are mostly comprised of single grains and aggregates of grains. Most of the individual grains are in the fine-grained fraction (< 63µm) (Stow, 1981), while the coarse-grained particles (> 63 µm) mostly occurred as aggregates (Figure 3).

The grains are coarser at Aussinanis, collecting dust from the central area, in comparison to all other sites. The particles size distribution at the central stations ranges from below the Qemscan detection limit to 250 µm at Aussinanis, and to 125 µm at Vogelfederberg (Figure 3). The majority of the particles collected at these central stations are between 20 and 63 µm, similar to the dust

characteristics observed at the station GK collecting dust from inland. Most of the individual grains at the central stations are found in the very fine grained fraction (Figure 3), while aggregates are more common in the coarse fraction. The particles from the station GK were the finest were all particles ranged from below detection limit to only 63 µm.

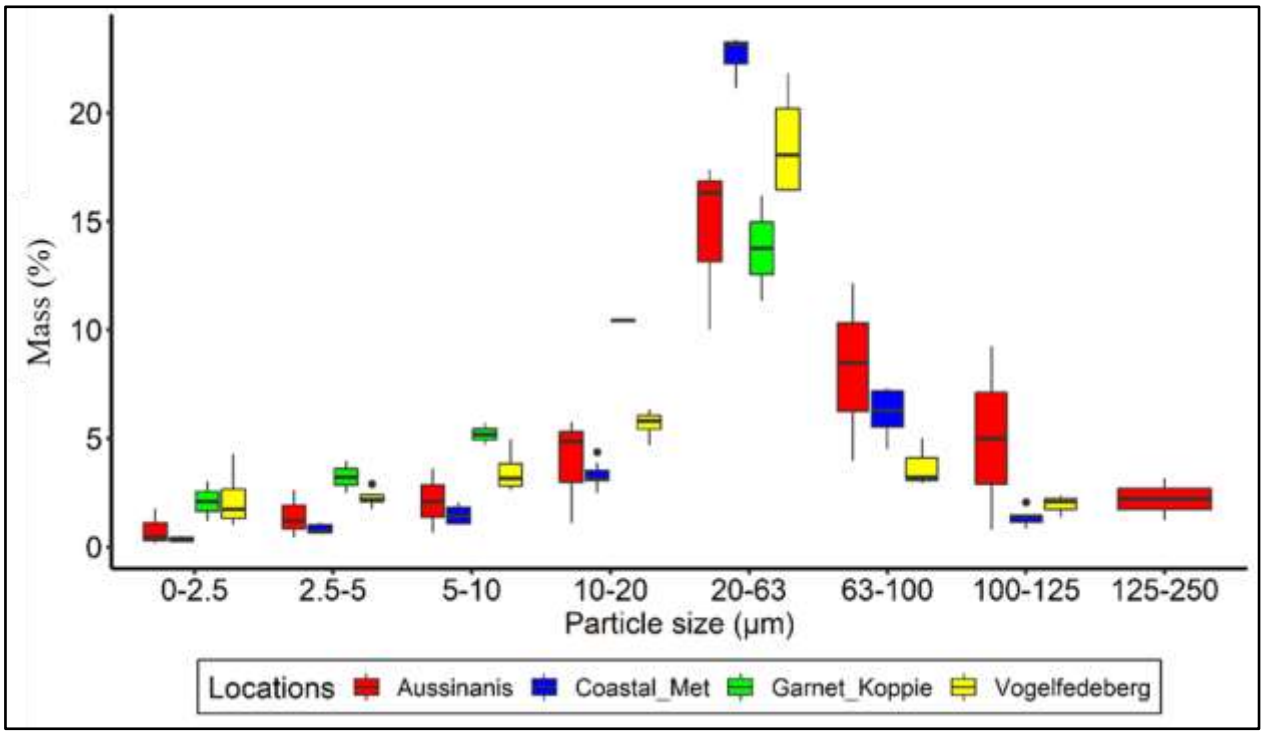

Figure 3*. Size fractions of the dust particles collected from four sites in the Namib Desert. The x-axis represents the particle size classes. The y-axis represents the mass percentage of particles for the classified size as mass percentage of total sample. The black dots are the outliers.*

3.4.2.2. Mineralogical characteristics and shape (MWAC samples)

Particle size and shape are used in this study to link the characteristics with trace metal composition and solubility, and as indicators of long-range transport. The mineralogical characteristics presented here include angular and rounded aggregates, individual platelets (flaky) and consolidated fine-grained particles at the four sites (Figure 5). A variety of Qemscan images illustrating individual high resolution particles are provided see Figure S6.

All collected samples showed abundant quartz and feldspar in the coarse fractions (i.e., in the 5 to 250 µm fraction) (Table 3). In contrast, individual Fe oxides grains and pyroxenes occurred in low abundance and were mostly found in the fine fraction (0-5 µm) (Figure 3). In some cases, intertwining of particles and coating of finer particles around the larger (coarse) particles can be observed. For example, Fe-oxides such as magnetite and hematite are observed coated around the clay minerals. As a result, elongated, plate-like shaped particles of micas, thinly plate shape clay minerals and rounded

aggregates of different minerals such as FeO, garnet, aluminosilicates and pyroxenes in cohesion with larger sized particles are apparent (Figure 4).

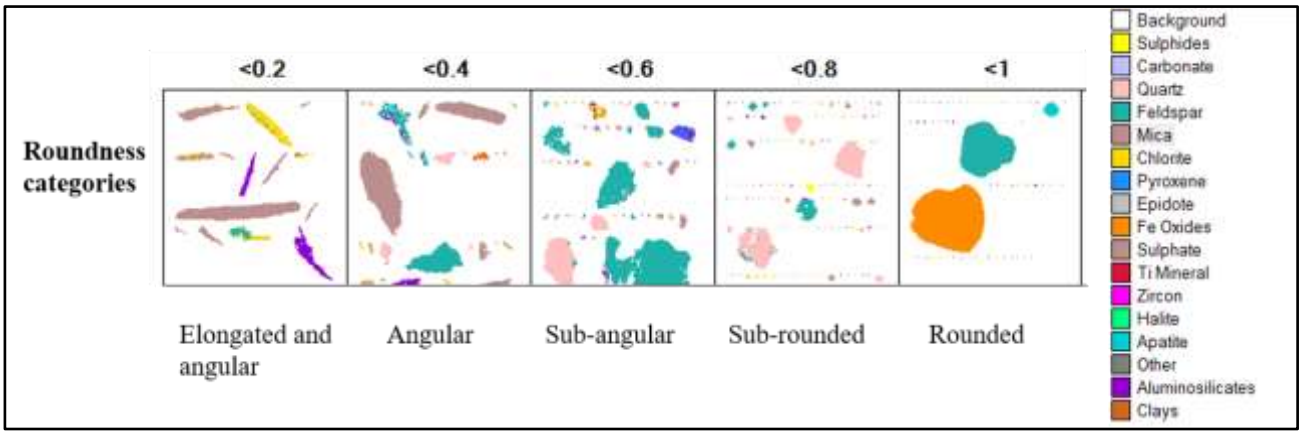

***Figure 4**. Example of the roundness distribution of observed samples, at the Coastal station which was similar at the four stations.*

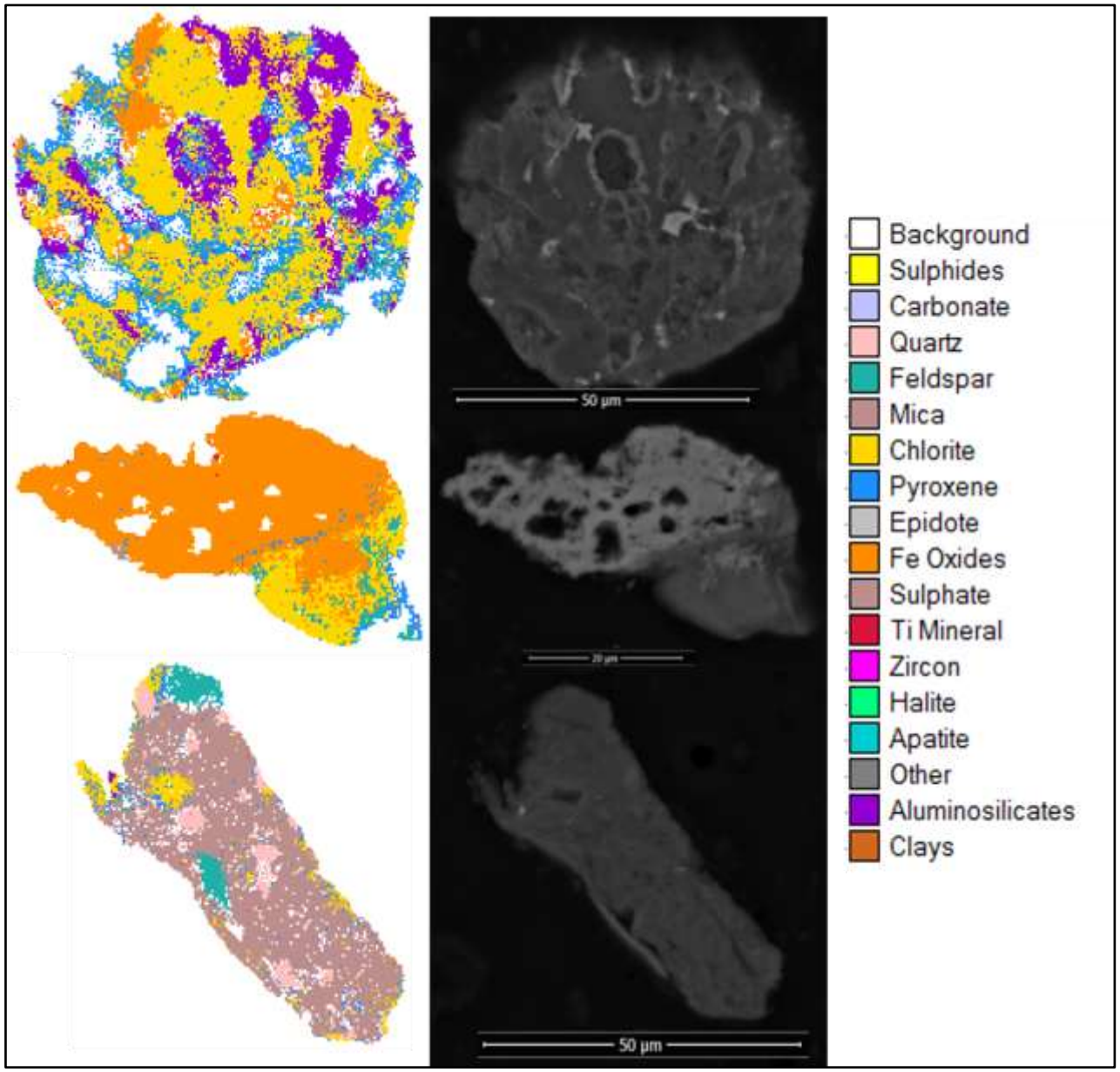

***Figure 5**. Examples of mineral aggregates from the four stations in the Namib Desert, (a) Chlorite aggregated with aluminosilicates and Fe oxides at the Coastal station, (b) Iron-oxides intertwined with pyroxenes at Coastal station, (c) Chlorite intertwined with* with micas and clays at inland station. The mineral particles shown in panels a, b, and c are not to scale.

Table 3. *Minerals composition observed in the dust collected at the four stations in the Namib Desert.*

A) Common minerals at all sites			
Quartz (15 to 40%), feldspar (17 to 32%), alumino-silicates (3 to 6%), biotite (~15%), muscovite (~10%), garnet (~4%), chlorite (~2%), pyroxene (~2%), clays (~0.5%)			
B) Mineral composition at each site in the fine fraction (0 to 2.5 µm)			
Coastal Met (Coastal Station)	**Aussinanis (Central Station)**	**Vogelfederberg (Central Station)**	**Garnet Koppie (Inland Station)**
Halite (5%), biotite (18%), muscovite (15%), chlorite (14%)	Goethite (17%), sulphides (13%), Fe-oxides (10%) and muscovite (10%)	Sulphides (10%), carbonates (47%), goethite (5%)	Sulphides (37%), Fe-Oxides (18%), goethite (12%), garnet (18%)

3.4.3. Total trace metal and leached concentrations (BSNE samples)

3.4.3.1. Total and soluble trace metal concentrations

Due to the low dust load, we could only analyse one sample for VF and GK for bulk concentrations, (but used duplicates for leaching experiments, cf. section 3.3.2). The low dust might have been influenced by the sampling method. Highest Al concentration of 23 259 ± 1140 ppm is observed at the stations closest to the coast (CM), compared to lower concentrations at the central stations (AS and VF) has a lower total Al concentrations (e.g., 19 238 ± 292 ppm for AS) (Table 4). Lowest Al concentration of 18 964 ppm is observed at the inland station (GK) (Table 4). The total Fe concentration is highest at the inland station (GK) (28 484 ppm) than at the coastal (25 052 ± 1183 ppm) and the central stations (15 516 ± 3229 ppm). The Cu concentration was highest at the inland station (30 ppm), which was almost twice as high as at the central (15.7 ± 7.7 ppm) and coastal stations (17.5 ± 0.88 ppm). Similarly, Zn is also highest at the inland station (22 372 ppm) compared to the central (18 623 ± 4251 ppm) and central station (12581 ± 159 ppm). The total Mn concentration is highest at the coastal station (318 ± 26 ppm), in comparison to central (227 ± 48 ppm) and inland station (237 ppm). The Pb concentration is also highest at the inland station (365 ppm) followed by the central station (200 ± 58 ppm), while the lowest total concentration is observed at the coastal station (14 ± 11 ppm), while the Central stations (AS and VF) had a higher total Al concentration (19 238 ± 292 ppm) than the Inland station (GK) with concentration of 18 964 ppm. The total Fe concentration is highest at the inland station (GK) (28 484 ppm), while the coastal station (25 052 ± 1183 ppm) had relatively higher Fe in comparison to the central stations (15 516 ± 3229). The highest

total Cu concentration was at the inland station (30 ppm), which was almost twice as high compared to the central (15.7 ± 7.7 ppm) and coastal station (17.5 ± 0.88 ppm). Similarly Zn was also highest Zn at the inland station (22 372 ppm) compared to the central (18 623 ± 4251 ppm) and central station (12581 ± 159 ppm). The total Mn concentration was highest at the coastal station (318 ± 26 ppm), in comparison to central (227 ± 48 ppm) and inland station (237 ppm). The total Pb concentration is also highest at the inland station (365 ± 0 ppm) followed by the central station (200 ± 58 ppm), while the lowest total concentration was observed at the coastal station (14 ± 11 ppm).

Table 4. Total trace metal concentrations for the four stations in the Namib Desert. Concentrations are presented in ppm as average of two and standard deviation where duplicates could be analysed.

Location	**Al**	**Fe**	**Zn**	**Cu**	**Pb**	**Mn**
Coastal Met	23 259 ± 1140	25 052 ± 1183	12 850 ± 159	18 ± 0.9	11 ± 4	318 ± 26
Aussinanis	19381 ± 218	17 836 ± 2276	16 215 ± 1163	18 ± 9	212 ± 77	252 ± 27
Vogelfederberg	18951	10 875	23 438	10	175	176
Garnet Koppie	18 964	28 484	22 372	30	366	237

3.4.3.2. Trace metal solubility

The solubility of the trace metals in the dust is low when assessed instantaneously leached with Milli-Q water (often considered the lower limit of the soluble fraction, (Perron et al., 2020). For example, the concentration of the soluble fraction of Fe in dust from the coastal station (CM) is 1.5 ± 0.8 ppm. Similarly, the concentration of the soluble fraction of Fe of 1.1 ± 0.07 ppm (at AS) and 0.6 ± 0.1 ppm (at VF) is low at the central stations.The lowest concentration of the soluble fraction of Fe of 1 ± 0.4 ppm is reported at the inland station (GK) (Table 5). The highest concentration of the soluble fraction of Al is observed at the central station AS (7.1 ± 4.3 ppm), while it is lowest (3.6 ± 0.5 ppm) at the central station VF . The coastal station (CM) (6.8 ± 3.4 ppm) and the inland station (GK) (6.4 ± 4.9 ppm) have similar concentration of the soluble fraction of Al. Mn shows a similar distribution to Al with highest soluble concentrations reported at the central station (AS) with 4.6 ± 2 ppm, while the lowest was observed at VF (0.4 ± 0.001 ppm). The soluble Mn concentrations for the coastal station (CM) (1.8 ± 0.2 ppm) was more than twice as high as at the inland station (GK) (0.5 ± 0.05 ppm).

Table 5. *Soluble trace metal concentrations for the four stations in the Namib Desert when leached with Milli-Q water. Concentrations are presented in ppm as average of duplicates and standard deviation.*

Location	**Al**	**Fe**	**Zn**	**Mn**	**Pb**
Coastal Met	6.8 ± 3.4	1.5 ± 0.8	257 ± 52	1.8 ± 0.2	0.01 ± 0.0003
Aussinanis	7.1 ± 4.3	1.1 ± 0.07	261 ± 117	4.6 ± 2	0.1 ± 0.12
Vogelfederberg	3.6 ± 0.5	0.1 ± 0.63	72 ± 2.8	0.4 ± 0.01	0.01 ± 0.007
Garnet Koppie	6.4 ± 4.9	1.0 ± 0.4	78 ± 8.6	0.5 ± 0.05	0.1 ± 0.03

The labile fractions assessed using the weak acid leach (also referred to as the upper limit of the soluble fraction) are summarised in Table 6 for selected trace metals, such as Fe, Cu, Zn, Mn, Pb, and Al discussed in this study. At the Coastal station (CM), the concentrations of labile Al (128 ± 12 ppm) were highest compared to the central (76 ± 21 ppm) (AS) and (30 ± 7 ppm) (VF), while the inland station (GK) has a soluble Al concentration of 76 ppm. The concentrations of labile Fe were higher at the inland station (GK) (579 ppm), than at the coastal station (CM) (66 ± 14 ppm). Inland station AS (66 ± 8 ppm) has similar concentration of labile Fe as CM, but lower than station VF (20 ± 6 ppm). The highest concentration of labile Cu (1.3 ± 0.05 ppm) was observed at the coastal station (CM), while the concentration, decreased from central (0.9 ± 0.2 ppm) to the inland stations (GK) (0.5 ppm). The concentration of labile Zn was higher at the coastal station (1893 ± 220 ppm), than at the inland station (1432 ppm), and lowest the central station (949 ± 251 ppm). The Mn concentrations were higher at the inland station (22 ppm), than at the coastal (16 ± 5.4 ppm) and central station (8 ± 3.6 ppm). The soluble Pb concentrations were higher at the inland station (12.2 ± 0 ppm), than at the central station (4.1 ± 3.8 ppm) and coastal station (0.78 ± 0.19 ppm).

Table 6. *Labile trace metal concentrations for the four stations in the Namib Desert when leached with weak acid leach. Concentrations are presented in ppm as an average duplicates and standard deviation where available.*

Location	**Al**	**Fe**	**Zn**	**Mn**	**Cu**
Coastal Met	128 ± 12	66 ± 14	1893 ± 220	16 ± 5	1.3 ± 0.05
Aussinanis	76 ± 25	80 ± 8	1100 ± 250	11 ± 2	0.93 ± 0.2
Vogelfederberg	30 ± 7	20 ± 6	798 ± 188	8 ± 1.2	1.3

Garnet Koppie	76	579	1431	22	0.45

Following from the concentrations observed in the pure water and weak acid leaching experiments, we further present the solubilities as fractions (in %) of the bulk metal composition. The solubility of Fe in Milli-Q water for the dust samples from the Namib Desert is very low, ranging from 0.001 to 0.009% (Table 6). The solubility of other trace metals in Milli-Q water such as Al (0.02 to 0.05%), Pb (0.05 to 0.16%), Mn (0.15 to ~2%) and Zn (0.3 to ~2%) is higher than that of Fe, but also generally low (less than ~2.5%, Table 6). The central station has the highest fractional solubility in Milli-Q water for most of the trace metals (Table 6). Our leaching in weak acid furthermore shows higher solubilities for some trace metals such as Zn (~3 – 16%) and Mn (~2 – 9%). Other trace metals, such as Fe and Al have much lower fractional solubilities of less than 0.6% even in the weak acid, except for station Garnet Koppie, where the fractional solubility of Fe in the weak acid was 2% (Table 6).

Table 7. *Range of trace metal concentrations and fractional solubilities of the Namib dust when leached with Milli-Q water and a weak acid solution ("Berger leach").*

Trace metals	**Leaching in Milli-Q (instantaneously solubile fraction in % of bulk trace metal concentration)**	**Leaching in weak acid (labile fraction in % of bulk trace metal concentration)**
Fe	0.001 to 0.009	0.14 to 2
Al	0.02 to 0.05	0.13 to 0.6
Mn	0.15 to 2.2	2 to 9
Zn	0.3 to 2.3	2.8 to 15.8
Pb	0.05 to 0.16	0.48 to 7.8

3.4.4. Air mass trajectories and wind directions

Forward trajectories were calculated to predict where the dust from the Namib Desert may be deposited in different seasons. They mostly indicate trajectories northwest towards the east Atlantic or southeast towards the Indian Ocean (Figure 6) following a similar pathways across the different seasons (Figure 6). Hence, air masses potentially carrying the dust aerosols from this area mostly influence the southeast Atlantic (up to 22 %), southwest Indian Ocean (up to 58%). Regions with

high dust trajectory density would presumably receive more dust from the Namib compared to regions with low trajectory density. Considering that, most of the short range dust likely impacts the Benguela system, while the longer range impacts may occur in the southeast Atlantic and Indian Ocean.

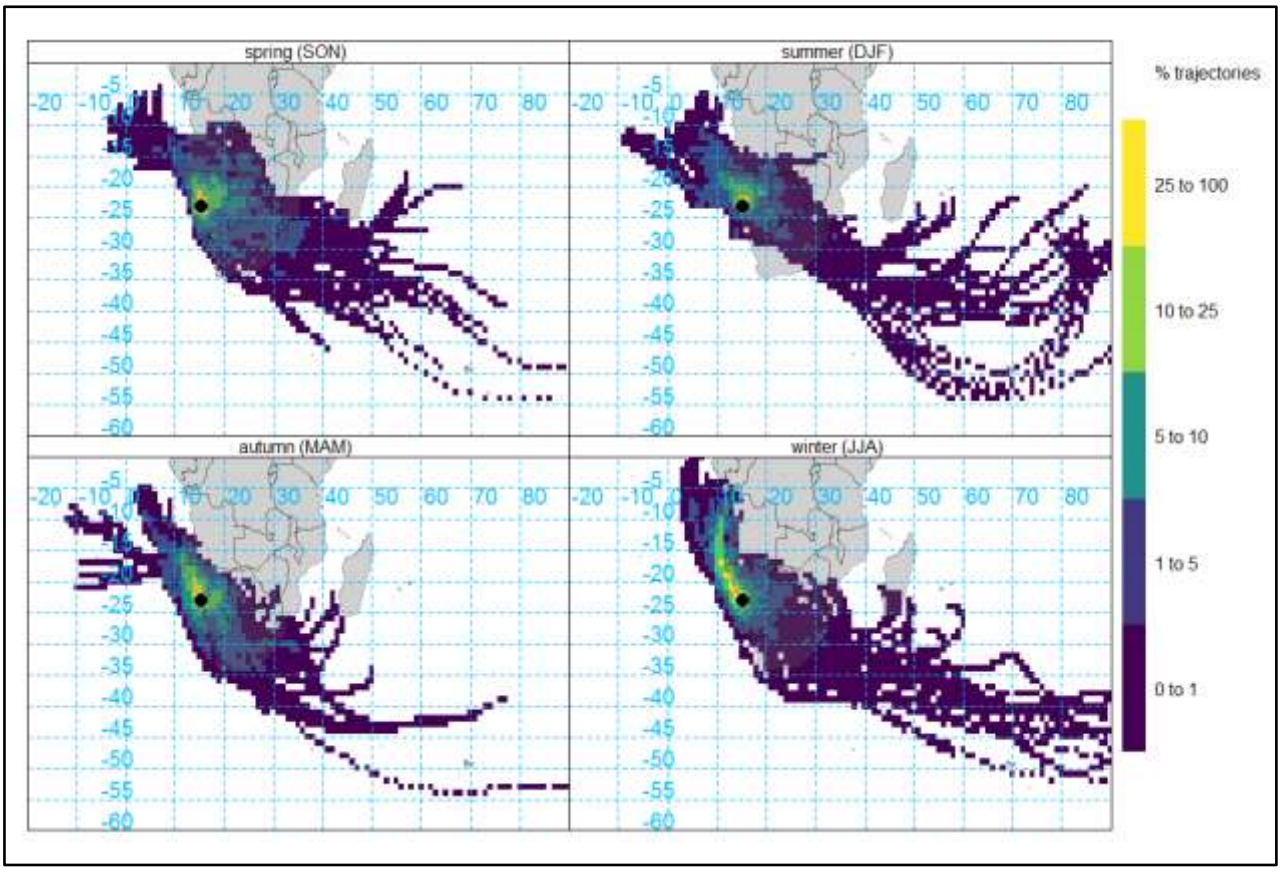

***Figure 6**. The forward trajectories after 7 days from the Namib Desert at different seasons (a) Autumn, (b) Spring, (c) Summer and (d) Winter. Calculated and plotted using the R package: SplitR.*

3.5. DISCUSSION

3.5.1. Dust loads and potential contributions to open oceans

Aeolian particles from the Namib Desert have been identified offshore in ocean bed core sediments (Stuut et al., 2002), highlighting the deposition of Namib Desert dust along the coastline. In addition, remote sensing techniques recorded persistent dust emissions, especially close to our coastal station (Vickery et al., 2013; von Holdt et al., 2017). Indeed, the coastal station had highest dust loads compared to the other stations, with aprroximately twice the dust load. This is likely due to the close proximity to the Kuiseb River and Delta located south of the coastal station. Both emit high volumes of dust (Vickery et al., 2013; von Holdt et al., 2019), and the Kuiseb River is considered the dustiest river in southern Africa contributing the majority of the Namib Desert total dust (von Holdt and Eckardt, 2018). The wind roses for the coastal station also indicated that most of the dust at the coastal station is transported from the southwest and would entail the Kuiseb River and Delta.

Both MWAC and BSNE samplers recorded low dust loads at the central and inland stations, although the BSNE sampler captured relatively high dust loads at the inland station (GK). The central and inland stations collected less dust loads most likely because of the greater distance from the Kuiseb River and Delta in comparison to the coastal station and because the dominant wind direction at this station is from the northeast, which is in the opposite direction from the major known dust sources. Also, in contrast to the coastal station, rock outcrops with presumably very low dust emissions surround the inland station in the dominant wind direction. The low abundance of quartz in the coarse fraction of the inland station is an indication that the dunes are at greater distance and the dominant wind direction from the east, preventing high volumes of dune sediments to reach the area, resulting into lower dust loads from these sources. Another factor may be that the central station is located in gravel plains that contains stone pavements with dry washes (von Holdt et al., 2019), which may have contributed to low dust loads. The latter is uncertain as gravel plains can also emit large volumes of dust after ground disturbances, usually caused by human activities such as off road driving (von Holdt et al., 2019). Lastly, the relatively high moisture content and frequent fog at the coastal station formed a crust at the bottom of the dust collector preventing the sample from escaping when the wind blew again, while the fog was much less at the inland stations, and some dust particles could have escaped without this crust formed by fog.

3.5.2. Particles shape and their role in transport

Even though most models assume that particles are spherical (Liu et al., 2016), most of the particles in this study are aspherical due to an abundance of mica minerals. In addition, the angular minerals appeared to have inclusions of other minerals. Platy and flatter particles can travel further compared to rounded spherical particles (Formenti et al., 2011) due to the lower settling velocities when in suspension in comparison to rounded particles (Cheng et al., 1988). As a result, these aspherical particles have more drag in the atmosphere, and can stay longer in suspension, which hence could increase the solubility (Barkley et al., 2021). The assumption that dust minerals are mostly spherical in models is therefore not consistent for all dust emitting sources and could lead to inaccuracies in some dust models. An aerodynamic diameter could be used in models rather to account for the aspherical shapes. The relatively high abundance of plate-shape minerals close to the coastline can mean that these particles will be susceptible to long-range transport. As such they are interesting for ocean biogeochemistry.

3.5.3. Particle sizes and their role in transport and potential impact on oceans

At all the stations, more than 80% of the collected particles were smaller than 100 µm. The inland station collected the finest grained particles. The particle size ranges are similar to other reported dust sources in the region, such as the ephemeral rivers (Kuiseb, Huab and Tsauchab River) along the Namibian coastline as well as the ephemeral pans, Etosha and Makgadikgadi Pans (Bhattachan et al., 2015; Dansie et al., 2017a). The grain size distributions at our four stations on land are indeed in a similar range to grain sizes ranging from 0 – 100 µm (modal range of 7 and 13 µm) observed in sediments offshore along the Namibian coastline (Stuut et al., 2002) indicating potential for coastal deposition. Nonetheless, These small (<100 µm) particles can be transported over long distances (> 1000 km from sources) (Ginoux et al., 2004; Goudie and Middleton, 2001). Thus, the Namib dust also has potential for long range transport further than 4000 km (Dansie et al., 2017b; Goudie and Middleton, 2001) and deposition in the remote, open ocean. These particles that are susceptible to long distance transport may supply high bioaccessible trace metals to impact oceans at depositional sites, which will be discussed further below.

3.5.3.1. Particle aggregation and their role in transport and potential impact on the ocean

As mentioned above (section 4.1): the Kuiseb River mostly supplies dust to the central and coastal stations, while finer reworked particles reach the inland station. In addition, the particles from the inland station were mostly singular grains, while the particles were aggregated at the coastal station.

This aggregation could be due to the close proximity to the river as aggregates can be formed from the collision and sticking of particles during fluvial transport. Aggregation can also be due to the fog conditions experienced close to the coastline, which can cause particles to be more aggregated and clusters (Andersen et al., 2019; Heather-Clark, 1996). Aggregates in the dust are important for the impact on the ocean as they can provide more nutrients to open oceans because particles that in cohesion are not dissolved until upon deposition (Raiswell et al., 2006). Hence, the particle shape and size characteristics from this region demonstrates suitable particles for long range transport and potential high nutrient content when deposited on surface oceans.

3.5.4. Mineralogical composition as an indicator of the dust sources and trace element content and solubility

The mineral compositions in the coarse-grained fraction at all sample sites were similar. However, important differences were observed in the fine-grained fractions. For example, clay minerals were abundant and likely responsible for the high Al content at the coastal station. Most of the chlorite, muscovite and biotite were found at the coastal station, which can be attributed to the Kuiseb Schist formation in the area. In addition, the sulphide content was high in the fine grain size fraction at the central station. This can be an attributing factor to the high solubility of Fe at this station. Other highly soluble elements from this station are Pb and Zn, which could be released from the sulphide containing minerals such as galena (PbS) or sphalerite (Zn, Fe)S.

The mineralogy at the inland station, in contrast revealed more Fe-oxides and sulphides than at the other stations. The inland station also had the highest Fe solubility. Previous studies in playa environments in the Namib Desert have shown that such dust has high amount of bioavailable Fe (Dansie et al., 2017a). Bhattachan et al (2015), also reported high bioavailable Fe content in Kalahari Desert dust, attributing the high bioavailable Fe to the weathering of Fe-rich minerals. This is in line with our observation. Journet et al. (2008) indicated that iron oxides such as hematite are less soluble compared to clay minerals coated with Fe. Our results contradict the Journet et al. (2008) findings, to some extent, as the inland station indicated high iron solubility in the weak acid leach along with a high contribution of iron oxides. The relatively high content of labile Fe in the fine-grained fraction of Namib Desert dust likely to result from the Fe-oxides and sulphides is an indication that the region might be an important fertilizer to the open oceans.

3.5.4.1. Influence of meteorological conditions and anthropogenic impact on the trace metal solubility

In addition to the mineralogy, the location and meteorological conditions at sources also play a role in the potential solubility of the dust. For example, fog has been reported as an enhancing factor in promoting more soluble Fe (Shi et al., 2020), as fog in the atmosphere increases atmospheric processing in the aerosols droplets, hence increasing the solubility (Fu et al., 2012; Shi et al., 2020). However, our study reported lower Fe solubility at the coastal station (an area more susceptible to foggy conditions) in comparison to the inland station. In addition to the fog, biomass burning is recorded annually along the Namibian. Biomass burning enhances the solubility of trace metals (Paris et al., 2010). Consequently, these persistent low-level clouds from inland biomass burning smoke found off the coast of Namibia can possibly enhance the solubility of dust in the region.

3.6. TOTAL AND BIOACCESSIBLE TRACE METALS

The trace metal concentrations in the Namib dust are slightly lower than in in dust from other global sources such as the Sahara although the samples are not from the same size ranges. For example, Al concentrations in dust from the Sahara ranged from 60 000 to 83 000 ppm (Guieu et al., 2002) in comparison to ~19 000 to 30 000 ppm for this study (Namib). Fe ranged from ~38 000 to 51 000 ppm in dust from the Sahara (Guieu et al., 2002) compared to 15 000 to 35 000 ppm for this study. Pb ranged from 26 to 80 ppm for Saharan dust (Guieu et al., 2002) compared to 13 to 366 ppm in this study. Most of the desert soils/dust are relatively insoluble (~0.5%) but solubility of dust tends to increase during atmospheric transport (1-90%), as well with anthropogenic influence mostly driven by difference in experimental methods (Mahowald et al., 2005a). Considering that Saharan dust is known to impact large parts of the Amazon forest despite its low solubility (Moskowitz et al., 2016), dust from southern African can be bioaccessible when deposited into oceans because of the similar trace metal composition and solubility range at the sources. Our fractional solubilities are higher than what had been previously reported in the dry river valleys along the Namibian coastline by Dansie et al., (2017). Dansie et al. reported bioavailable Fe content ranging between 5 to 17 ppm at stations from Huab and Tsauchab Rivers whereas our labile Fe concentrations ranged between 20 to 579 ppm. This could mean that certain dust emitters contain much larger amounts of labile Fe (up to 10 times more) than others despite their close proximity to rivers.

It is, however, challenging to compare the fractional solubility of trace metals from this study with others in the area due to variation of analytical techniques in determining the extractable fractions (Anderson et al., 2010). For example, Fe bioavailable fractions often range from 0.01 to 80%

depending on the acidity of the extraction reagent and leaching time (Mahowald et al., 2018). Extractable Fe from dust in the Kalahari Delta varied between 170 to 3000 ppm (809 ± 897 ppm when using 1.2M HCl for 10 min (Humphries et al., 2020), which is twice as high compared to our study in the Namib Desert sample. This further highlights the importance of developing one standard method in order to be compare different studies (Perron et al., 2020). However, some of our results (central and coastal stations) are comparable to Saharan dusts fractional solubilities ranging from 0.1 – 0.8% when leaching with ammonium acetate (Shi et al., 2011). Most of the continental soils and dust tend to have a Fe fractional solubility range of ~1% (Jickells et al., 2005; Mahowald et al., 2009), some of our Fe results fall in this range especially from the coastal and inland stations.

3.6.1. Air mass pathways, directions and potential impact on the ocean

Dust plumes from the Namibian coastline towards the Atlantic Ocean have been observed with the aid of satellites (Dansie et al., 2017; Eckardt and Kuring, 2005; Vickery et al., 2013; von Holdt et al., 2017). Strong easterly winds with average speed between 11-12 m/s are necessary for dust plumes to be deposited into the Atlantic Ocean (Preston-Whyte et al., 1994). Dansie et al (2017) recorded wind speeds as high as approximately 8 to 11 m/s in valleys. Our wind speeds that averaged between 4-5 m/s are lower, but on occasions, the wind speed from our study area is as high as 20 m/s which indicates that dust from these sources can be transported as plumes and deposited into the oceans.

Long-range air trajectory modelling from the Namib Desert was conducted to predict the regions of potential dust deposition. Most dust emissions are probably entrained with air masses that travel southeast towards the Indian Ocean, but some air masses travel towards the Atlantic Ocean. Our trajectories agree with previous Hysplit trajectories and modelling studies in this region (Bhattachan et al., 2012; Li et al., 2008; Neff and Bertler, 2015; Swap et al., 1996; Tatlhego et al., 2020). The Namibian coastline trajectories indicate that such dust would travel towards regions where the chlorophyll content is relatively high (Moore et al., 2002, 2001), which leads to the assumption that these non-playa environments and their fertilizing potential may contribute to the high primary production in these regions.

3.7. CONCLUSION

We investigated one of the dustiest non-playa sources of the Central Namib and showed the importance of this southern African dust as a source of nutrients to coastal and open oceans, especially the Indian Ocean and the southeast Atlantic Ocean. These Namib Desert dust is characterised by very fine-grained particles with high trace metal solubility. The dust loads decreased but the trace metal solubility increased from stations likely capturing dust from the coast to stations likely capturing dust from further inland. This study further confirmed that factors such as the location of site, meteorological conditions at the site, particle sizes, particle shapes and aggregation influence the solubility. These findings provide fundamental information for future studies to project the impact at depositional sites.

3.8. AUTHOR CONTRIBUTIONS

S.F., K. K., and F. E., conceived and designed the study and acquired funding; K.K., R.T., and G.R. contributed data and interpretation. K.K., F.D. and S.F. wrote the manuscript. All co-authors reviewed and edited this or previous versions of the manuscript and gave final approval for publication.

3.9. FUNDING

The work leading to these results received funding from the National Research Foundation (NRF) under the SANAP (110715, 110731), Bilateral (114677) and CPRR (105826) programmes. K. Kangueehi acknowledges funding from NRF through a Masters Innovation Scholarship.

3.10. ACKNOWLEDGEMENTS

The authors thank the Saldanha Bay municipality for providing the long-term monitoring data included in this study.

3.11. CONFLICT OF INTEREST STATEMENT

All authors declare no competing interests.

3.12. REFERENCES

Abrams, M.M., Jacobson, P.J., Jacobson, K.M., Seely, M.K., 1997. Survey of soil chemical properties across a landscape in the Namib Desert. J. Arid Environ. 35, 29–38. https://doi.org/10.1006/jare.1995.0139

Aguilar-Islas, A.M., Wu, J., Rember, R., Johansen, A.M., Shank, L.M., 2010. Dissolution of aerosol-derived iron in seawater: Leach solution chemistry, aerosol type, and colloidal iron fraction. Mar. Chem. 120, 25–33. https://doi.org/10.1016/j.marchem.2009.01.011

Andersen, H., Cermak, J., Fuchs, J., Knippertz, P., Gaetani, M., Quinting, J., Sippel, S., Vogt, R., 2019. Synoptic-scale controls of fog and low clouds in the Namib Desert. Atmos. Chem. Phys. Discuss. 1–27. https://doi.org/10.5194/acp-2019-924

Armstrong, A., Tuffin, I.M., Ramond, J.-B., Cowan, P.D.A., 2014. SEASONAL DYNAMICS OF EDAPHIC BACTERIAL COMMUNITIES IN THE HYPER-ARID NAMIB DESERT. University of the Western Cape.

Ashrafi, K., Shafiepour-Motlagh, M., Aslemand, A., Ghader, S., 2014. Dust storm simulation over Iran using HYSPLIT. J. Environ. Heal. Sci. Eng. 12, 9. https://doi.org/10.1186/2052-336X-12-9

Baker, A.R., Croot, P.L., 2010. Atmospheric and marine controls on aerosol iron solubility in seawater. Mar. Chem. https://doi.org/10.1016/j.marchem.2008.09.003

Baker, A.R., French, M., Linge, K.L., 2006. Trends in aerosol nutrient solubility along a west-east transect of the Saharan dust plume. Geophys. Res. Lett. 33, 10–13. https://doi.org/10.1029/2005GL024764

Barkley, A.E., Olson, N.E., Prospero, J.M., Gatineau, A., Panechou, K., Maynard, N.G., Blackwelder, P., China, S., Ault, A.P., Gaston, C.J., 2021. Atmospheric Transport of North African Dust-Bearing Supermicron Freshwater Diatoms to South America: Implications for Iron Transport to the Equatorial North Atlantic Ocean. Geophys. Res. Lett. 48, e2020GL090476. https://doi.org/10.1029/2020GL090476

Berger, C.J.M., Lippiatt, S.M., Lawrence, M.G., Bruland, K.W., 2008. Application of a chemical leach technique for estimating labile particulate aluminum, iron, and manganese in the Columbia River plume and coastal waters off Oregon and Washington. J. Geophys. Res. 113,

1–16. https://doi.org/10.1029/2007jc004703

Bhattachan, A., D'Odorico, P., Baddock, M.C., Zobeck, T.M., Okin, G.S., Cassar, N., 2012. The Southern Kalahari: a potential new dust source in the Southern Hemisphere? Environ. Res. Lett. 7, 024001. https://doi.org/10.1088/1748-9326/7/2/024001

Bhattachan, A., D'Odorico, P., Okin, G.S., 2015. Biogeochemistry of dust sources in Southern Africa. J. Arid Environ. 117, 18–27. https://doi.org/10.1016/j.jaridenv.2015.02.013

Buck, C.S., Landing, W.M., Resing, J.A., Lebon, G.T., 2006. Aerosol iron and aluminum solubility in the northwest Pacific Ocean: Results from the 2002 IOC cruise. Geochemistry, Geophys. Geosystems 7. https://doi.org/10.1029/2005GC000977

Capone, D.G., Hutchins, D.A., 2013. Microbial biogeochemistry of coastal upwelling regimes in a changing ocean. Nat. Geosci. 6, 711–717. https://doi.org/10.1038/ngeo1916

Cheng, Y.S., Yeh, H.C., Allen, M.D., 1988. Dynamic shape factor of a plate-like particle. Aerosol Sci. Technol. 8, 103–123. https://doi.org/10.1080/02786828808959176

Chester, R., Hughes, M.J., 1967. A chemical technique for the separation of ferro-manganese minerals, carbonate minerals and adsorbed trace elements from pelagic sediments. Chem. Geol. 2, 249–262. https://doi.org/10.1016/0009-2541(67)90025-3

Conway, T.M., John, S.G., 2014. Quantification of dissolved iron sources to the North Atlantic Ocean. Nature 511, 212–215. https://doi.org/10.1038/nature13482

Cutter, G., Casciotti, K., Croot, P., Geibert, W., Geochemistry, M., Heimbürger, L.-E., Lohan, M., 2017. Sampling and Sample-handling Protocols for GEOTRACES Cruises.

Dansie, A.P., Thomas, D.S.G., Wiggs, G.F.S., Munkittrick, K.R., 2018. Spatial variability of ocean fertilizing nutrients in the dust-emitting ephemeral river catchments of Namibia. Earth Surf. Process. Landforms 43, 563–578. https://doi.org/10.1002/esp.4207

Dansie, A.P., Wiggs, G.F.S., Thomas, D.S.G., 2017a. Iron and nutrient content of wind-erodible sediment in the ephemeral river valleys of Namibia. Geomorphology 290, 335–346. https://doi.org/10.1016/j.geomorph.2017.03.016

Dansie, A.P., Wiggs, G.F.S., Thomas, D.S.G., Washington, R., 2017b. Measurements of windblown dust characteristics and ocean fertilization potential: The ephemeral river valleys of Namibia.

Aeolian Res. 29, 30–41. https://doi.org/10.1016/j.aeolia.2017.08.002

Desboeufs, K. V., Losno, R., Colin, J.L., 2001. Factors influencing aerosol solubility during cloud processes. Atmos. Environ. 35, 3529–3537. https://doi.org/10.1016/S1352-2310(00)00472-6

Desboeufs, K. V., Sofikitis, A., Losno, R., Colin, J.L., Ausset, P., 2005. Dissolution and solubility of trace metals from natural and anthropogenic aerosol particulate matter. Chemosphere 58, 195–203. https://doi.org/10.1016/j.chemosphere.2004.02.025

Eckardt, F., Kuring, N., 2005. SeaWiFS identifies dust sources in the Namib Desert. Int. J. Remote Sens. 26, 4159–4167. https://doi.org/10.1080/01431160500113112

Eckardt, F.D., Livingstone, I., Seely, M., Von Holdt, J., 2013. The surface geology and geomorphology around Gobabeb, Namib desert, Namibia. Geogr. Ann. Ser. A Phys. Geogr. 95, 271–284. https://doi.org/10.1111/geoa.12028

Eckardt, F.D., Schemenauer, R.S., 1998. Fog water chemistry in the Namib Desert, Namibia. Atmos. Environ. 32, 2595–2599. https://doi.org/10.1016/S1352-2310(97)00498-6

Eltayeb, M.A.H., Van Grieken, R.E., Maenhaut, W., Annegarn, H.A.J., 1992. Aerosol-soil fractionationation for Namib desert samples. Aerosol Sci. 23, 983–986.

Formenti, P., D'Anna, B., Flamant, C., Mallet, M., Piketh, S.J., Schepanski, K., Waquet, F., Auriol, F., Brogniez, G., Burnet, F., Chaboureau, J.P., Chauvigné, A., Chazette, P., Denjean, C., Desboeufs, K., Doussin, J.F., Elguindi, N., Feuerstein, S., Gaetani, M., Giorio, C., Klopper, D., Mallet, M.D., Nabat, P., Monod, A., Solmon, F., Namwoonde, A., Chikwililwa, C., Mushi, R., Welton, E.J., Holben, B., 2019. The aerosols, radiation and clouds in southern Africa field campaign in Namibia overview, illustrative observations, and way forward. Bull. Am. Meteorol. Soc. 100, 1277–1298. https://doi.org/10.1175/BAMS-D-17-0278.1

Formenti, P., Schütz, L., Balkanski, Y., Desboeufs, K., Ebert, M., Kandler, K., Petzold, A., Scheuvens, D., Weinbruch, S., Zhang, D., 2011. Recent progress in understanding physical and chemical properties of African and Asian mineral dust. Atmos. Chem. Phys. 11, 8231–8256. https://doi.org/10.5194/acp-11-8231-2011

Fu, H., Lin, J., Shang, G., Dong, W., Grassian, V.H., Carmichael, G.R., Li, Y., Chen, J., 2012. Solubility of iron from combustion source particles in acidic media linked to iron speciation. Environ. Sci. Technol. 46, 11119–11127. https://doi.org/10.1021/es302558m

Ginoux, P., Prospero, J.M., Gill, T.E., Hsu, N.C., Zhao, M., 2012. Global-scale attribution of anthropogenic and natural dust sources and their emission rates based on MODIS Deep Blue aerosol products. Rev. Geophys. https://doi.org/10.1029/2012RG000388

Ginoux, P., Prospero, J.M., Torres, O., Chin, M., 2004. Long-term simulation of global dust distribution with the GOCART model : correlation with North Atlantic Oscillation. Environ. Model. Softw. 19, 113–128. https://doi.org/10.1016/S1364-8152(03)00114-2

Gottlieb, T.R., Eckardt, F.D., Venter, Z.S., Cramer, M.D., 2019. The contribution of fog to water and nutrient supply to Arthraerua leubnitziae in the central Namib Desert, Namibia. J. Arid Environ. 161, 35–46. https://doi.org/10.1016/j.jaridenv.2018.11.002

Goudie, A., Middleton, N.J., Ashrafi, K., Shafiepour-Motlagh, M., Aslemand, A., Ghader, S., Baker, A.R., Jickells, T.D., Witt, M., Linge, K.L., French, M., Linge, K.L., Bhattachan, A., D'Odorico, P., Okin, G.S., D'Odorico, P., Baddock, M.C., Zobeck, T.M., Okin, G.S., Cassar, N., Wang, L., Miller, M.F., Licht, K.J., D'Odorico, P., Bruland, K.W., Orians, K.J., Cowen, J.P., Bryant, R.G., Bigg, G.R., Mahowald, N.M., Eckardt, F.D., Ross, S.G., Duce, R., Tindale, N.., Irvine, U.C., Linage, D., James, S., Mahowald, N.M., Luo, C., 2015. The Southern Kalahari: a potential new dust source in the Southern Hemisphere? Geophys. Res. Lett. 7, 024001. https://doi.org/10.1088/1748-9326/7/2/024001

Goudie, A.S., Middleton, N.J., 2001. Saharan dust storms: Nature and consequences. Earth-Science Rev. 56, 179–204. https://doi.org/10.1016/S0012-8252(01)00067-8

Guieu, C., Loÿe-Pilot, M.D., Ridame, C., Thomas, C., 2002. Chemical characterization of the Saharan dust end-member: Some biogeochemical implications for the western Mediterranean Sea. J. Geophys. Res. Atmos. 107. https://doi.org/10.1029/2001JD000582

Heather-Clark, S., 1996. An environmental overview of the Walvis Bay'Bay Area', Namibia.

Heine, K., 2005. Holocene Climate of Namibia: a Review Based on Geoarchives. Afr. Study Monogr. 30, 119–133.

Hettiarachchi, E., Hurab, O., Rubasinghege, G., 2018. Atmospheric Processing and Iron Mobilization of Ilmenite: Iron-Containing Ternary Oxide in Mineral Dust Aerosol. J. Phys. Chem. A 122, 1291–1302. https://doi.org/10.1021/acs.jpca.7b11320

Holdt, J.R.C. Von, Eckardt, F.D., Baddock, M.C., Hipondoka, M.H.T., Wiggs, G.F.S., 2021. Influence of sampling approaches on physical and geochemical analysis of aeolian dust in

source regions. Aeolian Res. 50, 100684. https://doi.org/10.1016/j.aeolia.2021.100684

Humphries, M.S., Benitez-Nelson, C.R., Bizimis, M., Ralph, T.J., Larkin, Z.T., McCarthy, T.S., 2020. Dust provenance and its role as a potential fertilizing agent for the Okavango Delta, Botswana. Earth Surf. Process. Landforms 45, 1705–1716. https://doi.org/10.1002/esp.4840

Jacobson, P.J., Jacobson, K.M., Angermeier, P.L., Cherry, D.S., 2000. Hydrologic influences on soil properties along ephemeral rivers in the Namib Desert. J. Arid Environ. 45, 21–34. https://doi.org/10.1006/jare.1999.0619

Jenkins, W.J., Smethie, W.M., Boyle, E.A., Cutter, G.A., 2015. Water mass analysis for the U.S. GEOTRACES (GA03) North Atlantic sections. Deep. Res. Part II Top. Stud. Oceanogr. 116, 6–20. https://doi.org/10.1016/j.dsr2.2014.11.018

Jickells, T.D., An, Z.S., Andersen, K.K., Baker, A.R., Bergametti, C., Brooks, N., Cao, J.J., Boyd, P.W., Duce, R.A., Hunter, K.A., Kawahata, H., Kubilay, N., LaRoche, J., Liss, P.S., Mahowald, N., Prospero, J.M., Ridgwell, A.J., Tegen, I., Torres, R., 2005. Global iron connections between desert dust, ocean biogeochemistry, and climate. Science (80-.). https://doi.org/10.1126/science.1105959

Journet, E., Desboeufs, K. V., Caquineau, S., Colin, J.L., 2008a. Mineralogy as a critical factor of dust iron solubility. Geophys. Res. Lett. 35, 3–7. https://doi.org/10.1029/2007GL031589

Klopper, D., Formenti, P., Namwoonde, A., Cazaunau, M., Chevaillier, S., Feron, A., Gaimoz, C., Hease, P., Lahmidi, F., Mirande-Bret, C., Triquet, S., Zeng, Z., Piketh, S.J., 2020. Chemical composition and source apportionment of atmospheric aerosols on the Namibian coast. Atmos. Chem. Phys. 20, 15811–15833. https://doi.org/10.5194/acp-20-15811-2020

Knappett, C., Pirrie, D., Power, M.R., Nikolakopoulou, I., Hilditch, J., Rollinson, G.K., 2011. Mineralogical analysis and provenancing of ancient ceramics using automated SEM-EDS analysis (QEMSCAN®): A pilot study on LB I pottery from Akrotiri, Thera. J. Archaeol. Sci. 38, 219–232. https://doi.org/10.1016/j.jas.2010.08.022

Koffman, B.G., Yoder, M.F., Methven, T., Hanschka, L., Sears, H.B., Saylor, P.L., Wallace, K.L., 2021. Glacial Dust Surpasses Both Volcanic Ash and Desert Dust in Its Iron Fertilization Potential. Global Biogeochem. Cycles 35. https://doi.org/10.1029/2020GB006821

Kohfeld, K.E., Harrison, S.P., 2001. DIRTMAP: The geological record of dust. Earth-Science Rev. 54, 81–114. https://doi.org/10.1016/S0012-8252(01)00042-3

Lambert, F., Delmonte, B., Petit, J.R., Bigler, M., Kaufmann, P.R., Hutterli, M.A., Stocker, T.F., Ruth, U., Steffensen, J.P., Maggi, V., 2008. Dust - Climate couplings over the past 800,000 years from the EPICA Dome C ice core. Nature 452, 616–619. https://doi.org/10.1038/nature06763

Lancaster, J., Lancaster, N., Seely, M.K., 1984. Climate of the central Namib Desert. Madoqua 14, 5–61.

Li, F., Ginoux, P., Ramaswamy, V., 2008. Distribution, transport, and deposition of mineral dust in the Southern Ocean and Antarctica: Contribution of major sources. J. Geophys. Res. Atmos. 113, 1–15. https://doi.org/10.1029/2007JD009190

Liu, L., Huang, X., Ding, A., Fu, C., 2016. Dust-induced radiative feedbacks in north China: A dust storm episode modeling study using WRF-Chem. Atmos. Environ. 129, 43–54. https://doi.org/10.1016/J.ATMOSENV.2016.01.019

Lüthi, D., Le Floch, M., Bereiter, B., Blunier, T., Barnola, J.M., Siegenthaler, U., Raynaud, D., Jouzel, J., Fischer, H., Kawamura, K., Stocker, T.F., 2008. High-resolution carbon dioxide concentration record 650,000-800,000 years before present. Nature 453, 379–382. https://doi.org/10.1038/nature06949

Mahowald, N.M., Artaxo, P., Baker, A.R., Jickells, T.D., Okin, G.S., Randerson, J.T., Townsend, A.R., 2005a. Impacts of biomass burning emissions and land use change on Amazonian atmospheric phosphorus cycling and deposition. Global Biogeochem. Cycles 19. https://doi.org/10.1029/2005GB002541

Mahowald, N.M., Baker, A.R., Bergametti, G., Brooks, N., Duce, R.A., Jickells, T.D., Kubilay, N., Prospero, J.M., Tegen, I., 2005b. Atmospheric global dust cycle and iron inputs to the ocean. Global Biogeochem. Cycles 19. https://doi.org/10.1029/2004GB002402

Mahowald, N.M., Engelstaedter, S., Luo, C., Sealy, A., Artaxo, P., Benitez-Nelson, C., Bonnet, S., Chen, Y., Chuang, P.Y., Cohen, D.D., Dulac, F., Herut, B., Johansen, A.M., Kubilay, N., Losno, R., Maenhaut, W., Paytan, A., Prospero, J.M., Shank, L.M., Siefert, R.L., 2009. Atmospheric iron deposition: Global distribution, variability, and human perturbations. Ann. Rev. Mar. Sci. https://doi.org/10.1146/annurev.marine.010908.163727

Mahowald, N.M., Hamilton, D.S., Mackey, K.R.M., Moore, J.K., Baker, A.R., Scanza, R.A., Zhang, Y., 2018. Aerosol trace metal leaching and impacts on marine microorganisms. Nat.

Commun. 9. https://doi.org/10.1038/s41467-018-04970-7

Martin, J.H., Fitzwater, S.E., Gordon, M.R., 1990. Iron Deficiency Limits Phytoplankton Growth in Antartic Waters. Global Biogeochem. Cycles 5–12.

Marx, S.K., Lavin, K.S., Hageman, K.J., Kamber, B.S., O'Loingsigh, T., McTainsh, G.H., 2014. Trace elements and metal pollution in aerosols at an alpine site, New Zealand: Sources, concentrations and implications. Atmos. Environ. 82, 206–217. https://doi.org/10.1016/j.atmosenv.2013.10.019

Mcgowan, H., Clark, A., 2008. Identification of dust transport pathways from Lake Eyre , Australia using Hysplit. Atmos. Environ. 42, 6915–6925. https://doi.org/10.1016/j.atmosenv.2008.05.053

Meskhidze, N., Chameides, W.L., Nenes, A., 2005. Dust and pollution: A recipe for enhanced ocean fertilization? J. Geophys. Res. D Atmos. 110, 1–23. https://doi.org/10.1029/2004JD005082

Miller, R.M., Becker, T., Cartwright, J., Corner, B., Duncan, A.R., E., H.F., Frindt, S., Grotzinger, J.P., Haapala, I., Halverson, G.P., Hoffman, P.F., D.G.Hutchins, Mangongolo, A., Marsh, J.S., Meier, W.D., Prins, P., Reid, D.L., Retief, E.A., Schalk, K.E.L., Smithies, R.B., Swart, R., B.Teigler, Verwoerd, W.J., 2008. THE GEOLOGY OF NAMIBIA, 1st editio. ed. Library of Congress Subject Headings, Windhoek.

Moore, J.K., Doney, S.C., Glover, D.M., Fung, I.Y., 2001. Iron cycling and nutrient-limitation patterns in surface waters of the world ocean. Deep. Res. Part II Top. Stud. Oceanogr. 49, 463–507. https://doi.org/10.1016/S0967-0645(01)00109-6

Moore, J.K., Doney, S.C., Kleypas, J.A., Glover, D.M., Fung, I.Y., 2002. An intermediate complexity marine ecosystem model for the global domain, Deep-Sea Research II.

Moskowitz, B.M., Reynolds, R.L., Goldstein, H.L., Berquó, T.S., Kokaly, R.F., Bristow, C.S., 2016. Iron oxide minerals in dust-source sediments from the Bodélé Depression, Chad: Implications for radiative properties and Fe bioavailability of dust plumes from the Sahara. Aeolian Res. 22, 93–106. https://doi.org/10.1016/j.aeolia.2016.07.001

Muhs, D.R., 2013. The geologic records of dust in the quaternary. Aeolian Res. 9, 3–48. https://doi.org/10.1016/j.aeolia.2012.08.001

Neff, P.D., Bertler, N.A.N., 2015. Trajectory modeling of modern dust transport to the Southern Ocean and Antarctica. J. Geophys. Res. 120, 9303–9322. https://doi.org/10.1002/2015JD023304

Nie, J., Peng, W., 2014. Automated SEM-EDS heavy mineral analysis reveals no provenance shift between glacial loess and interglacial paleosol on the Chinese Loess Plateau. Aeolian Res. https://doi.org/10.1016/j.aeolia.2014.03.005

Paris, R., Desboeufs, K. V., Formenti, P., Nava, S., Chou, C., 2010. Chemical characterisation of iron in dust and biomass burning aerosols during AMMA-SOP0/DABEX: Implication for iron solubility. Atmos. Chem. Phys. 10, 4273–4282. https://doi.org/10.5194/acp-10-4273-2010

Paris, R., Desboeufs, K. V., Journet, E., 2011. Variability of dust iron solubility in atmospheric waters: Investigation of the role of oxalate organic complexation. Atmos. Environ. 45, 6510–6517. https://doi.org/10.1016/j.atmosenv.2011.08.068

Perron, M.M.G., Strzelec, M., Gault-Ringold, M., Proemse, B.C., Boyd, P.W., Bowie, A.R., 2020. Assessment of leaching protocols to determine the solubility of trace metals in aerosols. Talanta 208, 120377. https://doi.org/10.1016/j.talanta.2019.120377

Preston-Whyte, R.A., Diab, R.D., Sokolic, F., 1994. Thermo—topographically induced winds in the boundary layer over the Etosha Pan. South African Geogr. J. 76, 59–62. https://doi.org/10.1080/03736245.1994.9713576

Raiswell, R., Tranter, M., Benning, L.G., Siegert, M., De'ath, R., Huybrechts, P., Payne, T., 2006. Contributions from glacially derived sediment to the global iron (oxyhydr)oxide cycle: Implications for iron delivery to the oceans. Geochim. Cosmochim. Acta 70, 2765–2780. https://doi.org/10.1016/j.gca.2005.12.027

Sedwick, P.N., Sholkovitz, E.R., Church, T.M., 2007. Impact of anthropogenic combustion emissions on the fractional solubility of aerosol iron: Evidence from the Sargasso Sea. J. Earth Sci. 8, 1–21. https://doi.org/10.1029/2007GC001586

Shelley, R.U., Landing, W.M., Ussher, S.J., Planquette, H., Sarthou, G., 2018. Regional trends in the fractional solubility of Fe and other metals from North Atlantic aerosols (GEOTRACES cruises GA01 and GA03) following a two-stage leach. Biogeosciences 15, 2271–2288. https://doi.org/10.5194/bg-15-2271-2018

Shi, J., Guan, Y., Ito, A., Gao, H., Yao, X., Baker, A.R., Zhang, D., 2020. High Production of

Soluble Iron Promoted by Aerosol Acidification in Fog. Geophys. Res. Lett. 47, 1–8. https://doi.org/10.1029/2019GL086124

Shi, Z.B., Woodhouse, M.T., Carslaw, K.S., Krom, M.D., Mann, G.W., Baker, A.R., Savov, I., Fones, G.R., Brooks, B., Drake, N., Jickells, T.D., Benning, L.G., 2011. Minor effect of physical size sorting on iron solubility of transported mineral dust. Atmos. Chem. Phys. 11, 8459–8469. https://doi.org/10.5194/acp-11-8459-2011

Sholkovitz, E.R., Sedwick, P.N., Church, T.M., Baker, A.R., Powell, C.F., 2012. Fractional solubility of aerosol iron: Synthesis of a global-scale data set. Geochim. Cosmochim. Acta 89, 173–189. https://doi.org/10.1016/j.gca.2012.04.022

Spokes, L., Jickells, T., Jarvis, K., 2001. Atmospheric inputs of trace metals to the northeast Atlantic Ocean : the importance of southeasterly flow. Mar. Chem. 76, 319–330.

Stein, A.F., Draxler, R.R., Rolph, G.D., Stunder, B.J.B., Cohen, M.D., Ngan, F., 2015. Noaa's hysplit atmospheric transport and dispersion modeling system. Bull. Am. Meteorol. Soc. 96, 2059–2077. https://doi.org/10.1175/BAMS-D-14-00110.1

Stow, D.A. V., 1981. Fine-grained sediments: Terminology. Q. J. Eng. Geol. Hydrogeol. 14, 243–244. https://doi.org/10.1144/GSL.QJEG.1981.014.04.02

Stuut, J.B.W., Prins, M.A., Schneider, R.R., Weltje, G.J., Fred Jansen, J.H., Postma, G., 2002. A 300-kyr record of aridity and wind strength in southwestern Africa: Inferences from grain-size distributions of sediments on Walvis Ridge, SE Atlantic. Mar. Geol. 180, 221–233. https://doi.org/10.1016/S0025-3227(01)00215-8

Swap, R., Garstang, M., Macko, S, A., Tyson, P, D., Maenhaut, W., Artaxo, P., Kalberg, P., Talbot, R., 1996. The long-range transport of southern African aerosols to the tropical South Atlantic. Geophysical 101, 777–791.

Tatlhego, M., Bhattachan, A., Okin, G.S., D'Odorico, P., 2020. Mapping Areas of the Southern Ocean Where Productivity Likely Depends on Dust-Delivered Iron. J. Geophys. Res. Atmos. 125, 1–10. https://doi.org/10.1029/2019JD030926

Thomas, D.S.G., Leason, H.C., 2005. Dunefield activity response to climate variability in the southwest Kalahari. Geomorphology 64, 117–132. https://doi.org/10.1016/j.geomorph.2004.06.004

Vickery, K.J., Eckardt, F.D., Bryant, R.G., 2013. A sub-basin scale dust plume source frequency inventory for southern Africa, 2005-2008. Geophys. Res. Lett. 40, 5274–5279. https://doi.org/10.1002/grl.50968

Vogel, J.C., 1989. Evidence of past climate change in the Namib Desert. Palaeogeogr. Palaeoclimatol. Palaeoecol. 70, 355–366.

von Holdt, J.R., Eckardt, F.D., 2018. Dust activity and surface sediment characteristics of the dustiest river in southern Africa: the Kuiseb River, Central Namib. South African Geogr. J. 100, 104–121. https://doi.org/10.1080/03736245.2017.1339627

von Holdt, J.R., Eckardt, F.D., Wiggs, G.F.S., 2017. Landsat identifies aeolian dust emission dynamics at the landform scale. Remote Sens. Environ. 198, 229–243. https://doi.org/10.1016/j.rse.2017.06.010

von Holdt, J.R.C., 2013. Lower Kuiseb River sediments and their control on dust emmission 176.

von Holdt, J.R.C., Eckardt, F.D., Baddock, M.C., Hipondoka, M.H.T., Wiggs, G.F.S., 2021. Influence of sampling approaches on physical and geochemical analysis of aeolian dust in source regions. Aeolian Res. 50, 100684. https://doi.org/10.1016/j.aeolia.2021.100684

von Holdt, J.R.C., Eckardt, F.D., Baddock, M.C., Wiggs, G.F.S., 2019. Assessing Landscape Dust Emission Potential Using Combined Ground-Based Measurements and Remote Sensing Data, Journal of Geophysical Research: Earth Surface. https://doi.org/10.1029/2018JF004713

Winton, V.H.L., Bowie, A.R., Edwards, R., Keywood, M., Townsend, A.T., van der Merwe, P., Bollhöfer, A., 2015. Fractional iron solubility of atmospheric iron inputs to the Southern Ocean. Mar. Chem. 177, 20–32. https://doi.org/10.1016/j.marchem.2015.06.006

Winton, V.H.L., Edwards, R., Bowie, A.R., Keywood, M., Williams, A.G., Chambers, S.D., Selleck, P.W., Desservettaz, M., Mallet, M.D., Paton-Walsh, C., 2016. Dry season aerosol iron solubility in tropical northern Australia. Atmos. Chem. Phys. 16, 12829–12848. https://doi.org/10.5194/acp-16-12829-2016

Wu, J., Rember, R., Cahill, C., 2007. Dissolution of aerosol iron in the surface waters of the North Pacific and North Atlantic oceans as determined by a semicontinuous flow-through reactor method. Global Biogeochem. Cycles 21, 1–10. https://doi.org/10.1029/2006GB002851

3.13. SUPPLEMENTARY TABLE

***Table S1**. MWAC samples from the two year period. These samples were used for Qemscan analysis.*

Locations	Sample height	Orientation	Year	Analysed particles
Coastal Met	3 meter	060	2016	8250
Coastal Met	3 meter	220	2016	7237
Coastal Met	3 meter	220	2017	7316
Coastal Met	5 meter	060	2016	10071
Coastal Met	5 meter	220	2016	10821
Coastal Met	3 meter	060	2017	9080
Aussinanis	3 meter	220	2016	12 737
Aussinanis	3 meter	060	2017	8573
Aussinanis	3 meter	200	2016	4902
Vogelfederberg	3 meter	035	2017	18221
Vogelfederberg	3 meter	200	2017	36252
Vogelfederberg	3 meter	315	2017	16878
Vogelfederberg	3 meter	035	2016	9553
Garnet Koppie	3 meter	050	2017	10323
Garnet Koppie	3 meter	220	2017	36252
Total				**180229**

3.14. SUPPLEMENTARY FIGURES

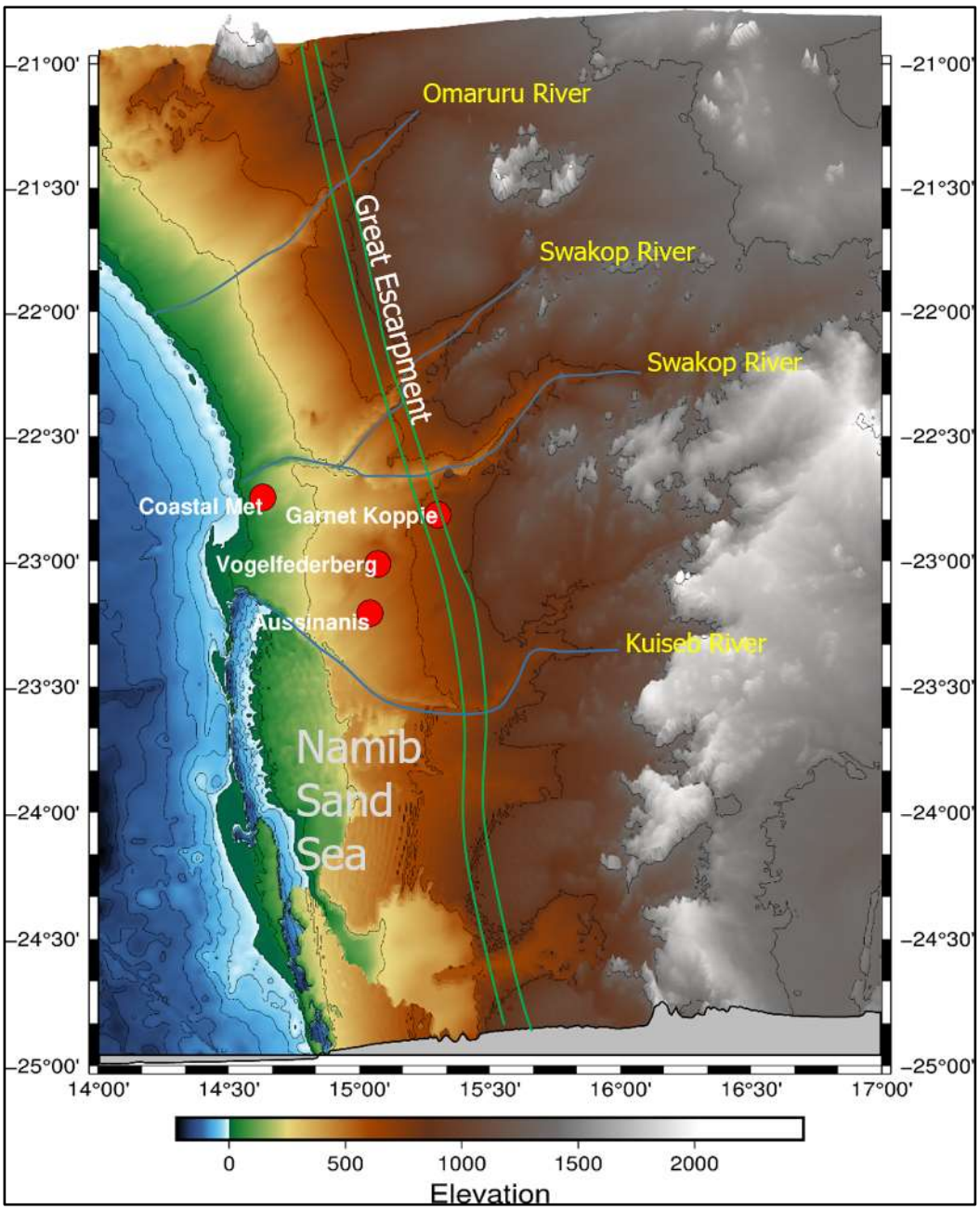

Figure S1*. Map of the sampling sites in the Namib Desert, Namibia. Station location coordinates are given in Table 2. In addition, the ephemeral rivers and the Great Escarpment are also shown in this figure.*

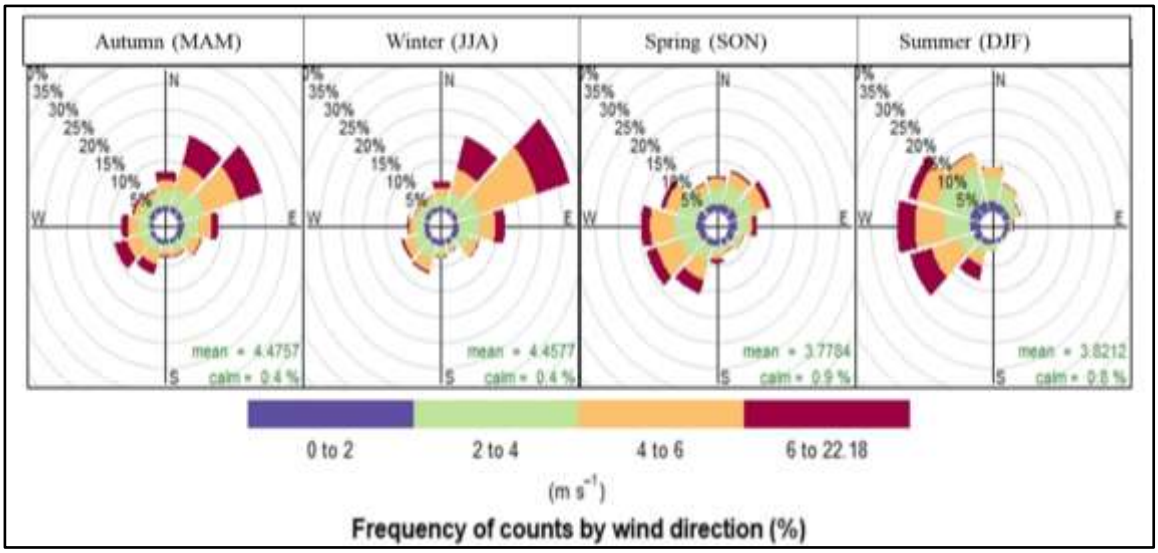

Figure S2. Wind roses for Garnet Koppie for data ranging from 2016 to 2017.

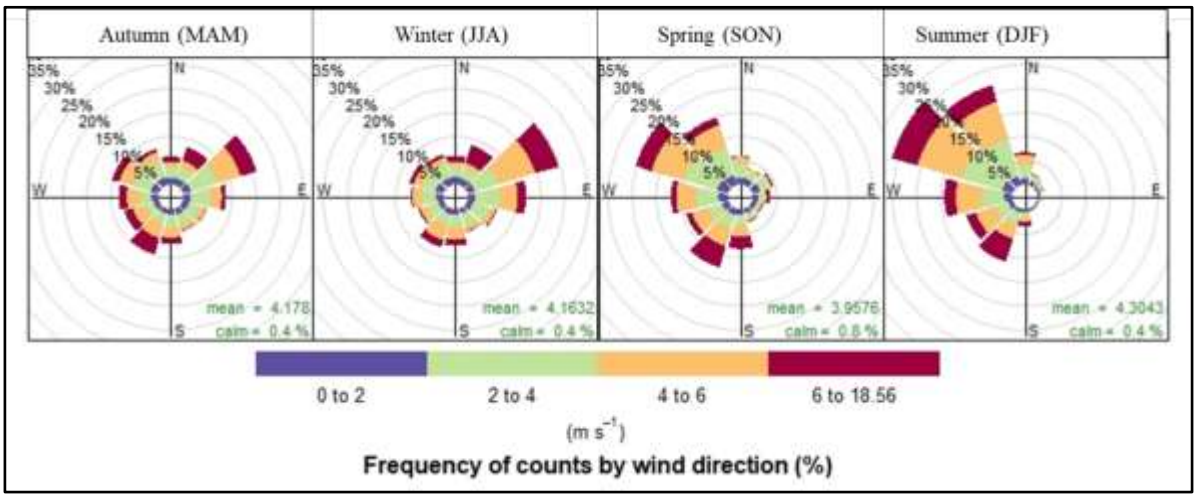

***Figure S3**. Wind roses for Aussinanis for data ranging from 2016 to 2017.*

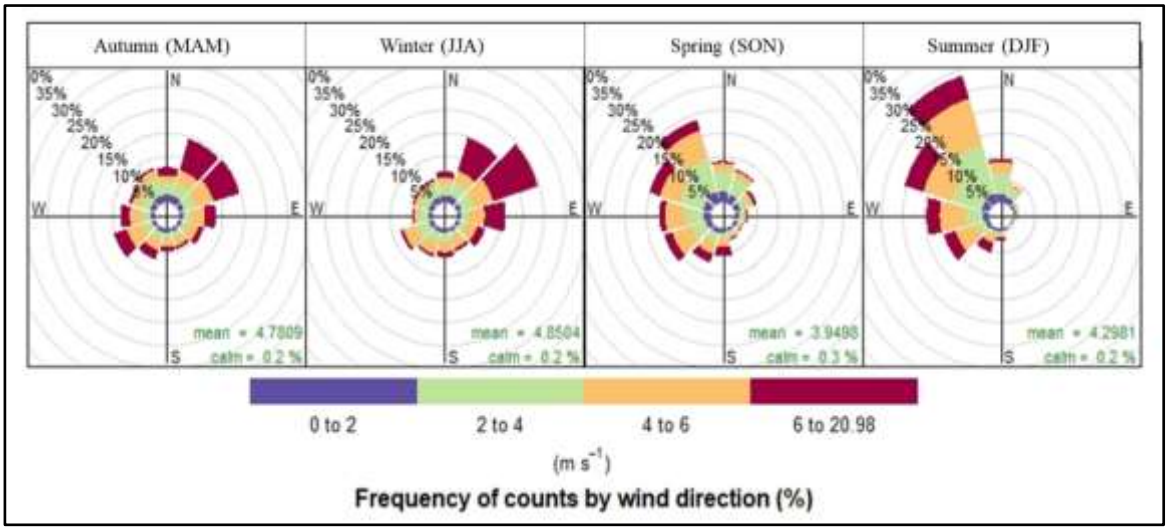

***Figure S4**. Monthly wind roses of Vogelfederberg for wind data from 2016 to 2017.*

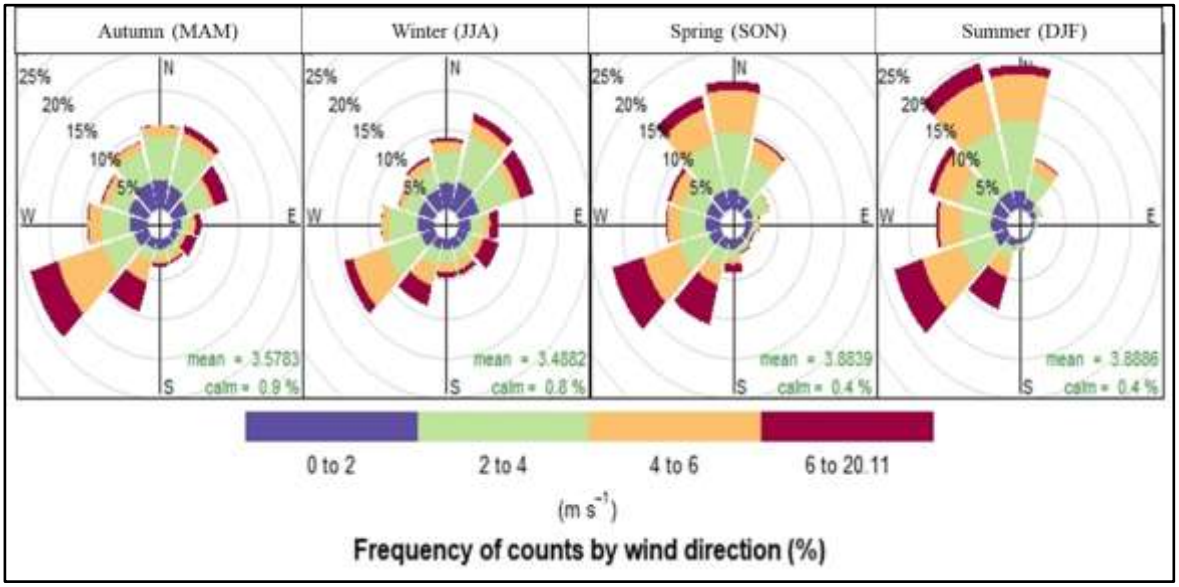

***Figure S5**. Wind roses for Coastal Met for data ranging from 2016 to 2017.*

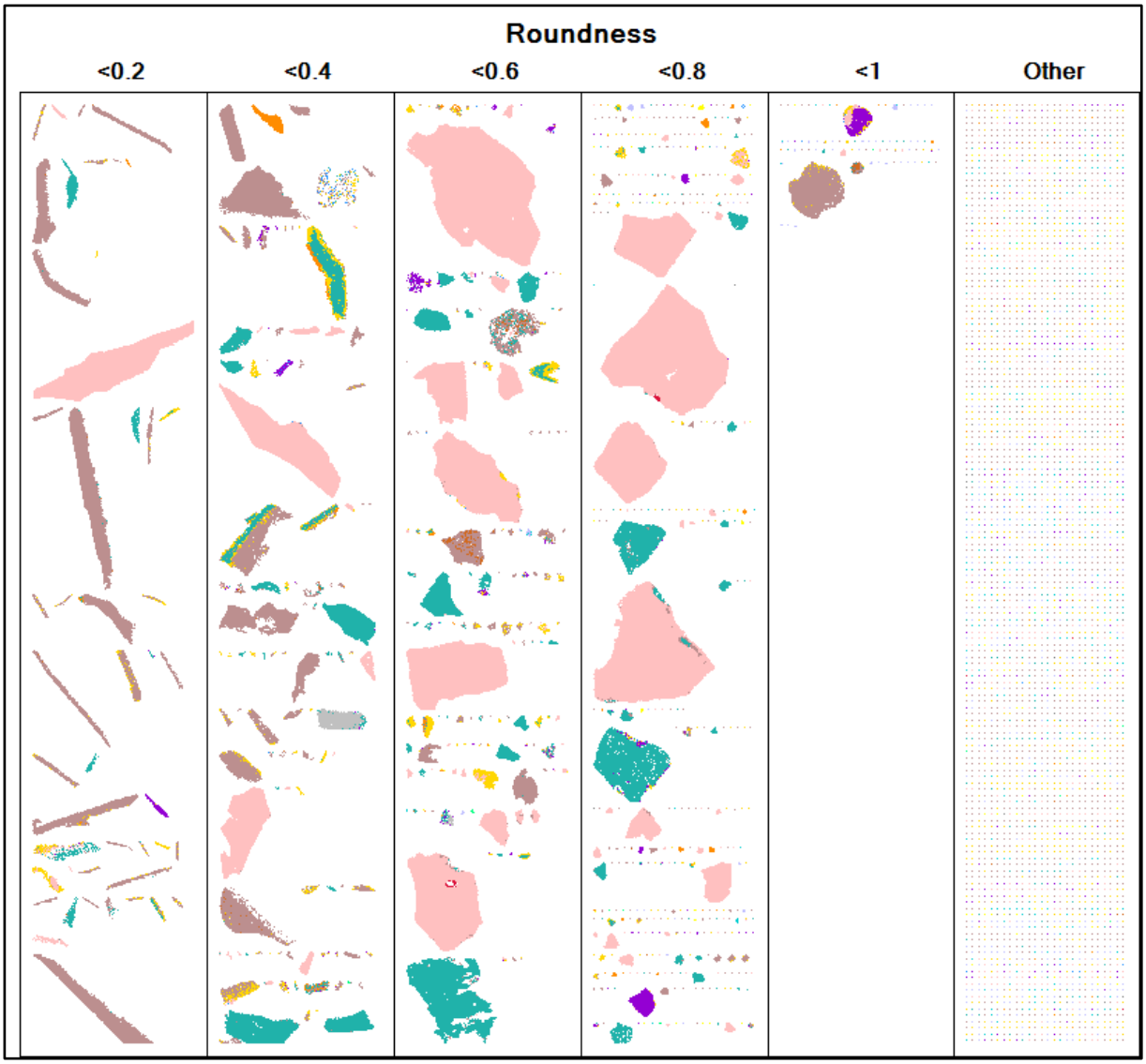

Figure S6. *The grid displaying the roundness of particles from angular to round. Sample from Coastal station used as an example*

CHAPTER 4: ATMOSPHERIC TRACE METAL DEPOSITION IN THE OCEANS SOUTH OF SOUTHERN AFRICA

A presentation of the prepared research paper

This research manuscript has been prepared for submission to Marine Chemistry. I am the lead author of the manuscript. S. Fietz, F. D. Eckardt, and A. N. Roychoudhury are co-authors. I was responsible for the collection of field data, data processing and writing of the manuscript.

This manuscript contributes the first winter and spring trace metal and solubility data of dust aerosols from the region south of South Africa. The data is compared to other global dust sources. This paper provides information on the link between solubility and potential sources. The aim is better understand the impact of aerosols on oceans south of southern Africa.

ATMOSPHERIC TRACE METAL OVER IN THE OCEANS SOUTH OF SOUTHERN AFRICA

Kaukurauee Ismael. Kangueehi[1], Frank D. Eckardt[2], Alakendra N. Roychoudhury[1], Susanne Fietz[1,*]

[1]Centre for Trace Metal and Experimental Biogeochemistry, Department of Earth Sciences, University of Stellenbosch, 7600 Stellenbosch, South Africa

[2] Environmental and Geographical Science Department, University of Cape Town, South Africa

*corresponding author: Department of Earth Sciences, Stellenbosch University, 7600 Stellenbosch, South Africa, sfietz@sun.ac.za, +27218083117

Keywords: Berger leach, Iron, Manganese, Southern Ocean, Bioaccessibility, GEOTRACES

4.1. ABSTRACT

Atmospheric deposition of aerosols can supply important micronutrients (trace metals) to surface oceanic waters and through this supply, enhance marine phytoplankton primary productivity. Various previous cruises have sampled trace metal aerosols over the Southern Ocean (SO) during summer, but data during the winter months is still missing. This is despite that most of the dust emissions from Southern Africa occurs during the drier winter and spring months. Hence, we conducted a sampling expedition during winter (July to August) and spring (October to November) in 2019 from South Africa towards the southwestern Indian Ocean and southeastern Atlantic Ocean. Since the impact of aerosols on marine biogeochemistry depends on the solubility of the aerosols particulate phases, we report the total composition and fractional solubility of atmospheric trace metals (Al, Fe, Mn, Cu, Co, Pb and Zn). For the latter we conducted two-stage leaching experiments (Milli-Q water and a weak acid reagent). The mean total concentration (±SD) in ng m^{-3} were 2388 ± 2494 (Fe), 197 ± 129 (Al), 295 ± 280 (Mn), 13.6 ± 17.3 (Cu), 1.8 ± 2.2 (V) and 26 ± 16 (Zn), respectively at five stations in winter, and 165 ± 71 (Al), 48 ± 21 (Fe), 1.22 ± 0.6 (Mn), 10 ± 20 (Cu), 40 ± 20 (Zn) and 0.6 ± 0.3 (V), at seven stations in spring. The fractional solubility in Milli-Q water ranged from 0 to 31 % for Fe, 2 to 30 % for Al, 0.2 to 23 % for V and 2.1 to 80% for Zn, 1 to 84% for Co, 0 to 45% for Cu and 0 to 47% for Mn. The labile fraction in the weak acid ranged from 0.5 to 41 % for Fe, 9 to 48 % for Al, 0.1 to 88 % for Mn, 25 to 72 % for Zn and 3.3 to 39 % for Co. Backward trajectories showed that some aerosols were from southern African sources, especially those collected closer to the continent, while the higher latitude samples originated either from South American or Antarctica. Here, we present one of the few studies that collected aerosols and determined the fractional solubility during winter and spring.

4.2. INTRODUCTION

Continental aerosols deposited into the upper surface mixed water bodies in oceans are important sources of macronutrients; such as nitrate (N), phosphate (P), silicate (Si)) and micronutrients such as iron (Fe), manganese (Mn), zinc (Zn), cadmium (Cd) and copper (Cu) (Jickells, 2005; Mackey et al., 2015). These micronutrients are key components in enzymes in phytoplankton and bacteria (Duce and Tindale, 1991; Moore et al., 2013) and a lack can thus constrain primary productivity (Bruland et al., 2001; Martin et al., 1990; Sunda, 2012). Trace metal availability, in contrast can stimulate phytoplankton growth, by increasing photosynthetic processes which will ultimately reduce carbon dioxide (CO_2) in the atmosphere (Hutchins & Bruland, 1998; Tagliabue et al., 2017). Different trace metals are required for various physiological roles in phytoplankton. For example, Zn is involved in many cell processes because among others, it can function as a Lewis acid (Frausto da Silva & Williams, 2001). In diatoms, the Mn superoxide dismutase is common (Twining & Baines, 2013). Cu plays a role in the transmembrane uptake of Fe and it is also utilized in both respiratory and photosynthetic electron exchange (La Fontaine et al., 2002; Maldonado et al., 2005; Twining & Baines, 2013). It is thus an essential micronutrient even though Cu, can be toxic to phytoplankton in high concentrations (Jordi et al., 2012; Paytan et al., 2009).

A key region where lack of micronutrients illustrate the role of dust emissions as an essential part of global climatic cycles is the Southern Ocean. The Southern Ocean has a potential capacity to sink more than 40% of all global anthropogenic atmospheric CO_2 (Frölicher et al., 2015; Shetye et al., 2015). The carbon removed from the atmosphere can be stored and deposited for millions of years in bottom oceanic sediments. One of the relevant processes is commonly known as the “biological pump” and currently, the biological pump is not working optimally in some areas of the Southern Ocean that are depleted in these micronutrients, especially, regions that are farthest from the continents (Jickells & Moore, 2015). The nutrients utilization efficiency is low due to the limitation of trace metals, especially iron. The biological pump drives carbon storage in the deep ocean and occurs through the gravitational settling of organic particles from surface waters (Boyd et al., 2019). These so-called High Nutrient Low Chlorophyll (HNLC) zones are regions with excess phosphate and nitrate but limited in micronutrients, such as iron, largely due to low external input (de Baar et al., 1995). The enhanced deposition of trace metals could enhance the efficiency of the biological pump, resulting into the sinking of organic particles (Boyd & Ellwood, 2010). Hence, dust emissions are an essential part of global climatic cycles.

The Southern Ocean is under-sampled for trace metals despite its importance to the global carbon flux (Anderson et al., 2014) leading to a data scarcity, especially on the role of atmospheric deposition. Most campaigns sampling aerosols in the Southern Ocean depart from Southern America (e.g., Basile et al., 1997; Gaiero et al., 2003; Gassó and Torres, 2019; Johnson et al., 2011; Li et al., 2008), and Australia (Gabric et al., 2010; Mackie et al., 2008; Struve et al., 2020; Winton et al., 2015). To our knowledge, only three studies have published mineral dust deposition between Southern Africa and Antarctica (Baker et al., 2006; Chance et al., 2015; Wagener et al., 2008). Wagner et al (2008) reported dust concentrations 13.0 ± 6.3 ng m^{-3} in the SO region. Solubilities reported by Chance et al (2015) for elements such as Fe, Mn and Al were less 20% but as high as 74% for Zn while using ammonium acetate as a leach. In addition, most sampling campaigns in the Southern Ocean south of Africa took place during the summer months for logistical reasons (Chance et al., 2015; Witt et al., 2006). The Southern Ocean is well known for severe weather conditions in winter and spring, challenging scientific expeditions during these seasons (Ansorge et al., 2017), while the summer months offer perfect sampling conditions (Henley et al., 2020). However, this is not ideal for two reasons (i) because the dust season in southern Africa and South America occurs in the dry winter months peaking between May to August (Eckardt and Kuring, 2005; Formenti et al., 2019; Vickery et al., 2013), and (ii) because the winter and spring aeolian deposition may be key to the Southern Ocean spring and early summer phytoplankton blooms. This rapid accumulation of phytoplankton biomass usually occurs seasonally. These blooms usually occur temporally and spatially and are depended on iron availability and vertical mixing in open ocean water.

Here, we sampled spring and winter aerosols in the Atlantic sector of the Southern Ocean, south of South Africa. Major known spring and winter dust sources in southern Africa and South America are for example, the Etosha Pan in Namibia, Makgadikgadi Pan in Botswana and Patagonian Desert in America (Bhattachan et al., 2012; Ginoux et al., 2012; Li et al., 2008). Dust plumes from these major emitters have been observed emanating from southern Africa towards the southwestern Indian Ocean and in some cases towards the southeastern Atlantic Ocean (Piketh et al., 2000, 2002; Swap et al., 2003). Similarly, dust plumes from South America also reach the southeastern Atlantic Southern Ocean (Gaiero et al., 2003). The Southern Hemisphere is expected to experience stronger winds and more drought conditions, likely strengthening the aerosol emission to the Southern Ocean (IPCC, 2019). Hence, the importance of Southern Hemisphere dust for the Southern Ocean biogeochemical cycle and carbon capture may strengthen in future.

Crucial for the relevance of the captured dust for the spring and summer phytoplankton development is the amount as well as the solubility that translates into bioaccessibility. In this study, we focused on the readily bioavailable and labile fractions similar to other studies by Shelley et al (2018) and Winton et al. (2015) in the north east Atlantic and Southern Ocean regions.

Hence, this study provides a unique opportunity of closing spatial and temporal gaps in aerosol sampling in the Southern Ocean. We provide atmospheric trace metal concentrations and their fractional solubility with an aim to contribute to data availability, and improve the knowledge of the potential impact of aerosol deposition during the winter and spring.

4.3. METHODS

4.3.1. Cruise track and aerosol sampling

The data used for this study was collected from two cruises onboard the research vessel SA Agulhas II that took place between Cape Town (South Africa) and Antarctica in winter and spring 2019 (Table 1). During the Southern oCean seAsonal Experiment (SCALE) 2019 Winter Cruise, the ship sailed for four weeks between June and July 2019. During the 2019 SCALE Spring cruise, the ship sailed for six weeks between October and December 2019. Both cruises mainly followed the so-called Bonus Good Hope Line from Cape Town to 60˚ S along the zero meridian in the East Atlantic sector of the Southern Ocean and on the return to Cape Town (Figure 1). Two samples were taken further east of the Bonus Good Hope Line, one in winter on an additional transect along the South African coast and one in spring on a longitudinal transect along the ice edge (Figure 1).

Bulk aerosol samples were collected on acid-washed Whatman W41 filters with 20 µm pore size. Air was pumped through the filters using a volumetric flow controlled high volume air sampler (5170DV-BL, Tisch Environmental) which draws approximately 100 L min^{-1} through the filter. The dust sampler was mounted on the 11th deck approximately 15 meters above sea level and opposite the direction of the ship's exhaust fume stacks during sailing (Figure 2). An automated sector control system (Campbell Scientific, Logan. Utah, USA) was set up to provide power to the dust sampler when the wind conditions were favorable (when the wind was ±60˚ from the bow of the ship and >0.5 m s^{-1}) and shut off when the wind directions came from the ship`s exhaust fume. This helps in preventing contamination from stack gases and other ship operations (Heimburger et al., 2013). Each sampling deployment lasted approximately one to two days (~48 hours). Filters were changed every 48 hours, because based on visual inspection, 24 hours was not sufficient to collect enough material for analyses. The filtration set-up differed between the winter and spring cruises in so far as during the winter cruises 8" x 10" W41 filter sheets were used, while during the spring cruise 47 mm

diameter W41 filter discs were placed on a 12-position PVC adapter plate (Shelley et al. 2015). Two duplicate sample filters were collected from each deployment.

The Whatman 41 filters were pre-cleaned according to GEOTRACES protocols (Cutter et al., 2017), in a certified 100-class clean laboratory and under a HEPA-filtered laminar flow at the University of Stellenbosch, South Africa, following Baker et al. (2006). The filters were placed into a 0.5 M (HCl) acid bath for one day and then individually rinsed with Milli-Q® water five times. After rinsing, the filters were placed in a Milli-Q® bath for 24 hours. Finally, the filters were soaked and rinsed five times with Milli-Q® water and left to dry for 12 hours before being individually stored in new plastic ziplock bags. Two duplicate sample filters were collected from each deployment.

After approximately 48 hours of sampling, filter holders with filters were placed in zip-lock bags and subsequent filter handling conducted in the on-board clean container. Under the laminar flow in the clean container, filters were removed from the filter holder, folded inwards and stored frozen at -20 ºC until analysis on land.

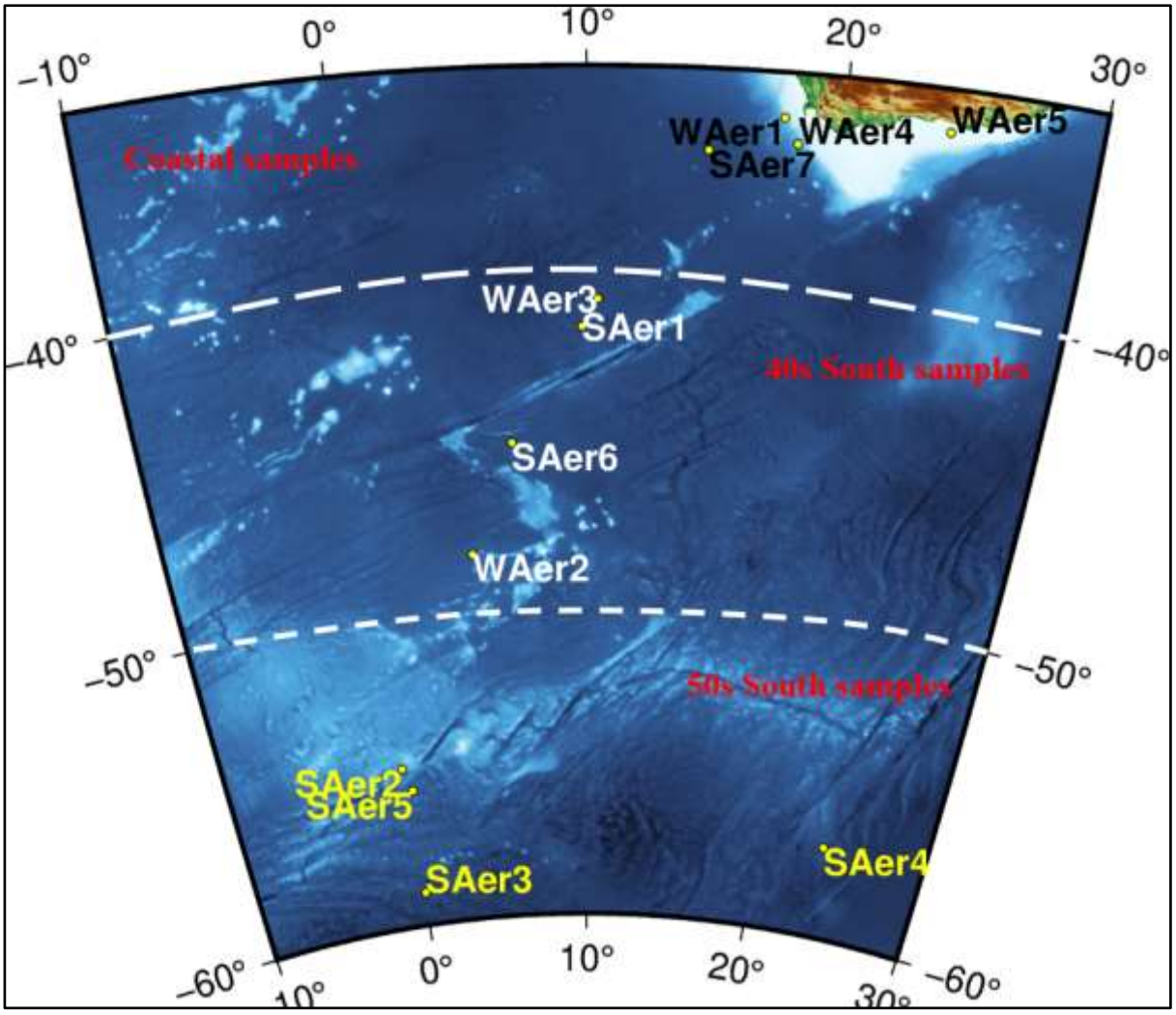

Figure 1. *Sample locations for the Southern oCean seAsonal Experiment 2019 (SCALE 2019) Winter Cruise (WAer) 2019 and Spring Cruise (SAer) 2019. In this study we use three operationally defined*

categories for the samples: samples collected in the coastal area, samples collected in the mid-ocean (40˚S) zone and samples collected furthest away from the continent (50˚S).

Table 1. *Aerosol sampling dates and number of samples collected during the South African led Southern oCean seAsonal Experiment 2019 (SCALE 2019) cruises into the Southern Ocean. Sampling duration was 48 hours for all samples.*

Sample ID	Ocean Sector	Latitude [˚N]	Longitude [˚W]	Dates
SAer_7	**Coastal**	-35.61627	14.79698	19/11/2019
WAer_1	**Coastal**	-34.4441	17.67923	06/08/2019
WAer_4	**Coastal**	-35.24377	18.24777	23/07/2019
WAer_5	**Coastal**	-34.36245	24.09932	11/08/2019
SAer_1	**40s South**	-41.32145	9.80482	15/10/2019
SAer_6	**40s South**	-44.97767	6.6326	15/11/2019
WAer_2	**40s South**	-48.45143	4.51788	03/08/2019
WAer_3	**40s South**	-40.43635	10.4721	19/07/2019
SAer_2	**50s South**	-54.99142	-0.27067	21/102019
SAer_3	**50s South**	-58.96347	0.0395	25/10/2019
SAer_4	**50s South**	-57.1516	23.99473	04/11/2019
SAer_5	**50s South**	-55.71673	0.15282	09/11/2019

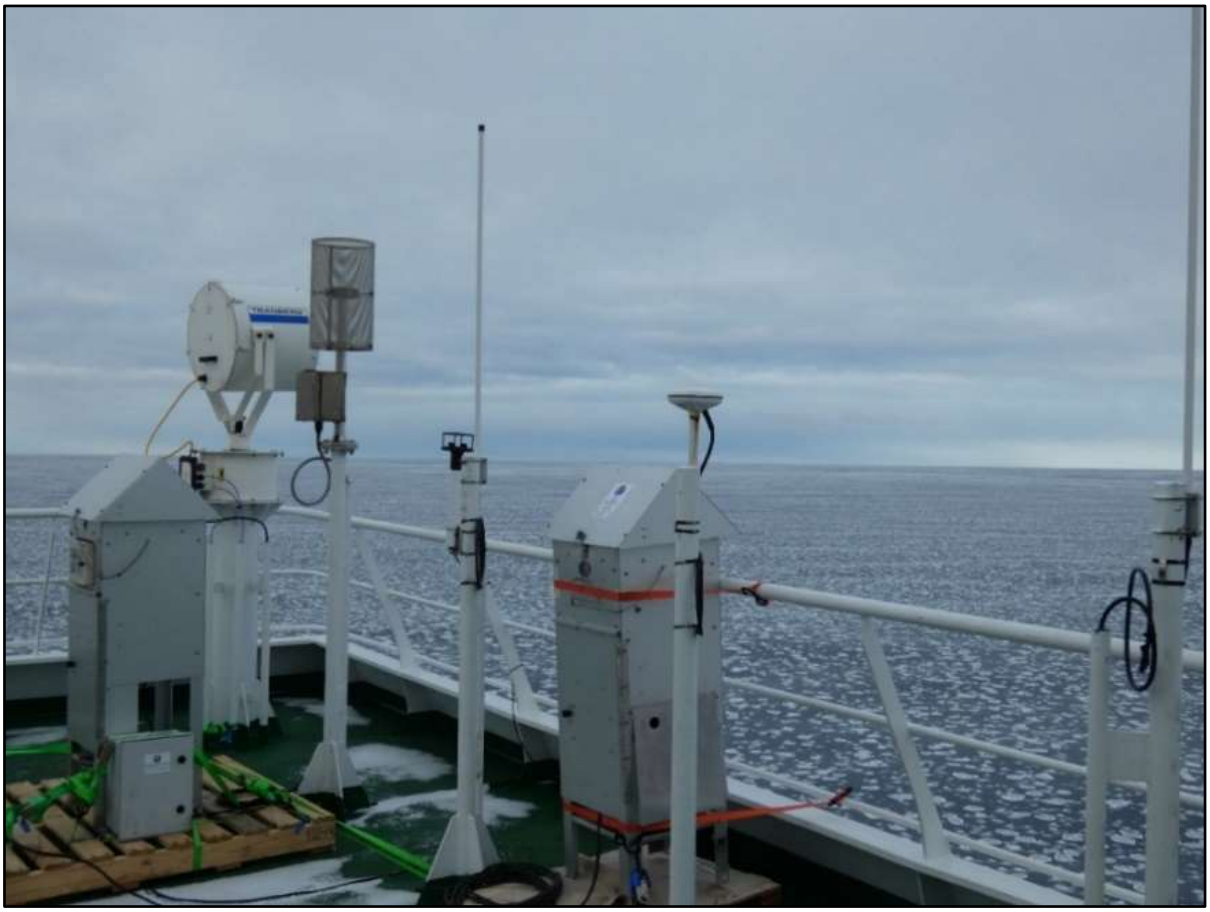

Figure 2. *The high-volume air sampler (Tisch Environmental) positioned on the monkey island on the SA Agulhas II during the winter cruise in 2019. In the background are pan cake ice sheets from approximately 58°S in the Atlantic sector of the Southern Ocean.*

4.3.2. Bulk trace metal analysis

After the cruise, under the laminar flow in the laboratory at Stellenbosch University, the aerosol samples were digested with HNO_3 prior to the determination of the bulk trace elemental concentration using an Agilent 7900 Inductively Coupled Plasma Mass Spectrometry (ICP-MS)**.** The trace metals had an internal standard accuracy range from 96 to 108% by repeat analysis (n=10). The blanks were subtracted from the sample results and corrected for dilution. Arizona Test Dust was analyzed along with our Southern Ocean aerosol bulk trace metal analysis. Results obtained for Arizona Test Dust are presented in Table 2 indicating mostly good correspondence with Baker et al. (2020).

Table 2. *Mean and standard error (duplicates samples) of elemental composition (concentration in ppm) of Arizona Test Dust determined in this study and Baker et al. (2020).*

Element	this study	Baker et al. (2020)
Fe	27 082 ± 1080	28 600 ± 1 100

Al	38 104 ± 742	60 300 ± 3 500
Ti	923 ± 58.9	2,510 ± 100
Mn	644 ± 16.4	658 ± 34
Co	13.0 ± 0.76	15.0 ± 0.5
Pb	31.9 ± 0.59	n/a

4.3.3. Leaching experiments

The sampled Whatman 41 filters as described in section 4.3. 1 were further used for leaching experiments. Sequential experiments were conducted with a trace metal clean flow through method following Winton et al. (2016) and Aguilar-Islas et al. (2010). All bottles and filters used in the leaching experiments were acid cleaned according to GEOTRACES protocols (Cutter et al., 2017). The sampled Whatman 41 filters were mounted to a single-staged PFA funnel stage connected to a front face. A peristaltic pump was used to pump the leachate at 24 rpm in order to push through 50 ml of solvent over approximately 10 min. The same set-up was used for a duplicate dust loaded filter and a blank.

4.3.4. Milli-Q leachate to determine the instantaneous water dissolvable (soluble) fraction

The Milli-Q water was used for the first leachate using the flow-through system described above (50 mL, ~2 min). The leachates were analysed using the same Agilent 7900 ICP-MS at Stellenbosch University as used for bulk metal analysis (cf. 2.2). The leachates were acidified to 2% final acid concentration using ultra-pure HNO_3 and particulates were left to settle out prior to analysis. Previously, published, similar continuous flow-through experiments indicated that the bioavailable and easily available iron and other trace metals could be extracted with Milli-Q water within the first 10 minutes (Wu et al., 2007). This fraction is thus considered as the instantaneous water dissolvable (soluble) trace metal fraction.

The fractional solubility of each trace metal in Milli-Q water was calculated following Winton et al., (2015), Eq. 1:

$$TM_{MilliQ} = \frac{TM_{MilliQ-leach}}{TM_{bulk}} x100 \qquad \text{(Eq. 1)}$$

After the leaching with Milli-Q water, the filters were used for further weak acid leaching experiments as described below in section 2.3.2.

4.3.5. WEAK ACID LEACHATE TO DETERMINE THE LABILE TRACE METAL FRACTION: "BERGER LEACH"

The reactive, labile fraction was determined following Berger et al. (2008; thus colloquially referred to as "Berger leach"), after completion of the Milli-Q water leaching (section 2.3.1). The same filters were transferred into acid-washed vials, dried in the laminar flow hood, and leached with 25% ultra-high purity glacial acetic acid (HAc) and 0.02 M hydroxylamine hydrochloride ($NH_2OH \cdot HCl$) at 90 °C for 10-15 min. The heating process enables dissolution of an additional labile fraction and acid-soluble fraction (Winton et al., 2015a), as the traditional 25% HAc room temperature leach tends to underestimate the labile metal fraction (Berger et al., 2008; Chester & Hughes, 1967). In addition, the heating step also serves to liberate the trace metals found in intracellular proteins in phytoplankton (Berger et al., 2008) and assists to release trace materials such as iron and manganese oxyhydroxides from biogenic materials (Bayon et al., 2004). The leachates were acidified with 2% HNO_3 solution and analysed with an ICP-MS as described for bulk metal analysis above (cf. 2.2). The fractional solubility in the weak acid was calculated according to Eq. 2 following Winton et al. (2015) similarly as shown in Eq. 1 for Milli-Q leachates:

$$TM_{acid} = \frac{TM_{acid-leach}}{TM_{bulk}} x100 \qquad \text{(Eq. 2)}$$

The bioavailable fraction is considered to be the sum of the fractional solubility in water (Milli-Q; cf. 2.3.1) and in the weak acid following Eq. 3.

$$TM_{labile} = TM_{MilliQ} + TM_{acid} \qquad \text{(Eq. 3)}$$

4.3.6. Air Mass Pathways

The online free available NOAA Hybrid Single Particle Lagrangian Integrated Trajectory Model (Hysplit) was used to determine the source of the air masses and thereby possible sources of aerosols (Stein et al., 2015). A 5-day air mass backward trajectories was modelled for each aerosol sample (Osipov et al., 2020; Strzelec et al., 2020). The model used vertical velocity simulation method and GDAS1 meteorology (Stein et al. 2015; Rolph 2016). The starting heights for the backward trajectories were 100, 500, 1500 m (e.g., Longo et al., 2016).

4.4. RESULTS

4.4.1. Bulk aerosol trace metal concentration

Spatial distribution: The total trace metal composition varies between sampling locations both in winter and spring (Table 3). The different stations have been grouped based on sampled locations into "Coastal", "40s South" and "50s South" groups (Figure 1). Presumably, aerosols collected at coastal sampling locations would deposit into subtropical waters, the 40s South would deposit into the subantarctic and polar frontal zone waters and the 50s South samples would deposit into the Antarctic waters (south of the polar front). The highest concentrations were recorded close to Southern Africa (Coastal group), while low concentrations were recorded in the 50s South group (Table 3). For example, Fe concentrations ranged from 60 to 5785 ng m^{-3} in the Coastal samples, but only from 22 to 63 ng m^{-3} in the 50s South group (Table 3) (Figure 3). Similar differences were observed for Mn. Cu concentrations were also high in the coastal samples, and very low or even below detection limits in the open ocean samples (Table 3). There is a large spatial variation, especially for metals such as Mn, while there is less variation for Al.

***Seasonal variability*:** Some of the apparent spatial differences resulted from seasonal sampling. Most of the bulk aerosol trace metal concentrations were much higher in winter than in spring (Table 3). For example, bulk Fe concentration ranged from 114 to 5786 ng m^{-3} in winter, but only from 8 to 79 ng m^{-3} in spring. Similarly, bulk Al concentrations ranged from 104 to 408 ng m^{-3} in winter, but only from 70 to 242 ng m^{-3} in spring (Table 3). Other bulk concentrations did not show such evident seasonal changes. The Pb concentration, for example, ranged from 0.23 to 1.95 ng m^{-3} in winter and 0.08 to 1.15 ng m^{-3} in spring (Table 3).

***Table 3**. Bulk trace metal concentrations (ng m^{-3}) at the different dust sampling locations grouped according to the distance from the South African coast (Figure 1). Bdl refers to below detection limit.*

Zones	Sample ID	Al	Fe	Mn	Zn	Cu	V	Pb
Coastal	SAer_7	120	60	1.6	47	43	0.1	0.27
	WAer_1	133	154	15	44	4.3	0.32	0.8
	WAer_4	182	4065	503	6.3	9.2	2.3	0.5
	WAer_5	312	5785	636	32	44	5.4	2.3
40s South	SAer_1	198	70	1.2	23	6.3	0.6	0.37
	SAer_6	127	43	0.8	26	17	0.3	017
	WAer_2	61	124	19	14	3.9	0.17	0.05
	WAer_3	329	3782	74	119	21	3.4	4.3
50s South	SAer_2	213	40	1.4	59	bdl	0.9	0.39
	SAer_3	237	63	1.9	44	bdl	0.7	0.38
	SAer_4	187	40	1.3	63	bdl	0.79	0.78
	SAer_5	73	22	0.4	18	7	1.1	0.17

***Table 4**. Total and fractional aerosol trace metal concentrations range in the proximal and distant open ocean water regions around Table 1 for sample locations. Bdl refers to below detection limit*

Trace metals	Total Concentration range (ng m^{-3})		Soluble fraction (ng m^{-3}), in Milli-Q water		Labile fraction (ng m^{-3}), in weak acid	
	min	max	min	max	min	max
Fe	124	5786	0.30	982	21	2101
Al	61	329	3.7	69	16	83
Mn	15	636	0.04	854	0.45	346
Pb	0.50	4.3	0.0006	0.40	0.38	2.3
V	0.17	5.4	0.01	0.30	0.12	3.4
Zn	6.3	118	0.13	221	12	108
Cu	3.9	44	bdl	4.6	bdl	10
Co	7.5	21	0.01	5.6	0.44	2.8

***Table 5**. Total and fractional aerosol trace metal concentrations ranges in the proximal and distant open ocean water regions around Southern Africa for the **Spring Cruise** 2019. See Figure 1, Table 1 for sample locations. Bdl refers to below detection limit.*

Trace metals	Total Concentration range (ng m^{-3})		Soluble fraction (ng m^{-3}), in Milli-Q water		Labile fraction (ng m^{-3}), in weak acid	
	min	max	min	max	min	max
Fe	8.0	79	1.1	4.7	8.0	47
Al	70	299	6.7	86	19	83
Mn	0.38	2.3	0.13	0.65	0.40	3.2
Pb	0.08	1.2	bdl	bdl	0.02	1.0
V	0.11	1.1	0.01	0.06	0.07	0.1
Zn	12	80	3.9	47	7.0	36
Cu	4.0	77	1.1	15	3.9	22

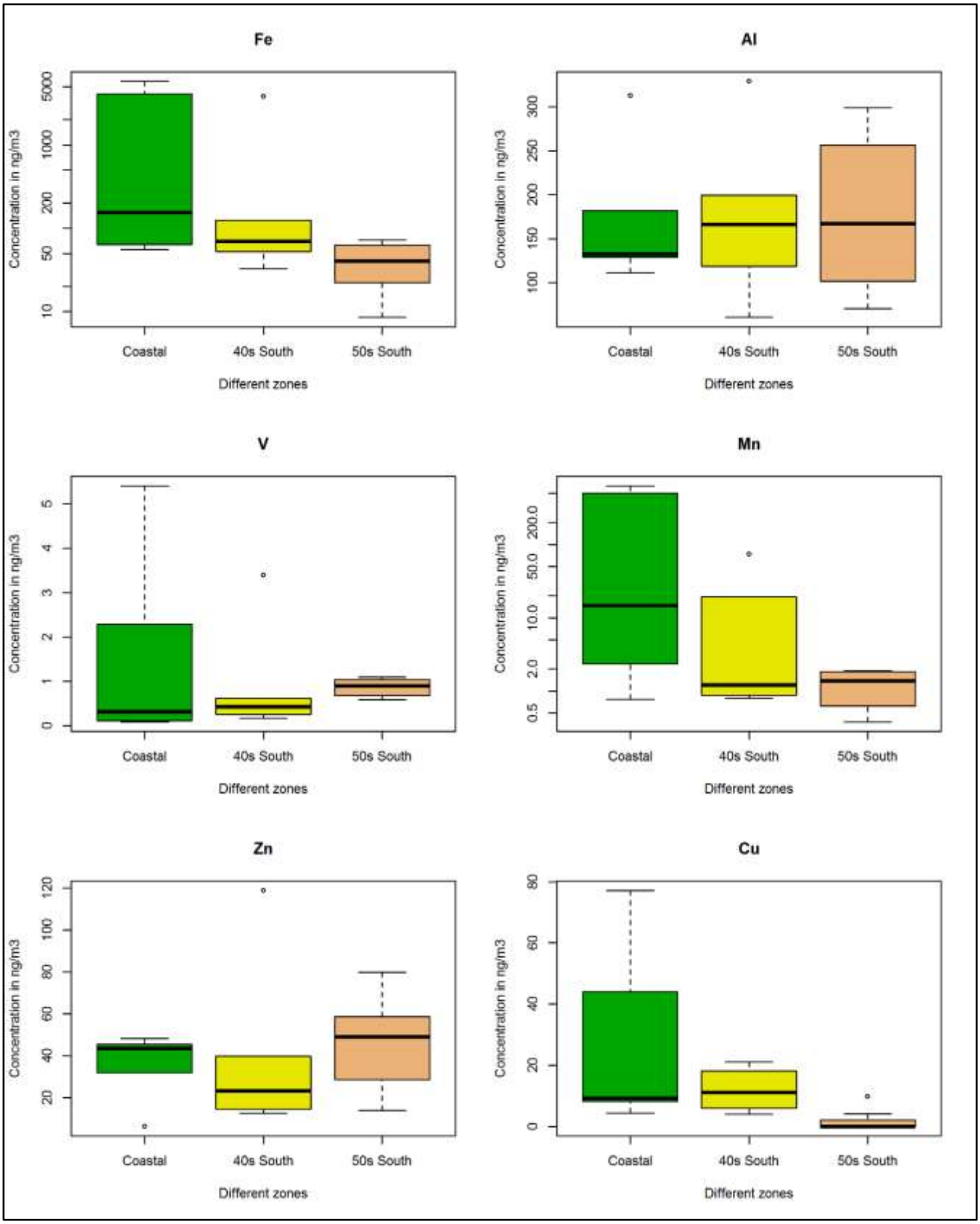

Figure 3. *Bulk total trace metal concentration of the different zones combining data gathered from winter and spring cruises 2019. The bottom line represents the first quartile (25%) and ends in the third (75%), the middle line represents the median, while drawn segment represents the furthest data without counting the boxplot outliers, while the dots represents the outliers.*

4.4.2. Soluble and labile fraction

Spatial distribution: The soluble fraction is considered to be the Milli-Q leachable fraction, while the labile fraction is considered to be the weak acid leachable fraction. The fractional solubility changed from the coastal to the open ocean samples for some trace metals. For example, the fractional solubility of Fe, Al and V decreased with distance from the coast to open ocean (Figure 4). In contrast, Mn and Zn differed from Fe, Al and V, as Mn and Zn had the highest solubility observed in the 40s South samples.

Seasonal variability: Some trace metals showed lower solubility in winter than in spring. The soluble Fe fraction, for example, ranged from 0.01 to 31% in winter, but only from 0.01 to 7.4% in spring (Table 3, Table 4). Others, in contrast, showed higher solubility in spring than in winter, such as Al (5 to 42% in spring, 1.9 to 8.3% in winter) (Table 3, Table 4). Nonetheless, the majority of the analysed trace metals had similar solubility in winter and spring (Table 2,Table 3). For example, solubility of V ranged from 0.16 to 20% in winter, and 1.5 to 23% in spring and solubility of Zn ranged from 2 to 80% in winter and 14 to 72% in spring (Table 2,Table 3). In winter, the solubility of the labile fraction, ranged from 0.53 to 52% Fe, from 8.6 to 74% Al, from 8 to 68% V, from 0.09 to 6.3% Mn and from 34 to 84% Pb. The Cu solubility was below detection when leached with weak acid (Table 3). In spring, the solubility of the labile fraction Fe ranged from 12 to 85% Fe, from 18 to 73% Al, from 5 to 79% V, from 26 to 79% Mn and from 20 to 84% Pb (Table 4).

Soluble versus labile fractions: All trace metals have a higher fractional solubility in the labile phase compared to the soluble phase (Table 3, Table 4) and fractional solubility in the labile phase roughly doubles compared to fractional solubility in the soluble phase for trace metals such as Al, Cu, Fe, Mn, V and Zn (Table 3,Table 4). These results indicate that the highest bioaccessible fraction of trace metals is a result of the labile fraction.

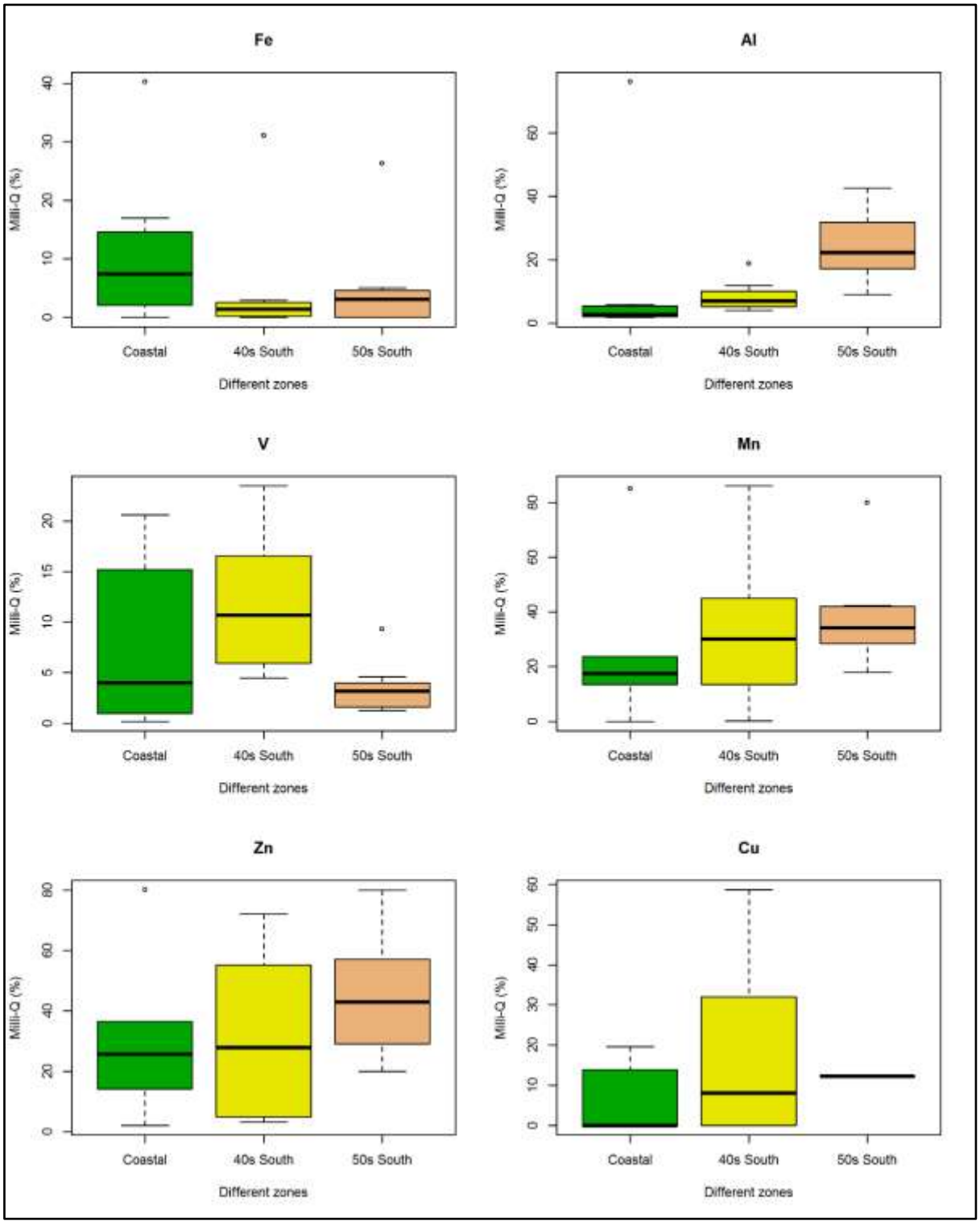

Figure 4*. Soluble fraction in (%) using Milli-Q water as a leachate (Milli-Q (%)) in aerosols collected in winter and spring 2019 over the Southern Ocean. The black dots represent the outliers. The reader is referred to Figure 1 and Table 1 for zonal grouping of the samples. The bottom line represents the first quartile (25%) and ends in the third (75%), the middle line represents the median, while drawn segment represents the furthest data without counting the boxplot outliers, while the dots represents the outliers.*

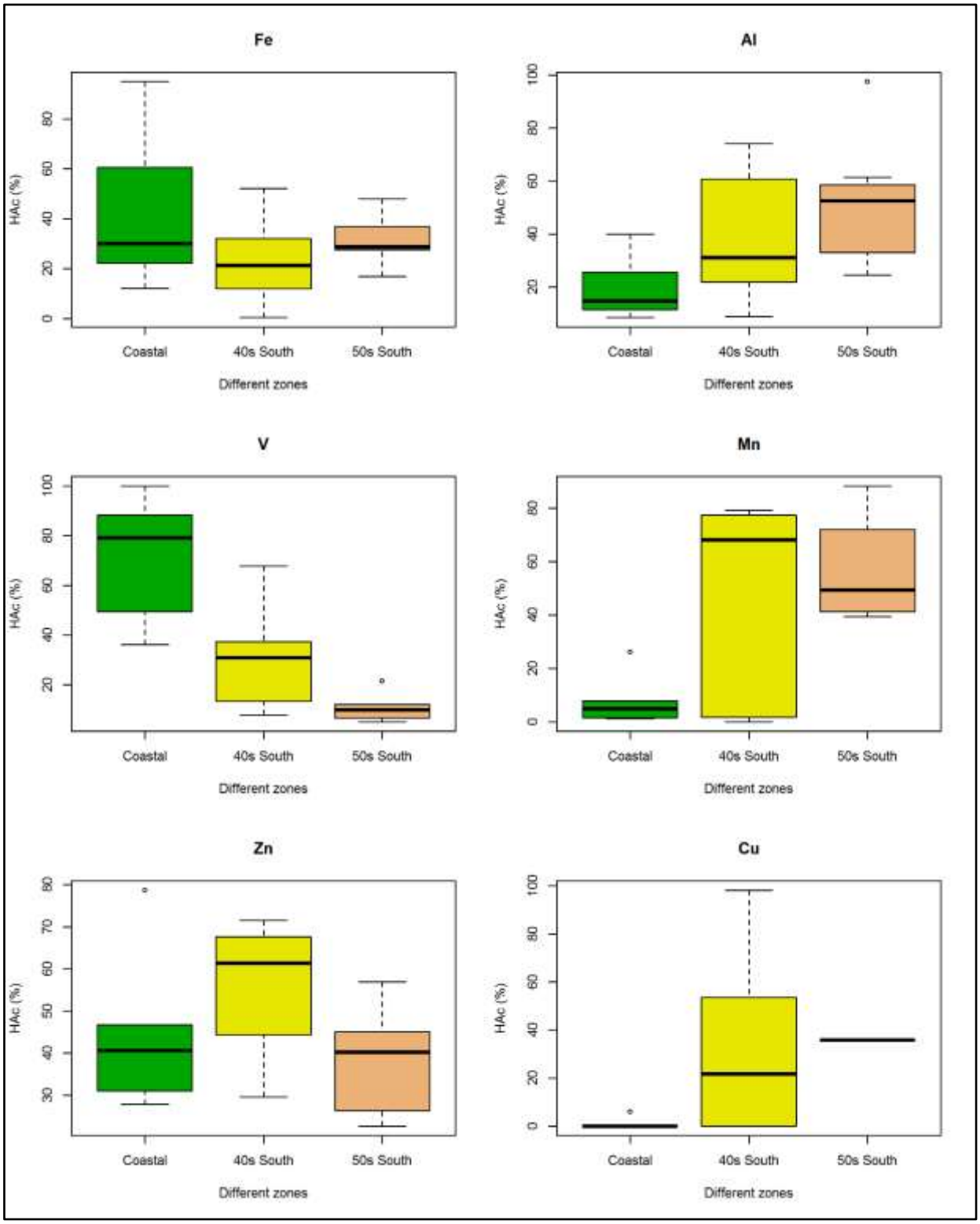

Figure 5. *Solubility (%) of labile fraction using a weak acid as a leachate in aerosols collected in winter and spring 2019 over the Southern Ocean. The black dots represent the outliers. The reader is referred to Figure 1 and Table 1 for zonal grouping of the samples. The bottom line represents the first quartile (25%) and ends in the third (75%), the middle line represents the median, while drawn segment represents the furthest data without counting the boxplot outliers, while the dots represents the outliers.*

4.4.3. Enrichment factors

The trace metals of interest in this study were normalised to Al concentrations, because Al is a lithogenic marker, most abundant in crustal soils and bedrock (Taylor & McLennan, 1985). The resulting enrichment factors are used as a strategy to identify and distinguish between the natural and anthropogenic sources. The enrichment factor ratios are calculated as given in Eq 4:

$$EF = [\frac{X}{Al}]_{aerosol} / [\frac{X}{Al}]_{UCC} \quad \text{(Eq. 4)}$$

Enrichment factors lower than ten roughly indicate that the target trace metal has a crustal source. Enrichment factors above ten are typically considered as indicative of enrichment through a source other than Earth crust, often from anthropogenic influence. The low enrichment factors for V, Fe and Mn (Table 6 indicate that the primary source is lithogenic. The enrichment factor for Mn was high (>10) for winter samples though and indicate potential anthropogenic impact (Table 6). Enrichment factors for Pb ranged from 5 to 55 across the different zones (Table 6), which shows strong anthropogenic influence especially for the winter samples. The enrichment factor for Cu was unusually high in winter and spring, especially in the coastal and 40s South samples (Table 6).

Table 6. *Enrichment factors at the different dust sampling locations grouped according to the distance from the South African coast.*

	Sample ID	V	Mn	Cu	Pb	Fe
Coastal	SAer_7	0.5	<<10	599	9	0.9
	WAer_1	1	12	56	26	2
	WAer_4	7	<<10	90	12	38
	WAer_5	9	<<10	250	29	31
40s South	WAer_2	1	44	127	13	5
	WAer_3	6	22	116	55	21
	SAer_1	2	<<10	51	8	0.6
	SAer_6	1	<<10	210	5	0.6
50s South	SAer_2	3	<<10	n/a	8	0.3
	SAer_3	2	<<10	n/a	7	0.5
	SAer_4	3	<<10	n/a	21	0.4
	SAer_5	9	<<10	152	9	0.5

4.5. BACKWARD TRAJECTORIES AND POSSIBLE SOURCES

Backward trajectories are commonly used to approximate aerosol sources and provenances (e.g. marine, deserts, anthropogenic). The five-day backward trajectory simulations indicate that most of the air masses at the sampling sites might originating from South America and some from Antarctica with a strong marine influence for most of the samples, especially for the coastal and 40s samples. The coastal samples also likely had some terrestrial input from Southern Africa (Figure 6).

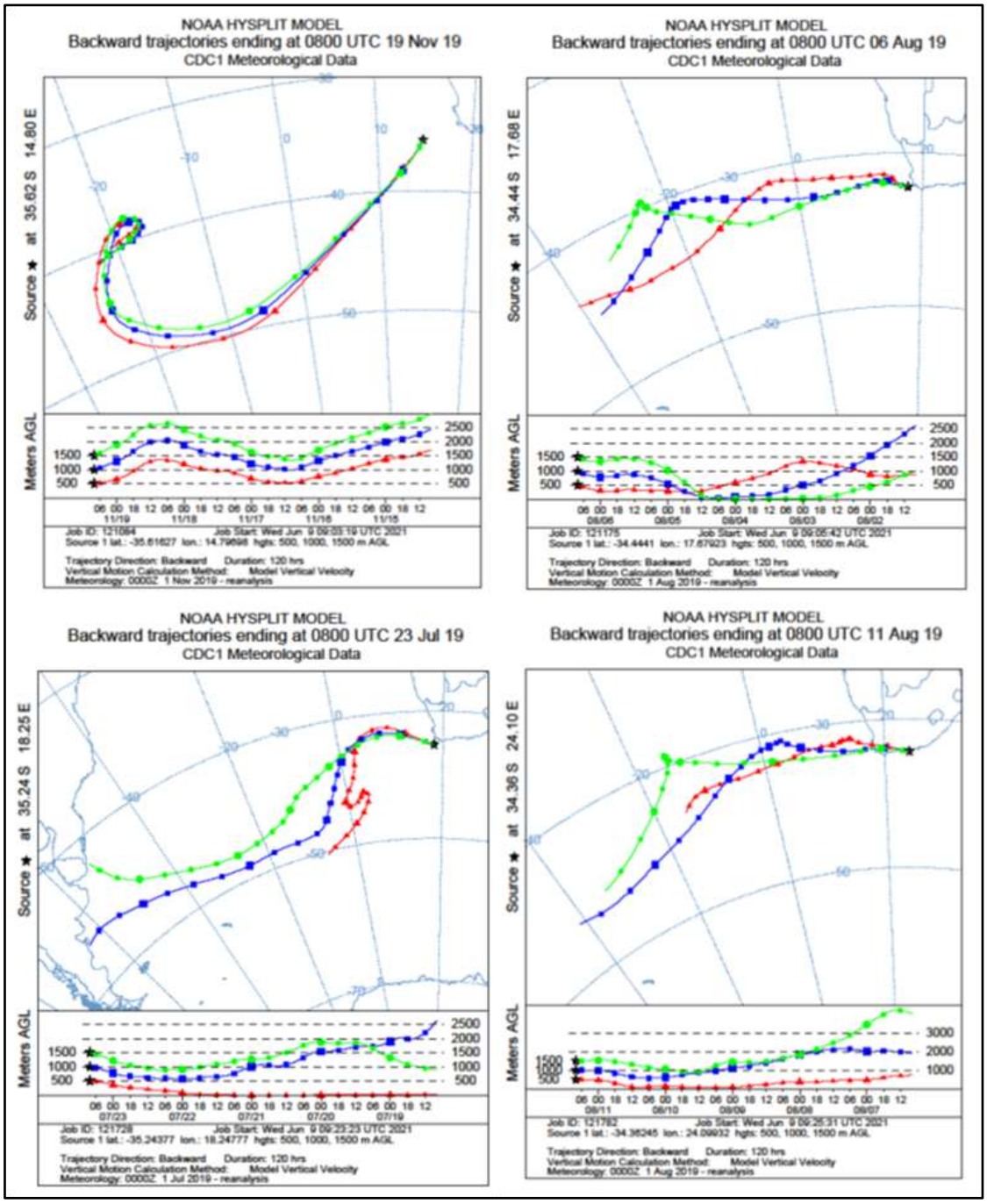

Figure 6. *Representative backward trajectories for the coastal stations.*

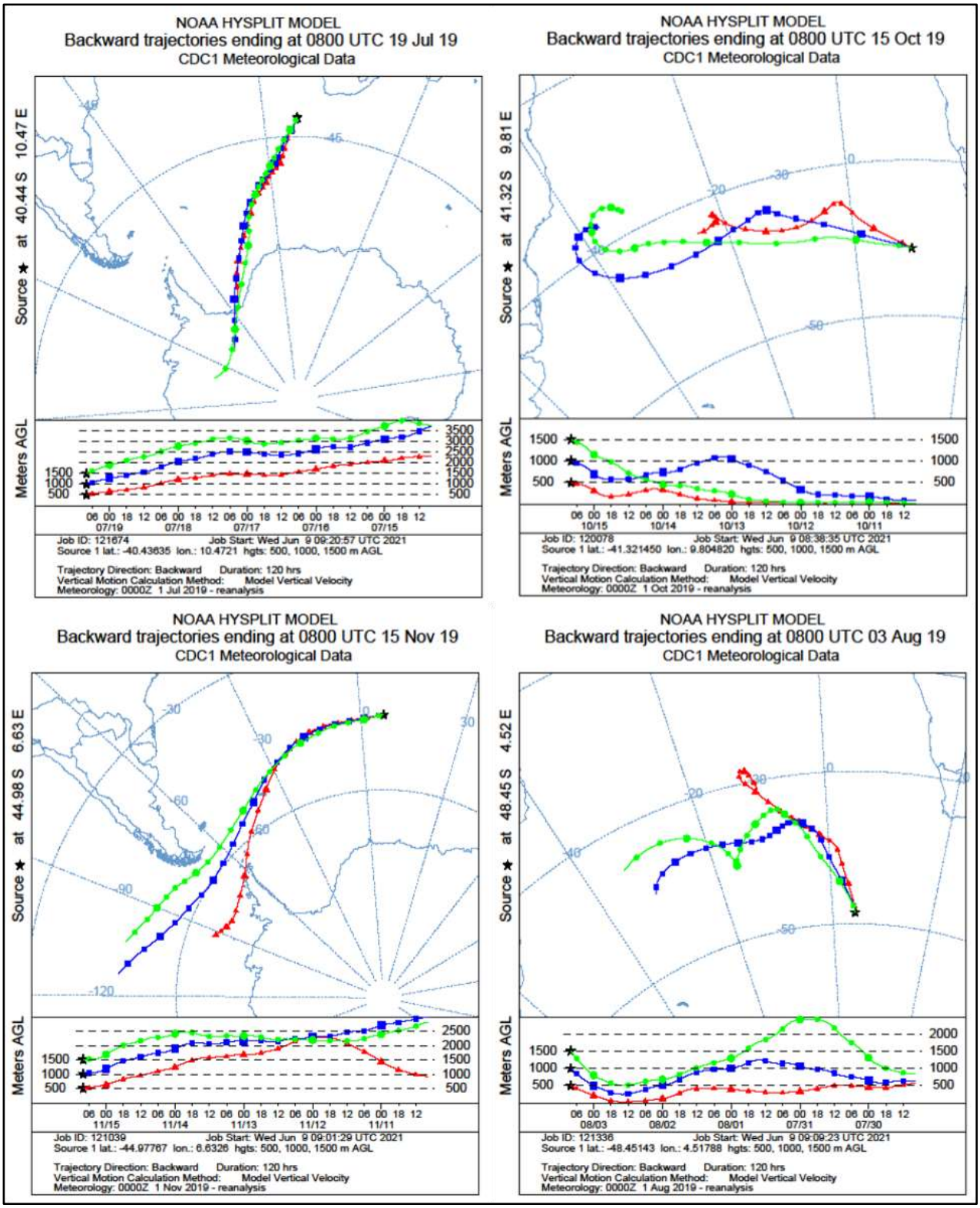

Figure 7*. Representative backward trajectories for the 40s South station.*

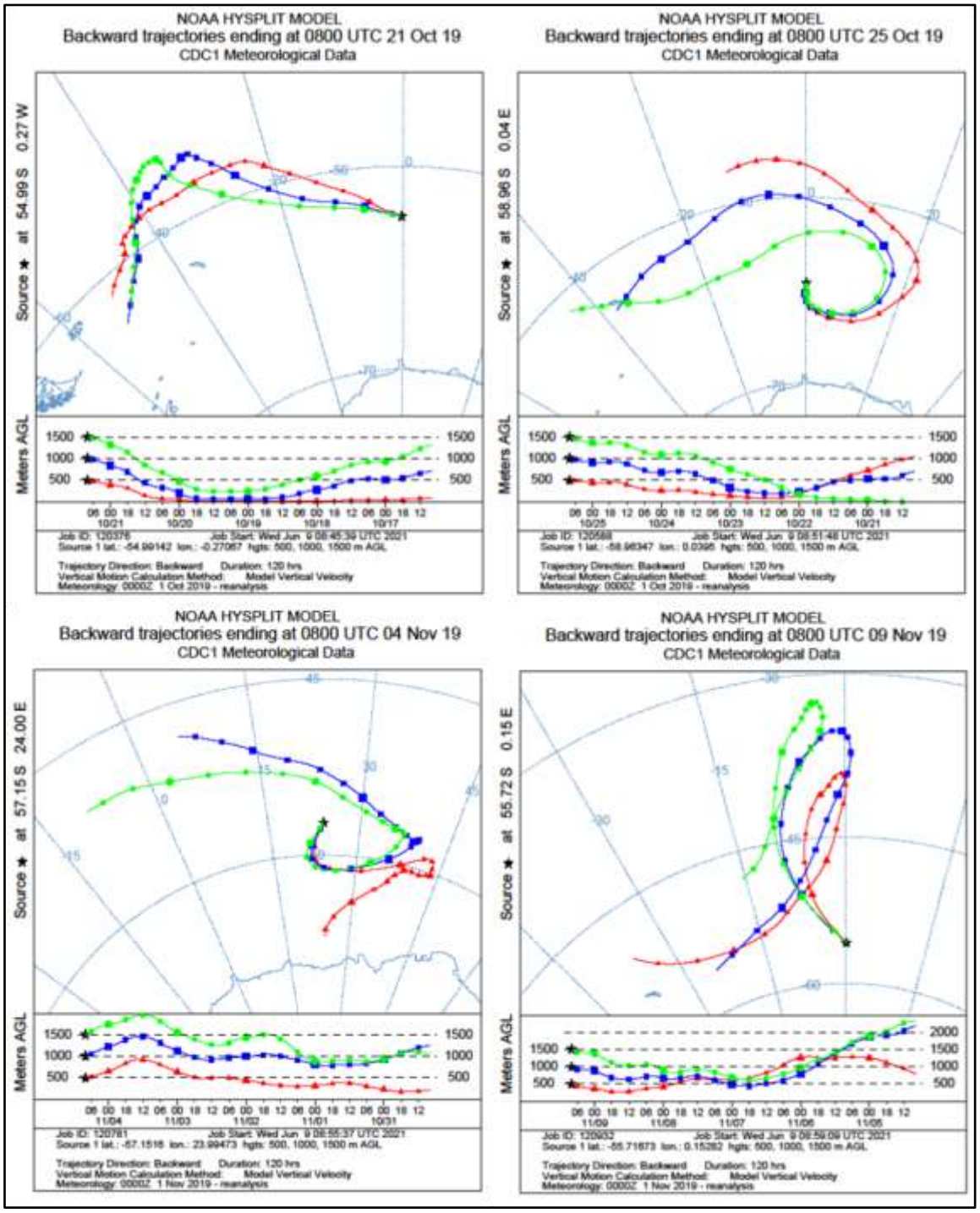

Figure 8. *Representative backward trajectories for the 50s South stations*

4.6. DISCUSSION

4.6.1. Bulk trace metals

4.6.1.1. Coastal dust aerosols

The seasonal and spatial distribution of the bulk trace metals is indicative of the origin as the different sources have led to a large variation in the aerosol trace metal loadings ranging for example from 22 to 5785 ng m^{-3} for bulk Fe. Trace metal concentrations were higher in our winter samples compared to our spring as well as existing summer data, e.g., 14. 5 ng m^{-3} Fe in summer in the same area (Chance et al., 2015). Since the winter sampling included samples along the South African coast this may be partially explained by the relatively high South African dust emissions that occur during the winter compared to summer and spring (peaking between August to September) (Piketh et al., 1999; Vickery et al., 2013). Hence, the high bulk trace metal concentrations especially observed in our winter near-coast samples, may be associated with Southern African dust sources. Klopper et al. (2020) recorded similarly high concentrations along the Namibian coastline. For example Klopper et al. (2020) reported 556 ± 643 ng m^{-3} Al in 2016; 446 ± 551 ng m^{-3} in 2017 with peak values of 4.7 µg m^{-3}. The same authors also reported 372 ± 480 ng m^{-3} Fe in 2016 and 338 ± 433 ng m^{-3} Fe in 2017, which is close to the Fe load of 246 ng m^{-3} observed by Annegarn et al. (1983) from the Namib Desert. Bulk trace metal concentrations collected close to the Southern Africa were also similar in range to the ones reported by Witt et al. (2006), (up to Cu=16.3 ng m^{-3}, Zn=20.7 ng m^{-3}, Pb= 14.1 ng m^{-3}), sampled between southern Africa and Australia. These results indicate that high trace metals loads are transported from the southern African coasts towards the open ocean.

The backward air mass trajectories indeed showed an inland source from southern Africa for our coastal stations (Figure 5). The strong easterly winds transport most of the air masses in southern Africa (Ross et al., 2001), whereas the weak westerlies drive air masses towards the Indian Ocean (Li et al., 2008). Numerous satellite images reveal that dust from Southern Africa follow this direction (see Figure S1) (Eckardt et al., 2020). This movement of air masses is further supported by forward trajectories in the region (Bhattachan et al., 2012; Tatlhego et al., 2020). In addition, there is strong correlation between air mass pathways from continental sources and elevated phytoplankton communities especially for the Southern Ocean (Neff and Bertler, 2015; Tatlhego et al., 2020).

Mineral dust particles can be blown over more than 1000 km from sources (Betzer et al., 1988). Some of the mineral grains travel more than 3500 km off the coast from west Africa (van der Does et al., 2018). Most of the nutrient rich aerosols fertilizing the proximal oceans are from the coastal sources (ephemeral rivers) and the exposed agricultural fields in Free State (South Africa) (Eckardt et al.,

2020). The extent of these southern African sources might be small, but their proximity makes them the main drivers of nutrient supply to coastal oceans. There is evidence that dust plumes from the Free State do reach the Indian Ocean passing over the area where some of our samples (e.g. WAer_4) were collected (Eckardt et al., 2020).

The calculated enrichment factors supported this notion of a Southern African source to some extent. The calculated enrichment factors revealed a strong lithogenic source for most of the aerosol samples (Table 5). Nonetheless, several trace metals in the coastal samples, such as Cu, Pb, Fe indicated a relatively strong anthropogenic influence (Table 5) likely due to the proximity to the industrial activities along the South African coastline. Similarly, Chance et al. (2015) reported high enrichment for Zn and Co from the same region (See appendix 2). Such high enrichment factors for elements such as Cu and Pb has been attributed coal-fired power plants, base metals smelters and burning of fossil fuels (Srinivas & Sarin, 2013). These results are in line with previous findings in aerosols collected on land over a major southern African export port on the West Coast (Kangueehi et al., in review).

4.6.1.2. Open ocean dust aerosols

Roughly 80% of our five-day long trajectories showed that the air masses reaching our collection sites are from marine areas and distant sources such as South America, Antarctica or Australia rather than southern Africa. Bulk concentrations for Fe, Zn, Cu and Cd were lower in the open oceans than at the coastal sites (Figure 3). Witt et al. (2006) similarly reported high aerosol trace metal concentrations close to South Africa decreasing towards the open Indian Ocean. Trace metal concentrations in the 50s South samples were much lower, for example, we reported Fe concentrations ranging from 22 to 63 ng m^{-3}. These lower concentrations in the southeast Atlantic sector compare well with marine aerosols collected over the southeast Indian sector of the Southern Ocean (19 ng m^{-3} Fe; Gao et al., 2013). These 50s South concentrations also compare well with areas in the Southern Ocean closer to Australia and South America, where total Fe aerosol concentration ranged from ~0.1 to > 200 ng m^{-3} were observed (Gao et al., 2013, 2020; Winton et al., 2015). For example, bulk Fe concentrations in marine aerosols collected close to Tasmania ranged from 5 to 17 ng m^{-3} (Bowie et al., 2009; Winton et al., 2015). Nonetheless, there is also an indication of a trace metal input from Antarctica in the 50s South samples, especially prominent in the relatively high Al concentrations. This Antarctic origin is supported by some of the backward trajectories from the 40s and 50s samples (Figure 7 , Figure 8). Gao (2014) also reported relatively high trace metal contents for Fe (14 ng m^{-3}), Mn (0.46 ng m^{-3}) and Al (150 ng m^{-3}) in samples collected over the East Antarctica

region. These concentrations are in similar ranges to our 50s South concentrations (41 ± 23 ng m^{-3} Fe), (1.24 ± 0.7 ng m^{-3} Mn), and (177 ± 88 ng Al m^{-3}). Our bulk trace metal concentrations at the station SAer4 (Table 2) are similar to concentrations observed on Larsemann Hills, close to East Antarctica, of 188 ng m^{-3} Fe, 177 ng m^{-3} Al, 13 ng m^{-3} Mn, and 19 ng m^{-3} Zn (Budhavant et al., 2015). and support the assumption that some fo the 50s South aerosols could be sourced from Antarctica.

4.6.2. Trace metal bioaccessibility

4.6.2.1. Leaching as an approximate for bioaccessibility

The solubility of dust is typically higher in a weak acid than in Milli-Q water. The laboratory pure water leaching approach is designed to mimic the short-term dissolution (instantaneous approach) of trace metals in surface oceans. It might underestimate the soluble fraction in the ocean upper mixed layer, because the leaching time is shorter than an assumed residence time of an aerosol in the ocean upper mixed layer (Winton et al., 2015). Hence, the instantaneous leach represents the lower estimate of the most soluble fraction (Shelley et al., 2018). This could explain the low solubilities observed when the samples were leached with our instantaneous Milli-Q. In contrast, the dissolution rate is faster when a weak acid is used, which mimics the involvement of atmospheric processes and a low atmospheric pH (Perron et al., 2020). Indeed, in our experiments, the solubility in the weak acid was much higher than the solubility in Milli-Q. The heating step used in our weak acid approach might further enhance the solubility. For example, Fe solubility increases with temperature (Cornell & Schwertmann, 2003). The variation in solubility percentages ranges from 0.01 to 90% from different aerosol leaching experiments (Mahowald et al., 2018; Perron et al., 2019). These large ranges along with our observed differences in solubility dependant on the leaching approach confirm the need for a standard protocol method for leaching of aerosols (Iron at the Air-Sea Interface Working Group 2021). Here, we assume the sum of both leachates as the bioaccessible fraction.

4.6.2.2. Seasonal and spatial variability in bioaccessibility estimates

As for the variation in the total concentration (cf. section 4.1) the differences in solubility of the labile fraction could be mainly due to the differentiation at the source areas (Conway & John, 2014). We illustrate this phenomenon here using Fe as, example as, solubility of Fe is through several previous studies. The labile fraction for Fe ranges from 0.5 to 52% in our study. This is higher than the 2.5 to 6.2% Fe that was reported by Gao et al. (2020) in aerosols collected over the Antarctic Peninsula during austral summer. As mentioned above (section 4.1) our samples had a higher variation of sources compared to Gao et al. (2020)'s samples collected at the Antarctic Peninsula. For example, our samples included coastal sites with a strong continental and possibly anthropogenic influence, where the latter likely increases solubility (Kangueehi et al., in review). However, Chance et al (2015) reported solubility in summer of 1.3 to 48% for labile Fe, which is similar to our range following the same transect. High concentrations of labile Fe were reported by Zhuang et al. (1992) ranging from 1 to 150 ng m^{-3} in aerosols originating from China collected over the Pacific Ocean. These concentrations are lower than our labile fractions of 0.3 to 982 ng m^{-3} Fe. Our labile trace metal concentrations for the 50s South zone were also much higher compared to recorded 0.53 ng m^{-3} of Fe (Gao et al., 2013) from shipboard sampling along eastern Antarctica.

Another reason for higher solubilities can be the distance from potential source. It is often assumed that aerosols become acidic with longer traveling distance (roughly after 15 days) due to atmospheric processing , leading to higher solubility for distant samples (Ito and Feng, 2010; Longo et al., 2016). For example, aerosol Fe solubility increased with travelling distance across the Atlantic from the Sahara towards North America (Rodriguez et al., 2020). However, our distant samples (50s South samples) did not show higher trace metal solubility than the coastal samples that were collected closer to terrestrial sources. The solubility for Fe for example was up to 5785 ng m^{-3} close to the shore and up to 63 ng m^{-3} in the 50s. Similarly, Buck et al. (2013) reported that aerosol Fe solubility did not increase with distance over the Pacific.

All other trace metal solubilities observed along our transects were broadly in range with previously published solubilities. For example, Witt et al. (2010) reported fractional solubilities higher than 50% for trace metals such as As, Pb, Ni, Cu, Cd and Zn, which is similar to our e.g., (Pb up to 84%). Similarly high solubilities have been reported by Chance et al., (2015) for Pb (~58%) and Cu (~55%) from the Southern Ocean region. Even Al was broadly similar to previous studies: Al solubility ranged from 10 to 98%, with an average and median of 41% and 35 in our study while, Chance et al

(2015) and Baker et al (2006) reported similar ranges of 3 to 78% for soluble Al from similar air masses. The fractional solubility of Mn ranged from 0.9 to 88%, which is also in similar ranges to Chance et al (2015; 1 - 82%) and Baker et al (2006; 18 - 75%). Our data suggest that considering the high Cu and Pb loads for example at the coastal sites and the relatively high solubility, the sites have potential to be negatively affected from the dust deposition.

4.6.3. Potential Impact on Phytoplankton Communities

Essential, bioactive trace metals: Most of the trace metals observed in the collected dust aerosols have fertilizing properties. This is especially true for Fe, and in addition some bioactive trace metals such as Mn, Zn, Cu and Co for example, that can be co-limiting in the Southern Ocean can be supplied by aerosols (Moore et al., 2013). The high solubilities for trace metals such as Fe, Mn, Cu, and Zn presented in this study, could mean that dust deposited in this region is in general highly soluble and become available quickly. In winter and spring, when primary productivity and thus micronutrient demands are relatively low, e.g. due to low temperatures and low light availability. These bioactive trace metals might not be fully utilized immediately by phytoplankton communities (Morel, 2008; Morel et al., 2020).

Potentially toxic trace metals: The high dissolution rates can have negative impacts on the phytoplankton also, especially for potentially toxic trace metals, such as Cd, Cu, and Pb (Paytan et al., 2009; Mackey et al., 2015. Some phytoplankton are known to acclimate at a faster rate, compared to the trace metal dissolution rates to avoid trace metal toxicity (Mackey et al., 2015). Hence, the toxicity of trace metals to phytoplankton community relies on the dissolution rate, acclimation rate, phytoplankton community uptake rate and the toxicity levels the phytoplankton community can handle.

The relatively high trace metal loads that we recorded during winter may thus not be utilised rapidly. However, this external wintertime supply could have two important impacts: (i) The excess trace metals might favour species that have intracellular storage capacity and utilize it during the summer, when there is more sunlight (Mackey et al., 2015). (ii) As the dissolution rate and suspension time might controls how long the trace metals might be available to the phytoplankton communities, the slow dissolution especially observed in the pure water leachates, might indicate that the trace metal concentrations can increase with time in seawater long after deposition and might be available up until the re-supply results from the higher spring bulk concentrations potentially fertilizing the spring

bloom. The trace metal load was much less during the spring season, which is the time when more productivity occurs compared to winter. Hence, when sunlight and primary productivity starts to increase, the dust load and trace metal supply towards the south Atlantic diminishes, potentially relying on the high winter load and possibilities. This shows that the dust emitted during the winter and might be key to support and maintain the spring and summer blooms.

4.7. CONCLUSION

This study investigated the distribution of trace metals and their solubility in the Southern Ocean. It is one of the first to provide atmospheric trace metal distribution in the southeast Atlantic during winter and spring. Comparison with existing summertime literature indicates that higher trace metal concentrations are deposited in winter and spring than in summer. Solubility and concentration vary between trace metals and also sites, i.e. from coast to open ocean. The dust loads that occur during winter could be stored and become bioaccessible during late spring to summer when productivity increases. These higher dust loads in winter could be essential nutrients for the summer when there is light and the primary productivity is higher.

4.8. AUTHOR CONTRIBUTIONS

K.K., F.D. and S.F. wrote the manuscript; S.F. and A.N.R. conceived and designed the study and acquired funding; K.K., and S.F. contributed data and interpretation. All co-authors reviewed and edited this or previous versions of the manuscript and gave final approval for publication.

4.9. FUNDING

The work leading to these results received funding from the National Research Foundation (NRF) under the SANAP (110715, 110731), Bilateral (114677) and CPRR (105826) programmes. K. Kangueehi acknowledges funding from NRF through a Masters Innovation Scholarship

4.10. ACKNOWLEDGEMENTS

The authors would like to thank the South African National Antarctic Programme (SANAP) as well as Captain Knowledge Bengu and the crew of the R/V SA Agulhas II for their professionalism and support during the Winter and Spring 2019 voyage. We acknowledge Chief Scientist Marcello Vichi

and all the participants involved in the expedition. We are grateful to the “TraceEx” team for their help in collecting aerosol samples during the cruise.

4.11. CONFLICT OF INTEREST STATEMENT

All authors declare no competing interests.

4.12. CHAPTER 4: REFERENCES

Anderson, R. F., Mawji, E., Cutter, G. A., Measures, C. I., & Jeandel, C. (2014). GEOTRACES: Changing the Way We Explore Ocean Chemistry. *Source: Oceanography*, *27*(1), 50–61. https://doi.org/10.2307/24862118

Ansorge, I. J., Skelton, P., Bekker, A., Nico De Bruyn, P. J., Butterworth, D., Cilliers, P., Cooper, J., Cowan, D. A., Dorrington, R., Fawcett, S., Fietz, S., Findlay, K. P., Froneman, P. W., Grantham, G. H., Greve, M., Hedding, D., Greg Hofmeyr, G. J., Kosch, M., Le Roux, P. C., … Van Vuuren, B. J. (2017). Exploring South Africa's southern frontier: A 20-year vision for polar research through the South African national antarctic programme. In *South African Journal of Science* (Vol. 113, Issues 5–6, pp. 7–7). Academy of Science of South Africa. https://doi.org/10.17159/sajs.2017/a0205

Ashrafi, K., Shafiepour-Motlagh, M., Aslemand, A., & Ghader, S. (2014). Dust storm simulation over Iran using HYSPLIT. *Journal of Environmental Health Science and Engineering*, *12*(1), 9. https://doi.org/10.1186/2052-336X-12-9

Baker, A R, Jickells, T. D., Biswas, K. F., Weston, K., & French, M. (2006). Nutrients in atmospheric aerosol particles along the Atlantic Meridional Transect. *Deep-Sea Research Part II: Topical Studies in Oceanography*, *53*(14–16), 1706–1719. https://doi.org/10.1016/j.dsr2.2006.05.012

Baker, Alex R, French, M., & Linge, K. L. (2006). Trends in aerosol nutrient solubility along a west-east transect of the Saharan dust plume. *Geophysical Research Letters*, *33*(7), 10–13. https://doi.org/10.1029/2005GL024764

Basile, I., Grousset, F. E., Revel, M., Petit, J. R., Biscaye, P. E., & Barkov, N. I. (1997). Patagonian origin of glacial dust deposited in East Antarctica (Vostok and Dome C) during glacial stages 2, 4 and 6. *Earth and Planetary Science Letters*, *146*(3–4), 573–589. https://doi.org/10.1016/S0012-821X(96)00255-5

Bayon, G., German, C. R., Burton, K. W., Nesbitt, R. W., & Rogers, N. (2004). Sedimentary Fe-Mn oxyhydroxides as paleoceanographic archives and the role of aeolian flux in regulating oceanic dissolved REE. *Earth and Planetary Science Letters*, *224*(3–4), 477–492. https://doi.org/10.1016/j.epsl.2004.05.033

Berger, C. J. M., Lippiatt, S. M., Lawrence, M. G., & Bruland, K. W. (2008). Application of a

chemical leach technique for estimating labile particulate aluminum, iron, and manganese in the Columbia River plume and coastal waters off Oregon and Washington. *Journal of Geophysical Research*, *113*, 1–16. https://doi.org/10.1029/2007jc004703

Bhattachan, A., D'Odorico, P., Baddock, M. C., Zobeck, T. M., Okin, G. S., & Cassar, N. (2012). The Southern Kalahari: a potential new dust source in the Southern Hemisphere? *Environmental Research Letters*, *7*(2), 024001. https://doi.org/10.1088/1748-9326/7/2/024001

Bowie, A. R., Lannuzel, D., Remenyi, T. A., Wagener, T., Lam, P. J., Boyd, P. W., Guieu, C., Townsend, A. T., & Trull, T. W. (2009). Biogeochemical iron budgets of the Southern Ocean south of Australia: Decoupling of iron and nutrient cycles in the subantarctic zone by the summertime supply. *Global Biogeochemical Cycles*, *23*(4). https://doi.org/10.1029/2009GB003500

Boyd, P. W., & Ellwood, M. J. (2010). The biogeochemical cycle of iron in the ocean. *Nature Geoscience*, *3*(10), 675–682. https://doi.org/10.1038/ngeo964

Bruland, K. W., Rue, E. L., & Smith, G. J. (2001). Iron and macronutrients in California coastal upwelling regimes: Implications for diatom blooms. *Limnol. Oceanogr*, *46*(7), 1661–1674. https://doi.org/10.4319/lo.2001.46.7.1661

Chance, R., Jickells, T. D., & Baker, A. R. (2015). Atmospheric trace metal concentrations, solubility and deposition fluxes in remote marine air over the south-east Atlantic. *Marine Chemistry*, *177*, 45–56. https://doi.org/10.1016/j.marchem.2015.06.028

Chester, R., & Hughes, M. J. (1967). A chemical technique for the separation of ferro-manganese minerals, carbonate minerals and adsorbed trace elements from pelagic sediments. *Chemical Geology*, *2*(C), 249–262. https://doi.org/10.1016/0009-2541(67)90025-3

Cloete, R., Loock, J. C., Mtshali, T., Fietz, S., & Roychoudhury, A. N. (2019). Winter and summer distributions of Copper, Zinc and Nickel along the International GEOTRACES Section GIPY05: Insights into deep winter mixing. *Chemical Geology*, *511*(February), 342–357. https://doi.org/10.1016/j.chemgeo.2018.10.023

Conway, T. M., & John, S. G. (2014). Quantification of dissolved iron sources to the North Atlantic Ocean. *Nature*, *511*(7508), 212–215. https://doi.org/10.1038/nature13482

Cornell, R. M., & Schwertmann, U. (2003). *The iron oxides – structure, properties, reactions, occurrence and uses* (Second Edi). VCH.

Cutter, G., Casciotti, K., Croot, P., Geibert, W., Geochemistry, M., Heimbürger, L.-E., & Lohan, M. (2017). *Sampling and Sample-handling Protocols for GEOTRACES Cruises*.

de Baar, H. J. W., de Jong, J. T. M., Bakker, D. C. E., Löscher, B. M., Veth, C., Bathmann, U. V, & Smetacek, V. (1995). Importance of iron for plankton blooms and carbon dioxide drawdown in the Southern Ocean. *Nature*, *373*, 412–415. https://doi.org/10.1038/373412a0

Duce, R. A., & Tindale, N. W. (1991). Atmospheric transport of iron and its deposition in the ocean. *Limnology and Oceanography*, *36*(8), 1715–1726. https://doi.org/10.4319/lo.1991.36.8.1715

Eckardt, F. D., Bekiswa, S., Von Holdt, J. R., Jack, C., Kuhn, N. J., Mogane, F., Murray, J. E., Ndara, N., & Palmer, A. R. (2020). South Africa's agricultural dust sources and events from MSG SEVIRI. *Aeolian Research*, *47*(March), 100637. https://doi.org/10.1016/j.aeolia.2020.100637

Eckardt, F., & Kuring, N. (2005). SeaWiFS identifies dust sources in the Namib Desert. *International Journal of Remote Sensing*, *26*(19), 4159–4167. https://doi.org/10.1080/01431160500113112

Formenti, P., D'Anna, B., Flamant, C., Mallet, M., Piketh, S. J., Schepanski, K., Waquet, F., Auriol, F., Brogniez, G., Burnet, F., Chaboureau, J. P., Chauvigné, A., Chazette, P., Denjean, C., Desboeufs, K., Doussin, J. F., Elguindi, N., Feuerstein, S., Gaetani, M., … Holben, B. (2019). The aerosols, radiation and clouds in southern Africa field campaign in Namibia overview, illustrative observations, and way forward. *Bulletin of the American Meteorological Society*, *100*(7), 1277–1298. https://doi.org/10.1175/BAMS-D-17-0278.1

Frausto da Silva, J. J. R., & Williams, R. J. P. (2001). *The Biological Chemistry of the Elements: The Inorganic Chemistry of Life*. Oxford University Press (OUP). https://books.google.com.na/books?hl=en&lr=&id=qXbKF1Pw_GsC&oi=fnd&pg=PA1&dq=The+Biological+Chemistry+of+the+Elements:+The+Inorganic+Chemistry+of+Life.+Oxford,+UK:+Oxford+Univ.+Press&ots=5tGzPYA2ca&sig=HgFX4ynbqrD4QI5WPYtt4I1dg_I&redir_esc=y#v=onepage&q=T

Frölicher, T. L., Sarmiento, J. L., Paynter, D. J., Dunne, J. P., Krasting, J. P., & Winton, M. (n.d.). *Dominance of the Southern Ocean in Anthropogenic Carbon and Heat Uptake in CMIP5 Models*. https://doi.org/10.1175/JCLI-D-14-00117.1

Gabric, A. J., Cropp, R. A., McTainsh, G. H., Johnston, B. M., Butler, H., Tilbrook, B., & Keywood, M. (2010). Australian dust storms in 2002-2003 and their impact on Southern Ocean biogeochemistry. *Global Biogeochemical Cycles*, *24*(2), n/a-n/a. https://doi.org/10.1029/2009GB003541

Gaiero, D. M., Probst, J. L., Depetris, P. J., Bidart, S. M., & Leleyter, L. (2003). Iron and other transition metals in Patagonian riverborne and windborne materials: Geochemical control and transport to the southern South Atlantic Ocean. *Geochimica et Cosmochimica Acta*, *67*(19), 3603–3623. https://doi.org/10.1016/S0016-7037(03)00211-4

Gao, Y., Xu, G., Zhan, J., Zhang, J., Li, W., Lin, Q., Chen, L., & Lin, H. (2013). Spatial and particle size distributions of atmospheric dissolvable iron in aerosols and its input to the Southern Ocean and coastal East Antarctica. *Journal of Geophysical Research Atmospheres*, *118*(22), 12,634-12,648. https://doi.org/10.1002/2013JD020367

Gassó, S., & Torres, O. (2019). Temporal Characterization of Dust Activity in the Central Patagonia Desert (Years 1964–2017). *Journal of Geophysical Research: Atmospheres*, *124*(6), 3417–3434. https://doi.org/10.1029/2018JD030209

Ginoux, P., Prospero, J. M., Gill, T. E., Hsu, N. C., & Zhao, M. (2012). Global-scale attribution of anthropogenic and natural dust sources and their emission rates based on MODIS Deep Blue aerosol products. *Reviews of Geophysics*, *50*(3), 1–36. https://doi.org/10.1029/2012RG000388

Heimburger, A., Losno, R., & Triquet, S. (2013). Solubility of iron and other trace elements in rainwater collected on the Kerguelen Islands (South Indian Ocean). *Biogeosciences*, *10*, 6617–6628. https://doi.org/10.5194/bg-10-6617-2013

Henley, S. F., Cavan, E. L., Fawcett, S. E., Kerr, R., Monteiro, T., Sherrell, R. M., Bowie, A. R., Boyd, P. W., Barnes, D. K. A., Schloss, I. R., Marshall, T., Flynn, R., & Smith, S. (2020). Changing Biogeochemistry of the Southern Ocean and Its Ecosystem Implications. In *Frontiers in Marine Science* (Vol. 7, Issue July). https://doi.org/10.3389/fmars.2020.00581

Hutchins, D. A., & Bruland, K. W. (1998). Iron-limited diatom growth and Si:N uptake ratios in a coastal upwelling regime. *Nature*, *393*(6685), 561–564. https://doi.org/10.1038/31203

Jickells, T. D. (2005). Global Iron Connections Between Desert Dust, Ocean Biogeochemistry, and Climate. *Science*, *308*(5718), 67–71. https://doi.org/10.1126/science.1105959

Jickells, T., & Moore, C. M. (2015). The Importance of Atmospheric Deposition for Ocean

Productivity. *Annual Review of Ecology, Evolution, and Systematics*, *46*(1), 481–501. https://doi.org/10.1146/annurev-ecolsys-112414-054118

Johnson, M. S., Meskhidze, N., Kiliyanpilakkil, V. P., & Gasso, S. (2011). Understanding the transport of Patagonian dust and its influence on marine biological activity in the South Atlantic Ocean. *Atmospheric Chemistry and Physics*, *11*(6), 2487–2502. https://doi.org/10.5194/acp-11-2487-2011

Jordi, A., Basterretxea, G., Tovar-Sánchez, A., Alastuey, A., & Querol, X. (2012). Copper aerosols inhibit phytoplankton growth in the Mediterranean Sea. *Proceedings of the National Academy of Sciences of the United States of America*, *109*(52), 21246–21249. https://doi.org/10.1073/pnas.1207567110

La Fontaine, S., Quinn, J. M., Nakamoto, S. S., Dudley Page, M., Göhre, V., Moseley, J. L., Kropat, J., & Merchant, S. (2002). Copper-dependent iron assimilation pathway in the model photosynthetic eukaryote Chlamydomonas reinhardtii. *Eukaryotic Cell*, *1*(5), 736–757. https://doi.org/10.1128/EC.1.5.736-757.2002

Li, F., Ginoux, P., & Ramaswamy, V. (2008). Distribution , transport , and deposition of mineral dust in the Southern Ocean and Antarctica : Contribution of major sources. *JOURNAL OF GEOPHYSICAL RESEARCH*, *113*(December 2007), 1–15. https://doi.org/10.1029/2007JD009190

Longo, A. F., Feng, Y., Lai, B., Landing, W. M., Shelley, R. U., Nenes, A., Mihalopoulos, N., Violaki, K., Ingall, E. D., Drive, F., & States, U. (2016). Influence of Atmospheric Processes on the Solubility and Composition of Iron in Saharan Dust. *Environmental Science & Technology*, *50*, 6912–6920. https://doi.org/10.1021/acs.est.6b02605

Mackey, K. R. M., Chien, C., Post, A. F., Saito, M. A., & Paytan, A. (2015a). Rapid and gradual modes of aerosol trace metal dissolution in seawater. *Frontiers in Microbiology*, *5*(January), 1–11. https://doi.org/10.3389/fmicb.2014.00794

Mackey, K. R. M., Chien, C. Te, Post, A. F., Saito, M. A., & Paytan, A. (2015b). Rapid and gradual modes of aerosol trace metal dissolution in seawater. *Frontiers in Microbiology*, *6*(JAN), 1–11. https://doi.org/10.3389/fmicb.2014.00794

Mackie, D. S., Boyd, P. W., McTainsh, G. H., Tindale, N. W., Westberry, T. K., & Hunter, K. A. (2008). Biogeochemistry of iron in Australian dust: From eolian uplift to marine uptake.

Geochemistry, Geophysics, Geosystems, *9*(3). https://doi.org/10.1029/2007GC001813

Mahowald, N. M., Hamilton, D. S., Mackey, K. R. M., Moore, J. K., Baker, A. R., Scanza, R. A., & Zhang, Y. (2018). Aerosol trace metal leaching and impacts on marine microorganisms. *Nature Communications*, *9*(1). https://doi.org/10.1038/s41467-018-04970-7

Maldonado, M. T., Strzepek, R. F., Sander, S., & Boyd, P. W. (2005). Acquisition of iron bound to strong organic complexes, with different Fe binding groups and photochemical reactivities, by plankton communities in Fe-limited subantarctic waters. *Global Biogeochemical Cycles*, *19*(4). https://doi.org/10.1029/2005GB002481

Martin, J. H. (1990). Glacial-interglacial CO2 change: The Iron Hypothesis. In *Paleoceanography* (Vol. 5, Issue 1, pp. 1–13). https://doi.org/10.1029/PA005i001p00001

Martin, J. H., & Fitzwater, S. E. (1988). Iron deficiency limits phytoplankton growth in the north-east Pacific subarctic. In *Nature* (Vol. 331, Issue 6154, pp. 341–343). https://doi.org/10.1038/331341a0

Martin, J. H., Fitzwater, S. E., & Gordon, M. R. (1990). Iron Deficiency Limits Phytoplankton Growth in Antartic Waters. *GLOBAL BIOGEOCHEMICAL CYCLES*, 5–12.

Mcgowan, H., & Clark, A. (2008). Identification of dust transport pathways from Lake Eyre , Australia using Hysplit. *Atmospheric Environment*, *42*, 6915–6925. https://doi.org/10.1016/j.atmosenv.2008.05.053

Middag, R., de Baar, H. J. W., Laan, P., Cai, P. H., & van Ooijen, J. C. (2011). Dissolved manganese in the Atlantic sector of the Southern Ocean. *Deep-Sea Research Part II: Topical Studies in Oceanography*, *58*(25–26), 2661–2677. https://doi.org/10.1016/j.dsr2.2010.10.043

Moore, C. M., Mills, M. M., Arrigo, K. R., Berman-Frank, I., Bopp, L., Boyd, P. W., Galbraith, E. D., Geider, R. J., Guieu, C., Jaccard, S. L., Jickells, T. D., La Roche, J., Lenton, T. M., Mahowald, N. M., Marañón, E., Marinov, I., Moore, J. K., Nakatsuka, T., Oschlies, A., … Ulloa, O. (2013a). Processes and patterns of oceanic nutrient limitation. *Nature Geoscience*, *6*(9), 701–710. https://doi.org/10.1038/ngeo1765

Moore, C. M., Mills, M. M., Arrigo, K. R., Berman-Frank, I., Bopp, L., Boyd, P. W., Galbraith, E. D., Geider, R. J., Guieu, C., Jaccard, S. L., Jickells, T. D., La Roche, J., Lenton, T. M., Mahowald, N. M., Marañón, E., Marinov, I., Moore, J. K., Nakatsuka, T., Oschlies, A., … Ulloa, O. (2013b). Processes and patterns of oceanic nutrient limitation. *Nature Geoscience*,

6(9), 701–710. https://doi.org/10.1038/ngeo1765

Morel, F. M. M. (2008). The co-evolution of phytoplankton and trace element cycles in the oceans. *Geobiology*, *6*(3), 318–324. https://doi.org/10.1111/j.1472-4669.2008.00144.x

Morel, F. M. M., Lam, P. J., & Saito, M. A. (2020). Trace Metal Substitution in Marine Phytoplankton. In *Annual Review of Earth and Planetary Sciences* (Vol. 48, pp. 491–517). Annual Reviews Inc. https://doi.org/10.1146/annurev-earth-053018-060108

Osipov, E. Y., Osipova, O. P., & Khodzher, T. V. (2020). Recent variability of atmospheric circulation patterns inferred from East Antarctica glaciochemical records. *Chemie Der Erde*, *80*(3), 125554. https://doi.org/10.1016/j.chemer.2019.125554

Paytan, A., Mackey, K. R. M., Chen, Y., Lima, I. D., Doney, S. C., Mahowald, N., Labiosa, R., & Post, A. F. (2009). Toxicity of atmospheric aerosols on marine phytoplankton. *PNAS*, *106*(12), 4601–4605.

Perron, M. M. G., Proemse, B. C., Strzelec, M., Gault-Ringold, M., Boyd, P. W., Sanz Rodriguez, E., Paull, B., & Bowie, A. R. (2019). Origin, transport and deposition of aerosol iron to Australian coastal waters. *Submitted*, *228*(October 2019), 117432. https://doi.org/10.1016/j.atmosenv.2020.117432

Perron, M. M. G., Strzelec, M., Gault-Ringold, M., Proemse, B. C., Boyd, P. W., & Bowie, A. R. (2020). Assessment of leaching protocols to determine the solubility of trace metals in aerosols. *Talanta*, *208*. https://doi.org/10.1016/j.talanta.2019.120377

Piketh, S. J., Annegarn, H. J., & Tyson, P. D. (1999). Lower tropospheric aerosol loadings over South Africa: The relative contribution of aeolian dust, industrial emissions, and biomass burning. *Journal of Geophysical Research Atmospheres*, *104*(D1), 1597–1607. https://doi.org/10.1029/1998JD100014

Piketh, S. J., Swap, R. J., Maenhaut, W., Annegarn, H. J., & Formenti, P. (2002). Chemical evidence of long-range atmospheric transport over southern Africa. *Journal of Geophysical Research Atmospheres*, *107*(24), 1–13. https://doi.org/10.1029/2002JD002056

Piketh, S. J., Tyson, P. D., & Steffen, W. (2000). Aeolian transport from southern Africa and iron fertilization of marine biota in the South Indian Ocean. In *South African Journal of Science* (Vol. 96, Issue 5, pp. 244–246).

Ross, K. E., Piketh, S. J., Swap, R. J., & Staebler, R. M. (2001). Controls governing airflow over the South African lowveld. *South African Journal of Science*, *97*(1–2), 29–40.

Shelley, R. U., Landing, W. M., Ussher, S. J., Planquette, H., & Sarthou, G. (2018). Regional trends in the fractional solubility of Fe and other metals from North Atlantic aerosols (GEOTRACES cruises GA01 and GA03) following a two-stage leach. *Biogeosciences*, *15*(8), 2271–2288. https://doi.org/10.5194/bg-15-2271-2018

Shetye, S. S., Mohan, R., Patil, S., Jena, B., Chacko, R., George, J. V., Noronha, S., Singh, N., Priya, L., & Sudhakar, M. (2015). Oceanic pCO2 in the Indian sector of the Southern Ocean during the austral summer-winter transition phase. *Deep-Sea Research Part II: Topical Studies in Oceanography*, *118*, 250–260. https://doi.org/10.1016/j.dsr2.2015.05.017

Srinivas, B., & Sarin, M. M. (2013). Atmospheric dry-deposition of mineral dust and anthropogenic trace metals to the Bay of Bengal. *Journal of Marine Systems*, *126*, 56–68. https://doi.org/10.1016/j.jmarsys.2012.11.004

Stein, A. F., Draxler, R. R., Rolph, G. D., Stunder, B. J. B., Cohen, M. D., & Ngan, F. (2015). Noaa's hysplit atmospheric transport and dispersion modeling system. *Bulletin of the American Meteorological Society*, *96*(12), 2059–2077. https://doi.org/10.1175/BAMS-D-14-00110.1

Struve, T., Pahnke, K., Lamy, F., Wengler, M., Böning, P., & Winckler, G. (2020). A circumpolar dust conveyor in the glacial Southern Ocean. *Nature Communications*, *11*(1). https://doi.org/10.1038/s41467-020-18858-y

Strzelec, M., Proemse, B. C., Barmuta, L. A., Gault-Ringold, M., Desservettaz, M., Boyd, P. W., Perron, M. M. G., Schofield, R., & Bowie, A. R. (2020). Atmospheric trace metal deposition from natural and anthropogenic sources in Western Australia. *Atmosphere*, *11*(5). https://doi.org/10.3390/ATMOS11050474

Sunda, W. G. (2012). Feedback interactions between trace metal nutrients and phytoplankton in the ocean. *Frontiers in Microbiology*, *3*(JUN), 1–22. https://doi.org/10.3389/fmicb.2012.00204

Swap, R. J., Annegarn, H. J., Suttles, J. T., King, M. D., Platnick, S., Privette, J. L., & Scholes, R. J. (2003). Africa burning : A thematic analysis of the Southern African Regional Science Initiative (SAFARI 2000). *JOURNAL OF GEOPHYSICAL RESEARCH*, *108*(Safari 2000), 1–15. https://doi.org/10.1029/2003JD003747

Tagliabue, A., Bowie, A. R., Boyd, P. W., Buck, K. N., Johnson, K. S., & Saito, M. A. (2017). The integral role of iron in ocean biogeochemistry. *Nature*, *543*(7643), 51–59. https://doi.org/10.1038/nature21058

Tatlhego, M., Bhattachan, A., Okin, G. S., & D'Odorico, P. (2020). Mapping Areas of the Southern Ocean Where Productivity Likely Depends on Dust-Delivered Iron. *Journal of Geophysical Research: Atmospheres*, *125*(3), 1–10. https://doi.org/10.1029/2019JD030926

Taylor, S. R., & McLennan, S. M. (1985). *The continental crust: Its composition and evolution*. Blackwell Scientific Pub.,Palo Alto, CA.

Twining, B. S., & Baines, S. B. (2013). The trace metal composition of marine phytoplankton. *Annual Review of Marine Science*, *5*, 191–215. https://doi.org/10.1146/annurev-marine-121211-172322

van der Does, M., Knippertz, P., Zschenderlein, P., Giles Harrison, R., & Stuut, J. B. W. (2018). The mysterious long-range transport of giant mineral dust particles. *Science Advances*, *4*(12), 1–9. https://doi.org/10.1126/sciadv.aau2768

Vickery, K. J., Eckardt, F. D., & Bryant, R. G. (2013a). A sub-basin scale dust plume source frequency inventory for southern Africa, 2005-2008. *Geophysical Research Letters*, *40*(19), 5274–5279. https://doi.org/10.1002/grl.50968

Vickery, K. J., Eckardt, F. D., & Bryant, R. G. (2013b). A sub-basin scale dust plume source frequency inventory for southern Africa, 2005-2008. *Geophysical Research Letters*, *40*(19), 5274–5279. https://doi.org/10.1002/grl.50968

Wagener, T., Guieu, C., Losno, R., Bonnet, S., & Mahowald, N. (2008). Revisiting atmospheric dust export to the Southern Hemisphere ocean: Biogeochemical implications. *Global Biogeochemical Cycles*, *22*(2), n/a-n/a. https://doi.org/10.1029/2007GB002984

Winton, V., Bowie, A., Edwards, R., Keywood, M., Townsend, A., van der Merwe, P., & Bollhfer, A. (2015). Fractional iron solubility of atmospheric iron inputs to the Southern Ocean. *Marine Chemistry*, *177*, 20–32. https://doi.org/10.1016/j.marchem.2015.06.006

Winton, V., Bowie, A., Edwards, R., Keywood, M., Townsend, A., van der Merwe, P., & Bollhöfer, A. (2015). Fractional iron solubility of atmospheric iron inputs to the Southern Ocean. *Marine Chemistry*, *177*, 20–32. https://doi.org/10.1016/j.marchem.2015.06.006

Winton, V. H. L., Bowie, A. R., Edwards, R., Keywood, M., Townsend, A. T., van der Merwe, P., & Bollhöfer, A. (2015). Fractional iron solubility of atmospheric iron inputs to the Southern Ocean. *Marine Chemistry*, *177*, 20–32. https://doi.org/10.1016/j.marchem.2015.06.006

Witt, M., Baker, A. R., & Jickells, T. D. (2006). Atmospheric trace metals over the Atlantic and South Indian Oceans: Investigation of metal concentrations and lead isotope ratios in coastal and remote marine aerosols. *Atmospheric Environment*, *40*(28), 5435–5451. https://doi.org/10.1016/j.atmosenv.2006.04.041

Wu, J., Rember, R., & Cahill, C. (2007). Dissolution of aerosol iron in the surface waters of the North Pacific and North Atlantic oceans as determined by a semicontinuous flow-through reactor method. *Global Biogeochemical Cycles*, *21*(4), 1–10. https://doi.org/10.1029/2006GB002851

4.13. SUPPLEMENTARY FIGURES

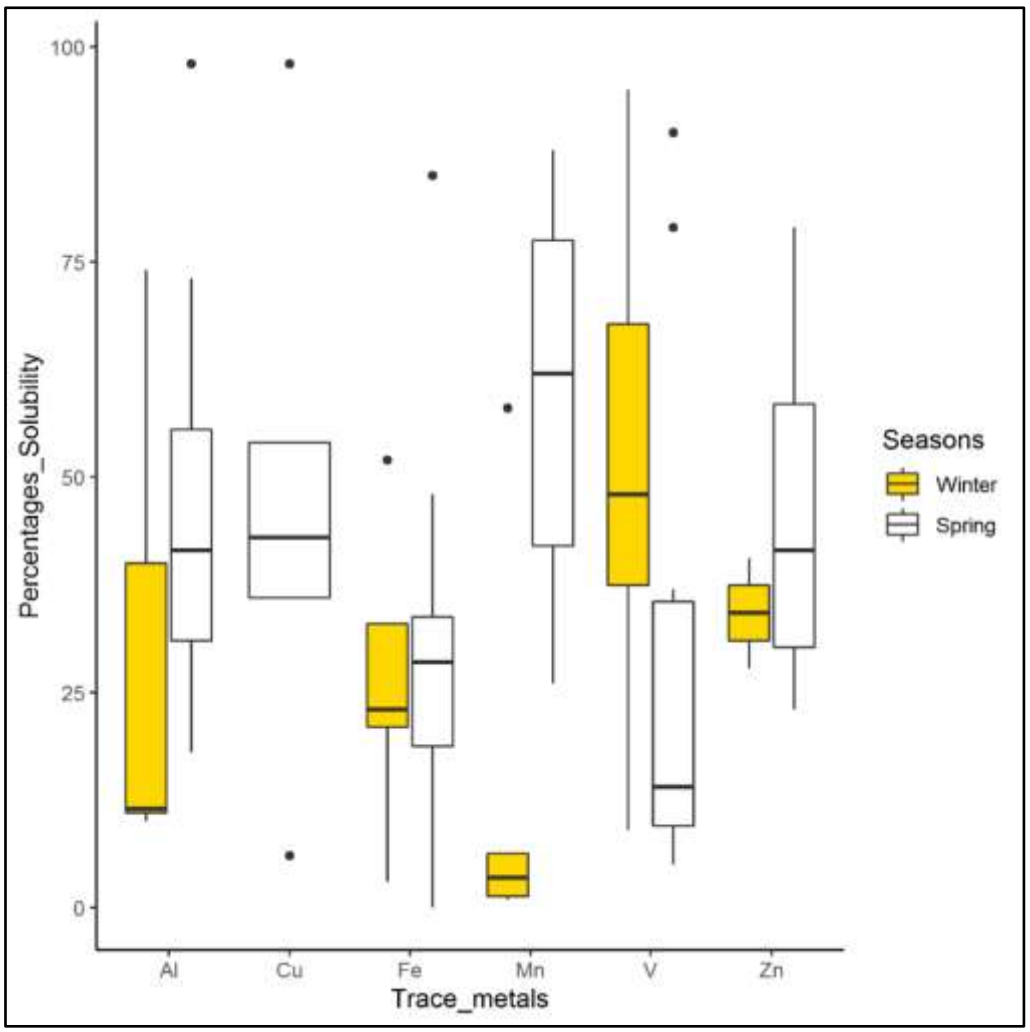

Figure S1. *Box and whisker plots showing the percentage of labile fraction of trace metal collected in winter and spring 2019 over the Southern Ocean. The black dots represent the outliers.*

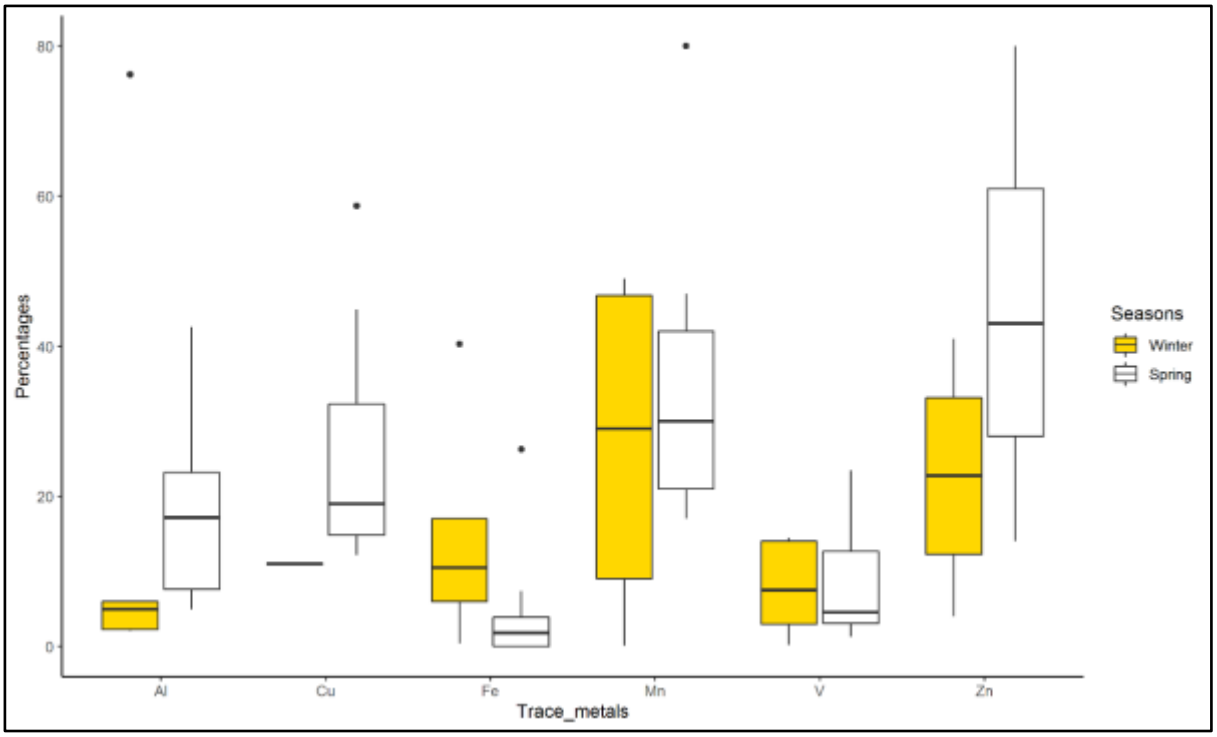

Figure S2. *Box and whisker plots showing the percentage of soluble fraction trace metal from spring 2019 collected over the Southern Ocean. The black dots represent the outliers.*

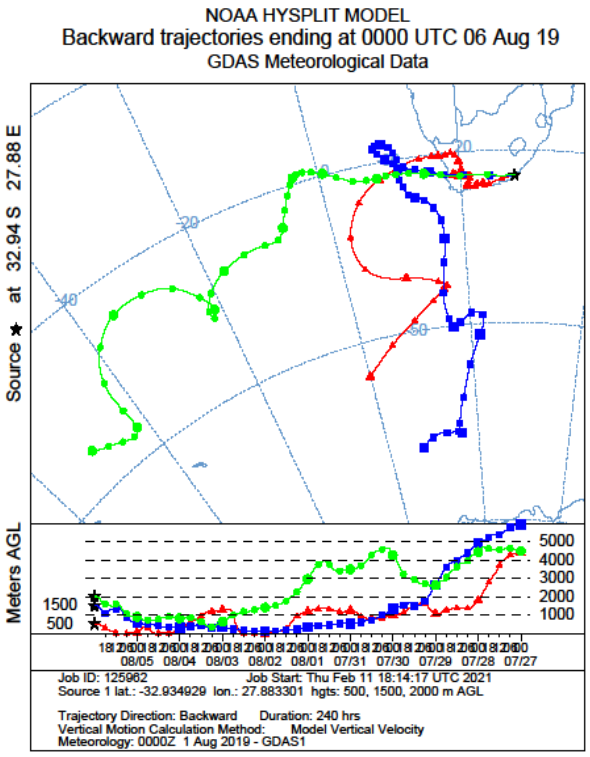

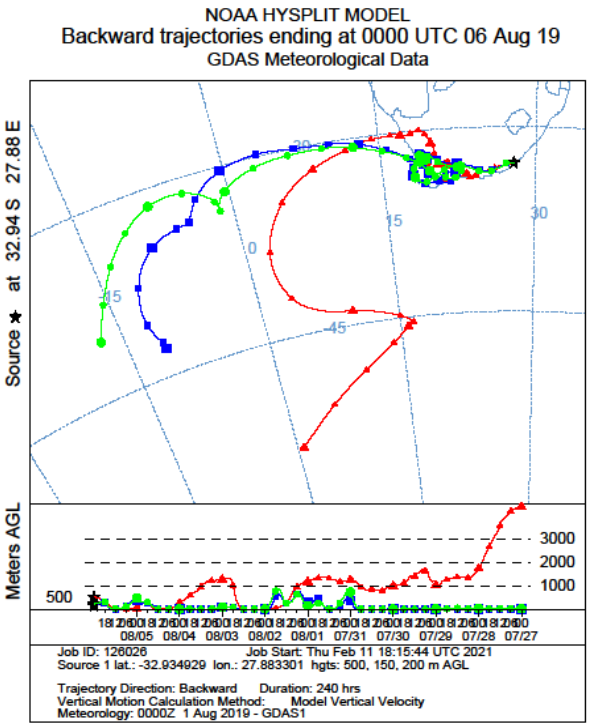

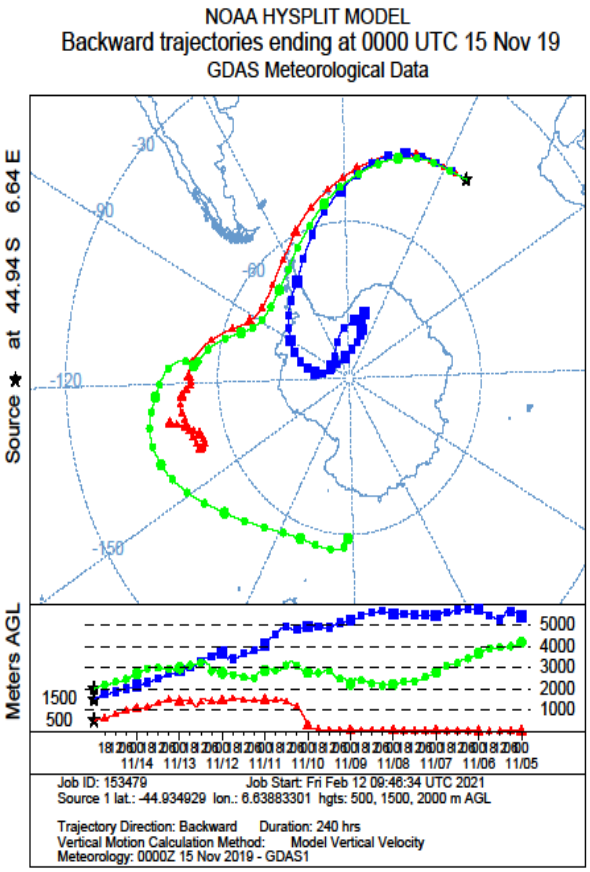

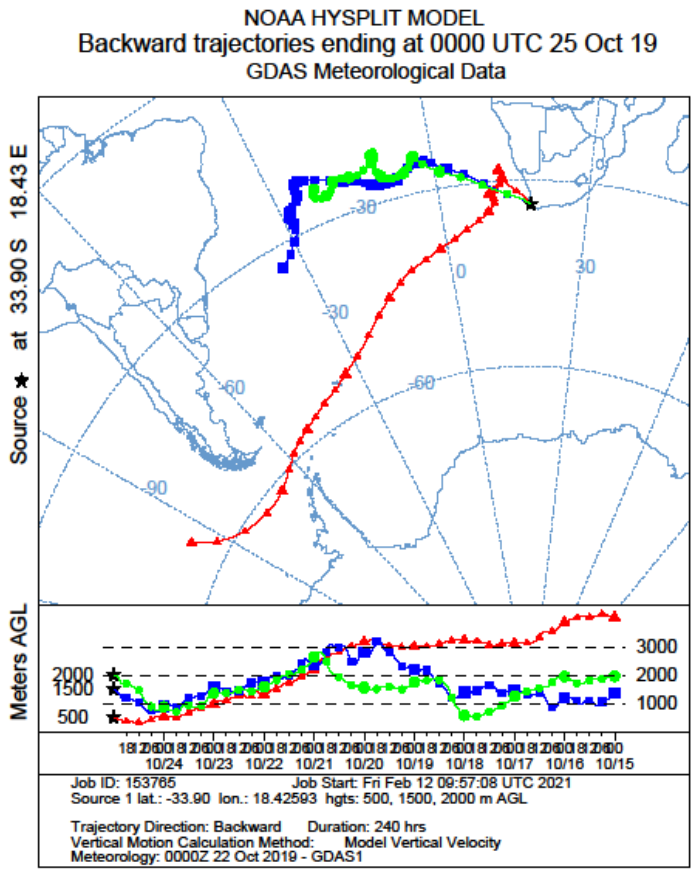

Figure S3 *Backward air masses trajectories showing the direction of air masses from two selected stations.*

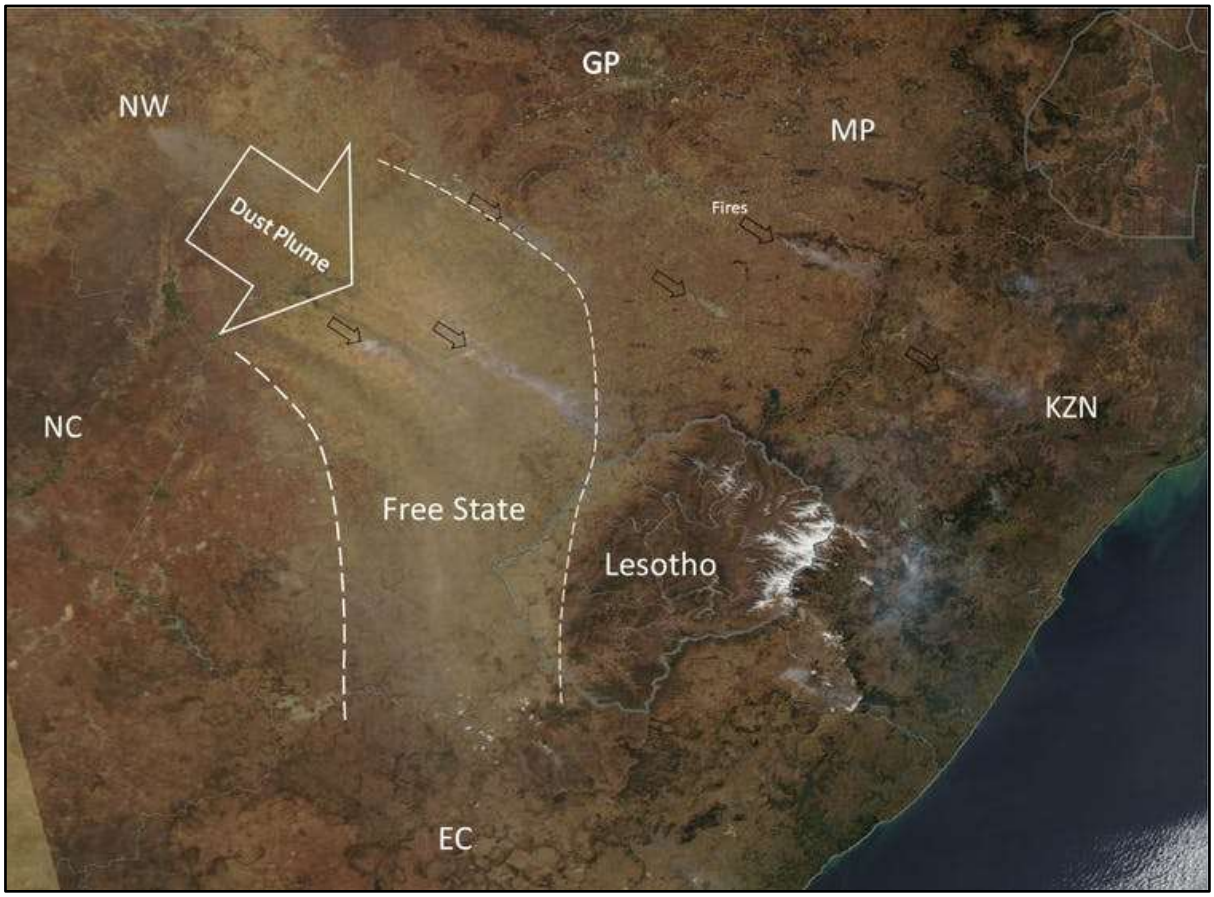

***Figure S4**. Some of the dust plumes from the agricultural fields in the Free State on the 23 September 2008 that can be seen exported through the Eastern Cape (EC) can be exported through this area. Image NASA MODIS satellite image.*

CHAPTER 5: SYNOPSIS

In this study, the all-encompassing aim was to investigate the trace metal concentration and solubility of aerosols from three different sources that can be categorized as anthropogenic or mixed, natural and marine. The aim was to study these important under-sampled dust sources and provide information of their fertilizing potential. This further highlights the importance of investigating some of the coastal towns where anthropogenic and natural emissions might be occurring. We added a component of physicochemical properties of dust aerosols, and how they can affect the nutrient dissolution. We provided information on how dust aerosols can impact the biogeochemical cycles and global climates. The findings of this study provides us with a new understanding of the possible impact that southern African dust can play by providing micronutrients to open oceans. The total composition and the soluble fractions are comparable to other global sources, where dust enhanced phytoplankton growth. Our findings also highlighted the impact and significance of anthropogenic dust to open oceans, especially from this region. Most of the emissions occur during the winter, and this could be confirmed by the higher concentrations observed in winter compared to the previous studies that sampled during the summer season. This dust emissions that were observed in winter could play a crucial role in supplying micronutrients during the spring and summer seasons. This winter deposited aerosols could be re-suspended in the mixed zone and potentially some of the spring blooms. The current need in atmospheric sciences is a standard protocol and method on how to determine the solubility of dust, currently, there are too many leaching experiments that have used different leaching methods, which makes it challenging to compare studies. All the objectives set out in this study were achieved by a combination of lab work analyses coupled with field work.

The three manuscripts addressed objectives set out for this thesis: The first manuscript focussed on a mixed (anthropogenic and natural) dust aerosol source. We report higher trace metal solubilities in these mixed sources compared to published solubilities from global, natural dust sources. This indicated how the contribution of combustion and other anthropogenically induced activities (e.g. mining) on dust aerosols can impact the solubility. Consequently, we presume that port towns, which handle large tonnages of mining ore could potentially be supplying highly soluble trace metals to marine environments. In summary, these findings highlighted the need to further investigate anthropogenic sources as important contributors of trace nutrients to ocean systems.

The second manuscript focussed on the bulk trace metal concentration and fractional of dust sources in the Namib Desert (as a natural source). Sources such as the Namib Desert are smaller than the world`s best known dust emitters, such as the Saharan Desert (Prospero et al., 2002). Nonetheless,

our findings showed that such smaller, less investigated dust emitting sources have a great potential to supply soluble trace metals to open oceans, but the solubility is low.

In the first two manuscripts, we also focussed on the mineralogical characteristics of the particles in order to link solubility with factors such as the particle size, shape and aggregation at a micrometer scale. Most particles in the sample collected from Saldanha Bay were rounded and spherical. In addition, elemental mapping of these Saldanha Bay particles showed internal mixing of particles. The internal mixing can enable fast dissolution and acid catalysed solubilisation due to higher surface area to volume ratios. In contrast, most of the particles were aspherical elongated particles of micas, clay minerals and feldspars.

Our findings supported previous recent suggestions (e.g., Kok et al., 2021) that desert dust coarse grained particles are important sources of nutrients to the ocean in addition to the traditionally considered nutrient input from fine particles. Most models also assume that particles are spherical, but our study confirmed that aerosol particles from natural sources such as the Namib Desert, are highly aspherical (due to an abundance of mica minerals). These aspherical particles have more drag in the atmosphere and, can thus travel further (Friese et al., 2016). This means that they stay longer in suspension and have more time to dissolve (Barkley et al., 2021). Consequently, the asphericity and density of the particles emitted by sources such as the Namib Desert, will likely affect the nutrient dissolution timescales. We thus recommend that future biogeochemical models include the impact of large, often aspherical particles from small-scale Southern Hemisphere emitters, such as the Namib Desert.

A key outcome of this dissertation resulted from the comparison of the dust from anthropogenic, mixed and natural sources, i.e., considering both studies shown in paper one and paper two. The dust loads were higher in samples from natural sources compared to samples from anthropogenic sources. However, the soluble fraction was higher in dust from anthropogenic sources compared to the dust from natural sources (Table 1). These southern African sources are located proximal to one of most biological productive upwelling cells in the world oceans of the west as well as to some trace nutrient limited areas to the south. It is thus likely that these southern African dust sources (natural and anthropogenic) play important roles in the ocean biogeochemistry. We further investigated this in paper three.

Table 1 *Comparison of trace metal concentrations and solubility in aerosol particles from different dust sources that were investigated in this dissertation. The data shown here represent a synthesis from (i) Paper 1 (Chapter 2 of Section 2.4.4.) for the anthropogenic and mixed sources, (ii) Paper 2 (Chapter 3 of Section 3.3.3.) for the natural dust sources, and (iii) Paper 3 (Chapter 4 of Section 4.3.1.) for the samples collected over the ocean.*

Sources	**Total trace metal concentrations**	**Solubility ranges (%)**
Aerosols collected on land with mixed & anthropogenic origin (Paper 1) (Saldanha Bay dust)	V (~18 ppm), Cu (~67 ppm), Pb (~1175 ppm), and Fe (~33 380 ppm), Al (26 029 ppm) and Zn (22 674 ppm)	Fe (up to 28%), Cu (up to 33%), Pb (up to 45%) and Zn (up to 38%)
Aerosols collected on land with natural origin (Paper 2) (Namib Desert dust)	Fe (15 500 to 28 000 ppm), Al (19 000 to 29 200 ppm), Cu (16 to 30 ppm), Zn (12 000 to 22 400 ppm)	Fe (up to 2 %), Cu (up to 7.8 %), Zn (up to 16%), Mn (up to 9%), Pb (up to 8%)
Samples collected over the ocean with anthropogenic and mixed origin (Coastal Ocean samples)	Fe (60 to 5785 ng m^{-3}), Al (120 to 312 ng m^{-3}), Mn (1.6 to 636 ng m^{-3}), Pb (0.27 to 2.3 ng m^{-3}), V (0.1 to 2.3 ng m^{-3}), Zn (6.3 to 47 ng m^{-3}), Cu (4.3 to 43 ng m^{-3}), Co (7.5 to 21 ng m^{-3})	Fe (0.5 to 36%), Al (8.6 to 95%), Mn (0.9 to 27 %), Zn (21 to 77 %) and Co (3.3 to 42%)
Samples collected over the ocean with marine or long-distance origin (40° to 50° South latitude samples)	Fe (124 to 3782 ng m^{-3}), Al (61 to 329 ng m^{-3}), Mn (0.4 to 74 ng m^{-3}), Pb (0.05 to 4.3 ng m^{-3}), V (0.17 to 3.4 ng m^{-3}), Zn (14 to 119 ng m^{-3}), Cu (3.9 to 21 ng m^{-3}), Co (7.5 to 21 ng m^{-3})	Fe (2 to 34%), Al (9 to 48%), Mn (0.1 to 88 %), Zn (25 to 72 %) and Co (3.3 to 39%)

The third manuscript focussed on trace metal composition and fractional solubility in aerosols collected over the ocean. We used the composition along with air mass trajectory modelling to attribute main sources (e.g., southern Africa, southern America, or marine origin). In this study we showed that trace metal concentrations and solubility changed with the sources and with the traveling distance. The solubility was much higher over the ocean compared to the solubility close to the land, which was an indication of atmospheric processing from long term dust transport (Zhuang et al., 1992). Some of the samples indicated that apart from South America and Antarctica, southern Africa can be an important source of soluble bioactive trace metals to open oceans.

In this dissertation, we intentionally investigated southern African anthropogenic and natural sources that have been potentially overlooked in dust research previously. Some models tend to underestimate trace metal solubility, such as Fe, by a factor of 15, mainly due to the exclusion of anthropogenic emission from models (Ito et al., 2019). Indeed, our comparison showed that omitting the dust aerosols with anthropogenic influence might underestimate total trace metal solubility considering that dust from the natural sources had lower trace metal solubilities compared to the mixed sources. (Table 1). This study thus closed crucial gaps in our understanding on the contribution of mixed and anthropogenic from southern African sources to the proximal oceans.

5.1. RECOMMENDATIONS

The studies of aerosols transport from Southern Africa are still limited. A long-term monitoring data set is needed at some of the major dust sources to better understand the seasonal cycles of dust emissions. Offshore sampling is limited from southern Africa towards the Southern Ocean, we recommend further aerosol sampling to better understand the seasonal supply of aerosols. Sampling of aerosols along other coastal towns is highly recommended as well as close to the coal mines to better understand the impact of dust to proximal oceans. In this dissertation, we aimed to add data to a region that is highly under-sampled for aerosols in the winter compared to the summer. More dust samples should be collected over all seasons to better quantify the impact of dust over different seasons. Despite the relatively smaller dust sources in southern Africa, their mineralogy and solubility is heterogeneous even at sources in close proximity. We recommend to modelers to consider the heterogeneity of southern African dust, our findings could assist in this regard. We have provided solubility from three different sources that have been under-sampled. We provided significant information and data on regional dust sources that have not yet been included in dust models or incorporated in global dust models. Hence the findings from this research can have relevance at a global and regional scale in terms of global dust models. Mesoscale incubation studies with southern African dust are recommended to investigate whether the dust will enhance the growth of phytoplankton communities. Current global climate predictions have indicated that dust emissions from the Sahara Desert (largest dust source) will decrease in the next century as global warming continues (Evan et al., 2016). This will further highlight the importance of focussing and studying smaller dust hot spots, especially once the global major dust source diminishes.

5.2. SYNOPSIS REFERENCES

Adebiyi, A. A., & Kok, J. F. (2020). Climate models miss most of the coarse dust in the atmosphere. *Science Advances*, *6*(15), eaaz9507. https://doi.org/10.1126/SCIADV.AAZ9507

Barkley, A. E., Olson, N. E., Prospero, J. M., Gatineau, A., Panechou, K., Maynard, N. G., Blackwelder, P., China, S., Ault, A. P., & Gaston, C. J. (2021). Atmospheric Transport of North African Dust-Bearing Supermicron Freshwater Diatoms to South America: Implications for Iron Transport to the Equatorial North Atlantic Ocean. *Geophysical Research Letters*, *48*(5), e2020GL090476. https://doi.org/10.1029/2020GL090476

Evan, A. T., Flamant, C., Gaetani, M., & Guichard, F. (2016). The past, present and future of African dust. *Nature*, *531*(7595), 493–495. https://doi.org/10.1038/nature17149

Friese, C. A., van der Does, M., Merkel, U., Iversen, M. H., Fischer, G., & Stuut, J. B. W. (2016). Environmental factors controlling the seasonal variability in particle size distribution of modern Saharan dust deposited off Cape Blanc. *Aeolian Research*, *22*, 165–179. https://doi.org/10.1016/J.AEOLIA.2016.04.005

Ito, A., Myriokefalitakis, S., Kanakidou, M., Mahowald, N. M., Scanza, R. A., Hamilton, D. S., Baker, A. R., Jickells, T., Sarin, M., Bikkina, S., Gao, Y., Shelley, R. U., Buck, C. S., Landing, W. M., Bowie, A. R., Perron, M. M. G., Guieu, C., Meskhidze, N., Johnson, M. S., … Duce, R. A. (2019). Pyrogenic iron: The missing link to high iron solubility in aerosols. *Science Advances*, *5*(5). https://doi.org/10.1126/sciadv.aau7671

Prospero, J. M., Ginoux, P., Torres, O., Nicholson, S. E., & Gill, T. E. (2002). Environmental characterization of global sources of atmospheric soil dust identified with the NIMBUS 7 Total Ozone Mapping Spectrometer (TOMS) absorbing aerosol product. *Reviews of Geophysics*, *40*(1), 1–31. https://doi.org/10.1029/2000RG000095

Schulz, M., Prospero, J. M., Baker, A. R., Dentener, F., Ickes, L., Liss, P. S., Mahowald, N. M., Nickovic, S., García-Pando, C. P., Rodríguez, S., Sarin, M., Tegen, I., & Duce, R. a. (2012). Atmospheric transport and deposition of mineral dust to the ocean: implications for research needs. *Environmental Science & Technology*, *46*(19), 10390–10404. https://doi.org/10.1021/es300073u

Zhuang, G., Yi, Z., Duce, R. A., & Brown, P. R. (1992). Chemistry of iron in marine aerosols. *Global Biogeochemical Cycles*, *6*(2), 161–173. https://doi.org/10.1029/92GB00756